

Development of a non-mammalian, pre-clinical screening tool for the predictive analysis of drug toxicity

Katy Saide

Thesis submitted for the degree of Doctor of
Philosophy
University of East Anglia
School of Biological Sciences
Norwich
United Kingdom
May 2018

Word count: 66460

©This copy of the thesis has been supplied on condition that anyone who consults it is understood to recognise that its copyright rests with the author and that use of any information derived there from must be in accordance with current UK Copyright Law. In addition, any quotation or extract must include full attribution

Abstract

The failure to predict drug-induced toxicity reactions is still a major problem contributing to a high attrition rate and tremendous cost in drug development. *Xenopus laevis* embryos are amenable for the early stage medium to high throughput small molecule screens. We hypothesise *Xenopus* embryos can assist *in vitro* drug-induced toxicity safety assessment in the early phases of drug development before moving on to expensive preclinical trials in mammals. The objective of this study was to assess the use of *Xenopus laevis* embryos for the prediction of organ-specific toxicity. To do this I used drugs known to generate toxicity reactions in humans. First of all I determined that *Xenopus* embryos treated with a drug from the age of stage 38 until stage 45, was an appropriate assay for the prediction of drug-induced toxicity. The embryos expressed major drug metabolism enzymes including CYP2E1, CYP2D6, CYP3A4 and glutathione S-transferases, sulphotransferases and glucuronosyltransferases. They also expressed KCNH2, which encodes the α -subunit protein of the potassium ion channel $K_V11.1$ that contributes to heart electrophysiology. For drug-induced liver injury, I used paracetamol treatment. *Xenopus laevis* embryos treated with paracetamol (0-5 mM) generated predicted paracetamol metabolites, had a dose-dependent depletion of free glutathione and increased expression of microRNA-122 (miR-122) in tissue that did not contain the liver. To investigate drug-induced cardiotoxicity, I treated *Xenopus* embryos with doxorubicin (0-100 μ M) and terfenadine (0-50 μ M). Embryo heart rates increased and decreased with these drugs respectively and arrhythmias occurred with both drug treatments. Embryos treated with doxorubicin had an increasing amount of arrhythmia that correlated with an increasing dose of doxorubicin treatment. Terfenadine treatment induced arrhythmia at a rate that was not concentration dependent. Wholemound *in situ* hybridisation (WISH) revealed the *Xenopus* embryos also express miR-208 specifically in the heart, similar to mammalian models. We conclude that *Xenopus laevis* embryos exhibit some similar characterisations of drug-induced hepatotoxicity and cardiotoxicity observed in mammalian models. These data indicate the *Xenopus* embryo could be a useful model to assess drug-induced toxicity and aid lead compound prioritisation in early drug development.

Abbreviations

1-ABT 1-aminobenzotriazole

ABC ATP-binding cassette

ADME Adsorption, distribution, metabolism and excretion

ADR Adverse drug reaction

AIF Apoptosis inducing factor

ALP Alkaline phosphatase

ALT Alanine aminotransferase

AMAP N-acetyl-meta-aminophenol

AMBIP Alpha-1-microglobulin/bikunin precursor

APAP Paracetamol (N-acetyl-para-aminophenol)

AST Aspartate aminotransferase

ATP Adenosine triphosphate

BMB Boehringer Mannheim blocking reagent

BCRP Breast cancer resistance protein

bpm beats per minute

BSEP Bile salt export pump

CB Cannabinoid

CiPA Comprehensive *in vitro* proarrhythmia assay

C_{max} peak serum drug concentration

COX Cyclooxygenase

CRM Chemically reactive metabolite

CYP450 Cytochrome P450

dH₂O Distilled water

DILI Drug-induced liver injury

DNA Deoxyribonucleic acid

DsRED Red fluorescent protein

DMPK Drug metabolism pharmacokinetics

DMSO dimethyl sulfoxide

EAD Early after-depolarisation

ECG Electrocardiogram

ECM Extra-cellular matrix

EDTA Ethylenediaminetetraacetic acid

EndoG Endonuclease G

ER Endoplasmic reticulum

EtOH Ethanol

FETAX Frog Embryo Teratogenesis Assay Xenopus

fps frames per second

GFP Green fluorescent protein

GLDH Glutamate dehydrogenase

GLP Good Laboratory Practice

GMP Good Manufacturing Practice

GSH Glutathione

GST Glutathione S-transferase

hCG human chorionic gonadotrophin

hERG human Ether-à-go-go-Related Gene

H&E Hematoxylin and eosin

HLA Human leucocyte antigen

HMGB1 High-mobility group box-1

hpf hours post-fertilisation

HPLC-MS/MS High-performance liquid chromatography-mass spectrometry

hSC-CM Human stem-cell derived cardiomyocyte

ICH International Conference on Harmonisation

I_{Kr} Rapid delayed rectifier K⁺ current

I_{Ks} Slow delayed rectifier current

INR International normalised ratio

IVF *In vitro* fertilisation

JVS juvenile visceral steatosis

K-18 Keratin-18

LB Luria Broth

LPS Lipopolysaccharide

LVEF Left ventricular ejection fraction

MABT maleic acid buffer, 0.1 % tween-20

MAPK mitogen-activated protein kinase

MHC Major histocompatibility complex

MICE Multiple ion channel effects

MMR Marc's Modified Ringers

MPT Mitochondrial membrane permeability transition

MRP2 Multidrug resistance-associated protein

miRNA micro RNA

mRNA messenger RNA

NAC N-acetyl cysteine

NADPH (reduced) Nicotinamide adenine dinucleotide phosphate

NCE New chemical entity

NIH National Institutes of Health

Nrf2 nuclear factor erythroid-2 related factor 2

NSAID Non-steroidal anti-inflammatory drug

NTEL No toxic effect level

PAPS 3'-phosphoadenosine-5'-phosphosulfate

PBS Phosphate buffered saline

PBST PBS 0.1 % tween-20

PMSG Pregnant Mare Serum Gonadotrophin

PTU Phenylthiourea

RAGE Receptor for advance glycation end-products

R&D Research and development

rRNA ribosomal RNA

RNA ribonucleic acid

ROS Reactive oxygen species

RT Room temperature

SM Safety margin

SNP Single-nucleotide polymorphism

snRNA Small nuclear RNA

SOD-2 Super-oxide dismutase-2

SSA Sulpho

SULT Sulphotransferase

TBL Total bilirubin

TdP Torsade de pointes

TLR Toll-like receptor

TUNEL Terminal deoxynucleotidyl transferase dUTP nick end labeling

UDP Uridine 5'-diphospho

UGT UDP-glucuronosyltransferase

ULN Upper limit of normal

UTR Untranslated region

WISH Wholemount *in situ* hybridisation

Acknowledgments

Grant Wheeler and Dan Antoine - Thank you for trusting me, giving me the opportunity to try new experiments and boosting my confidence in my abilities as a scientist.

Sam Fountain - For your great advice and listening to me when I needed to talk pharmacology.

Inès - Thanks for being Frangry, making me look less moody, all the hilarious and confusing French/English conversations, and forever lounging around in your onsie, singing badly and doing the chicken dance. Oh and being an amazing scientist. Indeed.

Nicole – Thanks for relentlessly advocating the Fine City as the best city in the UK to me and all the endless Nicole stories. I have no idea how I've managed to become friends with such a positive person.

Danielle – Thanks for putting up with my insults and being an inspirational meal prep queen.

Geoff - Thanks for listening to my many stupid questions but also reminding me that my experiments are very easy and simple compared to yours. And entertaining me with your awful knowledge of simple English sayings, even though you are in fact, British.

Marta and Angels - Thank you for being patient and being overall excellent sources of science advice.

The rest of the Wheeler/Münsterberg lab - Thank you for all your help and guidance.

Soph, Zo and Ros - Thank you for all the many compliments, constant laughs, visits “up North” to Norwich and generally being the best bunch.

Anna and Emma - Thanks for creating a place to call home for me in Norwich, being supportive and putting up with living with me.

Lizy and Danni – Thanks for keeping me grounded and the continuous, unwavering friendship.

Norwich Dragons Hockey Club - Thank you for being so welcoming and helping me keep some sort of sanity away from PhD life. Proud to be a dragon.

Mum – For the many visits to Norwich and all the support despite still not quite understanding what I have been doing for the past 4 years.

Contents

Abstract	ii
Abbreviations	iii
Acknowledgments	ix
Contents	x
Figure index	xv
Table index	xviii
1 Chapter 1: Introduction	1
1.1 General Overview of Drug Development	1
1.2 Drug Safety Assessment in Drug Development	3
1.3 Problems with Drug Safety Assessment	5
1.3.1 In Drug Development: Drug attrition	5
1.3.2 After Drug Development: Adverse drug reactions	5
1.4 Drug-induced toxicity: Organ-specific	7
1.4.1 Liver	7
1.4.2 Heart	28
1.5 An ideal preclinical animal model for the prediction of drug-induced toxicity 38	
1.5.1 Where is the gap?.....	39
1.6 Xenopus laevis	39
1.6.1 The Xenopus laevis liver.....	41
1.6.2 The Xenopus laevis heart.....	41
1.7 Rationale	42
2 Chapter 2: Materials and Methods	43
2.1 Xenopus laevis egg collection	43
2.2 Embryo fixing	43
2.3 Photographing embryos	44
2.4 RNA isolation and cDNA synthesis	44
2.4.1 1. mRNA: TRIzol® method	44
2.4.2 2. miRNA: miRCURY™ RNA (Exiqon) method	45
2.5 RT-PCR	45
2.6 qRT-PCR	46
2.6.1 qRT-PCR statistical analysis	46
2.7 Wholemout in situ hybridisation (WISH)	46

2.7.1	1. mRNA probe synthesis: for Cardiac Troponin 1c and alpha-1-microglobulin/bikunin precursor (AMBP).....	46
2.7.2	2. XenmiR probes: miR-122 and miR-208.....	48
2.7.3	WISH staining protocol.....	49
2.8	Sectioning.....	50
2.8.1	Cryostat with OCT compound.....	50
2.8.2	Microtome with wax.....	50
2.8.3	Hematoxylin and Eosin staining.....	50
2.9	Treatment with drugs.....	51
2.9.1	Chapter 3 Drug screens.....	51
2.9.2	Chapter 4 and 5 screens.....	51
2.9.3	The preparation of samples for the measurement of miR-122 expression using qRT-PCR.....	52
2.9.4	1-aminobenzotriazole (ABT) and paracetamol.....	52
2.9.5	N-acetyl cysteine (NAC) and paracetamol.....	52
2.9.6	Doxorubicin and dexrazoxane.....	53
2.10	Measuring free GSH.....	53
2.10.1	Sample preparation.....	53
2.10.2	GSH assay.....	53
2.10.3	Bradford assay.....	54
2.11	Heart rate assay.....	54
2.11.1	Anaesthetic assays.....	54
2.11.2	Drug treatment: doxorubicin and terfenadine.....	54
2.11.3	Post-treatment doxorubicin recovery.....	55
2.11.4	Video analysis.....	55
2.12	Mass spectrometry analysis of paracetamol (APAP) and paracetamol metabolites.....	56
2.12.1	Preparation of samples.....	56
2.12.2	Analysis of HPLC-MS/MS.....	57
2.13	Positive control.....	57
2.14	Statistical analysis.....	57
3	Chapter 3: Characterisation of the <i>Xenopus laevis</i> embryo as a model for drug-induced toxicity.....	58
3.1	Introduction.....	58
3.2	Aim.....	66
3.3	Hypothesis.....	66

3.4 Results	67
3.4.1 Initial drug dose response screens	67
3.4.2 Characterisation of <i>Xenopus</i> embryo drug metabolism machinery	81
3.4.3 Atlas of stage 45 <i>Xenopus laevis</i>	81
3.5 Discussion	103
3.6 Conclusion	105
4 Chapter 4: Assessing the use of <i>Xenopus</i> as a model for the prediction of Drug-induced Liver Injury using paracetamol as the model hepatotoxin	106
4.1 Introduction	106
4.1.1 Paracetamol-induced Liver Injury	106
4.1.1 Animal Models for Paracetamol-Induced Liver Injury	110
4.2 Aim	112
4.3 Hypothesis	112
4.4 Paracetamol Results	112
4.4.1 Paracetamol dose response in <i>Xenopus laevis</i>	112
4.4.2 Free GSH content in Paracetamol Treated Embryos	121
4.4.3 Liver expression pattern in <i>Xenopus laevis</i> and liver injury biomarker expression.....	123
4.4.4 Characterisation of the metabolic profile of paracetamol-treated <i>Xenopus laevis</i> embryos	128
4.1.1	130
4.4.5 Analysis of time-dependent and dose-dependent multidrug resistance-associated protein 2 (MRP2) expression	131
4.4.6 Treatment with acetyl-meta-aminophenol (AMAP).....	132
4.1.2	134
4.4.7 Characterisation of the metabolism of paracetamol in <i>Xenopus</i>	135
4.4.8 <i>Xenopus</i> incubation with the human clinical treatment for paracetamol overdose	137
4.5 Investigating an alternative drug known to be associated with drug-induced liver injury	139
4.5.1 Diclofenac-induced liver injury	139
4.6 Diclofenac Results	140
4.6.1 Diclofenac dose response in <i>Xenopus laevis</i>	140
4.7 Discussion	144
4.7.1 Paracetamol Overdose Concentration Range and Phenotypes	144
4.7.2 Characterising the <i>Xenopus</i> embryo response to paracetamol overdose ...	145

4.7.3	AMAP: the non-toxic regioisomer of APAP.....	150
4.7.4	Investigating an additional hepatotoxin: diclofenac.....	151
4.8	Conclusion	152
5	Chapter 5: Assessing the use of <i>Xenopus</i> as a model for the prediction of Drug-induced Cardiotoxicity using doxorubicin and terfenadine as the model	
	cardiotoxins.....	153
5.1	Introduction	153
5.1.1	Doxorubicin-induced cardiotoxicity	153
5.1.2	Animal models for doxorubicin-induced cardiotoxicity	155
5.1.3	Terfenadine-induced cardiotoxicity	157
5.1.4	Animal models for terfenadine-induced cardiotoxicity	157
5.2	Aim	158
5.3	Hypothesis.....	158
5.4	Results	158
5.4.1	Doxorubicin dose response in <i>Xenopus laevis</i> embryos	158
5.4.2	Dexrazoxane dose response in <i>Xenopus laevis</i> embryos	163
5.4.3	Treatment with combined doxorubicin and dexrazoxane incubation	167
5.4.4	Identification of the anaesthetic concentration suitable for the experiments that will investigate <i>Xenopus</i> embryo heart rate	171
5.4.5	Video analysis.....	172
5.4.6	Investigating the effect of doxorubicin treatment on <i>Xenopus</i> embryo heart rate	172
5.4.7	Terfenadine dose response in <i>Xenopus laevis</i> embryos	177
5.4.8	Investigating the effect of terfenadine treatment on <i>Xenopus</i> embryo heart rate	177
5.4.9	Heart expression pattern in <i>Xenopus laevis</i>	185
5.5	Discussion.....	190
5.5.1	Doxorubicin dose range and phenotype	190
5.5.2	Terfenadine dose range and phenotype	191
5.5.3	The heart rate assay	191
5.5.4	Doxorubicin and dexrazoxane combined treatment	195
5.5.5	MiR-208 expression in <i>Xenopus</i> embryos	195
5.6	Conclusion	196
6	Chapter 6: General discussion	197
6.1	Project aims.....	197
6.2	Introduction	197

6.3	Characterisation of the <i>Xenopus laevis</i> embryo as a model for drug-induced toxicity	200
6.4	<i>Xenopus laevis</i> embryos and the prediction of DILI: paracetamol	201
6.5	<i>Xenopus laevis</i> embryos and the prediction of cardiotoxicity: doxorubicin and terfenadine	203
6.6	Limitations and future experiments	204
6.7	Conclusion and the 'bigger picture'	209
7	Chapter 7: References	211
8	Chapter 8: Appendix.....	242
8.1	Heart rate assay	244

Figure index

Figure 1-1 Drug Development pipeline	1
Figure 1-2: Action potential of a cardiac myocyte	30
Figure 1-3: Electrocardiogram (ECG) trace	31
Figure 1-4: <i>Xenopus</i> heart	42
Figure 3-1: The monooxygenase CYP450 enzyme cycle.....	65
Figure 3-2: Stage 15 – stage 38 dose-response 0.78-100 μ M drug screens.....	80
Figure 3-3: Incidence of phenotypes for the stage 15 to stage 38 screen.....	83
Figure 3-4: Stage 38 – stage 45 dose-response 0.78-100 μ M drug screens.....	91
Figure 3-5: Incidence of phenotypes for the stage 38 to stage 45 screen.....	93
Figure 3-6: RT-PCR for drug metabolism enzymes in untreated <i>Xenopus laevis</i> embryos.	94
Figure 3-7: Transverse sections of untreated stage 45 <i>Xenopus laevis</i> embryos.	99
Figure 3-8: Sagittal sections of untreated stage 45 <i>Xenopus laevis</i> embryos.	102
Figure 4-1: Paracetamol metabolism with a therapeutic dose.....	107
Figure 4-2: Paracetamol metabolite hepatocyte transporters.....	108
Figure 4-3: The mechanism for paracetamol-induced liver injury.....	110
Figure 4-4: Paracetamol dose response 0-5 mM.....	116
Figure 4-5: The percentage of <i>Xenopus</i> embryo survival with 0-5 mM paracetamol treatment.....	117
Figure 4-6: Paracetamol dose response 0, 5.5-10 mM.....	119
Figure 4-7: The percentage of <i>Xenopus</i> embryo survival with 5.5-10 mM paracetamol treatment.....	120
Figure 4-8: The amount of free GSH inside <i>Xenopus</i> embryos treated with paracetamol.	122
Figure 4-9: Illustration of the location of the liver in <i>Xenopus</i> embryos.	124
Figure 4-10: Wholemout <i>in situ</i> hybridisation (WISH) for liver markers.	125
Figure 4-11: Sections of miR-122 WISH stage 45 embryos.	126
Figure 4-12: Expression of miR-122 in paracetamol-treated embryos.	127
Figure 4-13: Mass spectrometry detection of paracetamol.....	129
Figure 4-14: Mass spectrometry detection of paracetamol metabolites.	130
Figure 4-15: Expression of MRP2 in paracetamol-treated embryos.....	131
Figure 4-16: AMAP dose response 0, 5.5-10 mM.....	134
Figure 4-17: The percentage of <i>Xenopus</i> embryo survival with 5-10 mM AMAP treatment.	134

Figure 4-18: The amount of free GSH inside <i>Xenopus</i> embryos treated with paracetamol (APAP) or <i>N</i> -acetyl-meta-aminophenol (AMAP).....	135
Figure 4-19: The amount of free GSH in embryos treated with 1-aminobenzotriazole (1-ABT) and paracetamol.....	136
Figure 4-20: Free GSH in embryos treated with paracetamol and <i>N</i> -acetyl cysteine (NAC).	139
Figure 4-21: Diclofenac mechanism of toxicity	140
Figure 4-22: Diclofenac dose response 0-10 μ M.....	143
Figure 4-23: The percentage of <i>Xenopus</i> embryo survival with 1-10 μ M diclofenac treatment.....	144
Figure 5-1: Doxorubicin dose response 0-100 μ M.....	162
Figure 5-2: The percentage of <i>Xenopus</i> embryo survival with 0-100 μ M doxorubicin treatment.....	162
Figure 5-3: The percentage of <i>Xenopus</i> embryo survival with 0-150 μ M doxorubicin treatment.....	163
Figure 5-4: Dexrazoxane dose response 0-1 mM.....	166
Figure 5-5: The percentage of <i>Xenopus</i> embryo survival with 0-1 mM dexrazoxane treatment.....	166
Figure 5-6: Doxorubicin (0-100 μ M) and Dexrazoxane (0-1 mM) treatment.....	170
Figure 5-7: The percentage of <i>Xenopus</i> embryo survival with doxorubicin (0-100 μ M) and dexrazoxane (0-1 mM) treatment.	171
Figure 5-8: Investigation of anaesthetic concentration and heart rate.	172
Figure 5-9: The effect of doxorubicin treatment on heart rate.....	174
Figure 5-10: Heart rate assay embryo survival and incidence of arrhythmias with doxorubicin treatment.	175
Figure 5-11: Characterisation of heart rate for doxorubicin-treated embryos after 3 days without treatment.	176
Figure 5-12: Terfenadine dose response 0-100 μ M.....	182
Figure 5-13: The percentage of <i>Xenopus</i> embryo survival with 0-100 μ M terfenadine treatment.....	182
Figure 5-14: The effect of terfenadine treatment on heart rate.....	183
Figure 5-15: Heart rate assay embryo survival and incidence of arrhythmias with terfenadine treatment.....	184
Figure 5-16: Illustration of heart location in <i>Xenopus laevis</i> embryo.	186
Figure 5-17: Cardiac troponin 1c sections.	187
Figure 5-18: Wholemout <i>in situ</i> hybridisation (WISH) for miR-208.	188
Figure 5-19: miR-208 sections for stage 38 <i>Xenopus</i> embryos.....	189

Figure 6-1: Summary of project results.....	199
Figure 6-2: Future experiments to be conducted	208
Figure 6-3: Drug development with <i>Xenopus laevis</i>	209
Figure 8-1: Heart rate analysis and an example of a physiological heart beat	245
Figure 8-2: Graphs that indicate arrhythmic heart beats.....	246

Table index

Table 1-1: Clinical presentation of DILI.....	11
Table 1-2: Mechanisms of DILI and associated examples	15
Table 1-3: Advantages and Disadvantages of <i>in vitro</i> models for DILI	19
Table 1-4: Major DILI mechanisms and corresponding useful <i>in vitro</i> models	21
Table 3-1: A summary of the key mechanisms of action for drugs known to be associated with drug-induced toxicity.	61
Table 3-2: Summary of the major phase II metabolism enzymes.....	66
Table 8-1: miRNA qRT-PCR primer sets	242
Table 8-2 miRNA LNA probes	242
Table 8-3: mRNA qRT-PCR primers.....	242
Table 8-4: mRNA RT-PCR primers.....	242

1 Chapter 1: Introduction

1.1 General Overview of Drug Development

On average it takes a compound 10-15 years to progress from the discovery phase to being registered and legally available on the market for the appropriate patients. This does not leave much time to recover the cost of development before the drug is taken off patent. The drug development process can differ slightly according to the pharmaceutical company and the type of compound being pushed through, but in general the pipeline consists of the following stages (**Figure 1-1**).

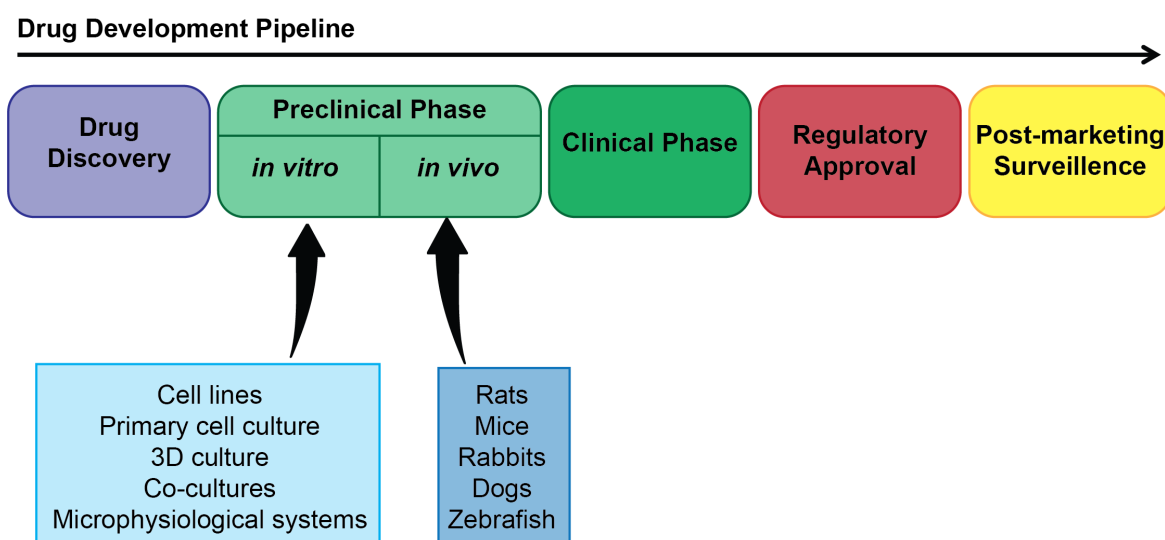


Figure 1-1 Drug Development pipeline

Typically, a drug will take 10-15 years in drug development from drug discovery until approval. The *in vitro* and *in vivo* models are used for pharmacokinetics studies and in drug safety assessment, which continues as the clinical studies are performed. The earlier a drug-induced toxicity reaction is identified for a drug candidate, the less time and money is wasted on the further development for a drug that has the potential to be a greater risk than benefit to the general population. Post-marketing surveillance is often when idiosyncratic adverse drug reactions are identified because they are too rare to be noticed in the clinical phase that is comprised of smaller cohorts.

To begin with, there is the discovery phase, a target has been identified and new chemical entities (NCEs) are put forward to determine which are good new potential therapeutic compounds for that target. Here, one is either looking at an entirely new therapeutic target for a disease model, or it could be the same target as a currently marketed medicine, and the aim is to find a NCE that is more efficient or has less side-effects. The “best” NCEs, termed lead compounds, are picked via analysis of their basic pharmacological properties. This is now often carried out by robotics so several tens of thousands NCEs can be processed at once, this is high throughput screening. For the last part of drug discovery, the lead compounds are optimised to generate more potent and more selective compounds, to be the best version of themselves with regards to their desired target. The compounds generated here are called drug candidates. Some preliminary toxicity studies are carried out during lead optimisation, however the majority of the toxicity studies begin in the preclinical phase of drug development.

The aim of the preclinical phase is to generate data that will provide enough information to understand the properties of the drug candidates as much as possible before they progress into the clinical phase, into humans. The regulatory authorities such as the European Medicines Agency or the US Food and Drugs Administration, judge the plethora of information generated during the preclinical phase studies for a drug candidate and choose whether to allow it through to clinical phase studies in humans or not. The data submitted to the regulatory authorities is generated under the Good Laboratory Practice (GLP) code to ensure they are of a certain standard and this data is therefore deemed more reliable and trustworthy compared to non-GLP experiments (Sullivan, 1995). In addition to safety pharmacology and toxicological testing, the preclinical phase also involves pharmacokinetic studies, which consist of studies to look at the drug candidate adsorption, distribution, metabolism and excretion (ADME). These additional studies are divided into primary and secondary pharmacology. Primary pharmacology investigates the drug candidate mechanism of action that is directly associated with the therapeutic target. Secondary pharmacology considers the mechanism of action not directly associated with the target (ICH (International Conference on Harmonization), 2014). The preclinical phase consists of *in vitro* and *in vivo* studies; the latter tends to follow the former. However, findings in the initial *in vivo* studies such as organ-specific toxicity can be evaluated retrospectively using target organ specific *in vitro* assays. Altogether, the preclinical phase will help to generate a first-in-human starting dose of the drug candidate, identify potential target organs for drug-induced toxicity and build a good idea of the parameters to be monitored in humans during the clinical phase to help to protect the phase I clinical phase healthy volunteers.

Finally, the successful drug candidate is submitted into the clinical phase, where it is administered to humans. The trials start with smaller groups of healthy volunteers in phase I clinical trials, and progress to phase III large, multiple groups of patients, that the drug candidate could provide a therapeutic use for.

These 3 phases of drug development (drug discovery, preclinical and clinical) do not necessarily strictly occur one after the other, they sometimes overlap and preclinical studies are often continued whilst the clinical phase has begun. Furthermore, the length of time spent in each phase can be significantly different for a compound for which there is a great demand. An anti-cancer drug candidate that shows promise at extending the lives of cancer patients could spend a shorter amount of time in the preclinical phase and be pushed through to the clinical phase more quickly because it could be the only chance for some patients, who are willing to take on the potential risks associated with the drug candidate as the benefit could be a longer life. However for the majority of drug candidates, the regulatory authorities prefer a robust set of preclinical studies are carried out to assess the toxicological potential.

1.2 Drug Safety Assessment in Drug Development

The regulatory guidelines, for assessing the safety pharmacology of a drug candidate, are issued by the International Conference on Harmonisation (ICH). ICH was established in 1990 in an attempt to integrate all of the existing regulations from different parts of the world such as Japan, the US and Europe. It is important to note that these are only guidelines and ultimately it is the drug company, not the regulator, which determines which safety studies are performed for a drug candidate in drug development. This is to help inject some flexibility into the drug development process and to encourage good experimental design for the studies that are necessary and justified for each individual drug candidate. Although there may be an initial catalogue of studies conducted for every drug candidate (Redfern et al., 2002), there is not a finite battery of studies that are, perhaps thoughtlessly, always conducted. Every drug candidate will have additional studies conducted in answer to their unique results from the initial studies. Overall the aim of the safety pharmacology studies is to investigate the potential undesirable pharmacodynamic effects of a substance on physiological functions in relation to exposure in the therapeutic range and above (ICH (International Conference on Harmonization), 2014). There are 2 main toxicological studies that are carried out: exploratory toxicology and regulatory toxicology. Exploratory toxicology studies typically consist of a single dose administered for 2 weeks at 2-day intervals. A large range of drug concentrations are used and the dose is increased throughout the 2 weeks and the studies are often not in accordance with GLP. These studies can help to determine which

organs are affected by the drug candidate and estimate the no toxic effect level (NTEL). These experiments provide preliminary, rough, quantitative information about the drug-associated toxicity. On the other hand, regulatory toxicological studies are performed under GLP and GMP (good manufacturing practice) (Chorghade, 2006). The regulatory authorities and ethical committees require them to be performed before the drug candidate is given to humans, and they support marketing approval in parallel to clinical trials. The current major safety pharmacology ICH guidelines include ICH S6, S7A, S7B, S9 and M3. The so-called “core battery” of safety studies for compounds that are being developed for the purpose of human pharmaceuticals are found in ICH S7A (ICH (International Conference on Harmonization), 2014). Guideline ICH S7A encourages the design of studies that will test the effects of the drug candidate on the vital organ systems, usually cardiovascular, respiratory and central nervous systems. The ICH M3 (ICH (International Conference, 2009) focuses on the preclinical safety studies with regards to the conduct of human clinical trials and marketing authorization and the ICH S6 guidelines assess the evaluation of biotechnology-derived pharmaceuticals. The ICH S9 guidelines are helpful for anticancer drug candidate study design. The ICH S7B guidelines stipulate the preclinical testing strategy for the evaluation of the potential for delayed ventricular repolarization (ICH (International Conference on Harmonization), 2005). This is the one preclinical study that the regulatory authorities state must be investigated (Bowes et al., 2012). An *in vitro* assay must be performed to investigate the effects of the drug candidate on the alpha subunit of the voltage-gated potassium ion channel (K_v11.1) encoded by the gene human Ether-à-go-go-Related Gene (hERG). A drug candidate that interacts with this protein encoded by the hERG, a gene that is also known as KCNH2, will often be strongly associated with cardiotoxicity. The hERG channel and drug candidate relationship will be discussed later in this chapter. As well as the core battery of safety studies, other experiments that are popular in preclinical drug candidate safety assessment include genetic toxicity assays, studies that investigate drug-drug interactions and metabolite-mediated toxicity. The ability of the drug candidate to cause DNA damage (mutagenicity), chromosome aberration and chromosome breakage can be assessed using the Ames test (Ames et al., 1975; Maron and Ames, 1983), the micronucleus assay (Galloway et al., 1994) and clastogenicity assays respectively (Kirpnick et al., 2005). It is a good idea to investigate if a drug candidate interacts with a popular enzyme or membrane transporter protein that other existing drugs are known to inhibit or induce, such as cytochrome P450s and P-glycoprotein (Wienkers and Heath, 2005). And increasingly, the generation of reactive metabolites is important to investigate in drug development, particularly with regards to their association with organ-specific toxicity and idiosyncratic toxicity (Baillie et al., 2002). Many reactive metabolites are responsible for the formation of

adverse drug reactions (Park et al., 2005b) which can have a detrimental effect on a marketed drug.

1.3 Problems with Drug Safety Assessment

1.3.1 In Drug Development: Drug attrition

It is widely acknowledged that in the past few decades, improved techniques such as high-throughput screening (Mayr and Fuerst, 2008), increasingly sensitive liquid chromatography mass spectrometry, (Feng, 2004; Kramer et al., 2007), combinatorial chemistry, faster DNA sequencing (Scannell et al., 2012) and improved X-ray crystallography has helped the drug discovery phase be more efficient. A larger number of NCEs are available to be screened quicker thus accelerating the time taken to identify a lead compound and subsequently reducing discovery phase costs. However there has been a decline in research and development (R&D) productivity (Pammolli et al., 2011) this is thought to be, in part, due to what has been referred to as “development-limiting toxicity” (Kramer et al., 2007), defined as a toxicity that has an undesirable safety margin and cannot be monitored, therefore it will affect the drug marketability.

Toxicity associated with NCEs is a dominant cause for attrition in all phases of drug development (Kramer et al., 2007). Consequently, an effort has been made by pharmaceutical companies to move safety studies towards the early stages of development (Hamdam et al., 2013; Redfern et al., 2002) to identify and remove the compounds which are more likely to induce a toxicity phenotype as early as possible in drug development in an attempt to select the compounds which should be a better investment of time and money. Early safety assessment can help in the decision making process in lead generation, give chemists the opportunity to remove hazardous aspects of the lead compound during lead optimization, introduce risk assessment early in drug development and help to manage safety margins in preclinical and clinical development studies (Bowes et al., 2012). It is thought about 70 % of all drug attrition in drug development associated with safety concerns, occurs in the preclinical phase (Kramer et al., 2007). As a result, a more strategic and efficient assessment of safety pharmacology in the preclinical phase will increase the quality of the drug candidates selected for the clinical phase, they will be more likely to make it through to the marketing stage.

1.3.2 After Drug Development: Adverse drug reactions

An adverse drug reaction (ADR) is defined as a response to the application of a drug at a standard dose for therapeutic, prophylactic and diagnostic use that is considerably harmful and likely to become hazardous with continuous administration (Anonymous, 1972; Edwards and Aronson, 2000). The drug treatment responsible for the ADR is

usually withdrawn or the dosage can be altered. ADRs are typically categorised into two types according to their mechanistic process. Type A are the most common ADRs and account for approximately 80% of all ADRs. They are predictable from the pharmacological properties of the implicated drug and are dose-dependent. Type B are idiosyncratic ADRs, and they tend to be more severe than type A and make up 10-15% of all ADRs. Type B can be further divided into immune and metabolic-mediated reactions (Gomes and Demoly, 2005; Pirmohamed et al., 2002) and they are more difficult to detect during drug development than type A ADRs. The reason for this can be put down to the fact that some type B ADRs only occur in 1 in 1000 to 1 in 10000 people, which when one considers the group size for human clinical trials is smaller, it is likely that these ADRs will be missed. There are additional, less common ADR types C, D and E: long-term adaptive changes, delayed effects and rebound effects when the drug is discontinued in patients respectively (Redfern et al., 2002). The delayed type D ADRs include examples such as carcinogenicity and teratogenicity and are investigated using preclinical toxicological studies. Type E is usually only detected during post-marketing surveillance. Type C ADRs occur with some drugs as a result of chronic use and dose accumulation. Some evidence exists for long-term methotrexate administration and its association with liver fibrosis, although the literature is not sure this is a valid association (Salliot and Van Der Heijde, 2009). Antimalarial drugs and ocular toxicity have also been implicated as a type C ADR (Carr et al., 1968).

ADRs are responsible for 1 in 16 UK hospital admissions, of which 2% are fatal. Pirmohamed and colleagues estimate that ADRs cost the NHS £499 million annually (Pirmohamed et al., 2004). Pharmaceutical companies stand to lose a significant amount of time and money if it becomes apparent that a compound causes moderate to severe or even fatal ADRs. It is particularly detrimental if the ADR is not discovered until the later stages of drug development such as the clinical phases, or after the compound has been approved and is in use in the general population. It is also in the patient's best interest to reduce the number drugs that cause ADRs and associated drug attrition rate, not just for the obvious safety reasons, but also to guarantee there is an effective therapeutic drug option to treat the patient's disease. Unfortunately, if a drug is the only effective treatment option, a patient will have to continue to use it even if drug-induced toxicity or hypersensitivity reactions are apparent. Therefore, it is important to remember that the decision to withdraw a drug also takes into account the availability of other treatments for that disease and the severity of the disease to be treated. Herein lies a similar challenge for pharmaceutical companies; determining when the potential adverse effects of a compound outweigh the therapeutic benefits to the targeted population of a specific disease (Stevens, 2006). Cancer is a good example of one such disease where patients

are more willing to tolerate risk of ADRs or a greater number of side effects associated with a drug, if the drug can extend their life.

1.4 Drug-induced toxicity: Organ-specific

1.4.1 Liver

1.4.1.1 Structure and Function

The human liver is located in the upper right part of the abdomen and extends across the centre to the upper left abdominal region. It is the largest visceral organ, the heaviest gland (approximately 1.4 kg) and the second largest organ to the skin in the human body (Tortora and Derrickson, 2014). The human liver divides into two lobes that are separated by a fold of mesentery called the falciform ligament, the inferior vena cava and the gallbladder. The right lobe is bigger than the left and has two functionally distinct lobes: the quadrate lobe and the caudate lobe, which are anterior and posterior respectively (Drake et al., 2012). The liver can be separated into approximately 1 million structural units called lobules. A lobule has a hexagonal shape that contains a central vein at its middle point and portal triads at its corners. A portal triad consists of connective tissue that envelops an artery, a vein and a bile duct. The population of hepatocytes supplied by 1 portal triad is a hepatic acinus, which is divided into 3 zones: (1) periportal, (2) transitional and (3) perivenous. Zone 1 is closest to the portal triad vasculature and therefore receives highly oxygenated blood whereas zone 3 is close to the central vein and receives poorly oxygenated blood (Bacon et al., 2006).

The three main components of the human liver are the hepatocytes, the bile canaliculi and the hepatic sinusoids. The hepatocytes make up about 80 % of the total volume of the liver and are therefore a major contribution to the overall function of the liver, they have metabolic, secretory and endocrine functions (Tortora and Derrickson, 2014). Hepatocytes secrete bile into the bile canaliculi, which are situated between neighbouring hepatocytes. The bile canaliculi aid the transportation of bile towards the gallbladder. Bile helps digestion in the duodenum of the small intestine, in particular, the emulsification and absorption of lipids. Oxygenated blood from the hepatic artery and deoxygenated blood from the hepatic portal vein is distributed into the blood capillaries found between hepatocytes known as hepatic sinusoids. This blood is then transported back to the right atrium of the heart via the inferior vena cava.

As well as bile secretion, the liver also has role to play in many other vital human bodily functions, notably for this project, it is the key site of drug metabolism. Compared to other organs, the liver has a very high concentration of drug metabolising enzymes such as cytochrome P450s (CYP450s), which are found in the smooth endoplasmic reticulum.

Furthermore, drugs absorbed from the gastrointestinal tract are initially taken to the liver via the portal vein, this is known as first pass metabolism. If the liver and the gastrointestinal tract extract a drug effectively, it may never reach the systemic circulation. Consequently the liver can reduce drug bioavailability. The liver also functions to synthesise plasma proteins such as albumin as well as deaminate amino acids, which results in the generation of ammonia. When blood glucose is low, the liver can generate glucose from glycogen, specific amino acids, lactic acid and sugars, for example fructose and galactose. And vice versa, when blood glucose is high, the liver converts glucose to glycogen and triglycerides. Vitamins A, B₁₂, D, E and K are stored in the liver alongside iron and copper. And finally, the liver contains Kupffer cells, which serve to phagocytise old red blood cells and white blood cells.

1.4.1.2 Drug metabolism

The liver contains a high concentration of the enzymes involved in drug metabolism. Drug metabolism is conventionally divided into phase 1 and phase 2 which are catabolic and anabolic respectively. Overall, the aim of drug metabolism is to decrease the lipophilicity of the drug and increase the polarity to excrete the compound quickly and avoid long-term exposure and excessive build-up of the compound. The kidneys find it easier to excrete polar compounds than non-polar compounds into urine. Phase 1 usually, although not always, precedes phase 2 and consists of oxidation, reduction and hydrolysis reactions that introduce a reactive, functional group to which a phase 2 conjugating system can add a substituent (Rang et al., 2016). The CYP450 enzymes are important for the phase 1 oxidation reactions. They require the co-factor (reduced) nicotinamide adenine dinucleotide phosphate (NADPH) and molecular oxygen to ultimately transfer a single oxygen atom onto the drug substrate. In the human genome, 57 genes encode 18 mammalian CYP450 families (Nebert et al., 2013) which are categorized according to their protein sequence homology. Most of the drug metabolising CYP450s belong to the 3 families: CYP1, CYP2 and CYP3. The 8 major active CYP450 isoforms found in human hepatocytes have been described as CYP1A2, CYP2B6, CYP2C8, CYP2C9, CYP2C19, CYP2D6, CYP2E1, and CYP3A4 (Utkarsh et al., 2016). However, over half of all oral drugs are metabolised by the CYP2D6 and CYP3A4 isoforms in humans (Li et al., 1995). Two or more enzymes can catalyse the same type of oxidation, indicating a redundant and broad substrate specificity. In humans, genetic polymorphisms and diet account for major variations in CYP450 activity between individuals. Many single-nucleotide polymorphisms (SNPs) can be found in the gene encoding CYP2D6. Patients with the ultra-metaboliser CYP2D6 phenotype metabolise codeine to morphine quickly, and if given the “recommended common dose”, these patients could suffer brain damage or it

could even be fatal (Eichelbaum and Evert, 1996). Dietary and environmental factors can influence CYP450 activity by inhibiting and inducing the enzymes. Grapefruit juice is well known to contain a CYP450 inhibitor and herbal medicine St John's wort induces CYP450 activity. These environmental factors can be detrimental if a patient is taking a drug metabolised by CYP450s.

Like phase 1 reactions, phase 2 anabolic conjugation reactions mainly take place in the liver, although some occur in the lungs and kidneys. Phase 2 reactions include glucuronidation, sulphation, acetylation, methylation, conjugation with amino acids and with the tripeptide glutathione (GSH). Conjugation usually results in a larger, inactive, more polar compound that is easier to excrete (Rang et al., 2016). The majority of the phase 2 conjugation reactions require enzymes, and isoforms exist for these too, much like the CYP450s. For example, glucuronidation involves the enzyme uridine 5'-diphospho-glucuronosyl transferase (UGT), which transfers the glucuronosyl group of uridine 5'-diphosphoglucuronic acid (UDP-glucuronic acid) to target drug molecules, can be divided into 4 families in mammals: UGT1, UGT2, UGT3 and UGT8 (Mackenzie et al., 2005). Sulphotransferases (SULTs) catalyze sulphation conjugation, they add a sulpho group from 3'-phosphoadenosine-5'-phosphosulfate (PAPS) to the target drug molecule. There are 13 known SULTs in humans that are divided into 4 families: SULT1, SULT2, SULT4 and SULT6 (Lindsay et al., 2008).

1.4.1.3 Drug-induced Liver Injury (DILI)

Drug-related liver injury (DILI), also known as drug-induced hepatotoxicity, is associated with impaired liver function and it is a common reason for drug candidate attrition in the late stages of drug development. It is also a leading cause of acute liver failure and the subsequent patient need for organ transplant. Consequently DILI is a big problem for the pharmaceutical industry as it can waste a lot of time and money invested in a drug candidate. It is also considered a major public health problem. DILI can manifest as different clinical pathologies (**Table 1-1**). The drug-induced liver pathological phenotype that occurs in a minority of patients is specific to the drug; that is to say that each hepatotoxic drug will usually present as a certain type of liver injury, if a liver-specific ADR was to occur. DILI can be resolved following discontinuation of the culprit drug or it can continue even after withdrawal, this can result in death. Fatality from DILI is not unusual. Nearly all patients will develop DILI if the dose of the hepatotoxic drug is high enough; this is predictable and dose-dependent DILI (Dragovic et al., 2016). The problematic type of DILI is idiosyncratic DILI which is much more unpredictable and manifests according to each individual's physiology, for example their immune response to the drug and genetic variants in isoenzymes (such as the previously mentioned CYP450s) which influences

their drug metabolism. The incidence of idiosyncratic DILI ranges from 1 in 1000 to 1 in 100000 patients that have been given the recommended therapeutic doses. These idiosyncratic ADRs are considered rare and can have a latency period ranging from 5 to 90 days (William M Lee, 2003). Therefore they are regularly not detected in the clinical phase of drug development. The rarity of idiosyncratic drug-induced hepatotoxicity makes it near impossible to detect in a relatively small cohort clinical trial size of approximately 3000 patients (Larrey, 2002; William M Lee, 2003). Over half of acute liver failure cases are drug-induced (Larrey, 2002) and more than 600 drugs have been associated with hepatotoxicity (Park et al., 2005a) which has led to numerous drug withdrawals from the market and black box labelling. For example, out of 51 drugs withdrawn from the market in the United States, European, or Asian markets between the years 1998 to 2008, the primary reason for withdrawal in 29 % was DILI (MacDonald and Robertson, 2009).

DILI is particularly difficult to predict and is often not identified until post-marketing surveillance, when the drug has been approved and used for several years by a much more diverse population of people with different treatment durations and possibly different dose range exposure than that experienced by the controlled clinical phase population the drug candidate was tested on before it was approved. The mechanism of hepatotoxicity related to drug treatment is often not completely understood and consequently it is hard to investigate during early stage drug development, especially because frequently, there is no relationship between the drug pharmacokinetic properties and the incidence of hepatotoxicity. Factors that affect drug metabolism also contribute to the occurrence of DILI, such as age, gender, body-mass index, pregnancy, renal disease and liver disease (Hunt et al., 1992).

Although the exact mechanism of DILI for each offending hepatotoxic drug is not always completely understood, a set of general mechanisms that contribute to DILI has been described (**Table 1-2**). The mechanisms described have been separated for clarity, but in reality a DILI reaction involves several mechanisms, which when combined, generate the liver injury and this leads to liver function impairment. Furthermore, there are additional mechanisms described in the literature, however not all the hypotheses have been completely proven. The mechanisms in **Table 1-2** focus on the role of the hepatocyte in DILI; other cell types are involved as well. The Kupffer cells are resident liver macrophages that can be activated to stimulate the release of cytokines and therefore exacerbate DILI, possibly helping to push past the liver immune tolerance to an immune response (Godoy et al., 2013; Jonsson et al., 2000). This cytokine response, secondary to the primary antibody-mediated or cytolytic response drug-protein adducts, can also activate neutrophil-mediated hepatotoxicity. Neutrophils can adhere to and release proteases into hepatocytes, causing cell necrosis (Jaeschke et al., 2002). The cells that

store fat are known as the stellate cells. The stellate cells are also involved in DILI reactions, they can produce fibrosis or form granulomas (William M Lee, 2003).

Table 1-1: Clinical presentation of DILI

Clinical Title	Observed Characteristics
Fatty Liver with lactic acidosis	Microvesicular steatosis, systemic mitochondrial dysfunction
Nonalcoholic Fatty Liver	Microvesicular or macrovesicular steatosis with or without ballooning and steatohepatitis
Acute Hepatic Necrosis	Collapse and necrosis of liver parenchyma
Acute Liver Failure	Collapse and necrosis of liver parenchyma with INR (international normalized ratio) >1.5 and encephalopathy
Acute Viral Hepatitis-like Liver Injury	Early onset symptom of DILI, fatigue, lack of energy
Autoimmune-like Hepatitis	Detectable autoantibodies and/or autoimmune features on liver biopsy specimen
Cholestasis without Inflammation	Severe itchiness with hyperbilirubinemia
Cholestatic Hepatitis	Elevated serum levels of ALP and total bilirubin
Immune-mediated hepatitis	Skin rash
Bile duct damage	Insufficient quantity of interlobular bile ducts with cholestasis
Sinusoidal disorders	Obliteration of central veins
Fibrosis and cirrhosis	Variable degrees of collagenization
Nodular regeneration	Formation of microscopic or macroscopic liver nodules

Adapted from Navarro & Senior (2006) and Tujios & Fontana (2011)

Immune-mediated DILI is associated with genetic variance. Patients that have a particular human leucocyte antigen (HLA) haplotype encoding their major histocompatibility complex (MHC), can have a higher chance of developing DILI than patients that don't have that haplotype. For example, flucloxacillin and amoxicillin-clavulanate -induced liver injury are associated with HLA-B*57:01 and the SNP HLA-DRB1*1501-DQB1*0602 respectively (Lucena et al., 2011; Monshi et al., 2013). Genetics can also contribute to the generation of chemically reactive metabolites (CRMs). Specific polymorphisms in the enzymes involved in phase 1 and phase 2 drug metabolism have potential to (1) increase the amount of CRMs produced to above average relative to the general population (2) reduce the efflux of CRMs from hepatocytes or (3) alter the metabolic pathway for a drug (Godoy et al., 2013). In addition, it is important to remember that although **Table 1-2** describes the mechanisms of DILI in accordance with a drug, it is often the case that the drug metabolite (or CRM) not the parent drug is the small molecule responsible for the DILI reaction.

1.4.1.4 The role of chemically reactive metabolites (CRMs) in DILI

Through drug metabolism, a reactive metabolite can be generated. This reactive metabolite may be a temporary intermediate before the next drug metabolism reaction, however it can be enough to bind to intracellular proteins and provide a significant contribution to the generation of a DILI reaction. Although there are animal models that are good for testing the safety of stable metabolites, this is not true for reactive metabolites. The vast majority of DILI reactions detected, associated with drug metabolites that are detected once the drug is available for patient use, are due to reactive (not stable) metabolites (Stepan et al., 2011). This is due, in part, to the lack of understanding the mechanisms of CRM-mediated DILI. In general, a CRM can irreversibly and covalently bind to endogenous proteins in the human body. This can disrupt cellular pathways and generate an ADR phenotype. The total amount of dose that covalently binds is known as the "body burden" (Thompson et al., 2016). But covalent binding alone does not always result in an ADR, it can be regarded as a drug bioactivation marker, not necessarily a direct indication of toxicity (Park et al., 2011). It is because most drug biotransformation occurs in the liver, that the generation of reactive metabolites is often associated with a hepatotoxic ADR. The production of CRMs from a parent drug does not necessarily indicate an ADR will definitely occur. The human body can neutralise the CRM, for example with phase 2 metabolism conjugation to GSH. To assess the ADR generation potential for an individual CRM, the following factors need to be considered: (1) parent drug exposure in metabolic tissues, (2) the rate of parent drug conversion to a metabolite, (3) the accumulation of the metabolite, (4) the cell's ability to neutralise the CRM and (5) the physicochemical properties of the metabolite. The CRM is usually

electrophilic as it is frequently the product of phase 1 oxidation from CYP450 enzymes. This electrophilic characteristic is exploited in drug development as a method of CRM detection. Radiolabeled or fluorescently tagged nucleophilic trapped agents, such as GSH, are identified using mass spectroscopy and can indicate the presence of CRMs generated from a parent drug candidate (Park et al., 2011; Prakash et al., 2008). Electron spin resonance spectroscopy can also be used to detect CRMs using a spin trapping agent, for example N-tert-butyl- α -phenylnitron (Albano and Tomasi, 1987). The enzyme that is responsible for generating a CRM could also become inactive as a result of this interaction with the CRM. This time dependent inactivation of a drug metabolising enzyme is another method of CRM detection (Hollenberg et al., 2008).

It has been speculated that a drug candidate with a high lipophilicity is more likely to form a CRM because a high fraction of it has to be eliminated by drug-metabolising enzymes (Thompson et al., 2016). An octanol-water partition coefficient (also known as logP) greater than 3 indicates the drug candidate has a high potential for causing DILI (Chen et al., 2013). Chen and colleagues state that when combined with a high dosage, that is ≥ 100 mg/day, a $\log P \geq 3$ drug candidate is very likely to cause a hepatotoxic ADR. This combination is known as a "rule of two". Although a structure cannot predict the type, severity or incidence of an ADR, there are certain structures of drug candidates that are known to be more likely to generate CRMs and subsequently increase the risk of a DILI reaction developing; so-called "structural alerts". These are established based on evidence of previously marketed drugs known to cause DILI reactions. Drug candidates are evaluated using *in silico* techniques to identify offending structural moieties (Hsiao et al., 2012; Liew et al., 2012).

For all these methods of CRM generation detection, the most common *in vitro* protocols include the incubation of the drug candidate with liver microsomes, cytosolic fractions or S9 subcellular fractions (Thompson et al., 2016). Despite all the methods mentioned above the exact mechanisms of CRM-mediated DILI reactions remain elusive. Regulatory guidelines do not exist for the detection of drug bioactivation and the assessment of drug safety associated with the metabolic process (Park et al., 2011). It is difficult to make models that will detect CRM-mediated DILI potential for several reasons. The most obvious reason is that CRMs are reactive and therefore short-lived, most do not enter the circulatory system so the human body is only exposed to them for a short period of time and this makes CRMs difficult to detect, identify and quantify (Guengerich, 2005). CRM-mediated DILI reactions also tend to be part of the idiosyncratic and rare type of ADRs, thus even detecting the phenotype in drug development is challenging (Stachulski et al., 2013). Immune cells contain some drug-metabolising enzymes and so are also capable of generating CRMs. A CRM that is covalently bound to an endogenous protein to form an

antigenic determinant, can activate drug-specific T-cells and bring about an immune-mediated ADR (Lavergne et al., 2008). There are 3 major mechanistic pathways for immune-mediated ADRs: (1) the hapten or pro-hapten hypothesis, (2) the pharmacological interaction concept and (3) the altered self-peptide repertoire hypothesis. Briefly, the hapten/pro-hapten hypothesis states that parent drug- or drug metabolite-protein adducts are displayed as antigenic determinants on the MHC molecule by antigen presenting cells and trigger T-cells and a subsequent immune-mediated ADR (Brander et al., 1995). Drugs are too small to initiate an immune response, but by covalently binding to a protein the combination is large enough to be antigenic and can stimulate an immune response. A hapten compound is protein reactive whereas a pro-hapten compound requires drug metabolism to become a reactive molecule. In the pharmacological interaction concept, the parent drug or CRM binds non-covalently and reversibly to a peptide-MHC complex and a T-cell receptor to stimulate a T-cell response (Pichler et al., 2011). The third hypothesis was demonstrated using abacavir as the culprit drug. Abacavir binds to HLA-B*57:01, changing the structure of the peptide groove and consequently altering the self-peptide repertoire for that MHC molecule. Different peptides can now bind to this abacavir-bound MHC molecule and activate a pathogenic-like T-cell-mediated immune response known as abacavir hypersensitivity syndrome (Illing et al., 2012; Norcross et al., 2012; Ostrov et al., 2012). This syndrome is associated with a rash. In general, the skin is more susceptible to pathogenic T-cells reactions than other organs and indeed, most ADRs seen in hospitalised patients are associated with an ADR skin phenotype (Hunziker et al., 1997). This susceptibility is thought to be because the skin has a large surface area, a dense network of dendritic cells and a large network of blood vessels (Clark et al., 2006).

Table 1-2: Mechanisms of DILI and associated examples

Mechanism of DILI	Type of Reaction	Examples of Drugs
<p>1. Cell Swelling, Cell Rupture and Cell Lysis</p> <p>High energy drug reactions with CYP450 can cause the drug to covalently bind to an intracellular protein. This can lead to intracellular dysfunction and subsequent actin disruption, loss of ionic gradients, change in calcium homeostasis and a decrease in the amount of ATP. All of these factors contribute to hepatocyte swelling, rupture and lysis, this manifests as liver injury, which can affect liver function.</p>	<p>Hepatocellular Mixed Hepatocellular and Cholestatic</p>	<p>Isoniazid Trazodone Diclofenac Nefazodone Venlafaxine Lovastatin</p>
<p>2. Bile Transport Inhibition</p> <p>Drugs can bind to the transport proteins at the canalicular membrane or the surrounding actin. This can inhibit bile export or interrupt bile flow.</p>	<p>Cholestasis Mixed Hepatocellular and Cholestatic</p>	<p>Chlorpromazine Estrogen Erythromycin</p>
<p>3. Immune stimulation</p> <p>A drug is too small to initiate an immune response, but it can covalently bind to a protein and form a drug-protein adduct. This larger product can travel to the hepatocyte surface and be recognised by the immune system; it is considered an antigen. This antigen can elicit an antibody-mediated cytotoxic immune response via the adaptive immune system, or a direct T-cell-mediated cytolytic reaction via the innate immune system. Both reactions can activate further cytokine activity and subsequent inflammation in the liver. However, as with other organs, the liver can tolerate and suppress an immune response. Liver injury only occurs if the</p>	<p>Immunoallergic Granulomatous Autoimmune Fibrosis</p>	<p>Halothane Phenytoin Sulfamethoxazole Methyldopa Methotrexate Flucloxacillin Ximelagatran</p>

natural tolerance is overcome.		
<p>4. Programmed Cell Death</p> <p>A drug can activate the caspase cascade via tumour necrosis factor α (TNFα) or Fas resulting in apoptosis: cell shrinkage and nuclear chromatin fragmentation.</p>	Apoptosis and/or necrosis are involved in almost all types of drug-induced adverse reactions	Many drugs including paracetamol and ethanol
<p>5. Mitochondrial Dysfunction</p> <p>If a drug inhibits β-oxidation, binds to a respiratory-chain enzyme or the mitochondrial DNA, this can cause oxidative stress. Subsequently, anaerobic metabolism, lactic acidosis and triglyceride and reactive oxygen species accumulation can occur. The lack of fatty acid oxidation and associated triglyceride accumulation in the liver leads to microvesicular steatosis; tiny lipid vesicles in the cytoplasm of hepatocytes (Jaeschke et al., 2002).</p>	Microvesicular fat Steatohepatitis	Valproic acid Nucleoside reverse transcriptase inhibitors Tetracycline Aspirin Troglitazone Amiodarone

Adapted from Lee (2003), Kaplowitz (2005), Tujios & Fontana (2011) and Godoy *et al* (2013)

1.4.1.5 Current *in vitro* models for Drug-induced Liver Injury

At present, there is not a single *in vitro* test that alone, can assess all the potential mechanisms of DILI in a drug candidate. In preclinical drug development, a combination of *in vitro* assays are used and the results are combined to evaluate the overall potential risk of DILI for a drug candidate. However, even once the risk has been calculated, it is difficult to determine the scale of the risk – will the DILI reaction be fatal or is it the case that all drugs have some potential to cause DILI but in reality, the human body can control this and there will never be any symptomatic patients. The complexity and tolerance ability of the human body cannot be captured in relatively simpler *in vitro* assays that may only consist of 3 different cell types. Drug candidate DILI assessment could be accurate at predicting DILI reactions in humans, but the reaction could be a low level reaction that patients can tolerate, much like most drugs have side effects. In either case, a promising drug candidate with good therapeutic predictions could be unnecessarily removed from drug development. So, it is important to develop assays that can mimic the mechanisms

of human DILI as closely as possible, but it is more important to understand the limitations of these studies and interpret the results correctly.

The advantages and disadvantages of some of the common *in vitro* cell models used to help predict DILI are summarised in **Table 1-3**. Traditionally, immortalized hepatic cell lines HepG2, Huh7 and HepaRG have been used for *in vitro* hepatotoxicity prediction assays because they are easy to use and share similarities with hepatocytes (Funk and Roth, 2017). Both the HepG2 and the Huh7 cell lines are derived from well-differentiated hepatocellular carcinomas, from 2 different patients. The HepaRG cell line is derived from a patient with a liver carcinoma and hepatitis C infection. The HepaRG cell line is considered a “step-up” from the HepG2 and Huh7 cell lines because unlike those cell lines, the HepaRG appears to be more sensitive to known DILI compounds and exhibits a change in oxidative stress, mitochondrial damage, and disorders of neutral lipid metabolism in the presence of them (Wu et al., 2016). However overall, the cell lines do not mimic the human drug-metabolizing enzyme system as well as primary human hepatocytes, and this is an important characteristic as some DILI reactions are dependent on the generation of CRMs, as previously described.

For the preclinical hepatotoxicity studies, primary cultured human hepatocytes are considered the “gold standard” (Gomez-Lechon et al., 2010; LeCluyse, 2001). They are much closer physiologically to *in vivo* human hepatocytes and preserve good drug metabolism mechanisms. However, they are unstable, they rapidly de-differentiate, the quality is dependent on the donor and the quantity can be irregular if you do not have a reliable surgical source that can supply liver tissue routinely. The instability of the primary human hepatocytes is reflected in the quick deterioration of drug-metabolizing enzyme activity (e.g. CYP450s) and transporter function (e.g. ATP-binding cassette (ABC) transporters) (Funk and Roth, 2017; Rowe et al., 2013). The phase 1 metabolism enzyme rate of activity declines quicker than the phase 2 enzyme rate in what is known as the phase 1 to phase 2 “shift” (Richert et al., 2016). Primary human hepatocytes can be cultured between two layers of gelled collagen; this is known as the sandwich model. The sandwich-cultured hepatocyte model has been proven to be particularly useful in the assessment of the ability of the drug candidate to inhibit bile acid transport (Kostrubsky et al., 2003). The uncertainty of when researchers will be able to obtain fresh primary human hepatocytes has led to the optimisation of cryopreservation. However, cryopreserved hepatocytes have a reduced cell attachment ability and transporter expression and are therefore not always suitable for the sandwich model (Swift et al., 2010). Primary human hepatocytes can also be cultured in 3D models either by use of scaffolds, hollow-fiber bioreactors, or spheroids. Overall, the 3D models tend to be even more liver-like than 2D monolayer cell culture with regards to the gene expression, phenotype and cell surface

receptor expression (Godoy et al., 2013). In the 3D models that use scaffolds, the hepatocytes can grow around the scaffolds that provide an artificial extra-cellular matrix (ECM). The scaffolding can be made from synthetic or natural materials. The majority of scaffolds are inexpensive; the exception is 3D printed scaffolds. Spheroids can be generated using hydrogels, through self-assembly in non-adhesive wells (Friedrich et al., 2009), with the help of a bioreactor (Chang and Hughes-Fulford, 2008) or via the hanging drop method (Kelm et al., 2003). Cell lines, as well as primary human hepatocytes, can be used to generate spheroids. Primary human hepatocyte spheroids are popular because it is thought they closely resemble the complex structure of the human liver, they can retain human liver proteomes, retain morphological and molecular phenotypes and maintain a good level of liver function (Bell et al., 2016; Messner et al., 2013).

Hepatocytes and non-parenchymal cells can be co-cultured to recapitulate the interaction of the cells of the human liver. Co-culturing can be performed in the sandwich and the 3D models. The non-parenchymal cells have included sinusoidal endothelial cells, Kupffer cells and stellate cells.

Finally, microfluidic *in vitro* systems appear to be an option that can combine the advantages of all the other *in vitro* models whilst providing solutions to the problematic disadvantages. Co-culture of human liver cells onto bio-compatible plastic material is combined with the addition of structures such as small channels, which can be perfused to, for example, remove the build up chemically reactive metabolites, or add oxygen to the cells (Novik et al., 2010). There is already a semi-automated 3D culture microfluidic system called the HepaChip®. The HepaChip® is still being optimised, but it is known to have good phase 1 and phase 2 enzyme activity compared to standard co-cultures and it could be useful as a holistic model to investigate specific mechanisms of DILI reactions as the ECM, co-culture cell ratio and metabolic activity can be easily changed to mimic particular DILI mechanisms (Godoy et al., 2013).

All of the *in vitro* models described have limitations, outlined in **Table 1-3**, but they can all be useful by picking an appropriate model to assess each DILI mechanism (**Table 1-4**) so long as the limitations of the model are taken into account when analysing the results.

Table 1-3: Advantages and Disadvantages of *in vitro* models for DILI

Cell model	Advantages	Disadvantages	Reference
HepG2 Huh7	<ul style="list-style-type: none"> • Technically easy to use • Stable phenotype • Experimentally reproducible • Genetic manipulation 	<ul style="list-style-type: none"> • No communication between different cell types • Low or partial expression of drug metabolising enzymes, hepatic transcription factors and nuclear receptors 	(Funk and Roth, 2017; Godoy et al., 2013)
HepaRG	<ul style="list-style-type: none"> • Same cell-line advantages as HepG2 and Huh7 • More stable, sensitive and superior predictability of known DILI compounds than HepG2 and Huh7 • Higher levels of drug-metabolising enzymes than HepG2 and Huh7 	<ul style="list-style-type: none"> • Low CYP450 expression (except CYP3A4) comparable to primary human hepatocytes 	(Lübberstedt et al., 2011; Wu et al., 2016)
Primary human hepatocytes: monolayer	<ul style="list-style-type: none"> • Retain the entire hepatic drug-metabolizing enzyme equipment (phase I and phase II) in an integrated, functional and inducible form 	<ul style="list-style-type: none"> • Unstable - can only be used for 1-2 day experiments • Not always readily available • High variation between batches • Require expert skill to isolate and 	(Gomez-Lechon et al., 2003)

		maintain	
Primary human hepatocyte: sandwich culture	<ul style="list-style-type: none"> • Formed and functional bile canalicular networks • Polarized excretory function 	<ul style="list-style-type: none"> • Cryopreserved hepatocytes are less suitable than fresh hepatocytes • Degradable • Inconsistent 	(Swift et al., 2010)
3D culture: hydrogel	<ul style="list-style-type: none"> • Longer hepatocyte function observed than that with sandwich culture 	<ul style="list-style-type: none"> • Degradable • Central cells show signs of necrosis 	(Moghe et al., 1997; Prestwich et al., 2007)
3D culture: scaffold based	<ul style="list-style-type: none"> • Overall inexpensive • Good porosity 	<ul style="list-style-type: none"> • Drug can bind to scaffold • Low throughput 	(Godoy et al., 2013)
3D culture: spheroids	<ul style="list-style-type: none"> • Stable long-term culture of primary human hepatocytes • Functional bile ducts • Good cell-cell and cell-ECM interaction • Polarized cells 	<ul style="list-style-type: none"> • Difficult to organize co-cultures 	(Bell et al., 2016)
Co-cultures	<ul style="list-style-type: none"> • Hepatocyte cell-non-parenchymal cell communication 	<ul style="list-style-type: none"> • Not high-throughput, labour intensive 	(Godoy et al., 2013)
Microphysiological systems: Liver-on-a-chip	<ul style="list-style-type: none"> • Physiological relevance - perfusion • Long-term 	<ul style="list-style-type: none"> • Limited widespread use as requires sophisticated equipment 	(Godoy et al., 2013)

Table 1-4: Major DILI mechanisms and corresponding useful *in vitro* models

DILI reaction mechanism	<i>In vitro</i> assessment model	Reference
Drug metabolism: 1. Lipophilicity 2. The generation of CRMs	<ul style="list-style-type: none"> • logP\geq3 and a dose\geq100 mg/day is indicative of a high risk factor for DILI • Cell-free glutathione (GSH)-trapping assays • Covalent binding using a radiolabeled drug • Cytotoxicity assays using cell lines that overexpress the major CYP450s 	(Brink et al., 2017; Chen et al., 2013; Thompson et al., 2016)
Interference with transporters, for example: <ul style="list-style-type: none"> - Bile Salt Export Pump (BSEP) - Multidrug resistance-associated protein 2 (MRP2) 	<ul style="list-style-type: none"> • Inverted membrane vesicles recombinantly expressing the respective transporter to measure transporter vesicles 	(Funk et al., 2001; Funk and Roth, 2017)
Intrahepatic cholestasis	<ul style="list-style-type: none"> • Sandwich model using primary human hepatocytes to measure the increase of bile acids and its effect on cytotoxicity and mitochondrial damage 	(Köck et al., 2014)
Mitochondrial dysfunction	<ul style="list-style-type: none"> • Use isolated mitochondria • Measure cytotoxicity on primary human hepatocytes or cell lines grown under specific conditions e.g. replace the glucose with galactose in the media for hepG2 cells and they are more susceptible to drug-induced mitochondrial dysfunction 	(Marroquin et al., 2007)

Combination of all mechanisms	<ul style="list-style-type: none"> • Primary human hepatocyte suspension and cell lines: <ul style="list-style-type: none"> - General cytotoxicity - measure lactate dehydrogenase (LDH) leakage, a change in ATP levels, the Resazurin assay - Other cytotoxicity – measure the level reactive oxygen species, free GSH decline and caspase activation 	(Richert et al., 2016; Zhang et al., 2016)
--------------------------------------	---	--

Adapted from the text of (Funk and Roth, 2017)

Pharmaceutical companies have turned to optimising *in vitro* methods to predict and characterise DILI mechanisms because often, a hepatotoxic reaction is first detected in the clinical phase or the phase 4 post-marketing surveillance, of drug development in humans. Therefore the hepatotoxic reaction associated with the drug candidate was not significant, or just did not occur, in the animal models. For the liver especially, the current animal models have poor correlation with human toxicity reactions. In approximately 45 % of human DILI cases, the rodent and non-rodent species did not detect DILI in the regulatory toxicology studies performed in drug development (Olson et al., 2000). Nonetheless, as previously described in this chapter, the drug regulatory authorities require a drug candidate to be tested in non-rodent and rodent species before it is assessed for human clinical trials.

1.4.1.6 Current *in vivo* and *ex vivo* models for Drug-induced Liver Injury

An ideal animal model would undertake the same mechanism as humans towards the mechanism of DILI and the potential impairment of liver function that could follow (Shenton et al., 2004). However, as previously discussed in this chapter, the exact mechanisms that result in an idiosyncratic DILI reaction are largely unknown. A good animal model can be determined by using it to assess drugs that are known to be associated with DILI reactions and liver function impairment. The animal model should be able to distinguish between these hepatotoxins and drugs that have not been associated with any DILI reactions. As with the *in vitro* assays, the *in vivo* models can be separated into the mechanisms of DILI.

For the immune stimulation mechanism, Halothane has been the popular model drug that is thought to act via stimulation of the adaptive immune system and consequently, it is the drug animal models are being developed against to detect this mechanism. An animal

model for this mechanism would require a drug candidate to sensitise their immune system, stimulate it upon re-challenge with the drug candidate, and overcome immune tolerance to overtly display an immune response that is manifested in the liver (Roth and Ganey, 2011). There are very few animal models for this mechanism; one example however, is the mouse model for flucloxacillin-induced cholestatic liver injury. Natrass and colleagues used a CD4⁺ deficient mouse model, with a MHC-II $\alpha\beta$ gene mutation to try to mimic sensitisation to the β -lactam antibiotic flucloxacillin (Natrass et al., 2015). Flucloxacillin is thought to initiate hepatotoxicity through the activation of CD8⁺ T-cells, particularly in patients with the HLA-B*57:01 allele. This model found similarities to human flucloxacillin-induced liver injury such as elevated plasma DILI biomarkers and possible CD8⁺ T-cell-mediated hepatocyte apoptosis. However further investigation is needed to find an animal model that can be routinely used in drug development to represent the immune stimulation mechanism that leads to severe liver injury in humans.

The mitochondrial dysfunction DILI mechanism, has in part, been captured in the superoxide-deficient-2 (SOD-2) heterozygous deficient mouse model. The reduction of SOD-2 available in the mouse cells, results in a mouse that has reduced mitochondrial function and the mice are more sensitive to drug-induced mitochondrial damage, especially from drug candidates that intensify oxidative stress (Roth and Ganey, 2011). Unfortunately, the liver injury in this model appears to be modest compared to that observed in humans and the duration of drug-candidate treatment required to get the hepatotoxic reaction varies (Corsini et al., 2012). Other mitochondrial dysfunction animal models have been developed, but they are more specific to the known hepatotoxic drug. Examples include fialuridine in woodchucks (Tennant et al., 1998), panadiplon in rabbits (Ulrich et al., 1998) and valproic acid in juvenile visceral steatosis (jvs) heterozygous mice (Knapp et al., 2008).

As previously stated, drug metabolism is an important factor that can contribute to the generation of a DILI reaction. But there are differences in drug metabolism enzyme expression and activity between animals and humans, between animals themselves and interindividual variance within humans, which makes it difficult to develop an animal model that can detect DILI via CRM generation. An enzyme isotype that manifests as a reduced metabolism phenotype can result in an accumulation of the parent drug in the liver, to potentially toxic concentrations. On the other hand, a fast metaboliser enzyme isotype could generate a high concentration of reactive metabolites, which could lead to liver injury. To better translate these genetics factors from animal models into humans, transgenic mice have been developed that express human CYP450s. Chimeric mice with a humanized liver, generated via human hepatocyte transplantation, also have the potential to produce good translatable data. One popular *ex vivo* method to detect CRM-

mediated liver injury is the isolation of liver subcellular fractions such as microsomes. Microsomes are not usually found in healthy human cells, they are typically isolated from human or rat hepatocytes via ultra-centrifugation. The high rotation speed (100000 xg) produces pellets that contain fragments of the endoplasmic reticulum, known as microsomes, which have a high concentration of CYP450 enzymes. Liver microsomes taken from a rodent model dosed with a radiolabeled drug can be assessed for drug protein-adduct formation by isolating proteins. Alternatively, a radiolabeled drug candidate that covalently binds could be measured indirectly using non-invasive autoradiography (Takakusa et al., 2008). Covalently bound drug or drug metabolite to intracellular proteins is an indication the drug candidate has the potential to cause liver injury. Furthermore, drug metabolite binding to GSH is also a risk factor that predisposes individuals to hepatotoxicity. Drug metabolites and drug protein-adducts or drug lipid-adducts can now be detected without the need for radiolabeling using mass spectrometry techniques. The amount of covalent binding in drugs known to be associated with DILI due to the production of reactive metabolites, has been estimated using antibodies to the reactive metabolite protein adducts and subsequent western blot or immunohistochemistry experiments (Bourdi et al., 2001).

An animal model that only focuses on one DILI mechanism is often not enough to recapitulate the severity of liver injury that occurs in humans. Multiple determinants contribute to overcome liver tolerance including environmental factors such as inflammatory stress. A bacterial or viral infection in combination with a therapeutic dose can result in a DILI reaction. To mimic this in an animal model, the animal is co-treated with the culprit drug and lipopolysaccharide (LPS). LPS binds to the toll-like receptors (TLRs) on mammalian cells and initiates the expression and release of pro-inflammatory mediators, for example, cytokines, reactive oxygen species (ROS) and toxic proteases (Arbour et al., 2000). The LPS plus drug animal DILI model has successfully identified drugs known to be associated with DILI such as diclofenac, chlorpromazine, trovafloxacin and halothane, and perhaps more importantly, no severe or moderate DILI reaction was produced with drugs not associated with DILI. However, a positive result can sometimes depend on getting the timing between the administration of the drug and the LPS correct. It is different for every drug and between animal species, consequently, it is difficult to implement this animal model as a good throughput DILI detection model in drug development (Roth and Ganey, 2011).

Rodents are usually the first animal species used in drug development, however zebrafish have also had some interest as a model for the prediction of DILI. Zebrafish possess similar drug metabolising enzymes to humans, including CYP450s, and accordingly, they follow similar drug metabolism pathways. Once validated and the limitations have been

determined, a zebrafish DILI model could be useful to bridge the gap between preclinical *in vitro* assays and rodent models (Vliegenthart et al., 2014b).

1.4.1.7 Biomarkers: Drug-induced liver injury

It is widely acknowledged that the current tests used in pharmaceutical industries to predict DILI are poor (Dragovic et al., 2016). Consequently, there has been a great effort in research to find biomarkers that are more sensitive and specific to DILI. A biomarker is defined as a characteristic that can be measured as an indicator of normal biological and pathogenic processes as well as pharmacologic response to a therapeutic dose (Biomarkers Definitions Working Group, 2001). A good organ-specific protein or gene biomarker should be approximately >10-fold higher than the maximal values of that gene (or protein) expression in any other tissue (Qin et al., 2016). Biomarkers are important in the preclinical and clinical phases of drug development, and in the clinic to diagnose and monitor disease. Many biomarkers have been used to try to detect DILI, however the sensitivity and specificity varies. The ideal biomarker for DILI should be non-invasive, is useful for the preclinical and clinical phases of drug development, specific to liver injury and easily detectable and measured through a uncomplicated laboratory assay (Antoine et al., 2009). It would also be useful if the biomarker reflected the state of liver function, because as mentioned previously, liver injury does not necessarily lead to impaired liver function. Here, I shall discuss the major DILI biomarkers that have been used in the past 70-80 years.

1.4.1.7.1 Alanine aminotransferase (ALT), aspartate aminotransferase (AST), alkaline phosphatase (ALP) and total bilirubin (TBL)

The enzymes ALT, AST and ALP are all intracellular in a healthy patient. When there is liver disease or a DILI incident, these enzymes are elevated in the blood serum. Hepatocyte damage, presented as hepatocellular liver injury in the clinic, exhibits an elevation of the aminotransferases. Whereas the cholestatic liver injury phenotype, is reflected with a dominant ALP serum increase, followed by raised TBL levels. In the mixed hepatocellular and cholestatic liver injury phenotype, both ALT and ALP levels are significantly greater than the healthy norm (William M Lee, 2003). However a liver biopsy and histological analysis would be the only way to know for certain what type of liver injury has occurred. The R formula, when measured at the onset of DILI, can help identify the type of liver injury, $R = \text{ALT (upper limit of normal, ULN)} / \text{ALP (ULN)}$. $R \geq 5$ indicates a hepatocellular liver injury phenotype, $R \leq 2$ indicates a cholestatic liver injury and finally $2 < R < 5$ is a mixed phenotype (Aithal et al., 2011; Benichou, 1990). ALT is predominantly present in liver cells and at low concentrations elsewhere in the human body. In contrast, AST can be found in the red and white blood cells, skeletal muscle, the heart, lung, brain,

kidney and pancreatic tissue as well as the liver. It is for this reason, elevated serum ALT is more specific to liver injury than an AST increase (Giboney, 2005; Robles-Díaz et al., 2016). However overall, ALT, AST and ALP can all be affected by other factors, none of these enzymes are entirely specific to DILI reactions. For example, hyperthyroidism (Cooper et al., 1979) and bone disease (King, 1953) can cause an increase in serum ALP, and serum ALT and AST can be elevated after exercise (Fowler et al., 1962). Furthermore, another limitation of the liver enzymes as biomarkers are the short half lives. ALT and AST have short circulation half lives at 47 h and 17 h respectively. Hy's Law dictates that an AST or ALT > 3 xULN with TBL > 2xULN indicates a hepatocellular DILI reaction, which has a 10-50 % high risk of mortality without liver transplantation (Zimmerman, 1999, 1978). But there has been a great effort in research to find a biomarker that is more specific to DILI reactions. The following biomarkers are some of the proposed biomarkers.

1.4.1.7.2 Glutamate dehydrogenase (GLDH)

GLDH is a mitochondrial enzyme abundant in the liver. It is more specific to the liver than ALT and AST, however some GLDH can be found in the kidney and in skeletal muscle. An increase in circulatory GLDH is indicative of mitochondrial dysfunction, a loss of mitochondrial membrane integrity and subsequent hepatocellular necrosis (Robles-Díaz et al., 2016). However GLDH can also be influenced by other factors, for example, it has been reported that the GLDH circulatory levels increase with subcutaneous heparin injections (Harrill et al., 2012).

1.4.1.7.3 Cytochrome c

Cytochrome c shuttles electrons between complexes II and IV of the electron transport chain. It is a small heme protein located in the inner membrane of the mitochondria. It is not liver-specific, but it is a biomarker for mitochondrial dysfunction that leads to apoptosis (Hu et al., 1999; Miller et al., 2008). Pathological mitochondria membrane permeabilisation causes the release of cytochrome c into the cytosol where it activates caspase-mediated apoptosis. Eventually cytochrome c is transferred into the serum and it can also be detected in urine. Saturated GSH conjugation or the binding of a reactive metabolite to a mitochondrial protein can lead to cytochrome c release into the serum (Antoine et al., 2009).

1.4.1.7.4 High-mobility group box-1 (HMGB1)

HMGB-1 is a nuclear protein and inflammatory mediator. Increased levels of serum HMGB-1 correlate with drug-induced liver injury. Its proinflammatory activity and stimulation of immune activation is mediated through signalling the toll-like receptor (TLR)

and receptor for advanced glycation end-products (RAGE) signalling (Antoine et al., 2012; Kubes and Mehal, 2012). HMGB-1 can recruit macrophages to the site of liver injury via TLR4 and RAGE. HMGB1 in the hypoacetylated form is released into the plasma from damaged cells that have compromised mitochondria. If the culprit drug or drug metabolite impairs mitochondria, the cellular production of ATP is reduced, and the cell death is a necrotic phenotype (as opposed to apoptotic) (Scaffidi et al., 2002). The hyperacetylated form of HMGB-1 is released from active immune cells.

1.4.1.7.5 Keratin-18 (K18)

Keratin-18 is an intermediate filament, it contributes to cell structure and support and it is present in the epithelial cells of the liver, although it is not liver-specific (Cummings et al., 2006). K-18 accounts for approximately 5 % of total hepatic protein. It is a caspase target during apoptosis and is released into the blood from unhealthy cells in a fragmented form and a full-length form indicating apoptosis and necrosis respectively (Schutte et al., 2004).

1.4.1.7.6 MicroRNA-122 (miR-122)

Micro ribonucleic acids (miRNAs) are non-coding RNAs, approximately 22 nucleotides long, and they regulate messenger RNA (mRNA) usually through binding to the mRNA 3' untranslated region (UTR) (Bartel, 2004). MiRNAs are stable and involved in a wide variety of physiological and pathological processes in humans and other animal species. In healthy humans they can be found inside cells and extracellularly. MiRNAs can also be cell- and tissue-specific and their abnormal presence in extracellular body fluids can indicate cell damage has occurred. Inflammation and different types of cancer can be identified through the detection of specific miRNAs in body fluids such as breast milk, urine and cerebrospinal fluid, in amounts that are not usually found in a healthy human (Brase et al., 2010; Osaki et al., 2014; J. feng Wang et al., 2010). Consequently miRNAs are widely accepted as good biomarkers (Weber et al., 2010). MiR-122 expression is specific to and highly expressed in the liver; 70 % of total human liver miRNA is miR-122. It is more specific to the liver than ALT, and can be useful in early phase human trials, where hepatotoxic drug candidates can go undetected if ALT is the biomarker in use (Thulin et al., 2014). When miR-122 is detectable in the blood, it can be a sign of hepatotoxicity. Circulating miR-122 has been identified in the early stages of hepatocellular damage and at lower doses compared to ALT (Antoine et al., 2013; Wang et al., 2009). Often, biomarkers for DILI are not detectable until the later stages of liver injury, when the prognosis can be worse. Circulating miR-122 is significantly increased in patients with diagnosed acute liver injury associated with paracetamol administration compared to patients that are taking paracetamol but do not present with acute liver injury

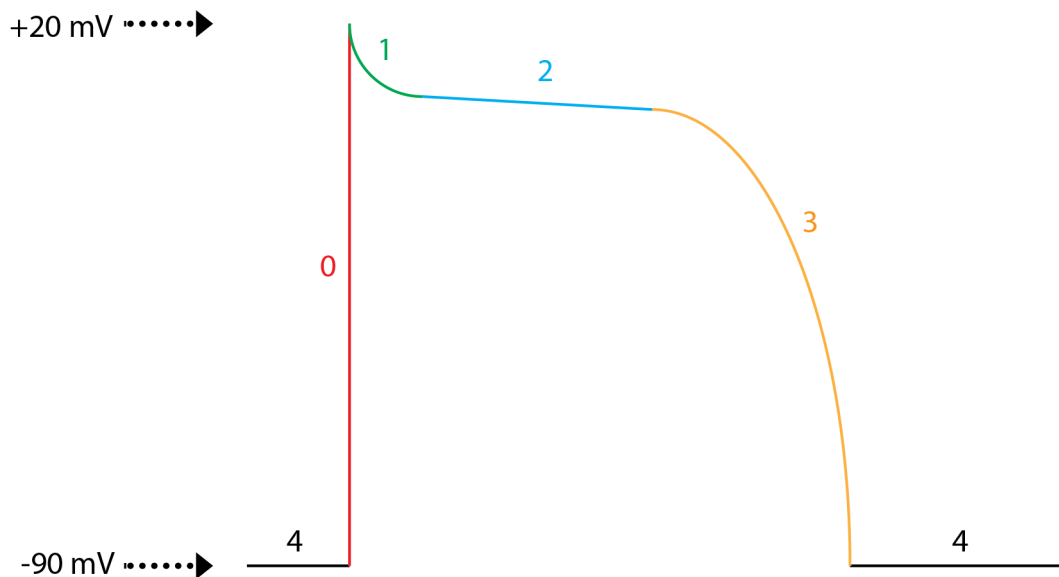
(Starkey Lewis et al., 2011). In other words, miR-122 has a good specificity for DILI identification.

1.4.2 Heart

1.4.2.1 Structure and Function

The human heart is a pyramid or cone-like shape, the apex extends to the left, anteriorly and inferiorly, towards the diaphragm and the base is opposite. The heart is in the mediastinum anatomical region of the human body, so between the sternum and the vertebral column, and from the first rib to the diaphragm. About two thirds of the mass of the heart is to the left of the midline. It about the size of a human fist: 12 cm long and 9 cm wide at it's widest point and 6 cm thick (Tortora and Derrickson, 2014). Cardiac muscle tissue is known as the myocardium, and it is the middle layer of the heart wall. The outer layer is called the epicardium and the inner layer is known as the endocardium. The myocardium layer contributes to 95 % of the heart wall and is responsible for the heart pumping movements, it is made up of cardiac muscle fibres. A cardiac muscle fibre contains 1 or 2 nuclei and is connected to a neighbouring fibre by an intercalated disc, which consists of desmosomes and gap junctions that are important for the propagation of action potentials and the coordination of atrial or ventricular contraction. In the human body, the heart consists of four chambers: two atria and two ventricles. The right side is separated from the left via the interatrial and interventricular septa. The ventricles have thicker walls than the atria and the left ventricle wall is thicker than the right. Blood is pumped into the atria of the heart first, through the atrioventricular valves, and then the ventricles pump blood out of the heart. The right atrioventricular valve is the tricuspid valve and the left is the bicuspid valve. The right atria and right ventricle receive deoxygenated blood from the body (from the inferior and superior vena cava) that is pumped to the lungs (via the pulmonary arteries), and the left atria and left ventricle pump oxygenated blood from the lungs (via the pulmonary veins) to the body (through the aorta). The pulmonary artery and aorta have semilunar valves, which prevent the flow of blood back into the heart ventricles. The atrioventricular and semilunar valves open and close according to the change in blood flow and the change in pressure exerted from atrial and ventricular contractions, in turn, contractions are controlled by the generation of action potentials. The autorhythmic cells of the sinoatrial node, located in the right atrial wall, repeatedly and spontaneously depolarise to overcome a threshold and trigger an action potential that causes the contraction of both atria. This action potential is conducted through the atrial muscle fibres to the atrioventricular node, located in the interatrial septum. During this conduction the atria have emptied their blood volume into the ventricles. From the atrioventricular node, the action potential enters the bundle of His,

then the right and left bundle branches towards the heart apex, and into the Purkinje fibres that extend up the walls of the ventricles. Ventricular contraction occurs. The action potential of a cardiomyocyte can be described in 5 phases (**Figure 1-2**). In a human, the baseline membrane potential is approximately -90 mV. In phase 0, the rapid entry of Na^+ through voltage-gated sodium channels depolarises the membrane potential to +20 mV. This Na^+ influx stimulates phase 1, where the transient potassium channels open to instigate rapid repolarisation via K^+ efflux. However the repolarisation plateaus as L-type Ca^{2+} channels and slow delayed rectifier K^+ channels open to allow Ca^{2+} influx and K^+ efflux respectively in phase 2. The plateau is overcome in phase 3 when additional K^+ rectifier channels open to increase the K^+ efflux and bring the membrane potential back to -90 mV, phase 4 (Li et al., 2016).



Phase number	Ion movement	Current and Channel	Name
Phase 0	Na ⁺ influx	Na	Rapid depolarisation
Phase 1	K ⁺ efflux	to	Rapid repolarisation: Transient outward
Phase 2	Ca ²⁺ influx K ⁺ efflux	L-type Ca Kr Ks	Plateau: Rapid delayed Slow delayed
Phase 3	K ⁺ efflux	Kr Ks K1	Repolarisation: Rapid delayed Slow delayed Inward rectifier
Phase 4	K ⁺ efflux	K1	Repolarisation: Inward rectifier

Figure 1-2: Action potential of a cardiac myocyte

Schematic of an action potential of a cardiac myocyte. In phase 0, sodium ions (Na⁺) enter the cell through voltage-gated Na channels for rapid depolarisation. Rapid repolarisation follows through the movement of potassium ions (K⁺) out of the cell in phase 1. In phase 2, calcium ions (Ca²⁺) entered the cell through L-type Ca channels which is counter-balanced by the efflux of K⁺ to result in a plateau. More K⁺ channels opened in phase 3 for further repolarisation until the membrane potential reaches the baseline of -90 mV in phase 4.

The movement of action potentials across the human heart produces an electrical current that can be detected, using an electrocardiograph, which generates an electrocardiogram (ECG) (**Figure 1-3**) The P wave is atrial depolarisation, the QRS complex is ventricular depolarisation and the T wave is ventricular repolarisation. The QT interval is defined as the start of the QRS complex until the end of the T wave. In a healthy human, the QT interval is approximately 350-440 ms and a QT interval >500 ms is indicative of an unhealthy individual (Li et al., 2016). A genetic predisposition can be the cause of a QT prolongation, or it can also be the result of a drug the patient is taking.

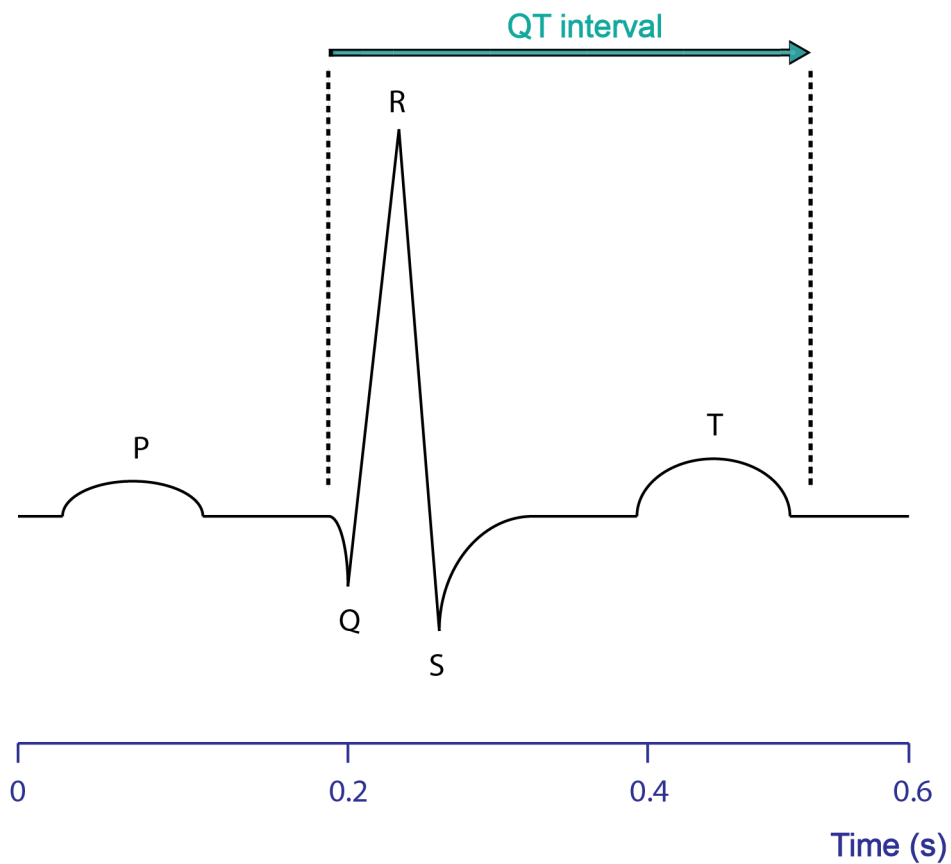


Figure 1-3: Electrocardiogram (ECG) trace

Schematic of the ECG trace for a human heart. The P wave is atrial depolarisation, the QRS complex is ventricular depolarisation and the T wave represents ventricular repolarisation. The QT interval is the time between the beginning of the QRS complex until the end of the T wave. Adapted from Rang *et al* (2016) and Li *et al* (2016).

1.4.2.2 Drug-induced cardiotoxicity

Drug-induced cardiotoxicity is a leading cause of drug attrition in drug development and the removal of drugs from the market after approval. Of the primary reasons for drug withdrawal in the US, Asia and European markets between 1998-2008, 33 % were due to cardiotoxicity (MacDonald and Robertson, 2009). This percentage includes drugs that were specifically marketed for antiarrhythmic therapeutic use as well as drugs that were developed for an entirely different therapeutic use, such as the antihistamine drug terfenadine. Cardiotoxicity can be split into 2 different types: (1) functional cardiac injury, where a change in the mechanical function of the myocardium is observed and (2) structural cardiac injury, a loss of cellular or subcellular parts of the heart or impaired heart or vasculature morphology, such as extracellular matrix remodelling. There are many different cardiotoxic effects including: myocardial dysfunction, ischaemia, hypotension, hypertension, QT interval prolongation, arrhythmias and thromboembolism. A drug that alters the contractility of the heart, can cause a reduced cardiac output that leads to toxicological peripheral tissue hypoperfusion; this is the ultimate functional cardiotoxic effect. These drug-induced cardiotoxicity effects can be observed immediately after drug administration or not until months or years after the start of drug therapy (Cross et al., 2015).

Delayed repolarisation, represented by QT prolongation on an ECG, is a surrogate marker for proarrhythmia for a drug candidate in drug development. Excluding anti-arrhythmics, over 100 drugs are known to cause QT prolongation (De Ponti et al., 2001). A large number of these drugs have a long history of safe use, consequently, QT prolongation does not always lead to drug-induced cardiotoxicity. The QT interval is the electrical systole of the ventricles in the heart. A prolonged QT interval equates to a prolonged action potential that will delay the ventricular repolarisation. In the majority of drug-induced QT prolongation, one cause is the inhibition of the rapidly activating delayed rectifier potassium ion current (I_{Kr}). The I_{Kr} current can be inhibited through blocking the voltage-dependent potassium channel. In this channel there is the protein known as $K_v11.1$, which is an alpha subunit of the channel encoded by the hERG (*human Ether-à-go-go-Related Gene*). The alternative, more official name for this gene, is KCNH2. This KCNH2 encoded alpha subunit is the major subunit for I_{Kr} and each subunit contains 6 α -helical transmembrane segments (Sanguinetti et al., 1995). Some drugs such as amiodarone and terfenadine inhibit not only the I_{Kr} current, but also the slow delayed rectifier current (I_{Ks}), which also contributes to delayed ventricular repolarisation (Kodama et al., 1997; Salata et al., 1995). The $K_v7.1$ voltage-gated potassium channel is the dominant channel type involved in the I_{Ks} current. The primary pore-forming alpha protein subunit of the channel is encoded by the KCNQ1 gene in humans (Jost et al., 2007). Like hERG, the

inhibition of this channel is associated with a long QT interval. Genetic mutations in the KCNQ1 gene are associated with long QT syndrome, hence the alternative name for the $K_{v7.1}$ channel is $K_{v}LQT1$ (Obiol-Pardo et al., 2011). Compounds that specifically block the $K_{v7.1}$ type potassium channel alone, have been identified in drug development such as the Hoechst/Aventis compound chromanol 293B and Merck-Sharpe&Dohme benzodiazepine derivatives L-735,821 and L-768,673 (Busch et al., 1996; Salata et al., 1996; Selnick et al., 1997). In addition to QT prolongation, these compounds are associated with T wave abnormalities and a longer action potential duration.

As mentioned previously, QT prolongation drug candidate potential must be measured in an *in vitro* assay during preclinical drug development, as outlined in the ICH S7B regulatory drug development guidance document. A drug candidate must be evaluated to determine if it is a potent hERG channel blocker, to the point where it is deemed sufficient to have the potential to cause arrhythmia. However not all drugs that inhibit the hERG channel cause QT prolongation. Verapamil is a potent hERG channel blocker, but is not associated with QT prolongation (Redfern et al., 2003; Zhang et al., 1999). There is evidence that drug-induced I_{Kr} inhibition is a risk factor for Torsade de pointes (TdP). TdP can be identified on an ECG as continuously changing QRS complexes that indicate extra ventricular beats as a result of early depolarisation initiated in the Purkinje fibres or midmyocardial cells (Dessertenne, 1966). TdP can lead to potentially life threatening ventricular tachycardia. Drugs associated with TdP in humans are often present in the blood plasma at a concentration that is similar to that which is needed to block the hERG channel (Redfern et al., 2003). In addition to hERG channel blocking, a drug candidate is also tested for its ability to inhibit of the I_{Ks} current or the $K_{v7.1}$ channel.

1.4.2.3 Current *in vitro* models for Drug-induced Cardiac Injury

As mentioned previously, ventricular repolarisation is governed not only by the opening of the hERG channel and associated K^+ efflux, but many other voltage-gated channels are also involved. Ventricular repolarisation occurs when the net outward current exceeds the net inward current in phase 3 of the action potential and the sodium and calcium voltage-gated channels contribute to this (Colatsky et al., 2016). Consequently, it makes sense to investigate drug candidate interaction with these channels in preclinical drug development, in addition to hERG blocking potential. This is the basis of the comprehensive *in vitro* proarrhythmia assay (CiPA) initiative. Once introduced, the ICH S7B document effectively removed the risk of approving drugs that cause TdP. However, a hERG channel blocker may not necessarily lead to QT prolongation, and QT prolongation does not always generate a TdP phenotype. Indeed, sometimes QT prolongation is not sufficient for TdP formation and an early after-depolarisation (EAD) is

required as well. Delayed repolarisation can stimulate a net inward current during the action potential plateau and cause an EAD. As a result, the low specificity of the hERG channel inhibition test has caused premature and inappropriate termination of good therapeutic drug candidates; it has generated false positives.

The CiPA method, consists of 3 elements: (1) *in vitro* evaluation of drug effect on multiple individual currents using human ion channels in a heterologous expression system, (2) integration of the information from (1) into *in silico* computational reconstruction of a human ventricular myocyte to assess proarrhythmic liability and (3) confirm any effects found, by investigating ionic currents identified using *in vitro* electrophysiological techniques in human stem cell-derived cardiomyocytes (hSC-CMs) (Cavero and Holzgrefe, 2014; Sager et al., 2014). For the first element, 7 ionic channel currents are assessed: the L-type Ca^{2+} , the depolarising late and fast Na^+ channel currents, these are the inward depolarising currents. The last 4 currents are outward repolarising currents and are made from K^+ channels they are: the slow delayed rectifier channel, the rapid delayed rectifier channel, transient K^+ channel and the inward rectifier channel (Colatsky et al., 2016; Sager et al., 2014). All of the ionic currents are assessed via automated patch clamp platforms expressed in the heterologous expression systems such as human embryonic kidney cells or Chinese hamster ovary cells. The disadvantage of this comprehensive ion channel screening tool is that the channel expressed in the heterologous systems can have different drug-binding kinetics and a different mode of channel inhibition to the wild-type channel, such is the case with the hERG channel expression (Di Veroli et al., 2014). However the use of hSC-CMs in the third element has many advantages. The hSC-CMs can detect drug candidate effects not observed in heterologous expression systems, for example, modulation of I_{Kr} via intracellular secondary messengers, oxidative stress and altered calcium handling (Clements, 2016; Mewe et al., 2010). hSC-CMs are stable in culture, therefore they can also be used to study the drug candidate long-term effects on hERG channel expression.

Prior to the CiPA initiative, Kramer *et al* (2013) investigated the use of models that measure the drug candidate multiple ion channel effects (MICE). They used 32 torsadogenic and 23 non-torsadogenic drugs to test which combination of ion channel assays can improve on the 70 % predictivity for cardiotoxicity associated with a positive hERG channel result alone. They discovered that the best MICE model involved testing the drug candidate blocking potency for a combination of hERG and the voltage-dependent calcium channel Cav1.2 (Kramer et al., 2013). The reason for this is that if a drug candidate blocks the hERG channel, the negative repercussions can be offset by simultaneous Cav1.2 blocking (Bril et al., 1996).

Manual patch clamp is considered the gold standard for hERG screening; it has a high predictive power and can measure the drug candidate effects on hERG channel function. However, it is too slow and costly to allow for the quick screening of a large amount of compounds in drug development, and requires a trained electrophysiologist (Murphy et al., 2006). One alternative method to detect drug candidate hERG channel inhibition is to investigate the ability of the drug candidate to compete with a known compound that binds to hERG channel. The rubidium efflux assay is one example of this method. In this assay, cells expressing the hERG channel (endogenous or otherwise) are loaded with rubidium ions (Rb^+), that can be the radioisotope, ^{86}Rb . The rubidium ions replace the potassium ions inside the cell. The cells are incubated with the drug candidate to be tested and subsequently a high concentration of potassium ions. The potassium ions depolarise the cells and open the hERG channel. Within minutes, the supernatant is collected and the content of rubidium ions is measured using atomic absorption spectroscopy or scintillation counting for ^{86}Rb . A low amount of rubidium ions in the supernatant is an indication the drug candidate has a high affinity to the hERG channel, and is a hERG channel inhibitor (Chaudhary et al., 2006; Cheng et al., 2002). In the [^3H]dofetilide assay, hERG channel inhibition is detected through the ability of the drug candidate to compete with the potent hERG channel antagonist, dofetilide (Redfern et al., 2003). A similar assay uses [^3H]astemizole, another potent hERG channel blocker, to measure drug candidate hERG channel potency (Chiu et al., 2004). Finally, fluorescent voltage-sensitive dyes offer another method to measure cardiotoxicity *in vitro*. A voltage-sensitive fluorescent dye, such as bis-(1,3-dibutylbarbituric acid)trimethine oxonol, can reflect the change in membrane potential for sodium and potassium ion voltage-gated channels (Tang et al., 2001). The alteration of this mechanism in the presence of a drug candidate can indicate its potential for hERG channel inhibition and the induction of a cardiotoxic reaction.

1.4.2.4 Current *in vivo* and *ex vivo* models for Drug-induced Cardiac Injury

Ex vivo female rabbit heart preparations are a popular model for drug candidate cardiotoxicity assessment. There are 2 major methods: the ventricular wedge preparation and the Langendorff Screenit model. Both models retain the structure and electrophysiology of the ventricle. The wedge preparation is maintained with an arterial perfusion, the left circumflex branch of the coronary artery whereas the Langendorff heart has a perfused aorta (Liu et al., 2006; Valentin et al., 2004). The Langendorff-perfused heart can be coupled to an automated computerized system that can measure the concentration-dependent electrophysiological effects of the drugs. This is the Screenit system. Both the rabbit ventricular wedge and Langendorff heart preparations are useful to define the mechanisms involved in proarrhythmia including QT prolongation, early after

depolarisation and transmural dispersion of repolarisation. In addition, the isolation of the heart is advantageous to study drug-induced cardiotoxicity because the drug is not exposed to hormonal and other physiological processes that are unique to the animal, not relevant to humans, and therefore could produce inaccurate cardiotoxicity assessment results. One disadvantage of these models is the need for a technical expert. Furthermore, these rabbit preparations have a different electrophysiology to humans, so it is hard to assess the proarrhythmic risk of a drug candidate using these assays (Gintant et al., 2016). Purkinje fibers isolated from dogs or pigs, can be used to assess the proarrhythmic potential of drug candidates. Gintant and colleagues demonstrated that drugs associated with QT prolongation and TdP in humans, cause a concentration-dependent prolongation of the action potential duration in isolated Purkinje fibers. Non-cardiotoxic drugs did not significantly alter the action potential duration (Gintant et al., 2001).

Zebrafish have a fully functional cardiovascular system at 48 hpf that consists of a 2 chambered heart (1 atrium and 1 ventricle, separated by an atrioventricular valve) which expresses the zebrafish equivalent of the hERG channel (zERG). The amino acid sequence produced from the human and zebrafish ether-a-go-go related genes are 99 % conserved (Langheinrich et al., 2003). Although the zebrafish does not have a pulmonary system, it is still considered a useful model to aid the assessment of a drug candidate cardiotoxic potential. The zebrafish embryos are transparent, a major advantage because the heart rate and rhythmicity can be visually determined in a live, whole mount embryo. De Luca and colleagues took advantage of the zebrafish transparency and generated a model system called Zebrabeat that can analyse variations in heart rate. In this model, a zebrafish double transgenic line was used that labelled endothelial and endocardial cells with green fluorescent protein (GFP) and red blood cells with red fluorescent protein (DsRED). The embryos were anaesthetised to remain stationary and the heart rate was recorded using a resonant laser-scanning confocal microscope coupled to a software called Zebrabeat that can recognise the GFP-labelled heart outline and the flow of fluorescent red, red blood cells. They were able to detect variation in heart contraction/relaxation and quantify red blood cell content in the heart chambers (De Luca et al., 2014). This model demonstrates the potential practicality of non-mammalian models in drug development.

One animal model limitation, is the difference in the physiological mechanisms of ventricular repolarisation between species (Gintant et al., 2016). In humans, dogs and rabbits, this is mediated by I_{Kr} . However guinea-pigs use I_{Kr} and I_{Ks} currents for ventricular repolarisation, and rats have minimal I_{Kr} , they rely on I_{to} .

1.4.2.5 Biomarkers: Drug-induced cardiotoxicity

Similar to biomarkers for DILI, there is room for improvement in biomarkers that have a high sensitivity and specificity for the prediction and detection of drug-induced cardiotoxicity. Many current biomarkers are not sufficient for early diagnosis and it has been suggested that a multiple biomarker strategy would be ideal (Osaki et al., 2014).

1.4.2.5.1 Cardiac myoglobin, creatine kinase-muscle/brain isoenzymes, and troponins

Cardiac troponin I is a protein specific to myocardial cells and as such, an altered concentration of troponin I in patient plasma indicates myocardial injury. It is a specific and sensitive biomarker that has a high diagnostic and prognostic value and considered the classic gold standard for the detection of myocardial injury (Adams et al., 1994; Cardinale et al., 2004; Osaki et al., 2014). Elevated plasma cardiac troponin I is associated with an increased risk of patients developing left ventricular dysfunction following a high dose of chemotherapy such as anthracyclines. Similarly, cardiac troponin T release into plasma, or into the media from cardiotoxic drug-treated cardiomyocytes, can also indicate cardiotoxicity, however it is not sufficient for the detection of late onset cardiotoxicity (Holmgren et al., 2015). But the cardiac troponins have a couple of disadvantages as biomarkers. One disadvantage is that they are rapidly cleared from the plasma after 24h and consequently they are not always reliable (Nishimura et al., 2015). Also, patients with chronic kidney disease but no cardiac symptoms have elevated plasma cardiac troponin (Ahmadi et al., 2014).

As well as cardiac troponins, cardiac myoglobin and creatine kinase-muscle/brain isoenzymes are routinely used for the assessment of myocardial injury and subsequently could be useful for the identification of drug-induced cardiotoxicity.

1.4.2.5.2 Heart-specific micro-RNAs

MiR-208 expression is specific to the heart and it was first demonstrated as a plasma biomarker of drug-induced cardiac injury in rats treated with isoproterenol (Ji et al., 2009). Many cardiovascular diseases are associated with specific miRNA plasma expression for example, plasma elevated miR-2 is associated with a reduced heart rate, widened QRS interval and a clinical presentation of a shortened PR interval (De Rosa et al., 2014). MiR-1, miR-133a, miR-208a and miR-499 are all elevated in plasma after acute myocardial infarction in rats (G.-K. Wang et al., 2010). Furthermore, rats treated with the cardiotoxic compounds isoproterenol and allylamine generated a significant elevation of plasma miR-208-3p (Glineur et al., 2016). Overall, miR-208 appears to be the most promising and heart-specific miRNA biomarker for drug-induced cardiotoxicity (Nishimura et al., 2015). In humans, it is specifically the miR-208a-3p, which is often shortened to miR-208.

1.4.2.5.3 Drug candidate interaction with hERG channel and subsequent association with QT interval prolongation

As previously mentioned, drug hERG channel activity is associated with TdP and QT prolongation. Inhibition of the hERG channel correlates with an increased risk of TdP, QT prolongation and subsequently, an increased risk of arrhythmia. Drugs that bind to the hERG (K_v11.1) channel slowly or drugs that dissociate from the channel faster, are less cardiotoxic compared to drugs that bind to the channel faster (Yu et al., 2015). The interaction of a compound with the hERG channel can be evaluated with hERG channel expressing cells mathematical modelling. A 30-fold difference between the drug candidate hERG IC₅₀ and the maximum plasma concentration (C_{max}) is regarded as the minimum margin required for safety when testing the cardiotoxicity of a drug (Redfern et al., 2003). The difference between these 2 measurements can be used to predict TdP incidence and arrhythmogenesis. However, there is a 30 % discordance between a positive hERG channel inhibition result and TdP generation (Kramer et al., 2013). Exceptions to this drug safety guideline include drugs that are associated with TdP despite a large difference between the hERG IC₅₀ and C_{max} including amiodarone (1400-fold) and nifedipine (35700-fold). Furthermore, verapamil has only a 2-fold difference but is not associated with QT prolongation or TdP (Redfern et al., 2003).

1.5 An ideal preclinical animal model for the prediction of drug-induced toxicity

In order to be able to evaluate a new animal model, it would be useful to determine what the ultimate ideal animal model for the prediction of drug-induced toxicity would be. First and foremost, a good study design is necessary when working with animal models in drug development. It is good practice ethically, so that each animal tested contributes reliable and useful data, but also scientifically, the experiments conducted should be designed to have clear endpoints and good statistical power. A clear endpoint will help determine if the animal has indicated a drug-induced toxicity reaction or not. An ideal safety animal model would have a similar clinical and anatomic pathology to humans. The drug metabolism and pharmacokinetics (DMPK) should also be similar because this can have a big impact on whether a drug-induced toxicity reaction will be generated, and determines the validity of the animal model for the evaluation of drug safety in humans (Redfern et al., 2002). The animal model should be able to distinguish between drugs associated with human toxicity and those not. Furthermore, any drug-toxicity reactions generated in the animal would ideally have been generated via the same mechanisms as in humans (Roth and Ganey, 2011). The development of a reaction should have a similar time of onset in the animals compared to what happens in humans. In addition, an excellent animal model

would demonstrate similar risk factors to humans that contribute to the generation of a drug-induced toxicity reaction.

1.5.1 Where is the gap?

Traditionally, drug candidates are tested on rodents and at least one non-rodent species, often the dog, before they are administered to humans. It has long been established that the concordance between animal and human drug-induced toxicity reactions is not as high as it should be to sufficiently predict the toxicity of a new drug candidate in humans. In a retrospective study of 150 compounds from 12 pharmaceutical companies, 221 human toxicity events were generated in the clinical phase of drug development. In non-rodents, 63 % predicted these toxicity events and there was a concordance of 43 % for rodents. The best correlation was observed for haematological, cardiovascular and gastrointestinal toxicities, and the worst was with cutaneous reactions (Olson et al., 2000). This study highlights the need for a better toxicity predictive model or multi-model system that is sensitive, reproducible and relevant to carry out an improved quantitative and qualitative assessment of drug safety. This applies to *in vitro* experiments, as well as *in vivo*. There is a conscious effort in research to try to fill this gap and ultimately save pharmaceutical companies time and money. As mentioned previously in this chapter, this would subsequently benefit patients and the healthcare system too. In general, there is a need for a model that is not expensive, and does not require long and complicated techniques. This model should be readily available and suitable for high throughput experiments to be conducted at the beginning of drug development. In addition, there is also a need for a model that can help study the delayed effects of drug candidates. Generally, the most popular safety pharmacology studies involve a single dose that is analysed up to 24 h (Redfern et al., 2002).

This project is funded by the UK National Centre for 3 Rs (NC3Rs). The major objective for the NC3Rs is to look for technologies that can replace, reduce and refine the use of animals for scientific purposes (NC3Rs, 2017; Prescott and Lidster, 2017). Overall, they aim to reduce the use of experiments that are irrelevant to humans and increase the efficiency of research and quality of study design. We hypothesise, the *Xenopus laevis* can help fill the gap for some of the ideal characteristics of an animal model for the prediction of drug-induced toxicity. The *Xenopus* can also contribute to the ideology of the NC3Rs as we shall explain below.

1.6 *Xenopus laevis*

Xenopus are non-mammalian, African clawed frogs that can develop *ex utero* at different rates according to the temperature at which they are incubated. At 25°C, a *Xenopus*

embryo can develop into an adult in 12 months, this is the temperature that elicits the fastest development rate. At <12°C the embryos will die however, between 12°C and 25°C, the embryos will develop at a rate proportional to the temperature. Consequently, the age of a *Xenopus* embryo cannot be given in hours post fertilisation (hpf), instead, the age can be identified using the developmental stages set out by Nieuwkoop and Faber (these can also be found on the NIH-funded website xenbase.org) (Nieuwkoop and Faber, 1994). The *Xenopus* embryos are easy to house, they can be obtained in large numbers following hormone stimulation and they are amenable for medium to high throughput small molecule screens. The Frog Embryo Teratogenesis Assay *Xenopus* (FETAX) uses developing *Xenopus* embryos to assess the teratogenic potential of small molecule compounds, therefore, it is possible that the *Xenopus* can help to detect drug-induced toxicity. At late stage development (stage 38-45) the *Xenopus* heart, liver and kidney are functional and adding compounds at this stage would assess drug-induced toxicity unlike the FETAX assay, which measures the affect on embryological development. Furthermore, toxicity can be assessed in embryos prior to coverage by the Animal Scientific Procedures Act and only a small amount of the compound to be tested would be required; this is important because in lead compound selection, the amount of compound available could be quite small. Toxicity assessment using the *Xenopus* combined with *in vitro* pharmacological cytotoxicity profiling and mathematical modelling can provide early *in vivo* testing without the need for early mammalian testing. This will be consistent with the ideology of the NC3Rs: **reduction** in the number of tests to be eventually conducted in mammalian experiments. The *Xenopus* could help prioritise the lead compounds and provide more information than *in vitro* safety tests. The *Danio rerio* (zebrafish) has already had some success as a possibly useful *in vivo* model for the assessment of drug-induced toxicity; this is encouraging for a *Xenopus* model which more anatomically similar to humans than *Danio rerio*. It is likely that a combination of both non-mammalian models could be used to help identify drug-induced toxicity potential in NCEs at early stage development. For this project, we used the *Xenopus laevis* species as the adults and the embryos are bigger than the *Xenopus tropicalis*, which was the other species available in our laboratory. From a practical point of view, the larger size makes the *Xenopus laevis* easier to handle and physically manipulate that is advantageous for techniques such as imaging and wholemount *in situ* hybridisation. However, the *Xenopus laevis* genome is allo-tetraploid compared to the diploid genome of the *Xenopus tropicalis*, so genetic alterations can be more challenging.

1.6.1 The *Xenopus laevis* liver

The *Xenopus* liver has the same cell types as found in humans including hepatocytes, stellate cells, Kupffer cells and sinusoidal endothelial cells (Blitz et al., 2006). The *Xenopus* hepatic tissue is generated from an area of suprablastoporal endoderm, which is close to the Spemann's organiser region (Chalmers and Slack, 2000). Similar to vertebrates, the liver is derived from the endoderm of the future gut tube, close to where the stomach and duodenum will meet (Nieuwkoop and Faber, 1994). By the age of stage 37-39, the *Xenopus* liver is a sac-like structure, with thick walls that fold inwards and fill the liver cavity with hepatocytes. Also at this time, the liver and biliary ductal systems are developing and the gall bladder is a thin-walled sac structure (Blitz et al., 2006).

1.6.2 The *Xenopus laevis* heart

The adult *Xenopus laevis* heart has 3 chambers: 2 atria and 1 ventricle and an outflow tract that extends from the ventricle, carrying blood from the heart to the body (**Figure 1-4**). The *Xenopus* ventricle is similar to the mammalian left ventricle (Hempel and Kühl, 2016). In the *Xenopus* embryo, a linear heart tube forms at stage 30, this consists of a bulbus cordis, ventricle, atrium and sinus venosus. From stage 35 onwards, the heart tube starts beating and the atrium is divided into left and right atria. Chamber specification is complete at stage 39, the outflow valve is matured by stage 41 and stage 44 is the maturation of the atrioventricular valve. By stage 46, the embryo has a fully functional 3 chambered heart (Bartlett et al., 2004; Nieuwkoop and Faber, 1994). The heart rate of *Xenopus* embryos is closer to that of the human than to the mouse (Blitz et al., 2006). Mice have a heart rate of 300-600 bpm (beats per minute) and *Xenopus* embryos have a heart rate of approximately 130 bpm at 22°C (Bartlett et al., 2004; Dhillon et al., 2013).

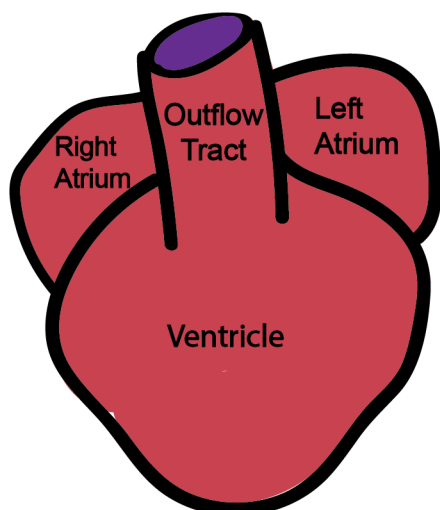


Figure 1-4: *Xenopus* heart

A schematic of the *Xenopus* heart at approximately stage 46 from a ventral view. The atria are slightly behind the ventricle. Blood flows from the atria into the ventricle, where oxygenated and deoxygenated blood mixes and exits the heart via the outflow tract.

1.7 Rationale

It is clear that there is room for new models and the improvement of existing models used to help predict drug-induced toxicity in humans. In accordance with the principles of the NC3Rs, the *Xenopus laevis* could be a useful model in the early preclinical phase of drug development to aid drug candidate prioritisation through drug-induced toxicity experiments.

Our project aims are to:

- Characterise the functional capacity of *Xenopus laevis* embryos in relation to drug metabolism and drug toxicity
- Optimise and adapt assays used in other drug toxicity models to the *Xenopus* system
- Investigate organ-specific toxicity in *Xenopus* embryos with drugs that are associated with hepatotoxic, cardiotoxic and nephrotoxic reactions in humans

In summary, in **chapter 3** we carried out preliminary drug screens using the *Xenopus laevis* embryos. In **chapters 4 and 5** we looked at drugs associated with hepatotoxicity and cardiotoxicity respectively in humans. We adapted existing *in vitro* experiments to assess the similarity of the drug response in the *Xenopus* embryos to humans, and we created new experiments that take advantage of the useful characteristics of the *Xenopus laevis* embryos. Our results show there are a lot of exciting potential directions for further experiments the *Xenopus laevis* embryos with regards to the prediction of drug-induced toxicity in drug development. Some suggestions for this are outlined in **chapter 6**.

2 Chapter 2: Materials and Methods

2.1 *Xenopus laevis* egg collection

Xenopus laevis females were primed 5-10 days prior to egg collection with 100 units of Pregnant Mare Serum Gonadotrophin (PMSG) into one dorsal lymph sac. Approximately 16 hours prior to egg collection, the primed females are injected with 500 units of human chorionic gonadotrophin (hCG, Chorulon®) into both dorsal lymph sacs. Embryos were obtained by *in vitro* fertilisation (IVF). Testes were isolated from a euthanized male frog 16 hours before egg collection. The male was anaesthetised in 300mL of 0.5 mg/mL tricaine (MS-222) dissolved in distilled water (dH₂O). The testes were kept at 4°C overnight in testes buffer.

On the day of egg collection, the eggs were obtained from the abdomen of the primed and induced female frogs through manual abdominal massage over a clean petri dish. The testes were crushed in 1 mL of 1X Marc's Modified Ringers (MMR) and spread on the eggs for 5 min at 18°C. 0.1x MMR covered the eggs for a further 20 min and the vitelline membrane was removed using 250 mL of 2 % (w/v) L-cysteine pH 8.0 (1X MMR). The eggs were washed further with 1X MMR and 0.1X MMR to remove the cysteine and then they were developed to the stage required for drug screening. Embryos were left to develop in 0.1X MMR solution on a petri dish coated with bovine serum albumin at 23°C. Stages were identified according to Nieuwkoop & Faber (1994).

Solutions:

- 10X MMR: 1 M NaCl, 20 mM KCl, 10 mM MgCl₂, 20 mM CaCl₂, 50 mM HEPES (pH 7.5)
- Testis buffer: 80% (v/v) fetal bovine serum, 20% (v/v) 1X MMR
- PMSG (Intervet): 1000U/ml PMSG prepared in solvent and stored at 4°C
- Chorulon® (Intervet): 1000U/ml Chorulon prepared in solvent and stored at 4°C

All experiments were performed in compliance with the relevant laws and institutional guidelines at the University of East Anglia. This research has been approved by the local ethical review committee according to UK Home Office regulations.

2.2 *Embryo fixing*

The required stage of development was determined according to Nieuwkoop & Faber (1994). Once the embryos reached their desired stage they were fixed using MEMFA (3.7% (v/v) formaldehyde, 1X MEM salts (0.1 M MOPS, 2 mM EGTA, 1 mM MgSO₄, pH7.4) made up with dH₂O). They were then dehydrated in 100 % ethanol (EtOH) and left at -20°C for storage.

2.3 *Photographing embryos*

When we were ready to photograph the embryos for phenotype identification, the fixed embryos were re-hydrated using a serial gradient of EtOH (phosphate buffered saline 0.1 % tween-20, PBST) to 100 % PBST. A clean petri dish was coated with a 2 % (w/v) agarose gel and the embryos, suspended in 100 % PBST, were photographed. For the stage 38 embryos, we captured the lateral view. The ventral and lateral views were captured for stage 45 embryos where possible.

2.4 *RNA isolation and cDNA synthesis*

2.4.1 1. mRNA: TRizol® method

After incubation until the stage required, 10 embryos were placed in a 1.5 mL eppendorf tube, all fluid was removed and they were then snap frozen in liquid nitrogen for at least 2 h. The sample frozen dried embryos could be stored at -80°C if need be.

Samples were kept on ice and all reagents were kept ice cold. 1 mL of TRizol® was added to the dried embryos. All animal tissue was broken by vortexing until homogenised. Then 500 µL of Chloroform was added and centrifuged at 4°C to separate proteins/lipids, DNA and RNA. The aqueous upper phase containing RNA was put into a new 1.5 mL eppendorf tube. To precipitate RNA: 500 µL of isopropanol, 50 µL of 5 M NaCl and 2 µL of glycogen-blue were added. After centrifugation at 4°C the supernatant was removed and replaced by 70 % EtOH prepared in RNase free water to wash RNA. After centrifugation at 4°C the EtOH was removed and the pellet was dissolved in 45 µL of RNase free H₂O. At this step, the RNA could be stored at -80°C.

5 µL 10X DNase buffer and 1 µL of DNase I (Roche) were added to each RNA sample. Samples were then incubated at 37°C for 30 min. To this, 50 µL of nuclease-free H₂O was added. Sample final volume was 100 µL. To extract RNA: 100 µL of acidic phenol/chloroform was then added. After centrifugation at 4°C the aqueous upper phase was put into a new 1.5 mL eppendorf tube. To precipitate RNA 70 µL of isopropanol, 7 µL of 5 M NaCl and 1 µL of glycogen-blue were added. This was centrifuged at 4°C. Then the supernatant was removed and replaced by 70 % EtOH prepared nuclease-free to wash RNA. After centrifugation at 4°C the EtOH was removed and the pellet was resuspended in 20 µL of nuclease-free H₂O. The concentration was determined by spectrophotometry (Nanodrop) and sample was stored at -80°C.

First strand cDNA Synthesis was performed using SuperScript II Reverse Transcriptase. For reverse transcription, 1 µg RNA and 1 µl Oligo(dT) (Promega) 12-18 primer were mixed and brought up to 11 µL using nuclease-free water. The mixture was heated to 70°C using a PTC- 100 Peltier Thermal Cycler (BIO-RAD) for 10 min before being put

back on ice where 4 μ L 5X First-Strand Buffer (Sigma, UK), 1 μ L 10mM dNTPs (Roche UK), 1 μ L RNasin (40U/ μ L; Roche, UK), 1 μ L of SuperScript II Reverse Transcriptase (200U/ μ L; Invitrogen, UK) and 2 μ L 100 mM DTT (Sigma, UK) were added to each tube. The samples were incubated at 42°C for 1 h, enzymes were deactivated at 65°C for 5 min and 30 μ L nuclease-free water was added to make a total of 50 μ L cDNA.

2.4.2 2. miRNA: miRCURY™ RNA (Exiqon) method

RNA extraction was completed using the miRCURY™ RNA Isolation (for tissue) kit according to manufacturer's instructions. Embryo tissue was placed into a 2 mL eppendorf tube and snap frozen in liquid nitrogen. To homogenise the tissue, 300 μ L of Lysis Solution was added to the sample and vortexed for 5 min. 600 μ L of RNase Free Water and 20 μ L of proteinase K was added to the lysate and incubated at 55°C for 15 min and spun for 1 min at 14000 x g. 450 μ L of 95 % EtOH was added and the lysate solution was passed through a column by centrifuging for 1 min at 14000 x g. 3X 400 μ L of Wash Solution was subsequently passed through the column at 14000 x g for 1 min to wash the resin. The resin was then dried by a 2 min spin at 14000 x g. The RNA was eluted by adding 50 μ L of nuclease-free water to the column and spun for 2 min at 200 x g followed by 1 min at 14,000 x g. RNA was quantified using a standard spectrophotometer, 260/280 and 260/230 ratios of 1.8-2.0 indicated good quality RNA.

To make cDNA the Universal cDNA synthesis kit II (Exiqon) was used: 2 μ L of 5 ng/ μ L RNA was added to 2 μ L 5 x Reaction Buffer, 5 μ L nuclease-free water and 1 μ L Enzyme mix. This was incubated at 42°C for 60 min then at 95°C for 5 min and cooled to 4°C. The cDNA was stored at -20°C.

2.5 RT-PCR

The amplification of templates was performed using a thermocycler. Total PCR reaction was 10 μ L containing 10-50ng of template cDNA 1 μ M of each forward and reverse primer, 1X of BioMix™ (2X reaction mix containing ultra-stableTaq DNA polymerase, Bionline). An initial denaturation step of 95°C for 3 min was followed by a denaturation of 1 min at 95°C for the start of the cycle. The annealing step was carried out at an annealing temperature calculated by subtracting 5°C from the primer melting temperature, for 1 min. This was followed by 1 min of extension step at 72°C (according to the expected size of the PCR product, 1 min/1 kbp) 25-35 cycles (depending on the level of expression of the gene of interest) of denaturation, annealing and extension were carried out. Amplified products were fractionated in 1 % (w/v) agarose Tris/Borate/EDTA (TBE 1X: 45 mM Tris-Borate, 1 mM EDTA (ethylenediaminetetraacetic acid), pH 8.0) gel electrophoresis with

0.0001 % (v/v) of 10 mg/mL ethidium bromide and visualised under UV light using a UV transilluminator (BIO-RAD).

2.6 qRT-PCR

The cDNA was diluted 1 in 80; we determined this was the optimum concentration to use in preliminary experiments. The reaction was performed in MicroAmp optical 96 well plate (Applied Biosystems). The final volume was 15 μ L containing 5 μ L of the diluted cDNA, 0.5 μ L of miRCURY™ LNA PCR Primer mix (Exiqon) or 10 μ M mrp2 (forward and reverse), 7.5 μ L of 2x SYBR® Green PCR Master Mix (Applied Biosystems) and 2 μ L of RNase free water. A 7500 real-time PCR instrument (Applied Biosystems) was used under the following conditions: 50°C for 2 min, 95°C for 10 min, 95°C for 10 s (for miRNA) or 15 s (for mRNA) cycles X40 and 60°C for 1 min. We used miR-103 as a quantitative control for miR-122 expression of paracetamol-treated embryos. To measure mrp2 expression, we used ornithine decarboxylase 1 (odc1) as a quantitative control. Samples were plated in triplicates (technical replicates). Samples derived from embryos produced from different mothers were our biological replicates.

2.6.1 qRT-PCR statistical analysis

Gene expression was analysed using the Livak method (Livak and Schmittgen, 2001). An average CT value was taken from the technical replicates, this was normalised to miR-103 or odc1 expression and also to the untreated samples (embryos that received no drug treatment). The fold change was determined using the formula: $2^{-\Delta\Delta CT}$, this number was converted into a logarithmic (\log_{10}). Mann-Whitney tests were performed between gut and tail tissues from embryos treated with the same concentration of drug to determine statistical significance. These were performed using Graph Pad Prism 6.

2.7 Wholemount *in situ* hybridisation (WISH)

2.7.1 1. mRNA probe synthesis: for Cardiac Troponin 1c and alpha-1-microglobulin/bikunin precursor (AMBP)

2.7.1.1 Purification of PCR product

PCR products were purified using the QIAquick PCR Purification Kit (Qiagen, UK) according to manufacturer's instructions. The concentration was determined by spectrophotometry (Nanodrop). Ligation reactions were carried out according to the ratio of vector and insert.

This ratio was calculated as follows:

$$\frac{([\text{ng of vector}] \times [\text{kb size of insert}])}{[\text{kb size of vector}]} \times \text{molar ratio} \frac{[\text{insert}]}{[\text{vector}]} = \text{ng of insert}$$

Ligation reactions were carried out according to two conditions of ratio 3:1 and 1:1. The reaction mixture was as follows: 10-100 ng of PCR products, 0.5 µL of pGEM®-T Easy Vector, 5µl of 2x ligase buffer (Promega), 1 µL of Ligase T4 DNA (3U/µL, Promega) made up to 10 µL with nuclease-free H₂O. The reaction was then incubated for 2-3 h at RT. Ligation reaction was then transformed into competent bacteria by the method outlined below.

2.7.1.2 Preparation of competent cells

A 5 mL culture of DH5α *Escherichia coli* was grown overnight in Luria Broth (LB) at 37°C and with shaking. 1 mL of this culture was added to 200 mL of LB medium and grown at 37°C with shaking until optical density (OD₆₀₀) reached 0.3 to 0.4. At this point the culture was divided into 3X 15 mL Falcon tubes and put on ice for 15 min. The cells were centrifuged at 4°C for 15 min at 6000 x g. The supernatant was discarded and the bacterial pellet was resuspended in 16 mL filter sterilized TB I buffer. Cells were put on ice for 15 min, centrifuged at 4°C at 20000 x g for 30 min. The supernatant was discarded and the pellet was resuspended in 4 mL of sterilized TB II. Aliquots were stored at -80°C.

Materials:

- TB I pH 5.8: 0.1 M RbCl₂, 0.068 M MnCl₂H₂O, 0.01 M CaCl₂, 1 M KAc pH 7.5, 37.5 mL Glycerol adjust to 250 mL and pH using 0.2 M HAc 26
- TB II: 0.5 M MOPS pH 6.8, 0.01 M RbCl₂, 1.04 M CaCl₂ H₂O, 37.5 mL Glycerol adjust to 250 mL aliquoted and stored at -80°C

2.7.1.3 Transformation

5 µL of plasmid was added into 200 µL of competent E.coli cells, left on ice for 30 min and heat shocked at 42°C for 90 s. 300 µL of LB media was added and cells were left for 1 h at 37°C. 300 µL of transformation mix was plated out onto LB agar containing the required antibiotic overnight at 37°C.

2.7.1.4 DNA midiprep

Colonies from the transformation were incubated in 50 mL LB/carbenicillin liquid media overnight at 37°C with rocking. Plasmid DNA was isolated using Qiagen midi plasmid purification kit (Qiagen, UK) according to manufacturer's instructions. 1 µL of the final product was analysed by gel electrophoresis and the sequence of the gene of interest was confirmed by sequencing with 0.1 µM M13 forward and reverse primers (Sanger Sequencing Service, Source BioScience). The Midi preparation of the plasmid was diluted

10 times and 1 μL was used for the PCR reaction, 1X of BioMix™ (2x reaction mix containing ultra-stableTaq DNA polymerase, Bioline) was added for a total volume of 10 μL . A thermocycler was used to perform the reaction under the following conditions: an initial denaturation step of 95°C for 3 min was followed by a denaturation of 1 min at 95°C. The annealing step was carried out at an annealing temperature of 55°C for 1 min. This was followed by 1 minute of extension step at 72°C. 25 cycles denaturation, annealing and extension were carried out. Amplified products were fractionated in 1 % (w/v) agarose Tris/Borate/EDTA (TBE 1x: 45mM Tris-Borate, 1mM EDTA, pH8.0) gel electrophoresis with 0.0001% (v/v) of 10mg/ml ethidium bromide and visualised under UV light using a UV trans-illuminator (BIO-RAD).

2.7.1.5 DNA quantification

DNA was quantified using a standard spectrophotometer, 260/280 and 260/230 ratios of 1.8-2.0 indicated good quality DNA.

2.7.1.6 Probe synthesis

Probe was synthesised with a promoter specific RNA polymerase (T7, Sp6 or T3) the following reaction conditions were used: 1 μL PCR template, 2 μL dithiothréitol (DTT, Promega), 1 μL Digoxigenin (DIG) labeled UTPs (Roche), 1 μL RNase inhibitor (Promega), 2 μL (40U) RNA polymerase (Promega) 4 μL 5x transcription buffer (Promega) made to a final volume of 20 μL with nuclease-free H_2O . The reaction was incubated at 37°C for 3 h. Any remaining DNA template was removed by adding 1 μL of DNase I (Roche) and incubating for 30 min at 37°C.

2.7.1.7 Purification of probes

30 μL of nuclease-free H_2O were then added to the 20 μL of the probe synthesis PCR product purify the probe. Probes were purified by using Illustra MicroSpin G-50 Columns (GE healthcare life sciences) according to manufacturer's instructions. 5 μL of probe was analysed on a 2 % (w/v) agarose to confirm probe integrity. 5 μg of purified probe was added to approximately 10 mL of hybridisation buffer depending on probe quality (determined on a 2 % (w/v) agarose gel) and stored at -20°C.

2.7.2 2. XenmiR probes: miR-122 and miR-208

Probes obtained from Exiqon arrived as 1 nmol dried pellets. We resuspended the pellet in 40 μL nuclease-free water, and added 10 μL of this into 12.5 mL hybridisation buffer to generate a final concentration of 20 nM. 1 mL of this probe solution was used in the WISH for the miRNAs.

2.7.3 WISH staining protocol

Embryos were rehydrated from 100 % EtOH by using a serial gradient of EtOH (PBST) 25 % to 100 % PBST for 5 min each followed by 2 x 5 min PBST washes, all with rocking at room temperature (RT). Embryos were then treated with 10 µg/mL proteinase K (no rocking) for varying times depending on the embryo stage age.

Xenopus stage 38 – 10 min and stage 45 – 20 min.

Xenopus embryos were then subsequently washed 2X PBST for 5 min and incubated in 3.7 % (v/v) formaldehyde/PBST for 45 min without rocking. Next, the embryos were washed with 50 % hybridisation buffer (PBST) followed by 100 % hybridisation buffer both for 10 min. Then embryos were prehybridised in 100 % hybridisation buffer for 4 h at hybridisation temperature (48°C for XenmiR probes: miR-122 and miR-208, and 65°C for mRNA probes: AMBP and cardiac troponin 1c). The embryos were incubated with XenmiR probes for 24 h and overnight with mRNA probes, at their respective temperatures.

Probes were removed and stored at -20°C and embryos were washed with fresh hybridisation buffer for 10 min followed by 2X 15 min washes with wash solution and 1X 10 min wash in 50% maleic acid buffer, 0.1 % tween-20 (MABT)/50% wash buffer. All steps were completed at the correct hybridisation temperature for the XenmiR and mRNA probes as stated. Next, 2X 30 min washes in 1X MABT (0.1 % tween-20), 1X 1 h wash in 2 % (w/v) Boehringer Mannheim blocking reagent BBR in MABT (BMB) and a 4 h wash in 20% (v/v) goat serum in 2 % (w/v) BBR, all at RT. BBR solution was replaced with antibody solution containing anti-Dig antibody (Roche, 150 U) (1:3000) made in 20 % (v/v) goat serum and 2 % (v/v) BBR at 4°C overnight. All steps with rocking.

Antibody solution was removed and embryos were washed 5X 1X MABT for 60 min each at RT and incubated 1 last 1X MABT wash overnight at 4°C with rocking. The colour reaction was then carried out by washing the embryos in fresh alkaline phosphate buffer twice for 10 min at RT with rocking. Embryos were then put in NBT/BCIP in alkaline phosphate buffer (4.5 µL/mL NBT, 3.5 µL/mL BCIP) protected from light using foil, until the desired level of colour was reached. Embryos were placed in 5X TBST solution overnight if needed to remove background staining and then photographed.

Materials for WISH:

- PBS – 10X: 2.5 g NaH₂PO₄.H₂O, 11.94 g NaHPO₄.H₂O, 102.2 g NaCl
- PBST – PBS with 0.1 % (v/v) tween-20
- Proteinase K (10 µg/mL): 1 µL proteinase K, 1 mL PBST
- Hybridisation buffer: 50 % (v/v) formamide, 5X SSC, 1 mg/mL Torula RNA, 100 µg/mL Heparin, 1X Denharts solution, 0.1 % (v/v) tween-20, 0.1 % (w/v) CHAPS, 10 mM EDTA
- Washing buffer: 50 % (v/v) formamide, 1X SSC, 0.1 % (v/v) tween-20

- MABT (1X): 100 mM Maleic acid, 150 mM NaCl, 0.1% (v/v) tween-20, (pH 7.5)
- BMB (10%): 10% (w/v) in BMB preheated (50°C), 1X MAB, stirred until dissolved and then autoclaved, aliquoted and stored at -20°C.
- Alkaline phosphatase buffer: 100 mM Tris (pH 9.5), 50 mM MgCl₂, 100 mM NaCl, 0.1% (v/v) tween-20.
- BCIP: 50 mg/mL in 100% DMF
- NBT (Nitro Blue tetrazolium): 75 mg/mL in 70 % dimethylformamide (DMF)
- TBST: 125 mL 1 M Tris pH 7.5 40 g NaCl, 1 g KCl and 450ml with dH₂O. Autoclaved then add 50 mL of tween-20.
- MEMFA: 10 % (v/v) MEM salts, 10 % (v/v) formaldehyde
- MEM salts: 0.1 M MOPS, 2 mM EGTA, 1 mM MgSO₄, pH 7.4

2.8 Sectioning

2.8.1 Cryostat with OCT compound

Embryos were fixed in MEMFA for 1 week, washed 2X 5 min with PBST and placed in 30% (w/v) sucrose overnight at 4°C. Embryos were transferred to cryo30 moulds filled with optimal cutting temperature (OCT) compound and left for 4 h at RT. Embryos were positioned appropriately for sectioning, frozen gradually in isopentane surrounded by dry ice for 30 min and then left overnight at -20°C. Embryos were sectioned to 15 µm thickness using the LEICA CM 1950 Cryostat and sections were placed on 5 % TESPA slides. Slides were washed 3X 5 min washes in PBS and coverslips were mounted using hydromount.

2.8.2 Microtome with wax

Embryos were fixed in MEMFA for 1 week, washed 2X 5 min with PBST and then dehydrated using a serial gradient to 100 % EtOH. 3X 100 % EtOH to remove PBST completely then put into 100 % histoclear (National Diagnostics) in glass vials in a 65°C oven for 10 min. Add wax in the ratio 1:1 with 100 % histoclear, incubate for 1 h at 65°C. 3X wax washes at 65°C to remove histoclear. Transfer embryos and wax to moulds and allow to set at RT for at least 1 h. Embryos were sectioned using a microtome to a 10 µm thickness onto 5 % TESPA slides and adhered to slides using water and manual pressure and dried at RT. Slides were washed 2X 5 min washes in histoclear to remove wax and mounted using hydromount and coverslips.

2.8.3 Hematoxylin and Eosin staining

After sectioning, the OCT or wax was removed from the slides as stated above. Hematoxylin (Sigma, UK) was diluted 1:1 in dH₂O and filtered using filter paper, ready for

use. Eosin Y (Sigma, UK) stock solution contained 0.1 % (w/v) dissolved in dH₂O with 3 drops of acetic acid. 100 mL of this stock was added to 700 mL of 80 % EtOH (dH₂O) and this solution was filtered using filter paper, ready for use. Acidic alcohol contained 396 mL of 95 % EtOH and 4 mL HCl. Test slides were conducted for the day to adjust the staining times for a optimal H&E stain. Approximately, the sections (without excess OCT or wax) were treated with 5 min hematoxylin, rinsed in dH₂O for 30 s, 5X dips in the acidic alcohol followed by another 30 s dH₂O rinse. Then, eosin treatment for about 30 s, dehydration with 75 % to 100 % EtOH (dH₂O) and 2X 10 s in histoclear. Mounted using hydromount and coverslips. Images were taken using a Zeiss CCD upright microscope with colour camera.

2.9 Treatment with drugs

2.9.1 Chapter 3 Drug screens

The following drugs were used for the chapter 3 screens Paracetamol (Acetaminophen; Sigma, UK), Indomethacin (Santa Cruz Biotechnology), Cisplatin (Santa Cruz Biotechnology), Gentamicin (Gentamicin sulfate; Santa Cruz Biotechnology), doxorubicin (doxorubicin hydrochloride; Sigma, UK), daunorubicin (daunorubicin hydrochloride; Sigma, UK), tobramycin (Santa Cruz Biotechnology), AMAP (N-acetyl-meta-aminophenol; Sigma, UK), diclofenac (diclofenac sodium salt; Sigma, UK). For these drugs, all of the concentrations (0.78 µM – 100 µM) contained 0.5 % DMSO (v/v). 1 well in a 96-well plate contained 125 µL of 2X final concentration of drug. Embryos at their desired stage according to Nieuwkoop & Faber (1994), were added to the well containing the drug solution, 1 embryo/well, with 125 µL 0.1X MMR. The final total volume of each well was 250 µL. For 1 biological replicate (n=1), we used 5 embryos for each drug concentration. Consequently 5 biological replicates (n=5) used a total of 25 embryos. The plates were sealed with Breathe-Eazy® Sealing membranes (Sigma, UK) to prevent evaporation, but allow the exchange of gases. For both stage 15 – stage 38 and stage 38 – stage 45 screens, the embryos were incubated at 23°C throughout drug treatment. Embryos were fixed and photographed as previously mentioned.

2.9.2 Chapter 4 and 5 screens

All drugs in these chapters were dissolved in 0.1X MMR alone. Except terfenadine, all final concentrations of terfenadine contained 0.5 % DMSO (v/v) (0.1X MMR). The untreated embryos for terfenadine experiments (0 µM terfenadine) also contained 0.5 % DMSO (v/v) (0.1X MMR). 1 well in a 96-well plate contained 125 µL of 2X final concentration of drug. Embryos at their desired stage according to Nieuwkoop & Faber (1994), were added to the well containing the drug solution, 1 embryo/well, with 125 µL

0.1X MMR. The final total volume of each well was 250 μ L. For 1 biological replicate (n=1), we used 7 embryos for each drug concentration. Consequently 5 biological replicates (n=5) used a total of 35 embryos.

2.9.3 The preparation of samples for the measurement of miR-122 expression using qRT-PCR

Stage 38 embryos were treated with paracetamol as described above until stage 45. At stage 45, the embryos were placed into a clean petri of 0.5 mg/mL tricaine (0.1X MMR) and incubated at 23°C for 1 h. Embryos were dissected into tail and gut tissue using a simple razor. The dissection technique was confirmed by analyzing the expression of the liver-specific marker AMBP. AMBP was expressed in the gut tissue dissected but not in the tail tissue.

1 biological replicate is defined as using 1 adult frog mother. In other words, a result generated from embryos that have the same mother, was only counted as 1 biological replicate.

2.9.4 1-aminobenzotriazole (ABT) and paracetamol

2.9.4.1 Pre-incubation

62.5 μ L 6 mM 1-ABT was put into 1 well of a 96-well plate with 1 embryo and 62.5 μ L 0.1X MMR to make a final concentration of 3 mM 1-ABT. This was incubated at 23°C for 2 h. Then 62.5 μ L of 4X final concentration of paracetamol was added with 62.5 μ L of 6 mM 1-ABT to create a final volume of 250 μ L/well. This was incubated for a further 70 h, until the embryos were stage 45 at 23°C. The embryos were processed with the GSH assay method.

2.9.5 N-acetyl cysteine (NAC) and paracetamol

2.9.5.1 1. Pre-incubation

62.5 μ L 1 mM NAC (Sigma, UK) was put into 1 well of a 96-well plate with 1X stage 38 embryo and 62.5 μ L 0.1X MMR to make a final concentration of 0.5 mM 1-ABT. This was incubated at 23°C for 2 h. Then 62.5 μ L of 4X final concentration of paracetamol was added with 62.5 μ L of 1 mM 1-ABT to create a final volume of 250 μ L/well. This was incubated for a further 70 h, until the embryos were stage 45 at 23°C.

2.9.5.2 2. Concurrent treatment

62.5 µL 2 mM NAC, 62.5 µL 4X final concentration of paracetamol, 125 µL 0.1X MMR and 1X stage 38 embryo were combined in 1 well of a 96-well plate. Final volume was 250 µL/well. The plate was incubated at 23°C for 72 h, when the embryos were stage 45.

2.9.5.3 3. 24 h NAC treatment prior to harvest

125 µL of 2X final concentration paracetamol and 125 µL 0.1X MMR were combined into 1 well of a 96-well plate with 1X stage 38 embryo. This was incubated at 23°C for 48 h. At 48 h we added 25 µL 6 mM NAC and 25 µL 2X final concentration of paracetamol to make a final volume of 300 µL/well with 0.5 mM NAC. This was further incubated for 24 h at 23°C until the embryos were stage 45.

All the embryos were processed with the GSH assay method at stage 45.

2.9.6 Doxorubicin and dexrazoxane

62.5 µL 4X final concentration doxorubicin, 62.5 µL 4X final concentration dexrazoxane, 125 µL 0.1X MMR and 1X stage 38 embryo were added to 1 well of a 96-well plate and incubated for 72 h at 23°C, until they were stage 45. Final volume was 250 µL/well. The doxorubicin to dexrazoxane ratio was 1:10 respectively.

2.10 Measuring free GSH

2.10.1 Sample preparation

At the end of the incubation period, embryos that were treated with the same conditions were transferred into 1 eppendorf and put on ice. As much as possible, the incubation solution was removed and 125 µL 10 mM HCl was added. Embryos were homogenized using the vortex and an eppendorf pestle. Then, they were centrifuged at 14000 x g for 5 min at 4°C. 25 µL of the supernatant was transferred to another tube to be kept at -80°C for protein quantification using the Bradford assay, this was replaced with 25 µL 6.5 % (w/v) 5-sulfosalicylic acid hydrate (SSA). Remove all of the supernatant including the SSA and keep at -80°C until perform the GSH assay.

2.10.2 GSH assay

Standard GSH concentrations: 0, 1, 2, 5, 10, 20, 30 and 40 nmol/mL were made up on the day of the experiment using GSH buffer and 0.1 mM GSH (Sigma, UK) and kept on ice. 20 µL of the standard or sample was mixed with 200 µL Assay Reagent in 1 well of a 96-well plate and incubated for 5 min. 50 µL/well 13 U/mL GSH reductase (diluted in GSH buffer) and the plate was read immediately at 405 nm absorption using the GloMax®

Explorer System spectrophotometer (Promega). 11 readings were taken at 15 s intervals. The reading with best standard curve was used to calculate the sample results (nmol/mL).

Solutions:

- GSH buffer: 143 mM NaH₂PO₄ and 6.3 mM EDTA dissolved dH₂O
- Assay Reagent: 0.28 mg/mL NADPH (Sigma, UK) and 0.4 mg/mL DTNB (5,5-dithio-bis-(2-nitrobenzoic acid; Sigma, UK) dissolved in GSH buffer

2.10.3 Bradford assay

Standard concentrations were made up using BSA dissolved in 10 mM HCl: 0, 0.1, 0.2, 0.4, 0.8, 1.2, 1.6, 2 and 4 mg/mL. The assay was completed according to the manufacturer's instructions (BIO-RAD). 5 µL of each sample was added to 1 well of a 96-well plate with 25 µL of reagent A + S (1 mL reagent A + 20 µL reagent S) and 200 µL of reagent B. This was incubated for 15 min at RT. The plate was read at 595 nm absorption using the GloMax® Explorer System spectrophotometer (Promega).

GSH results (nmol/mL) were divided by the BCA result (mg/mL) for the same sample to give the final result (nmol/mg).

2.11 Heart rate assay

I created and developed the method to detect heart rate in *Xenopus* embryos as detailed below. The method was originally adapted from Bartlett and colleagues (2004).

2.11.1 Anaesthetic assays

Untreated embryos were developed until the age of stage 45, when they were placed into 0.1, 0.2 0.3, 0.4 or 0.5 mg/mL (0.1X MMR) tricaine in a clean petri dish and incubated at 23°C for 1 h. We used 3 embryos and 3 biological replicates for each concentration in this anaesthetic assay: 9 embryos for each concentration in total. After this incubation, the embryos were kept in tricaine solution in the petri dish, placed so that the ventral side was in view and filmed in black and white using a Pulnix TM-840 CCD camera on top of a Zeiss CCD upright microscope. The camera was optimized to record 50 frames per second (fps) of 720p resolution, we recorded the embryo heart beat for 30 s.

2.11.2 Drug treatment: doxorubicin and terfenadine

Embryos were dosed with 0-100 µM doxorubicin or 0-50 µM terfenadine from stage 38 until stage 45 in a 96-well plate as described in "treatment with drugs". 7 embryos were used for each concentration and we conducted 3 biological replicates: 21 embryos in total for each concentration. At the age of stage 45, the embryos from the same drug concentration were pooled together and put into a final concentration of 0.2 mg/mL

tricaine in a clean petri dish along with a fresh solution of the concentration of drug they were receiving. They were incubated for 1 h at 23°C before they were filmed in black and white using a Pulnix TM-840 CCD camera on top of a Zeiss CCD upright microscope. The camera was optimized to record 50 frames per second (fps) of 720p resolution, we recorded the embryo heart beat for 30 s.

2.11.3 Post-treatment doxorubicin recovery

After the doxorubicin-treated embryos were filmed as above, the embryos that received the same concentration of doxorubicin were pooled together and were transferred into a clean petri dish containing only 0.1X MMR media. They were incubated at 23°C for a further 72 h. After 72 h, they were transferred into a clean petri dish containing a final concentration of 0.2 mg/mL tricaine and incubated at 1 h for 23°C. After 1 h, the embryos were filmed as previously mentioned in black and white using a Pulnix TM-840 CCD camera on top of a Zeiss CCD upright microscope. The camera was optimized to record 50 frames per second (fps) of 720p resolution, we recorded the embryo heart beat for 30 s.

2.11.4 Video analysis

The black and white video MP4 recordings were imported into Adobe Media Encoder CC 2017 and converted into a sequence of TIFF images, so 1 image is created for each frame. A 30 s video would create 1500 images. This TIFF image sequence is imported into ImageJ using the Time Series Analyzer V3 plugin. We identified the atrium and ventricle of the *Xenopus* embryo and created a circular region of interest (ROI) that was 70 pixels wide on top of each of these heart chambers. We also created a control third ROI of the same size that was placed in an area outside of the embryo in the images. Using the ImageJ plugin, we processed all the images to generate the average intensity within each ROI for every frame, which we pasted into Microsoft Excel. In excel, we converted the frame numbers into real time seconds, and normalized the atrium and ventricle ROI averages to the third ROI average. Occasionally in the recording, the entire image becomes brighter or darker and affects the intensity readings for the atrium and the ventricle. Consequently, the third ROI can be used to correct this.

The average ROI intensity was plotted against seconds. The higher the intensity number, the closer the pigment is to black on the greyscale, which equates as blood filling the chamber. We used the ventricle data to calculate the heart rate. The number of peaks in 30 s on the ventricle graph was counted manually and we converted this into beats per min (bpm). An arrhythmic heart beat was identified as irregular peaks and troughs in the graphs created from the atrium and ventricle ROIs. We validated the arrhythmic beat by

observing the heart beating in real time in the video. An irregular beat on the graph always correlated with an arrhythmic beat observed in the video.

An average heart rate (bpm) for 1 concentration from 1 biological replicate was taken. Subsequently we averaged the 3 biological replicates and calculated the standard error across these 3 replicates. 1 biological replicate is defined as using 1 adult frog mother. In other words, a result generated from embryos that have the same mother, was only counted as 1 biological replicate.

An example of a heart rate assay video, video analysis and representative graphs for normal heart beat rhythm and arrhythmia is shown in the **Appendix Figures A-1 and A-2**.

2.12 Mass spectrometry analysis of paracetamol (APAP) and paracetamol metabolites

2.12.1 Preparation of samples

Stage 38 embryos were treated with paracetamol as described above until stage 45. At stage 45, the embryos used for drug treatment were pooled into 1 eppendorf and put on ice to reduce the movement of the embryos. The incubation medium was removed and put into a new eppendorf and we snap froze the embryos in liquid nitrogen. Samples were stored at -80°C until they were analysed. These samples were analysed in the MRC Centre for Drug Safety Science at University of Liverpool by Dr. Mark Bayliss. The method for analysis was described recently in Eakins *et al* (2015).

We measured paracetamol and paracetamol metabolite content in our samples using high performance liquid chromatography-tandem mass spectrometry (HPLC-MS/MS). Test samples were treated with acetonitrile, to remove matrix-based interferences. They were diluted with water prior to analysis by LC-MS/MS on a Sciex API 4000 (Warrington, UK) equipped with a Turbo V™ electrospray source (ESI). The gradients were based on mobile phases containing 0.1% (v/v) formic acid in both water (A) and acetonitrile (B). Separations were performed on a 2.6 µm Kinetex® XB-C18 column (50 × 2.1 mm ID) obtained from Phenomenex (Macclesfield, UK), at a temperature of 40 °C and a flow-rate of 0.5 mL min⁻¹. The following gradient was used: 0 min 0% B, 0.3 min 0% B then 2.3 min 50% B. The column was flushed with 100% B, and then returned to 0% B using a flow-rate of 0.7 mL min⁻¹, giving a programmed cycle time of 4.2 minutes. A panel of deuterated internal standards was employed. The MS was operated in negative ion mode for measuring the major paracetamol metabolites (APAP-glucuronide, APAP-sulphate, APAP-NAC, APAP-glutathione, APAP-methoxy and APAP-cysteine) and high concentrations of paracetamol and it was operated in positive ion mode for measuring the remaining metabolite and low concentrations of APAP (Eakins *et al.*, 2015).

2.12.2 Analysis of HPLC-MS/MS

Where ratio of an analyte inside the embryo versus the analyte in the incubation medium is <0.02 , results for the embryo represent mainly concentrations in residual medium that is still coating embryos. We analysed 5 embryos for each paracetamol concentration, these embryos were generated from 1 adult female frog and used in the same paracetamol drug screen. Consequently, this experiment comprises of 1 biological replicate, therefore were could not perform any statistical analysis.

2.13 Positive control

Where possible, literature has been described to be able to compare the data we have generated with the *Xenopus* embryos to existing results from similar experiments. Within the experiments conducted with the *Xenopus* embryos, a negative control was included. However we were not able to conduct the experiments with a positive control, for example, an organism to which a reproducible response is established. In future experiments, it would be ideal to conduct the *Xenopus* experiments in parallel to a more established animal model such as zebrafish or a rodent.

2.14 Statistical analysis

Statistical tests were carried out using GraphPad Prism 6.0 software. I chose the appropriate test to use according to the parameters of the data and the comparisons I wanted to analyse. An ordinary one-way ANOVA was used for investigating the difference of the treated groups compared to the untreated embryos and Mann-Whitney non-parametric tests were used to compare unpaired treatment groups. For the paired data sets a parametric paired T test was performed.

3 Chapter 3: Characterisation of the *Xenopus laevis* embryo as a model for drug-induced toxicity

3.1 Introduction

Over the past 15 years the Wheeler laboratory, plus others, have shown that the *Xenopus laevis* embryos are amenable to medium throughput drug screens (Tomlinson et al., 2012; Wheeler and Brändli, 2009; Wheeler and Liu, 2012). Up to 5 embryos, that are stage 45, can fit into 1 well in a 96 well plate. This is advantageous because compared to other animal models such as rodents, the *Xenopus* model assay could test many drug candidates at one time and only a small amount of the compound would be required which suits early stage testing in drug development where often only a small amount of a drug candidate is available. Rodents are traditionally the first animal model used in drug development for preclinical drug safety studies and instinctively, they could be considered more relatable to humans than the non-mammalian *Xenopus laevis*. However, studies show that the correlation between rodent studies and other animal studies is not good. Only 4 in 24 toxicities were detected in animals that occurred in humans (Heywood, 1990). Another study found that for 114 drug-induced toxicity cases, only 6 had direct animal correlation (Spriet-Pourra and Auriche, 1994). In conclusion, there is definitely room for an improvement of the current practice for drug safety studies in drug development. There is a space for an animal model that **can** predict drug-toxicity reactions, or more likely, the solution may be to use a variety of animal models for which we really understand the use and limitations. Furthermore, although a non-mammalian model such as *Xenopus* may initially seem irrelevant for humans, many zebrafish models have proven there is some translation (Zon and Peterson, 2005).

To begin our investigation into the use of *Xenopus laevis* embryos as a model for the prediction of drug-induced toxicity, we decided to use a known *Xenopus* toxicity assay (previously mentioned in **chapter 1**) called the FETAX as a starting point. The FETAX can suggest the impact the drug candidate has on embryonic development. Next, we used *Xenopus* embryos at the age we believe is more relevant to drug-induced toxicity: stage 38 until stage 45. In both of these assays we decided to use drugs that are known to cause organ-specific toxicity in humans. The key mechanisms of action for these drugs are summarised in **Table 3-1**. The mechanisms of action for drug-induced toxicity with respect to paracetamol and doxorubicin will be discussed in more detail in **chapters 4 and 5** respectively.

Gentamicin is an aminoglycoside which is a class of antibiotics that consists of 2 or more amino sugars with a glycosidic linkage to an aminocyclitol ring (Weinstein et al., 1963).

Gentamicin is one of the most nephrotoxic aminoglycoside antibiotics. It is largely excreted unchanged via glomerular filtration in the kidneys (Gyselynck et al., 1971). This is because it is not lipophilic and therefore it is not readily absorbed into most tissues. But it does accumulate in the kidney proximal tubule epithelial cells (Vandewalle et al., 1981). Gentamicin enters these cells through the receptor megalin (Dagil et al., 2013). It is estimated 5 % of the gentamicin parent drug administered builds up in these cells which is a key step that leads to the generation of nephrotoxicity (Mingeot-Leclercq and Tulkens, 1999). Gentamicin-related toxicity occurs in 10-20 % of patients and presents as non-oliguric renal failure in the clinic. Although when gentamicin is stopped, the renal failure is reversed in almost all patients. Gentamicin is also associated with ototoxicity. The megalin receptor is present in the cochlea of the inner ear as well as in the kidneys, consequently the ears are susceptible to gentamicin-induced cell death (Mizuta et al., 1999).

Indomethacin is an anti-inflammatory drug, originally introduced to treat rheumatoid arthritis (Lione and Scialli, 1995). It inhibits prostaglandin synthesis in all tissues, however it especially affects the gastric prostaglandins. This is thought to be because the parent drug is the active component (it doesn't need to be activated like a prodrug). Therefore, with oral administration, it immediately affects the gastric prostaglandins causing gastrointestinal irritation and ulcer formation (Wilson and Kaymakcalan, 1981). Under physiological conditions, the gastric prostaglandins aid the formation of gastric mucus and inhibit acid secretion. Indomethacin also induces mitochondrial stress through the inhibition of complex I, and together with the interference of the gastric prostaglandins, the intestinal mucosal epithelia become more permeable thus making it easy for bacteria to penetrate the mucosa (Watanabe et al., 2011). This will recruit inflammatory cells, activate the innate immune system and overall cause more injury to the initial injury site (Boelsterli et al., 2013).

Cisplatin is a highly effective anticancer chemotherapeutic agent but it is unfortunately associated with dose-limiting nephrotoxicity (Arany and Safirstein, 2003). Renal impairment typically begins a few days after the first dose (Miller et al., 2010). Approximately 20-30 % of patients taking cisplatin present with acute kidney injury (Goldstein and Mayor, 1983; Madias and Harrington, 1978). The exact mechanism of therapeutic action is not known. In an aqueous environment, the cisplatin compound becomes a positively charged electrophile that reacts with DNA to form inter- and intra-strand crosslinks consequently inhibiting DNA synthesis and cell replication (Wang and Lippard, 2005). Tumour cells are less capable at DNA repair and therefore they are more sensitive to the mechanisms of cisplatin than healthy cells. It is thought that cisplatin particularly targets mitochondrial DNA. The renal proximal tubule cells contain a high density of mitochondria so this could be the reason for the high frequency of kidney-

specific toxicity associated with cisplatin. Cisplatin is metabolised by various enzymes to generate highly reactive thiols that are more potent toxins than the parent drug itself (Townsend et al., 2003). Positively-charged cisplatin metabolites accumulate in negatively-charged mitochondria. Furthermore, cisplatin-induced tubular epithelial cell injury activates TLR4-mediated inflammatory cell recruitment (Zhang et al., 2008). As with most anticancer drugs, cisplatin is associated with a number of organ-specific toxicities in addition to nephrotoxicity namely ototoxicity, gastrotoxicity and myelosuppression (Hartmann and Lipp, 2003). However nephrotoxicity is the dominant organ-specific phenotype for patients administered cisplatin.

To help validate our *Xenopus* toxicity assay, we looked at drugs that are not well known to be associated with toxicity in addition to the organ-specific toxic compounds named above. Tobramycin, also known as nebramycin, is an aminoglycoside antibiotic that was discovered in approximately the same decade as gentamicin (Stark et al., 1967). Tobramycin is associated with some nephrotoxicity but not as much as gentamicin (Begg and Barclay, 1995; Luft et al., 1978). It has the same therapeutic mechanism of action as gentamicin. Consequently, in order to validate an animal model for the prediction of nephrotoxicity, tobramycin is often used as a counter drug to gentamicin. Daunorubicin is an anthracycline antibiotic that has a similar therapeutic mechanism of action to doxorubicin, but is has a lower incidence of cardiotoxicity than doxorubicin (Dorr et al., 1991). For this reason it is often used in conjunction with more potent cardiotoxic compounds to validate a new animal model for the prediction of cardiotoxicity. Pouna and colleagues (1996) tested a number of anthracycline drugs including doxorubicin and daunorubicin to investigate the value of an isolated perfused rat heart for preclinical drug safety studies. In this model daunorubicin was significantly less cardiotoxic than doxorubicin, this reflects the incidence observed in humans (Pouna et al., 1996). N-acetyl-meta-aminophenol (AMAP) is the alleged non-toxic isomer of paracetamol. However toxicity to this compound does occur in some animal models. Overall the incidence of AMAP toxicity appears to be species-specific (Hadi et al., 2013). Consequently, we decided to see if we could see the difference between paracetamol and AMAP in the initial drug screens in this chapter using the *Xenopus* embryos. AMAP is discussed in more detail in **chapter 4**.

Table 3-1: A summary of the key mechanisms of action for drugs known to be associated with drug-induced toxicity.

Drug name	Therapeutic mechanism	Toxicity mechanism	Reference
Gentamicin	<p>Aminoglycoside antibiotic</p> <p>Bactericidal for Gram negative and some Gram-positive bacteria e.g. <i>Pseudomonas aeruginosa</i> and <i>Mycobacterium tuberculosis</i> respectively.</p> <p>Blocks the initiation of DNA synthesis by binding to the A site of 16s ribosomal RNA (rRNA) within the 30S subunit. This interferes with physiological ribosome-RNA interactions and transfer RNA specificity during translation and causes bacterial cell death.</p>	<p>Nephrotoxic and ototoxic</p> <p>Accumulates in the lysosomal and endosomal vacuoles in the epithelial cells of the proximal tubule. Gentamicin overloads the lysosomes and ruptures causing high concentrations of gentamicin and acid hydrolases to enter the cytoplasm. This disrupts cell structure and function causing non-oliguric renal failure.</p> <p>Gentamicin also causes the degeneration of hair cell death of the inner ear causing the loss of high and low frequency hearing. The mechanism for this is the interference with mitochondrial ribosomes, causing mitochondrial dysfunction and cell death.</p>	<p>(Begg and Barclay, 1995; Fourmy et al., 1996; Hutchin and Cortopassi, 1994; Mingeot-Leclercg and Tulkens, 1999; Silverblatt and Kuehn, 1979)</p>
Indomethacin	<p>NSAID</p> <p>Analgesic, antipyretic and anti-inflammatory drug.</p> <p>Nonselective inhibitor of COX-1/2 that blocks the synthesis of prostaglandins.</p>	<p>Gastrointestinal toxicity</p> <p>Parent drug specifically inhibits gastric prostaglandin synthesis. It also induces endoplasmic reticulum stress and mitochondrial stress,</p>	<p>(Boelsterli et al., 2013; Watanabe et al., 2011)</p>

		consequently exacerbating the site of inflammation and necrosis.	
Diclofenac	NSAID Analgesic, antipyretic and anti-inflammatory drug. Weak COX-2 selective.	Hepatotoxic The metabolites from oxidative reactions and phase II gluconide metabolite derivatives are involved in the generation of diclofenac-induced liver injury. The exact toxicity mechanism is unknown, however there is an involvement of mitochondrial dysfunction.	(Gómez-Lechón et al., 2003; Syed et al., 2016)
Doxorubicin	Anthracycline cytotoxic antibiotic Doxorubicin intercalates with the DNA and inhibits topoisomerase II activity consequently blocking DNA synthesis and cell replication, this induces cell death.	Cardiotoxic Doxorubicin can cause cumulative, dose-related cardiac damage through the generation of free radicals. Damaged cardiac tissue can cause dysrhythmias and lead to heart failure.	(Gu et al., 2015; Singal and Iliskovic, 1998)
Cisplatin	Anticancer alkylating-like agent Tumour cells tend to have insufficient DNA repair mechanisms. Cisplatin can covalently bind to DNA, cause intrastrand cross links and thus inhibit DNA synthesis and replication. This can trigger tumour cell death. It is thought	Nephrotoxic The nephrotoxicity associated with cisplatin is proportional to the dose. The high density of mitochondrial DNA in proximal tubular cells indicates this is why cisplatin-induced toxicity is particularly noticeable in the kidney.	(Miller et al., 2010; Wang and Lippard, 2005)

	mitochondrial DNA is more susceptible than nuclear DNA.		
Paracetamol	NSAID Analgesic and antipyretic but weak anti-inflammatory drug compared to other NSAIDs. It is often not classed as NSAID because it is a very weak COX inhibitor. The exact therapeutic mechanism for the analgesic effect is unknown but it could be due to an indirect action of the cannabinoid receptors (CB ₁).	Hepatotoxic The major metabolic pathway produces stable metabolites via sulfotransferase and glucuonyl transferase enzymes. However the minor metabolic pathway, catalyzed by CYP2E1, CYP1A2 and CYP3A4, generates the reactive metabolite NAPQI (N-acetyl-p-benzoquinone). If a dose greater than the recommended therapeutic dose is ingested (>4 g/day), this metabolite accumulates and can damage hepatocytes and instigate cell death through the generation of reactive oxygen species, stimulation of Ca ²⁺ -activated degradative enzymes and lipid peroxidation. NAPQI is particularly damaging when there is a reduction in the neutralising agent GSH (glutathione).	(Bertolini et al., 2006; McGill and Jaeschke, 2013)

Prior to the investigation into the use of *Xenopus* embryos towards the prediction drug-induced toxicity, we decided it was important to characterise the capabilities of the model. Drug metabolism can often play a crucial role in the generation of a drug-induced toxicity reaction. In humans, for the majority of drugs, the body alters the molecular structure of the parent compound administered with the aim to excrete the drug safely and quickly. The host organism can also affect the distribution of the drug through body compartments, so-called pharmacokinetics. However the body's reaction to a drug, under certain circumstances, is what leads to a drug-induced toxicity reaction. A drug associated with toxicity reactions is not inherently toxic itself, rather it is the way the body reacts to it that generates a toxicity reaction. For example the body can generate a metabolite that is reactive and responsible for the generation of drug-induced toxicity reactions, such is the case with paracetamol and its metabolite NAPQI (**Table 3-1** and **chapter 4**). The body can also favour the transport of a drug into a specific body compartment that can lead to detrimental accumulation for example cisplatin accumulation in proximal tubule epithelial cells results in nephrotoxicity. Environmental factors including age and diet can also influence the body's ability to safely excrete drugs. One famous example is that grapefruit reduces the expression of CYP3A4 in the gut (Bailey et al., 1998). Overall the way an organism reacts to a drug is important in determining an animal model that can predict drug-induced toxicity in humans.

Drug metabolism and the generation of chemically reactive metabolites (CRMs) are discussed in detail in **chapter 1**. CYP450 enzymes are a superfamily of haem proteins that have distinct but sometimes overlapping substrate specificities. Of 315 drugs tested, 57 % were predominantly cleared through the action of CYP450s in humans. The CYP450 isoenzyme that metabolised the most drugs was CYP3A4 (50 % of the drugs) then it was CYP2D6 (20 %), CYP2C9 and CYP2C19 (15 %) and <15 % included CYP2E1, CYP2A6 and CYP1A2 (Bertz and Granneman, 1997). CYP450 enzymes catalyse drug oxidation reactions via the mechanism summarised in **Figure 3-1**. The major enzyme involved in phase II drug metabolism is the uridine-5'-diphospho-glucuronyl transferase (UGT). The UGT superfamily consists of 22 proteins in humans, of which the UGT1A and UGT2B subfamilies are particularly involved in drug renal elimination (Rowland et al., 2013). The remaining key phase II enzymes are summarised in **Table 3-2**.

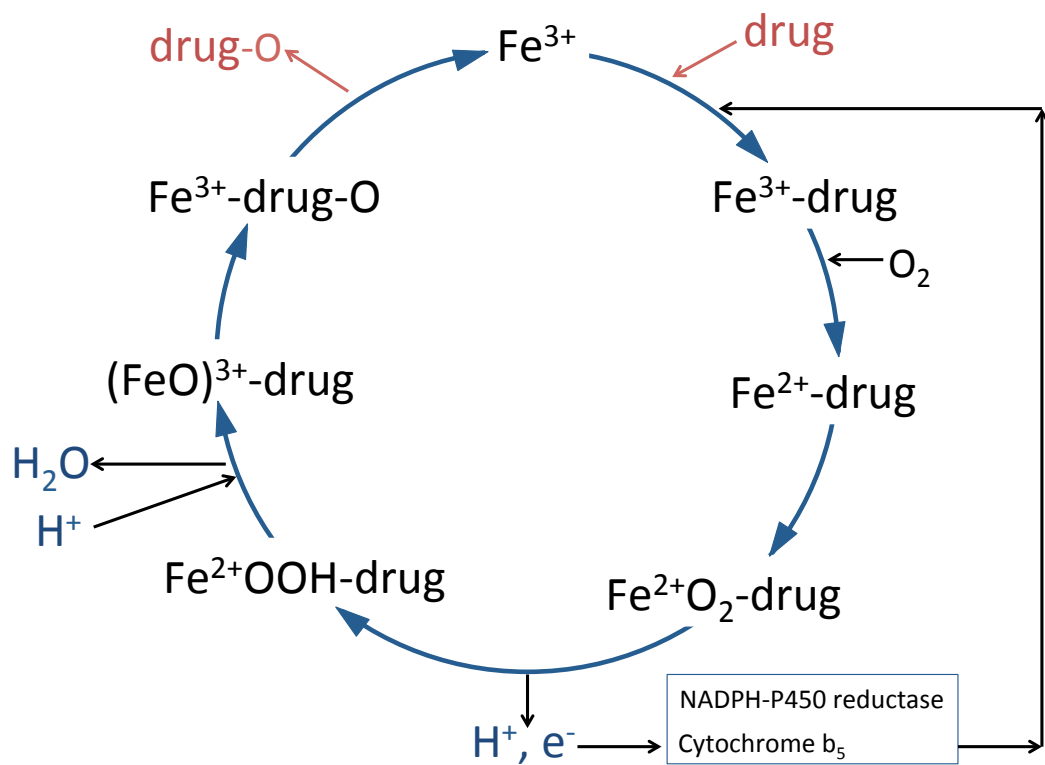


Figure 3-1: The monooxygenase CYP450 enzyme cycle.

Drugs that are metabolised by CYP450 enzymes undergo an oxidation reaction where they lose an electron and gain an oxygen atom. Iron is present in CYP450 enzyme in the ferric (Fe³⁺) or ferrous state (Fe²⁺). This figure is adapted from Rang *et al* (2016).

Table 3-2: Summary of the major phase II metabolism enzymes

Adapted from (Nassar et al., 2009)

Reaction	Conjugating agent	Enzyme	Target functional group
Glucuronidation	Uridine 5'-diphospho (UDP)-glucuronic acid	UDP-glucuronyl transferase (UGT)	-OH -COOH -NH ₂ -SH
Acetylation	Acetyl Coenzyme A	Acetyl transferase	-OH, -NH ₂
Amino acid conjugation	- Glycine - Glutamine, - Taurine	Acyl transferase	-COOH
Methylation	S-adenosyl-methionine	Methyl transferase	-OH, -NH ₂
Sulphation	3'-phosphoadenosine-5'-phosphosulphate (PAPS)	Sulphotransferase	-OH, -NH ₂
Glutathione conjugation	Glutathione	Glutathione-S-transferase	Electrophiles

3.2 Aim

To establish the appropriate stages of *Xenopus laevis* embryonic development for the investigation of *Xenopus* as a drug-induced toxicity model.

3.3 Hypothesis

From stage 38 to stage 45, the *Xenopus laevis* embryo is sufficient for the detection of drug-induced toxicity.

3.4 Results

3.4.1 Initial drug dose response screens

3.4.1.1 1. Stage 15-stage 38 *Xenopus laevis* embryos

In the drug discovery screens I generally tested compounds between stages 15 and 38 as this correlates with major organogenesis in the embryo. Stage 15 (18 hpf at 23°C) *Xenopus* embryos were treated with 0.78-100 µM of drug and harvested at stage 38 (36 h incubation). The embryos that survived to the age of stage 38 were photographed, and divided into phenotype groups. Embryos treated with paracetamol (n=5) developed an increasing variation of phenotypes that deviated from the normal stage 38 phenotype ("wildtype") (**Figures 3-2A and 3-3A**). In particular, the frequency of the developmentally delayed phenotype (orange bar) correlated with paracetamol concentration 12.5-100 µM. For embryos treated with the alleged non-toxic paracetamol isomer AMAP (n=3), the most frequent phenotype was the wildtype (blue bar) (**Figures 3-2B and 3-3B**). The incidence of an developmentally delayed embryo was less frequent in the embryos treated with AMAP compared to paracetamol. Gentamicin-treated embryos produced variable phenotypes in all of the concentration groups (n=4) (**Figures 3-2C and 3-3C**). The incidence of any particular phenotype did not correlate with the concentration of gentamicin the embryos received. In humans, tobramycin is the less nephrotoxic drug of the same class as gentamicin (the aminoglycosides). In the embryos treated with tobramycin the over incidence of abnormal phenotypes (not wildtype) was less compared to the gentamicin-treated embryos (n=2) (**Figures 3-2D and 3-3D**). The wildtype phenotype negatively correlates with 12.5-100 µM doxorubicin treatment (n=3) (**Figures 3-2E and 3-3E**). For embryos treated with indomethacin, there was not a concentration-dependent abnormal phenotype (n=3) (**Figures 3-2F and 3-3F**). The frequency of the wildtype phenotype decreases for embryos treated with 25-100 µM indomethacin. Cisplatin induced a variety of abnormal phenotypes including developmentally delayed, bent tail (pink bar), shortened body length (black bar) and oedema (green bar) in embryos treated with 25-100 µM concentrations (n=3) (**Figures 3-2G and 3-3G**). The wildtype phenotype frequency decreased in embryos treated with the same cisplatin concentration range. Finally, for embryos treated with diclofenac the overall incidence of any phenotype was significantly reduced with 50-100 µM concentrations (n=2) (**Figures 3-2H and 3-3H**). The absence of phenotypes at the higher concentrations correlates with the low percentage of embryos photographed. Only 40 % and 0 % of the embryos treated with 50 and 100 µM diclofenac respectively survived to be photographed. The most common abnormal phenotype observed in embryos treated with diclofenac is developmental delay.

A. Paracetamol

0.78 μM		
<p>wildtype 96 % 1 mm</p>		
1.56 μM		
3.13 μM		
6.25 μM		
12.5 μM		
25 μM		

50 μ M



100 μ M



B. AMAP

0.78 μM

1.56 μM

3.13 μM

6.25 μM

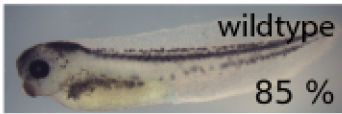
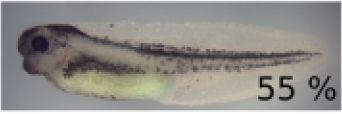
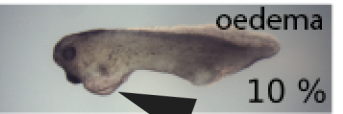
12.5 μM

25 μM

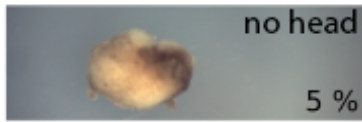
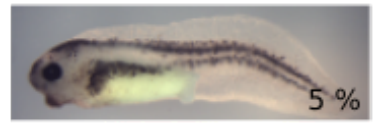
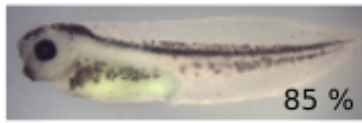
50 μM

100 μM

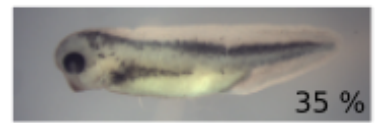

C. Gentamicin

0.78 μM		
 <p>wildtype 85 %</p>	 <p>developmentally delayed 5 %</p>	 <p>shortened body 5 %</p>
 <p>abnormal eye 5 %</p>		
1.56 μM		
 <p>55 %</p>	 <p>10 %</p>	 <p>oedema 10 %</p>
 <p>bent tail 5 %</p>	 <p>5 %</p>	
3.13 μM		
 <p>80 %</p>	 <p>15 %</p>	 <p>5 %</p>
6.25 μM		
 <p>80 %</p>	 <p>5 %</p>	 <p>5 %</p>
 <p>5 %</p>		
12.5 μM		
 <p>80 %</p>	 <p>10 %</p>	 <p>5 %</p>
25 μM		
 <p>70 %</p>	 <p>20 %</p>	 <p>5 %</p>

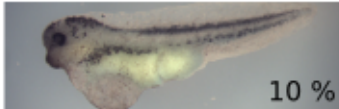
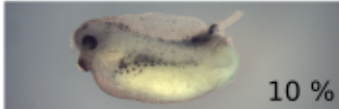
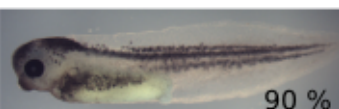
50 μ M



100 μ M



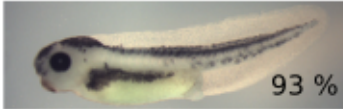
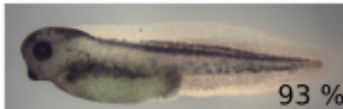
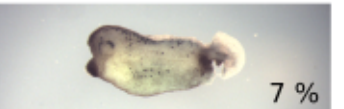
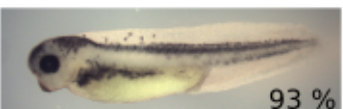
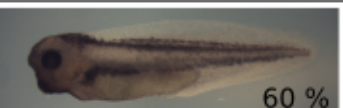
D. Tobramycin

0.78 μM		
 60 %	 10 %	 20 %
 10 %		
1.56 μM		
 100 %		
3.13 μM		
 70 %	 10 %	 20 %
6.25 μM		
 60 %	 10 %	 10 %
 10 %	 10 %	
12.5 μM		
 100 %		
25 μM		
 90 %	 10 %	
50 μM		
 100 %		

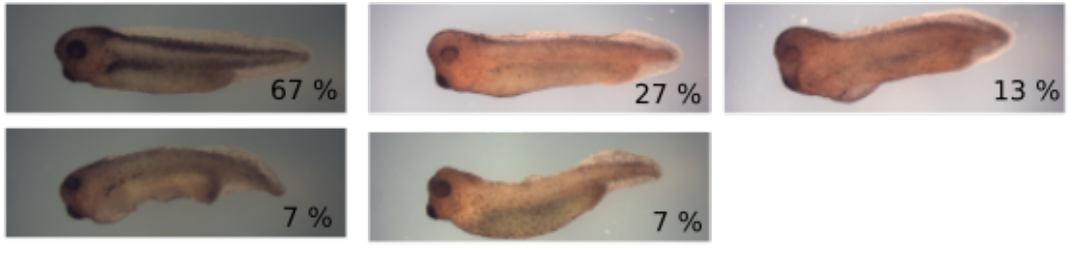
100 μ M



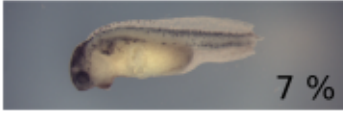
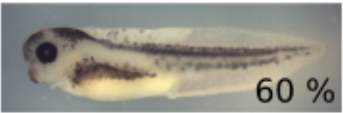
E. Doxorubicin

0.78 μM		
 80 %	 7 %	 7 %
1.56 μM		
 93 %	 7 %	
3.13 μM		
 93 %	 7 %	
6.25 μM		
 40 %	 7 %	 20 %
 7 %	 7 %	
12.5 μM		
 93 %	 7 %	
25 μM		
 67 %	 33 %	
50 μM		
 60 %	 13 %	 7 %
 13 %		

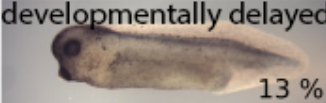
100 μ M



F. Indomethacin

0.78 μM		
 47 %	 7 %	 7 %
 7 %		
1.56 μM		
 53 %	 7 %	 7 %
3.13 μM		
 40 %	 20 %	 7 %
6.25 μM		
 60 %		
12.5 μM		
 60 %	 7 %	
25 μM		
 67 %	 13 %	 7 %
50 μM		
 40 %	 27 %	 20 %
 7 %	 7 %	

G. Cisplatin

0.78 μM		
 wildtype 67 %	 developmentally delayed 13 %	 20 %
1.56 μM		
 87 %	 7 %	 7 %
3.13 μM		
 87 %	 7 %	 7 %
6.25 μM		
 73 %	 20 %	 7 %
12.5 μM		
 60 %	 27 %	
25 μM		
 87 %	 13 %	
50 μM		
 53 %	 7 %	 27 %
 7 %	 7 %	
100 μM		
 47 %	 20 %	 7 %
 13 %	 7 %	

H. Diclofenac

0.78 μM			
	100 %		
1.56 μM			
		80 % 20 %	
3.13 μM			
			50 % 40 % 10 %
6.25 μM			
		50 % 50 %	
12.5 μM			
			40 % 10 % 40 %
25 μM			
			40 % 10 % 20 %
	30 %		
50 μM			
			10 % 10 % 10 %
	10 %		

Figure 3-2: Stage 15 – stage 38 dose-response 0.78-100 μ M drug screens.

Stage 15 *Xenopus laevis* embryos were incubated for 36 h with paracetamol (A), AMAP (B), gentamicin (C), tobramycin (D), doxorubicin (E), indomethacin (F), cisplatin (G) or diclofenac (H). Photographs were taken of the embryos that survived to age of stage 38 and embryos that displayed the same phenotype were grouped together, a representative embryo of the phenotype is depicted in this figure. A representation of each of the phenotypes has been labelled. The phenotypes included wildtype, no head, oedema, bent tail, developmentally delayed, shortened body and abnormal eye. The percentage of embryos that produced this phenotype out of the total embryos tested is indicated.

3.4.1.2 2. Stage 38-stage 45 *Xenopus laevis* embryos

For these screens, stage 38 embryos were incubated with 0.78-100 μ M drug for 72 h. The surviving stage 45 embryos were photographed and I noted the incidence of abnormal and wildtype phenotypes. Compared to the stage 15-stage 38 screens, the overall incidence of abnormal phenotypes in the stage 45 embryos was lower due to organogenesis being near completion. The wildtype phenotype was the most popular observed phenotype. For embryos treated with paracetamol (**Figures 3-4A and 3-5A**) and gentamicin (**Figures 3-4B and 3-5B**), the second most common phenotype was oedema. The frequency of this phenotype does not correlate with drug concentration for both paracetamol and gentamicin. There are less abnormal phenotypes in embryos treated with tobramycin compared to gentamicin (n=2) (**Figures 3-4C and 3-5C**). The wildtype phenotype frequency decreases with increasing doxorubicin concentration from 25-100 μ M (n=3) (**Figures 3-4D and 3-5D**). The oedema phenotype for doxorubicin-treated embryos occurs throughout the concentration spectrum. Embryos treated with 100 μ M doxorubicin produced developmentally delayed and shortened body length phenotypes. The embryos treated with 100 μ M indomethacin did not survive (**Figures 3-4E and 3-5E**). The wildtype phenotype was the most popular for indomethacin-treated embryos, and the incidence was not concentration-dependent for the 0.78-25 μ M indomethacin treatment groups (n=1). However for embryos treated with 50 μ M indomethacin, the most common phenotype observed was a shortened body length. At this concentration the embryos also produced a bent tail phenotype. All stage 38 embryos treated with a concentration of cisplatin within the range 0.78-100 μ M, produced a wildtype phenotype at stage 45 (n=1) (**Figures 3-4F and 3-5F**). For diclofenac, the wildtype phenotype was only observed in embryos treated from 0.78-12.5 μ M (n=1) (**Figures 3-4G and 3-5G**). The only phenotype observed in embryos in the 25 and 50 μ M diclofenac treatment group was a shortened body length. None of the 100 μ M diclofenac-treated embryos survived to the age of stage 45 to be photographed. Stage 38 embryos that were treated with a concentration of

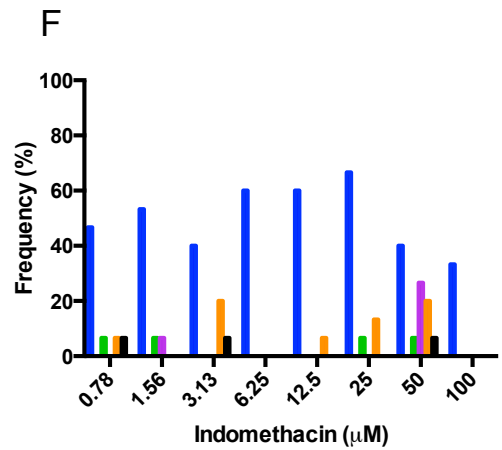
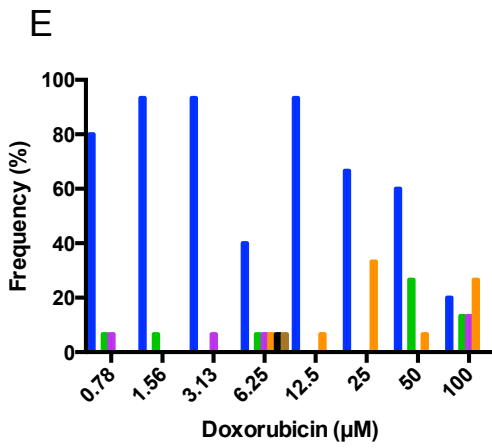
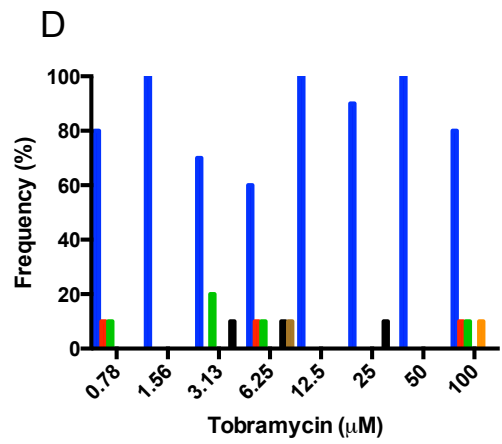
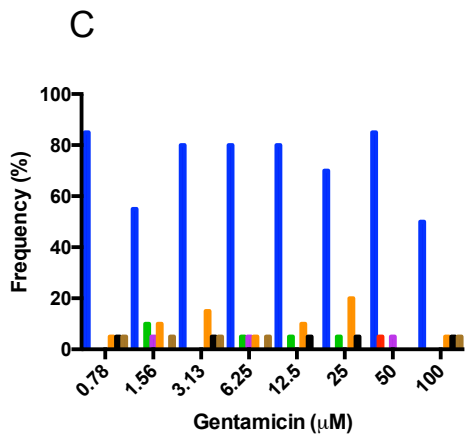
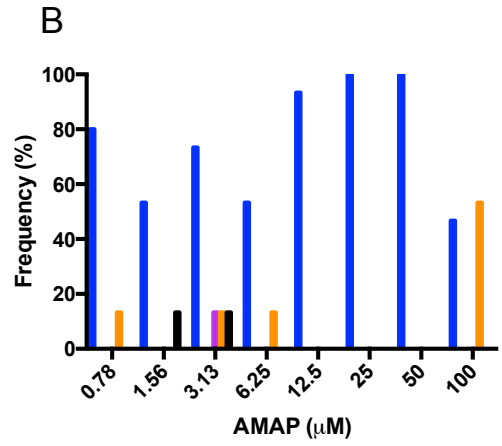
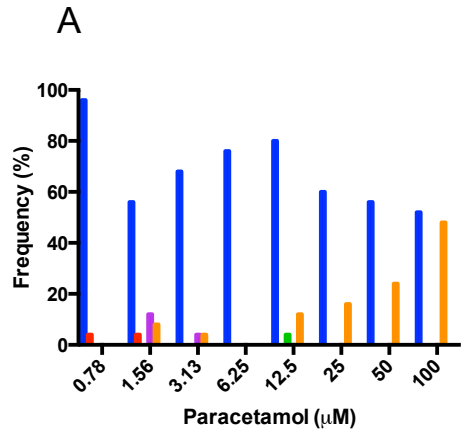
daunorubicin within the range 0.78-100 μ M all displayed wildtype phenotypes (n=1) (**Figures 3-4H and 3-5H**).

3.4.2 Characterisation of *Xenopus* embryo drug metabolism machinery

In all the future experiments for the investigation of the use of *Xenopus* embryos for the prediction of drug toxicity, I will use embryos aged stage 38 until the age of stage 45. I isolated RNA from whole stage 38 and stage 45 embryos and looked for the expression of major enzymes that are involved in drug metabolism in humans. The *Xenopus* CYP2E1, CYP2D6 and CYP3A4 isoenzymes were expressed in stage 38 and stage 45 embryos (n=5) (**Figure 3-6A**). The *Xenopus* gene that is the equivalent of the human KCNH2 gene was also present in both stage 38 and stage 45 embryos (**Figure 3-6A**). The KCNH2 gene encodes the alpha subunit of the potassium ion channel known as the hERG channel. The hERG channel is associated with a significant amount of drug-induced cardiotoxicity reactions in humans. Embryos that expressed the 3 CYP450 isoforms we looked for, also expressed the major enzymes that are involved with human phase II drug metabolism (**Figure 3-6B**). In particular, I looked for the major phase II enzymes that are important for paracetamol metabolism including the glutathione S-transferases (GSTs): GSTP1, GSTT1 and GSTM1. We measured the presence of sulphotransferase enzymes SULT1A1 and SULT2A1. And finally, I looked for UGT1A6 and UGT1A1, which are the major UDP-glucuronosyl-transferase enzymes that produce paracetamol-glucuronide conjugates. For these phase II enzymes I used 2 sets of primers designed for 2 different regions of the *Xenopus laevis* gene. Overall, all of these phase II enzymes were expressed in RNA isolated from whole stage 38 and stage 45 embryos (n=5).

3.4.3 Atlas of stage 45 *Xenopus laevis*

To our knowledge, there is not an existing atlas for *Xenopus laevis* embryos. Consequently, I decided to produce an atlas to help identify the structures within the embryos in future experiments. Untreated stage 45 embryos were sectioned transversely (**Figure 3-7**) and along the sagittal plane (**Figure 3-8**) (n=10). For the transverse sections, I sectioned from anterior to posterior until the end of the gastrointestinal region. This is because that is the area of the organs I am interested in for hepatotoxicity and cardiotoxicity in the future experiments of this projects. In the sagittal sections of the stage 45 embryos one can clearly see the length of the whole embryo.



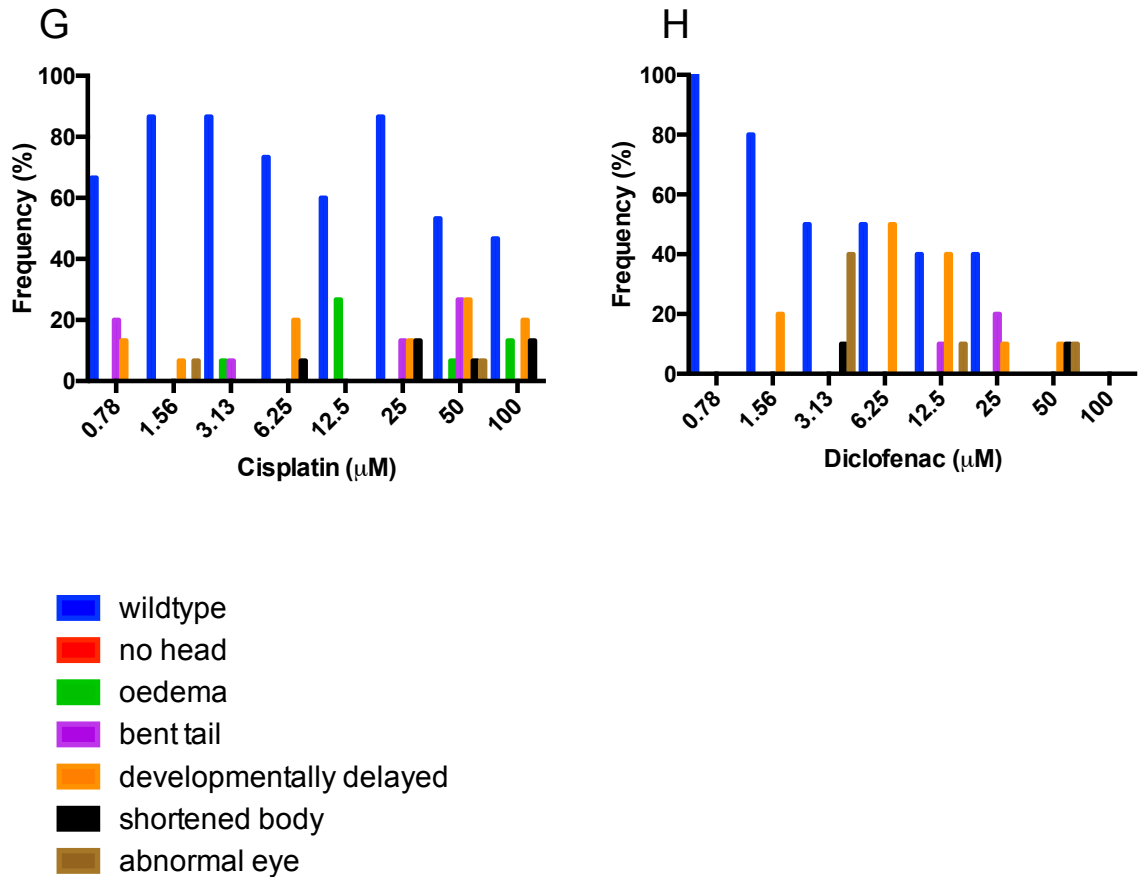
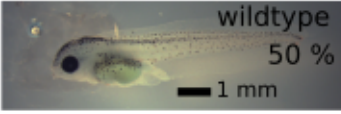


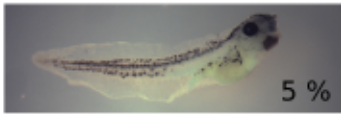
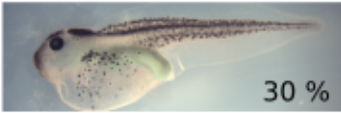
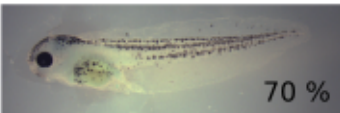
Figure 3-3: Incidence of phenotypes for the stage 15 to stage 38 screen.

The frequency of phenotypes observed after a 36 h 0.78-100 μM drug incubation in the stage 15-stage 38 screens (**Figure 3-2**) were plotted as a percentage of the total embryos tested for that drug. The stage 15 embryos were treated with paracetamol (A), AMAP (B), gentamicin (C), tobramycin (D), doxorubicin (E), indomethacin (F), cisplatin (G) or diclofenac (H). The wildtype phenotype (blue bar) indicates the phenotype is that of an untreated stage 15 that is incubated for 36 h.

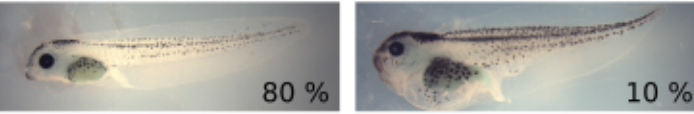
A. Paracetamol

0.78 μM		
 <p>wildtype 50 % 1 mm</p>	 <p>oedema 20 %</p>	 <p>30 %</p>
1.56 μM		
 <p>60 %</p>	 <p>30 %</p>	
3.13 μM		
 <p>70 %</p>	 <p>30 %</p>	
6.25 μM		
 <p>100 %</p>		
12.5 μM		
 <p>70 %</p>		
25 μM		
 <p>30 %</p>		
50 μM		
 <p>50 %</p>	 <p>50 %</p>	
100 μM		
 <p>70 %</p>	 <p>30 %</p>	

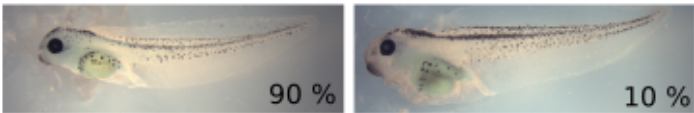
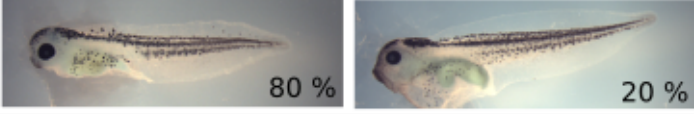
B. Gentamicin

0.78 μM		
 <p>wildtype 75 %</p>	 <p>oedema 5 %</p>	 <p>5 %</p>
1.56 μM		
 <p>70 %</p>	 <p>30 %</p>	
3.13 μM		
 <p>65 %</p>	 <p>35 %</p>	
6.25 μM		
 <p>75 %</p>	 <p>25 %</p>	
12.5 μM		
 <p>45 %</p>	 <p>5 %</p>	 <p>25 %</p>
25 μM		
 <p>70 %</p>	 <p>25 %</p>	
50 μM		
 <p>85 %</p>	 <p>15 %</p>	
100 μM		
 <p>70 %</p>	 <p>5 %</p>	 <p>25 %</p>

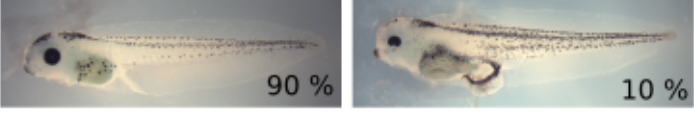
C. Tobramycin

0.78 μM

1.56 μM

3.13 μM

6.25 μM

12.5 μM

25 μM

50 μM

100 μM


D. Doxorubicin

0.78 μM		
 <p>wildtype 87 %</p>	 <p>oedema 13 %</p>	
1.56 μM		
 <p>80 %</p>	 <p>13 %</p>	
3.13 μM		
 <p>80 %</p>	 <p>20 %</p>	
6.25 μM		
 <p>73 %</p>	 <p>27 %</p>	
12.5 μM		
 <p>87 %</p>	 <p>13 %</p>	
25 μM		
 <p>100 %</p>		
50 μM		
 <p>80 %</p>	 <p>13 %</p>	
100 μM		
 <p>40 %</p>	 <p>20 %</p>	 <p>13 %</p>

E. Indomethacin

0.78 μM	
	
1.56 μM	
	
3.13 μM	
	
6.25 μM	
	
12.5 μM	
	
25 μM	
	
50 μM	
	

F. Cisplatin

0.78 μM
 wildtype 100 %
1.56 μM
 100 %
3.13 μM
 80 %
6.25 μM
 100 %
12.5 μM
 100 %
25 μM
 100 %
50 μM
 100 %
100 μM
 100 %

G. Diclofenac

0.78 μM

1.56 μM

3.13 μM

6.25 μM

12.5 μM
 
25 μM

50 μM


H. Daunorubicin

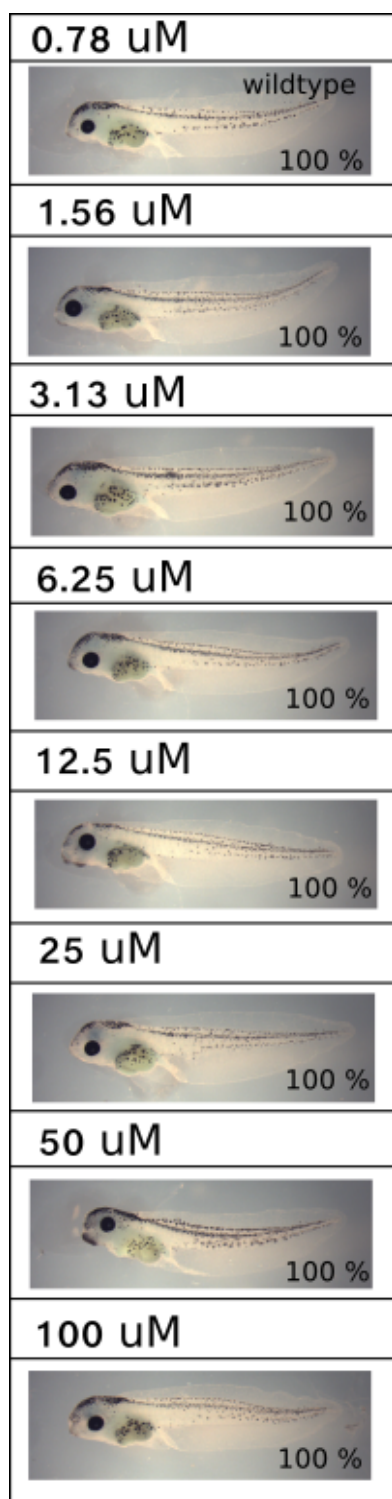
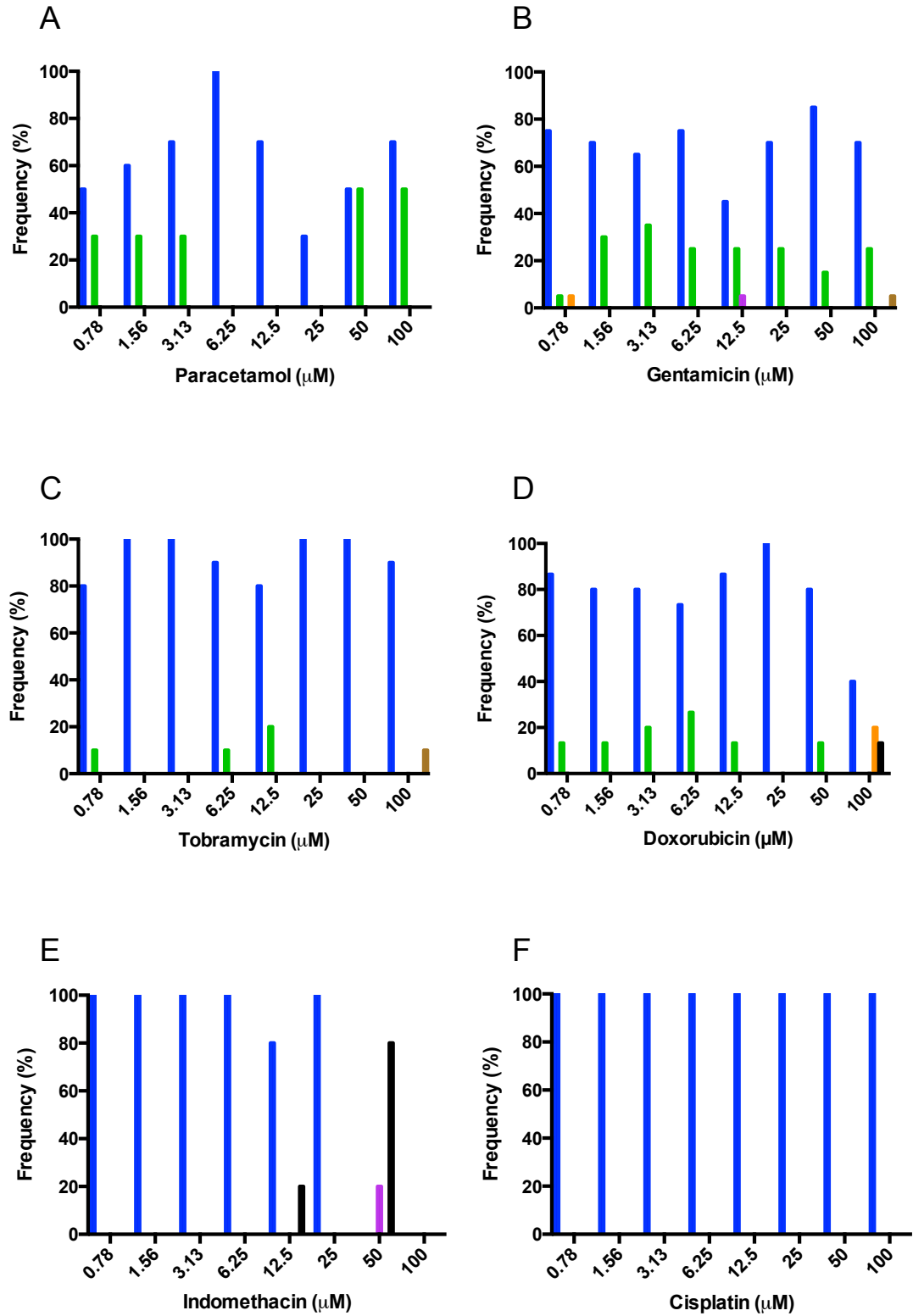


Figure 3-4: Stage 38 – stage 45 dose-response 0.78-100 μ M drug screens.

Stage 38 *Xenopus laevis* embryos were incubated for 72 h with paracetamol (A), gentamicin (B), tobramycin (C), doxorubicin (D), indomethacin (E), cisplatin (F), diclofenac (G) or daunorubicin (H). Photographs were taken of the embryos that survived to age of stage 45 and embryos that displayed the same phenotype were grouped together, a representative embryo of the phenotype is depicted in this figure. A representation of each

of the phenotypes has been labelled. The phenotypes included wildtype, no head, oedema, bent tail, developmentally delayed, shortened body length and abnormal eye. The percentage of embryos that produced this phenotype out of the total embryos tested is indicated.



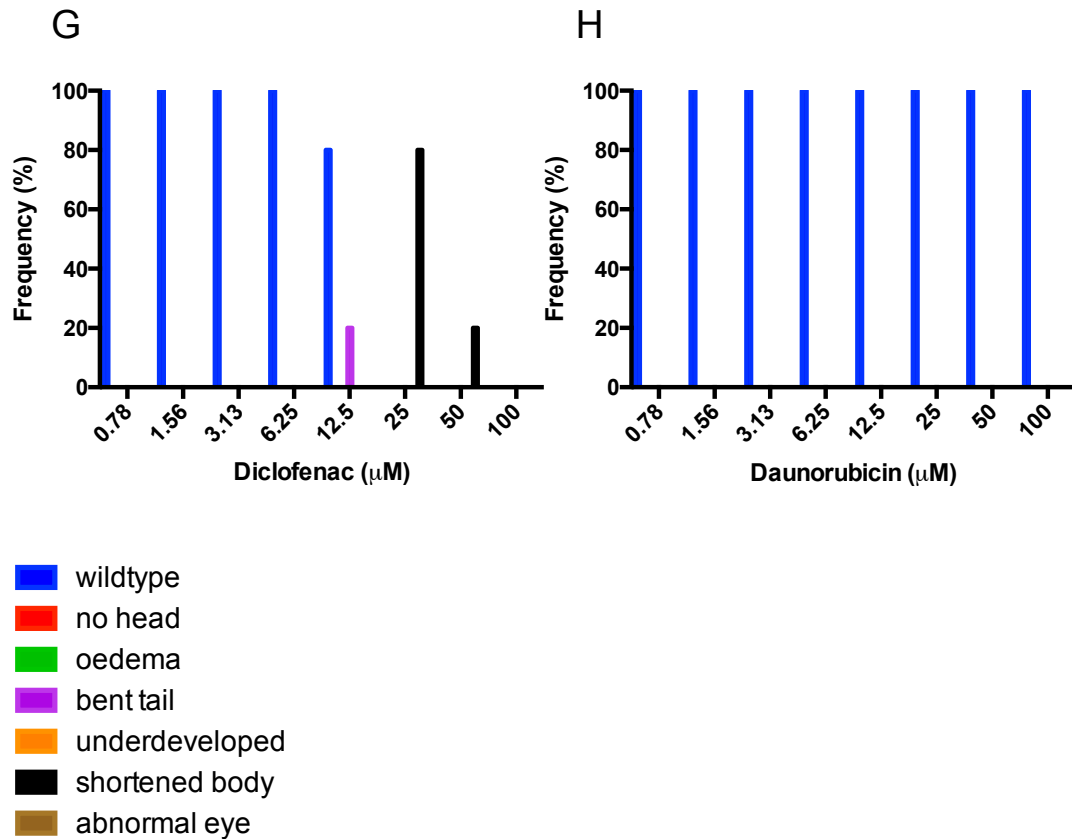
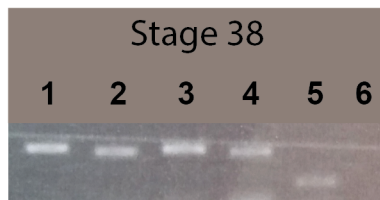


Figure 3-5: Incidence of phenotypes for the stage 38 to stage 45 screen.

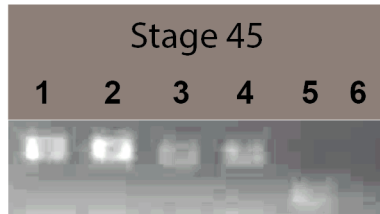
The frequency of phenotypes observed after a 72 h 0.78-100 μM drug incubation in the stage 38-stage 45 screens (**Figure 3-4**) were plotted as a percentage of the total embryos tested for that drug. The stage 38 embryos were treated with paracetamol (A), gentamicin (B), tobramycin (C), doxorubicin (D), indomethacin (E), cisplatin (F), diclofenac (G) or daunorubicin (H). The wildtype phenotype (blue bar) indicates the phenotype is that of an untreated stage 45 that is incubated for 72 h.

A i

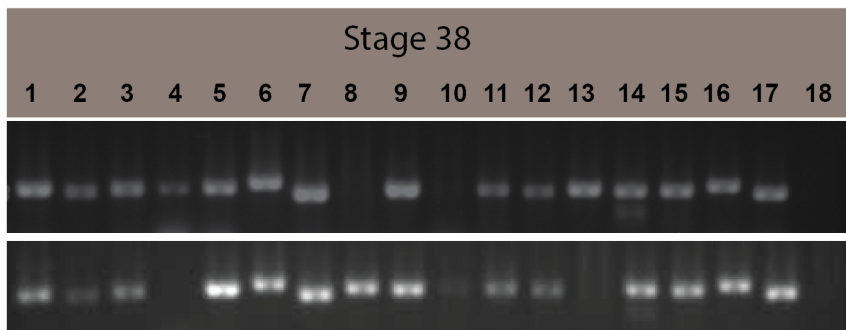


- 1 CYP2E1
- 2 CYP2D6
- 3 CYP3A4
- 4 KCNH2
- 5 H4
- 6 W

ii



B i



- 1 CYP2E1
- 2 CYP2D6
- 3 CYP3A4

- 4 GSTP1
- 5

- 6 GSTT1
- 7

- 8 GSTM1
- 9

- 10 SULT1A1
- 11

- 12 SULT2A1
- 13

- 14 UGT1A6
- 15

- 16 UGT1A1
- 17

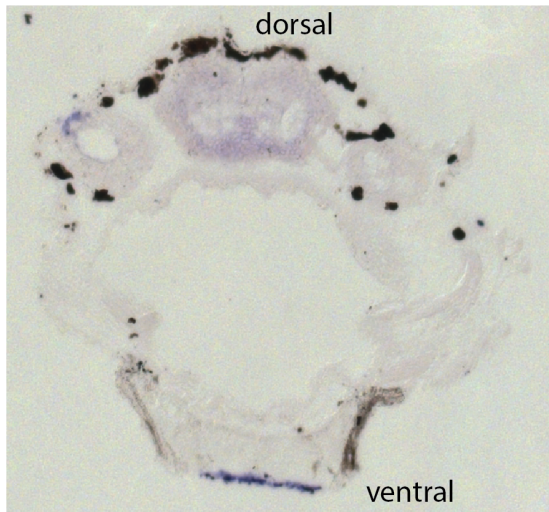
- 18 W

Figure 3-6: RT-PCR for drug metabolism enzymes in untreated *Xenopus laevis* embryos.

The expression of major drug metabolism enzymes in RNA isolated from whole stage 38 (i) and stage 45 (ii) untreated embryos. For the phase I enzymes (A) 1 representative gel

is displayed (n=5). Histone 4 (H4) was the positive control, water (W) was the negative control. For the phase II enzymes (B) 2 representative gels are shown for each stage (n=5). For the phase II enzymes, 2 primer sets designed for different sections of the gene are displayed, for example, lanes 4 and 5 are both amplicons for GSTP1 but using 2 different primer sets. The CYP450 enzymes were the positive controls and the negative control was water (W).

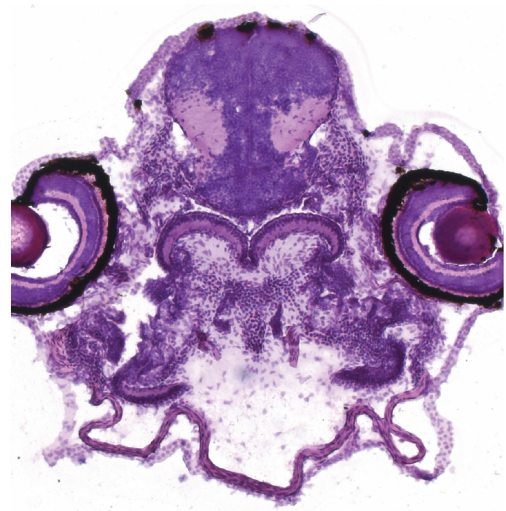
Ai



Bi



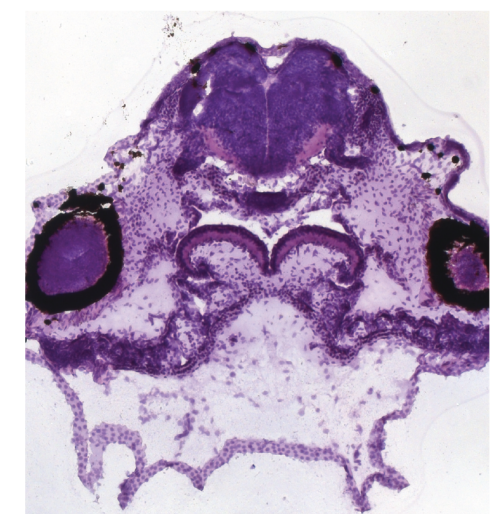
ii



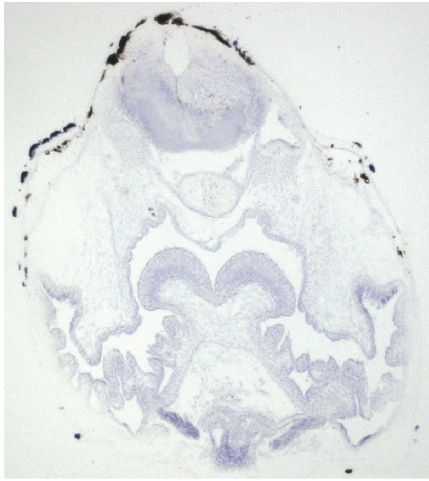
Ci



ii



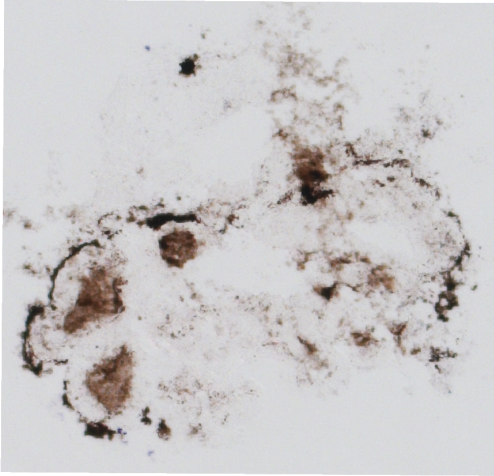
D i



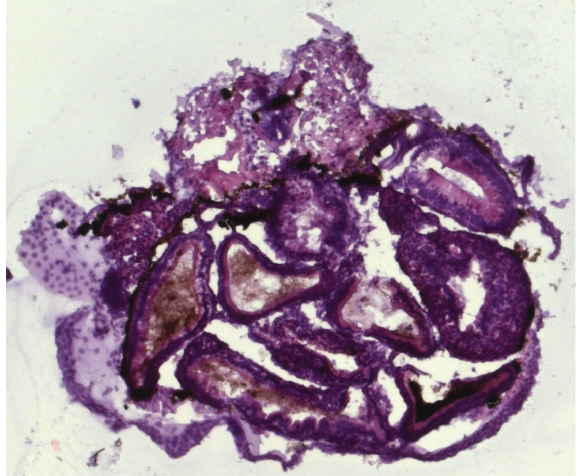
ii



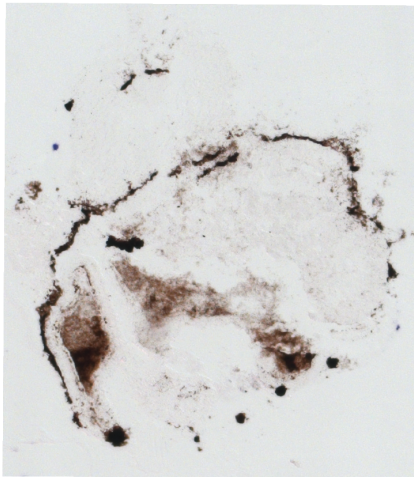
E i



ii



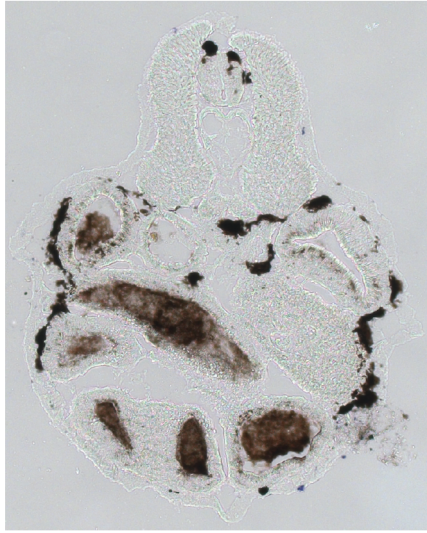
F i



ii



G i



ii



H i



ii



J i



ii



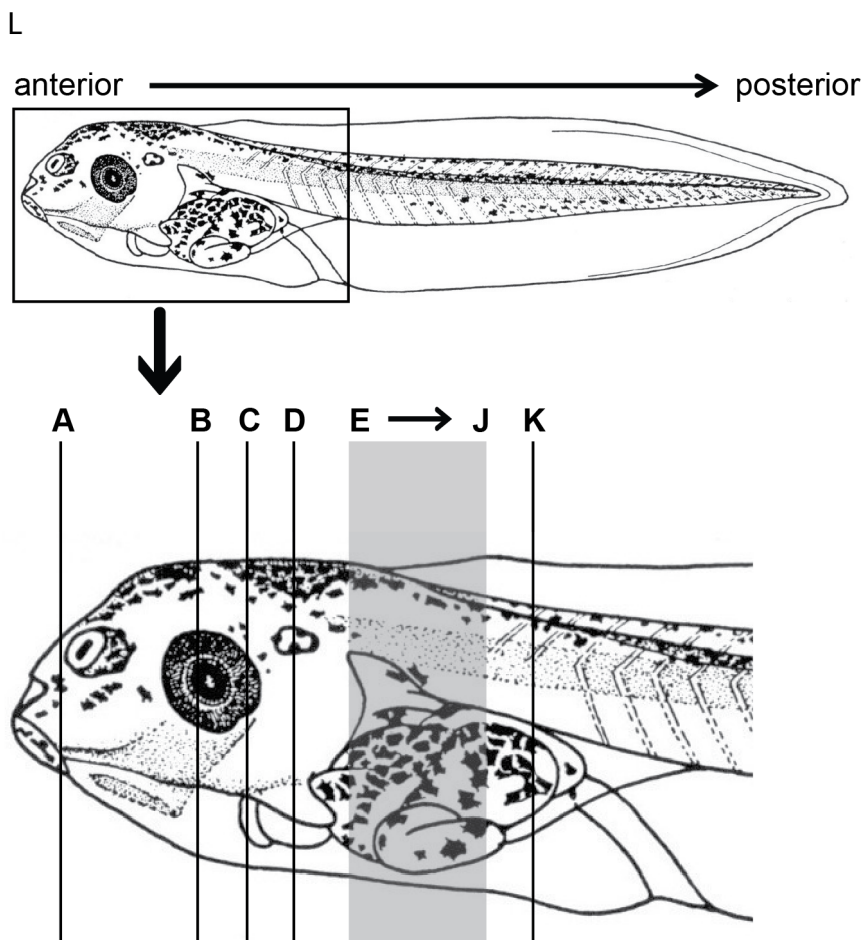
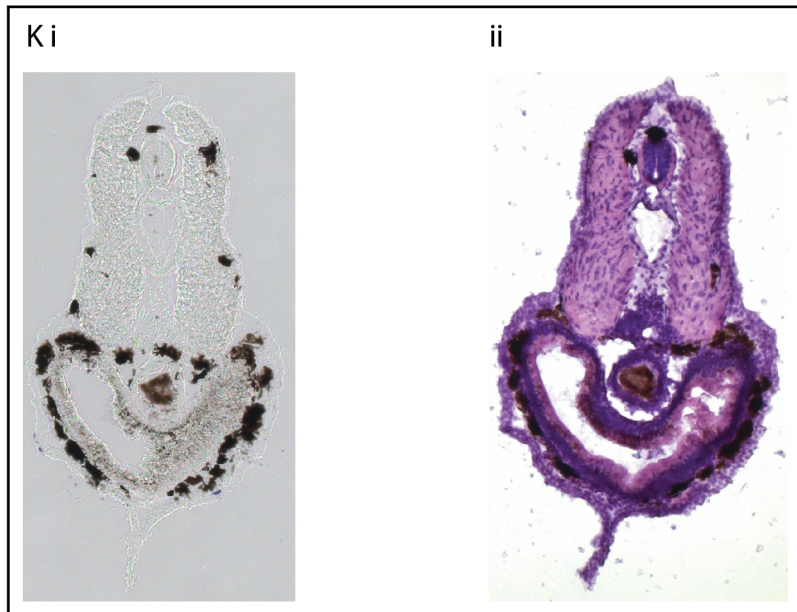
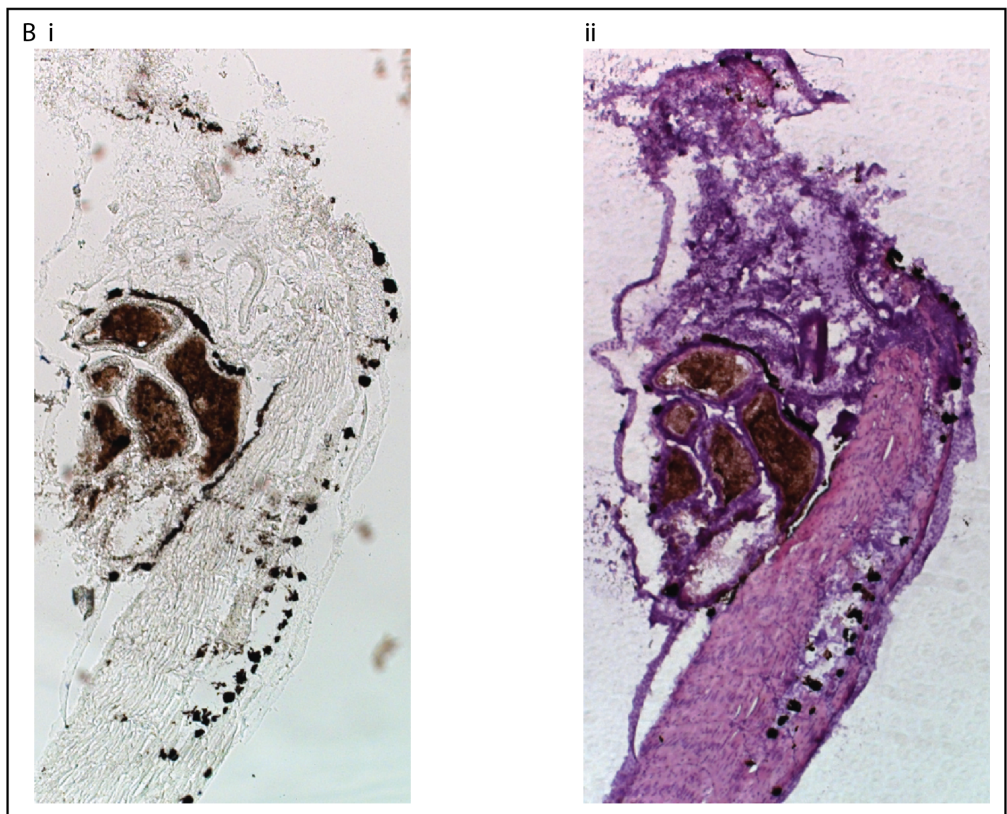
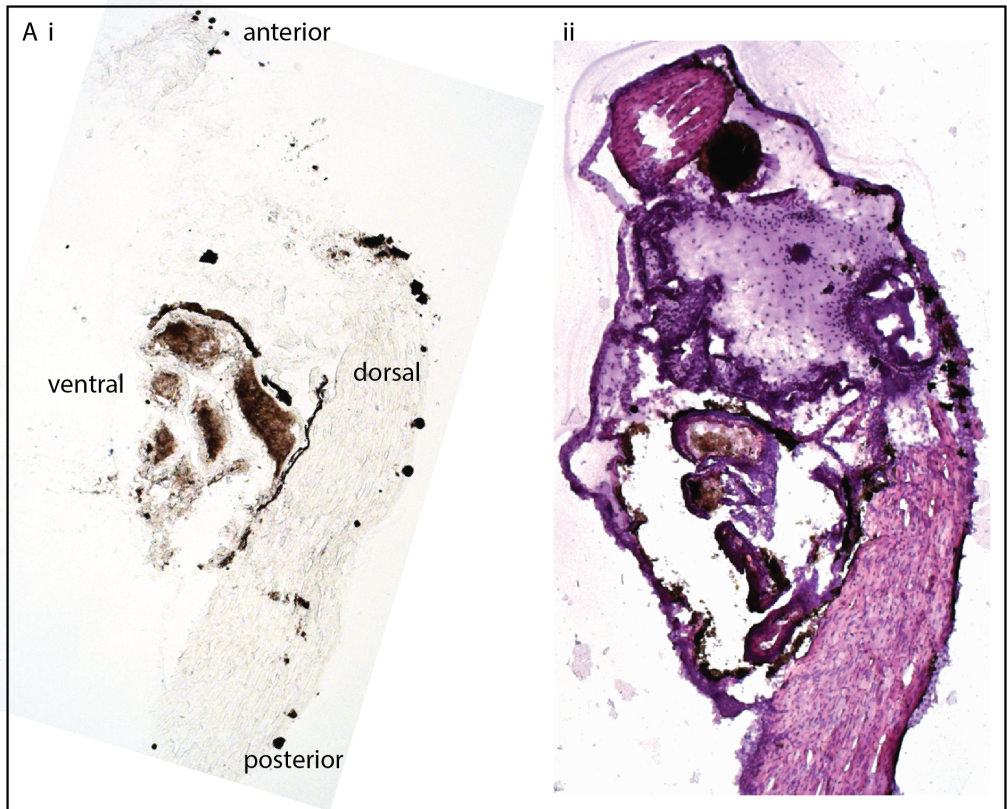
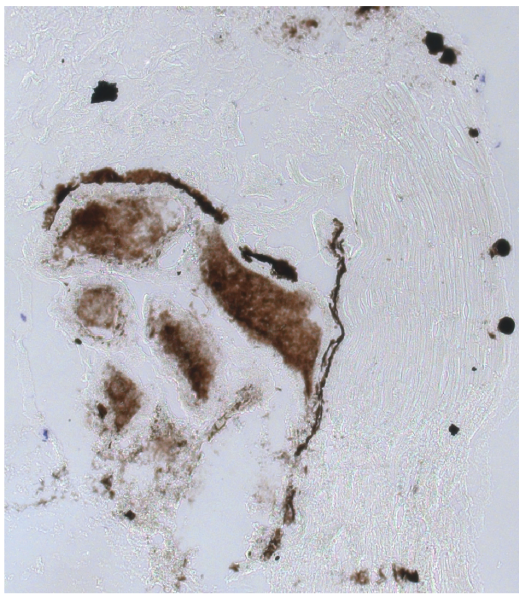


Figure 3-7: Transverse sections of untreated stage 45 *Xenopus laevis* embryos.

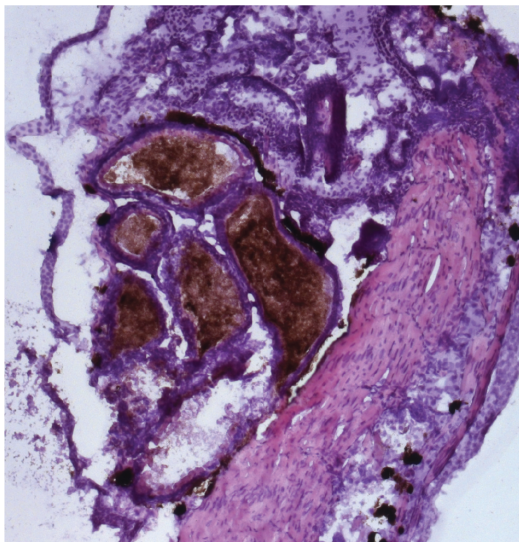
Transverse sections (15 μm) arranged in order from anterior to posterior (A to K) as shown in (L). The sections were either left without stain (i) or stained with H&E (ii).



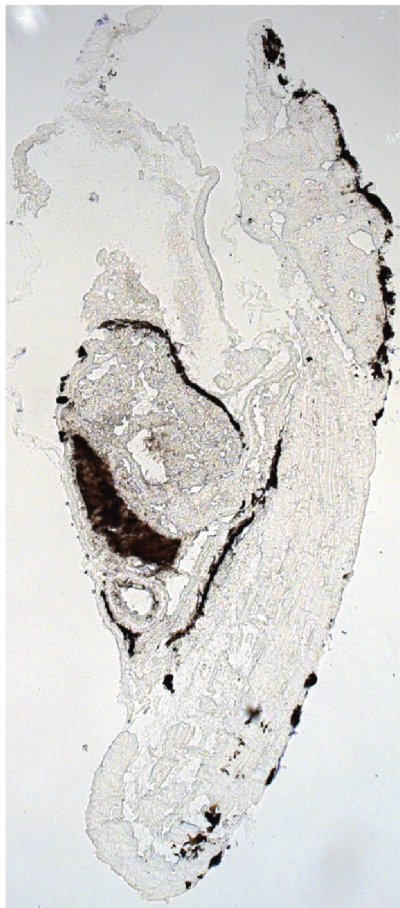
Ci



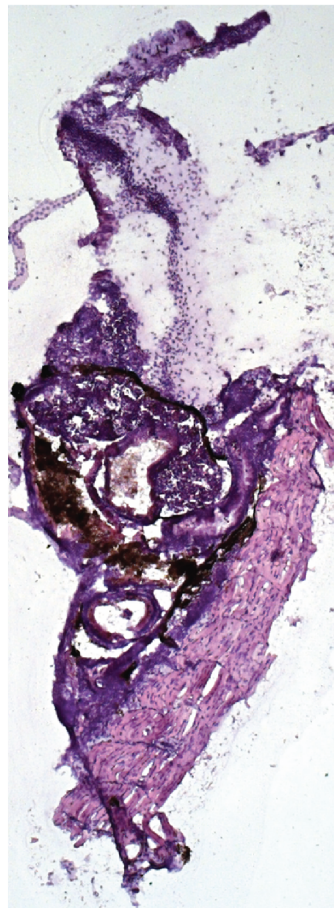
ii

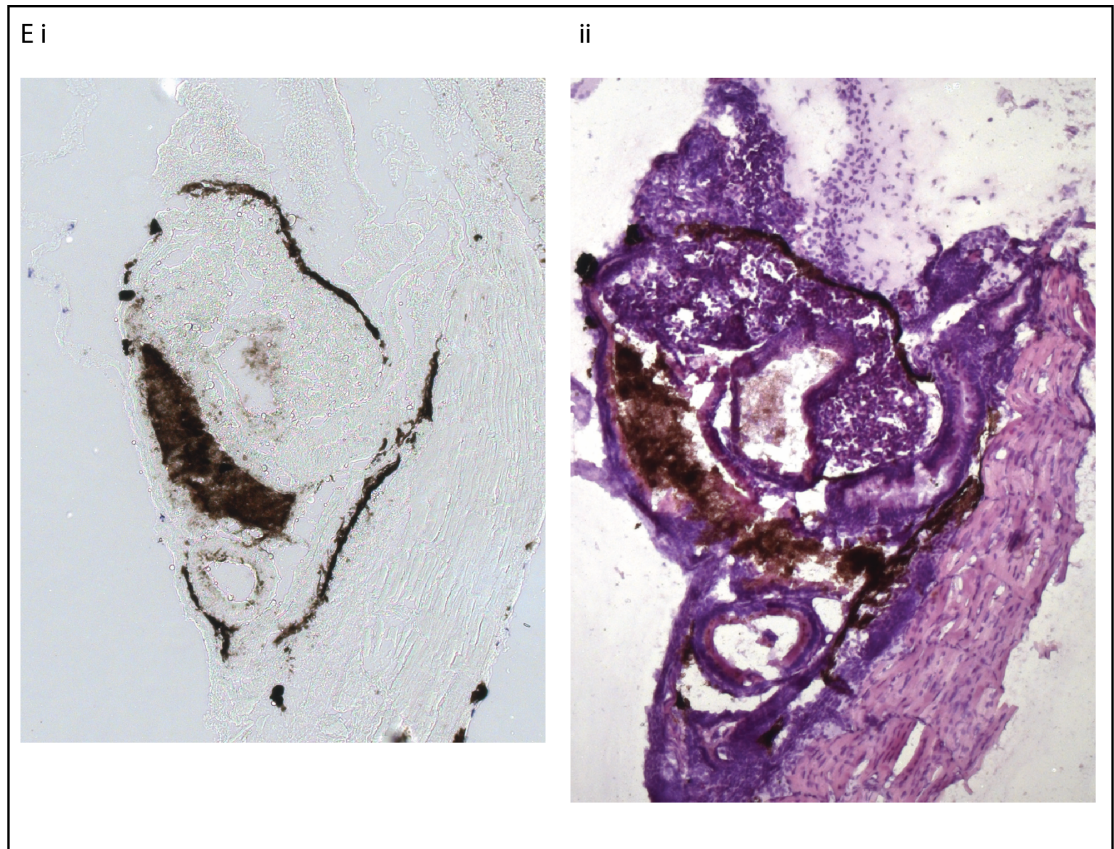


Di



ii





F

ventral view

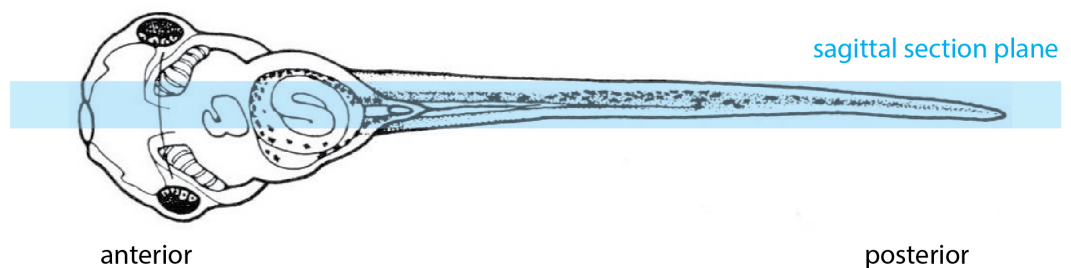


Figure 3-8: Sagittal sections of untreated stage 45 *Xenopus laevis* embryos.

Sagittal sections (15 μ m) taken from the region shown in (F). The sections were either left without stain (i) or stained with H&E (ii). Sections from approximately the same area are grouped together, for example, the sections in (A) are almost the same but with and without stain counterparts.

3.5 Discussion

In our laboratory, *Xenopus* embryos have been used for chemical and drug screens before (Tomlinson et al., 2012; Wheeler and Brändli, 2009; Wheeler and Liu, 2012). Therefore, we decided to test a known assay called the FETAX, which measures the effect of drugs on embryonic development as previously mentioned in **chapter 1**. The Frog Embryo Teratogenesis Assay *Xenopus* (FETAX) uses *Xenopus* embryos up to the age of stage 38 and it is thought to analyse small molecule teratogenicity. However, in terms of drugs, a teratogen is an agent that can disturb the development of the embryo or foetus. Teratogens halt the pregnancy or produce a congenital malformation (a birth defect). Classes of teratogens include radiation, maternal infections, chemicals, and drugs. The changes seen in the stage 15 to stage 38 screens I have measured in this project do not reflect teratogenicity, but rather they demonstrate developmental changes. To begin with, I decided to use the same concentration range for all the drugs, 0.78-100 μM . To perform the FETAX, I used stage 15 *Xenopus laevis* embryos and incubated them at 23°C with the drugs for 36 h (**Figure 3-2**). Typically, an untreated stage 15 embryo develops to the age of stage 38 after a 36 h incubation period at 23°C. Embryos that had the same phenotype were grouped together and we took a photograph of one of them, to represent the group. Each drug tested in the stage 15 to stage 38 screens produced at least 3 different abnormal phenotypes. There was not an obvious phenotype that indicated the toxicity of the drug. For example, the drugs associated with hepatotoxicity, paracetamol and diclofenac, did not exhibit one particular abnormal phenotype. Furthermore the most common abnormal phenotype observed for all the drugs was the developmentally delayed phenotype. The developmentally delayed phenotype was defined as an embryo that looks younger than stage 38 after the 36 h drug incubation. The high frequency and non-specificity of this phenotype for all the drugs tested suggests that any compound interference at this age will slow down embryonic development. Furthermore there was a greater variation of abnormal phenotypes produced in the stage 15-stage 38 screens compared to the stage 38-stage 45 screens. I believe this is because the older embryos have more functional organs and mature systems compared to the younger embryos. Unlike stage 15-38 embryos, organogenesis has more or less finished in stage 45 embryos, and therefore they are better equipped to process drugs. The stage 38-stage 45 embryos can tolerate the drugs better than the younger embryos. However, like every organism, the embryos have a limit, and this is reflected in the dose-dependent decrease in the wildtype phenotype for the higher concentrations of doxorubicin, diclofenac and indomethacin in the stage 38-stage 45 screens (**Figure 3-5**). The absence of a wildtype phenotype decline in these screens with drugs such as cisplatin,

paracetamol and gentamicin, that are associated with organ-specific toxicity in humans, suggests the 0.78-100 μM concentration range is not high enough. I cannot be certain that I am treating the embryos with a concentration that is high enough to induce organ-specific toxicity if there is an absence of significant mortality in the highest concentrations of cisplatin, paracetamol and gentamicin administered. To be clear, mortality does not necessarily indicate drug-specific toxicity, however a concentration of the drug just below that which causes death, is likely to be the dose that induces drug-specific toxicity. That is if the animal model is capable of generating a drug-induced toxicity reaction similar to that observed in humans.

Expression analysis using RT-PCR identified many of the drug metabolism enzymes characterised from human studies that play a major role in drug-induced toxicity (**Figure 3-6**). The drug metabolism enzymes I looked for are expressed at the embryo age that I will use to perform the toxicity screens for this project. Furthermore it is promising that the gene, *KCNH2*, which encodes the alpha subunit protein of the hERG channel ($\text{K}_{\text{v}}11.1$) is expressed. This is promising for characterising the use of the embryos for the prediction of drug-induced cardiotoxicity. As previously mentioned in **chapter 1**, the hERG channel is a voltage-gated K^+ channel that has a physiological role in the generation of the delayed rectifier current (I_{Kr}). This current is important for cell membrane repolarisation for the cardiac action potential. Some drugs associated with cardiotoxicity in humans bind to and block this potassium channel, which can lead to arrhythmic heart beats. I assumed that if the drug metabolism enzyme is expressed at stage 38 and stage 45, they will also be expressed at the stages in-between. The RT-PCR results in this chapter were generated from embryos that were not treated with any drugs. In the future, we would like to investigate the change in expression of drug metabolism enzymes in treated embryos. For example CYP2E1 expression in embryos treated with paracetamol. CYP2E1 is the major enzyme responsible for the production of the reactive metabolite that is important for the generation of paracetamol-induced hepatotoxicity in humans. This is discussed in more detail in **chapter 4**. The *Xenopus* CYP2E1 does not necessarily metabolise paracetamol at the same rate or to generate the same reactive metabolite produced by the human CYP2E1. In zebrafish, CYP3A65 is responsible for the production of the paracetamol reactive metabolite (Chng et al., 2012). The presence of mRNA expression does not help us to understand the activity of the enzyme. Drug metabolism enzyme activity can be crucial for the animal to be able to generate a drug-specific toxicity reaction, particularly when it is known that the toxicity reaction is mediated by a drug metabolite. In future experiments, I would look to measure the activity of the *Xenopus* CYP450, GST, UGT and SULT enzymes that could be involved in drug metabolism. We only measured the expression of the major enzymes involved in human drug metabolism. I would look to

investigate the expression of more drug metabolism enzymes in the *Xenopus* embryos to understand the potential usefulness and limitations of the model.

In the following chapters, I investigated drug-induced hepatotoxicity and drug-induced cardiotoxicity in the *Xenopus laevis* embryos. I decided to create an atlas to help identify structures, such as the heart and the liver (**Figure 3-7**). I chose to look at stage 45 embryos, because that is the age the embryos will be analysed at after drug incubation. The transverse sections were arranged in order from anterior to posterior in order to help determine at which level a section is taken from in future experiments. The different body compartments of the embryo are more apparent in the sections stained with hematoxylin and eosin (H&E). The sagittal sections demonstrate that one advantage of the *Xenopus* is that because of its small size, we are able to take a section of the full body. We could observe the effect of the drug on the tissue surrounding the target organ for drug-induced toxicity. This is not possible with larger animals, for which a costly magnetic resonance imaging (MRI) scan might be the equivalent.

3.6 Conclusion

Overall, from these results, I believe that the stage 38-stage 45 *Xenopus laevis* embryo screen has the potential to predict drug-induced toxicity as opposed to drug-induced teratogenicity. In the following chapters that explore organ-specific toxicity, for the most part, we decided to incubate the stage 38 embryos with the drug of interest and harvest the embryos at stage 45. It has been determined that up until and including the age of stage 45, the *Xenopus laevis* embryos do not feel pain, and consequently embryos younger than stage 46 are not subjected to home office restrictions. Furthermore the stage 45 embryos still fit comfortably into the wells of a 96 well plate to allow medium throughput screening. In conclusion, this drug screen protocol could be useful in terms of practicality for early preclinical drug safety studies in drug development.

4 Chapter 4: Assessing the use of *Xenopus* as a model for the prediction of Drug-induced Liver Injury using paracetamol as the model hepatotoxin

4.1 Introduction

4.1.1 Paracetamol-induced Liver Injury

It is estimated that paracetamol-induced liver injury is accountable for the majority of acute liver failure cases in developed countries. It contributes to 80 % of the liver failure cases associated with drugs. Over a 6 year period in the US, 42 % of acute liver failure cases were due paracetamol overdose, of which 48 % were unintentional, 44 % were intentional and the remaining 8 % were of unknown intent (Larson et al., 2005). In the UK, it is estimated approximately 90000 patients present with paracetamol overdose a year, resulting in 50000 hospital admissions and 150-250 deaths (Bateman et al., 2014; Hawton et al., 2013; Wong et al., 2014). Paracetamol is the second most common reason for a liver transplant. Overall, paracetamol is the single largest cause of acute liver failure in the US and the UK (Ostapowicz et al., 2002). At a therapeutic dose, that is 4 g/day, paracetamol is an antipyretic and an analgesic drug. The analgesic effect is due to the indirect activation of cannabinoid (CB₁) receptors (Bertolini et al., 2006). Additional therapeutic mechanisms of paracetamol includes the inhibition of cyclooxygenase (COX) activity, in particular it is COX2 selective and a reduction in prostaglandin synthesis (Hinz et al., 2007; Lucas et al., 2005). Severe liver injury is likely to occur when a single dose of 10-15 g of paracetamol is taken (Dart et al., 2006). The majority of paracetamol metabolism occurs in hepatocytes in the liver and therefore the liver is the target organ for paracetamol-induced toxicity, although it can be metabolised in the kidney and intestines too (Bessemers and Vermeulen, 2001). Paracetamol is a frequently used drug in developed countries and so the mechanism of paracetamol-induced liver injury is well defined in the literature (**Figure 4-1**). In humans, paracetamol (APAP) is metabolised predominantly by UDP (uridine 5'-diphospho)-glucuronosyl transferase (UGT) into the APAP-glucuronide conjugate, which is more water-soluble than the parent drug. The humans the major UGTs involved are UGT1A1 and UGT1A6 (Court et al., 2001). The second common pathway is APAP conjugation to sulphate with the help of the sulphotransferase (SULT) enzyme. The SULT1A1, SULT1A3/4 and SULT1E1 isoforms are important for paracetamol metabolism in humans (Adjel et al., 2008). In adult humans, approximately 50-70% and 25-35 % of paracetamol is metabolised via the glucuronide and sulphate pathways respectively and are excreted safely. Less than 5 % of the parent drug is

excreted unchanged and the remaining 5-15 % is metabolised by CYP450 enzymes to *N*-acetyl-*p* benzoquinone imine (NAPQI) (McGill and Jaeschke, 2013; Prescott, 1983). The CYP450 isoform mainly involved in the production of NAPQI is CYP2E1, however CYP1A2, CYP3A4 and CYP2D6 contribute as well (Dong et al., 2000; Patten et al., 1993). When a therapeutic dose of APAP is taken, the NAPQI is converted to the APAP-GSH conjugate, via the cysteine sulfhydryl group on the GSH tripeptide, with the help of the glutathione-S-transferase (GST) enzyme. APAP-GSH is then further metabolised to mostly the APAP-cysteine and APAP-mercapturate metabolites, which are then excreted.

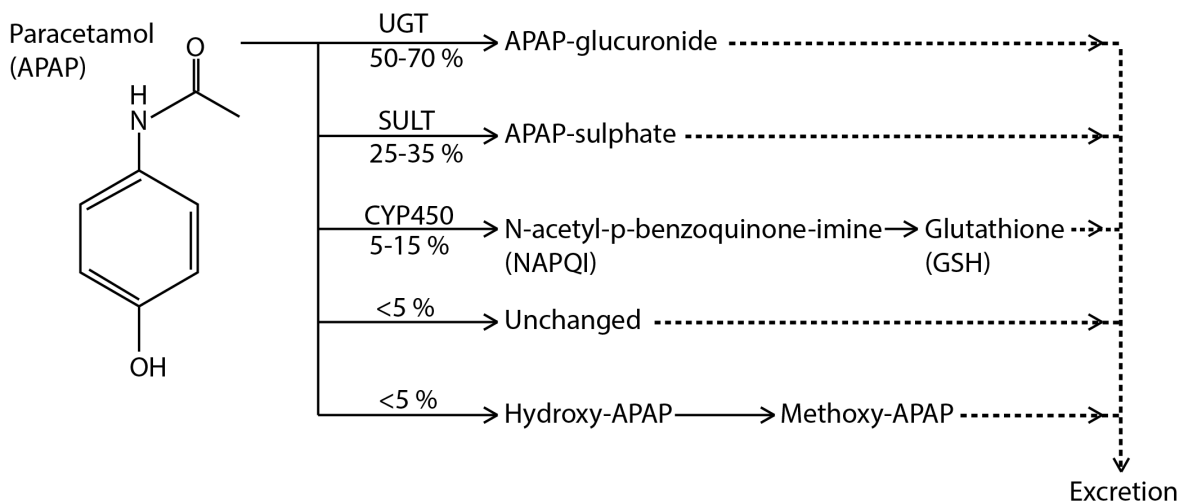


Figure 4-1: Paracetamol metabolism with a therapeutic dose.

Paracetamol (APAP) administered at a therapeutic dose (≤ 4 g/day) is metabolised to a number of metabolites in humans, the major metabolites are displayed in this schematic. Approximately 50-70 % of the APAP dose is converted to APAP-glucuronide through the action of uridine 5'-diphospho-glucuronosyltransferase (UGT). APAP-sulphate is the second major metabolite from APAP, contributing to approximately 25-35 % of all APAP metabolites and generated from sulphotransferase (SULT) enzymes. CYP450 enzymes convert 5-15 % of APAP to the reactive metabolite *N*-acetyl-*p*-benzoquinone imine (NAPQI), which is neutralised with the tripeptide glutathione (GSH). And <5 % of APAP is excreted unchanged or converted to the metabolite methoxy-APAP.

The paracetamol metabolites are predominantly excreted through ABC transporters. These ATP-binding transporters are found in the membranes of hepatocytes and use the hydrolysis conversion of ATP to ADP to provide the energy required to move substrates across membranes, sometimes against the substrate gradient (Klaassen and Aleksunes, 2014). The APAP-glucuronide and APAP-sulphate metabolites are excreted from the apical side of hepatocytes into the bile canaliculi through ABCC2 and ABCG2, also known

as multidrug resistance-associated protein-2 (MRP2) and cluster of differentiation w388 (CDw388) or breast cancer resistance protein (BCRP) respectively. Both of these metabolites are excreted into the liver sinusoids via ABCC3 and ABCC4, which are found on the basolateral side of hepatocytes (Ghanem et al., 2009). The APAP-GSH metabolite is also a substrate for MRP2 efflux into bile (Chen et al., 2003) (**Figure 4-2**).

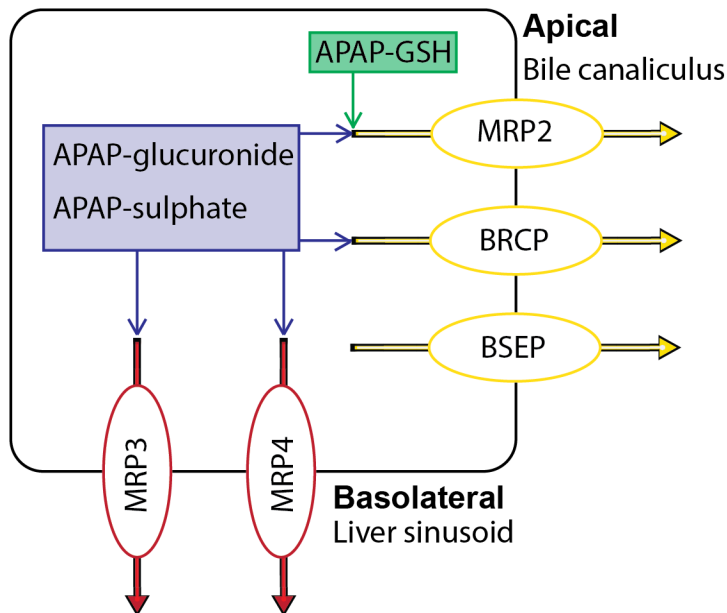


Figure 4-2: Paracetamol metabolite hepatocyte transporters.

Schematic of the hepatocyte transporters involved in the transport of major paracetamol (APAP) metabolites: APAP-glutathione (APAP-GSH), APAP- glucuronide and APAP-sulphate. The multidrug resistance-associated protein-2 (MRP2) and breast cancer resistance protein (BCRP) transporters expressed on the apical surface of the hepatocyte, transport APAP-glucuronide and APAP-sulphate into the bile canaliculus. MRP2 also transports APAP-GSH. On the basolateral surface, the APAP-glucuronide and APAP-sulphate metabolites are transported into the liver sinusoids via the MRP3 and MRP4 transmembrane proteins. BSEP, bile salt export pump.

When an overdose of APAP has been taken, the supply of GSH is saturated and so there is more free, unconjugated NAPQI (**Figure 4-3**). NAPQI is a reactive metabolite, and can bind to the sulfhydryl groups on cellular proteins such as mitochondrial proteins, or ion channels (Prescott, 1980). The NAPQI protein adducts formed can lead to mitochondrial dysfunction, nuclear DNA fragmentation, oxidative stress, hepatocyte death and subsequent acute liver failure and potentially patient death. The major cell death pathway by far is necrotic, although some apoptotic cell death also occurs. The initial ROS formation, exacerbates mitochondrial damage and cell death by activating the MAPK (mitogen-activated protein kinase) –JNK (c-Jun N-terminal kinase) pathway, which in turn,

amplifies oxidative stress (Jaeschke et al., 2012). Oxidative stress can activate the formation of the mitochondrial membrane permeability transition (MPT) pore. This allows solutes up to 1500Da to be able to pass through the inner mitochondrial membrane, the mitochondrial membrane potential is lost and mitochondrial proteins are released from the mitochondria and are able to fragment nuclear DNA (Kon et al., 2004). The mitochondrial proteins released include endonucleases such as AIF (apoptosis inducing factor) and endoG (endonuclease G) (Jaeschke et al., 2012; McGill and Jaeschke, 2013). Subsequently, necrotic cell death occurs. The exact mechanism for the initial incidence of oxidative stress, and it's relationship to NAPQI production is not yet understood (Jaeschke et al., 2012).

In the clinic, patients are administered *N*-acetyl cysteine (NAC) to prevent severe paracetamol-induced liver injury. The NAC replenishes the GSH stores, scavenges ROS in mitochondria and enhances the sulphation APAP metabolic pathway. The NAC therapeutic effect is more useful at preventing liver injury if it is taken less than 8 hours after the APAP overdose (Smilkstein et al., 1988; Waring, 2012). Some of the ABC transporters, in particular those involved in the efflux transport of paracetamol metabolites such as MRP2, BCRP and MRP4, are upregulated with paracetamol overdose (Barnes et al., 2007; Gu and Manautou, 2010). This is thought to be in a bid to reduce to accumulation of reactive metabolites inside the hepatocyte. Paracetamol-induced liver injury is an example of CRM-mediated DILI that is a result of the combination of CRM accumulation and a decline in cellular neutralising ability. The NAPQI protein adducts formed can be quantified by measurement of APAP-cysteine that is released into the protein fraction of the blood following a protease enzyme treatment (unlike the APAP-cysteine derived from APAP-GSH, which is present in the non-protein fraction of circulation) (Vliegenthart et al., 2017). The site of hepatotoxicity associated with paracetamol overdose is the zone 3 perivenous zone where there is more CYP450 bioactivation and more GSH generally available for detoxification. Paracetamol-induced liver injury has been recapitulated in several rodent and non-rodent animal models.

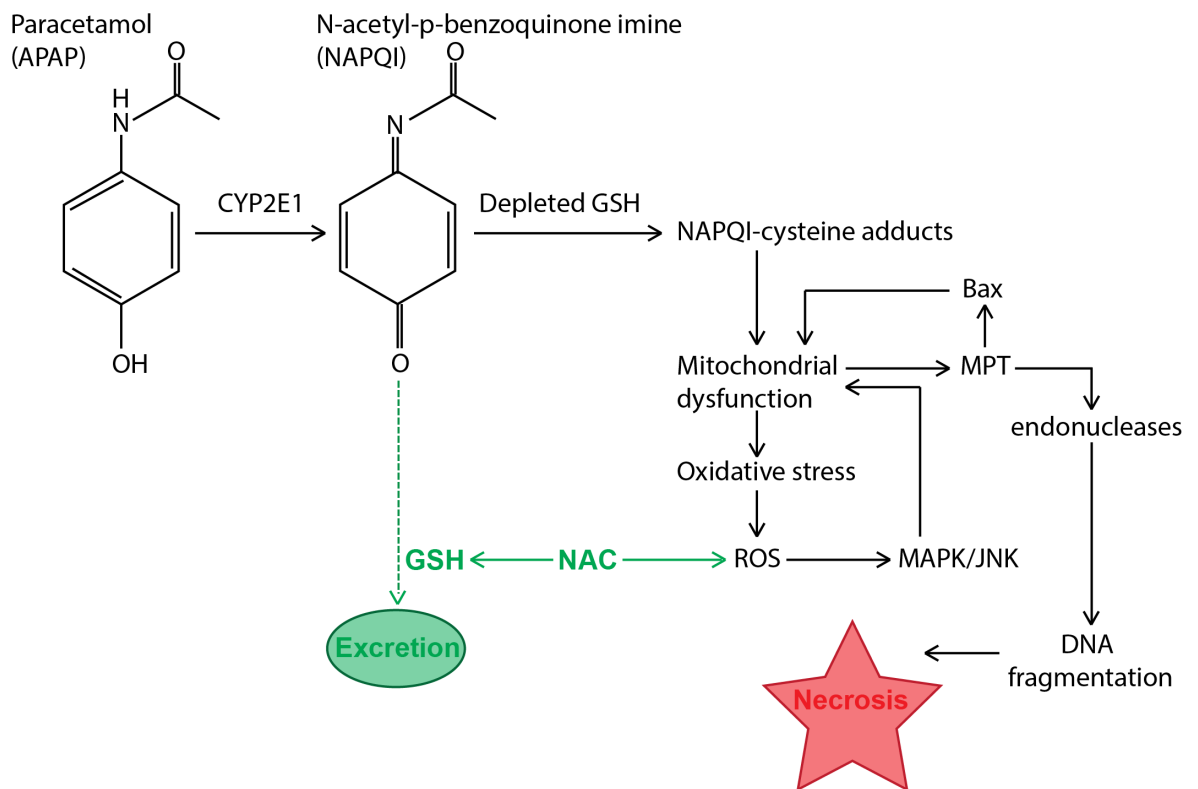


Figure 4-3: The mechanism for paracetamol-induced liver injury.

The majority of paracetamol metabolism occurs in hepatocytes, in the liver. The major reactive metabolite responsible for paracetamol-induced liver injury is *N*-acetyl-p-benzoquinone imine (NAPQI) that is produced from paracetamol (APAP) through the enzyme CYP2E1. In paracetamol overdose, the amount of glutathione (GSH) is reduced which allows NAPQI to covalently bind to the cysteine residues on mitochondrial proteins. This leads to the generation of reactive oxygen species (ROS), which exacerbates oxidative stress via the induction of the mitogen-activated protein kinase/c-Jun N-terminal kinases (MAPK/JNK) pathway. Mitochondrial dysfunction causes mitochondrial membrane permeability transition (MPT), which allows the translocation of proteins such as Bax into the mitochondria and release of endonucleases into the cytosol, which enter the nucleus and cause nuclear DNA fragmentation. All these mechanisms contribute to hepatocyte necrosis and liver injury. *N*-acetyl cysteine (NAC) is administered to paracetamol overdose patients. It replenishes GSH and scavenges ROS.

4.1.1 Animal Models for Paracetamol-Induced Liver Injury

A good animal model for the prediction of drug safety should be translatable to humans. However, a good way to determine the validity and limitation of a new animal model such as the *Xenopus* can be through comparison with existing animal models as well as to humans. Many animal models have attempted to mimic the paracetamol-induced liver injury phenotype. For rats, the paracetamol dose that has been used for studying

paracetamol overdose, ranges from 1500 to 2500 mg/kg (Bushel et al., 2007; Hadi et al., 2013; Kienhuis et al., 2009). The wildtype F344/N and Wister male rats are the most popular, and the method of paracetamol administration is often oral gavage. Wildtype CB57BL/6 mouse models are treated with a toxic dose of paracetamol within the range 300-375 mg/kg, also administered by oral gavage (McGill et al., 2012; Qin et al., 2016). Rats are less sensitive to hepatotoxicity associated with paracetamol overdose than mice (Davis et al., 1974). Rats do not form as much mitochondrial protein adducts, generate as much oxidative stress or activate the MAPK-JNK pathway unlike mice (McGill et al., 2012). Although rats metabolised APAP similarly to mice, the steps that mice carry out but rats don't, appear to be essential for the generation of APAP hepatotoxicity. The significant differences in response to a toxic APAP dose between the rat and mouse demonstrates the necessity for more than one animal species in drug development to pick up drug-induced toxicity reactions that could potentially be relative i.e. translatable to humans. It also indicates the complexity of decision-making in drug development: if APAP were a new drug candidate and the rat and mouse generated results that included conflicting hepatotoxicity incidence – which result should be considered? Would APAP be deprioritised? In this case, a drug that is very commonly used in the world today may not have made it to the market.

The zebrafish (*Danio rerio*) is an increasingly popular non-mammalian animal model to use for research and toxicology studies. It has been used by different laboratory groups to investigate paracetamol-induced liver injury. Similar to *Xenopus*, zebrafish liver development is very rapid in comparison to mammalian liver development and occurs in the embryo *ex utero*. In zebrafish, liver budding starts at 28 hours post-fertilisation (hpf), primary liver morphogenesis is completed by 48 hpf, hepatic organogenesis is finished at 72 hpf including blood perfusion and functionality. The liver is considered to be fully functional by 120 hpf (Isogai et al., 2001; McGrath and Li, 2008; Vliegthart et al., 2014b). Whereas mice do not have a mature liver until embryonic day 18.5, *in utero* (Zhao and Duncan, 2005). Zebrafish larvae models for paracetamol overdose were treated with within the range 1-10 mM APAP. This dose is administered into the media the embryos are swimming in, usually from the age of 72 hpf and harvested at or before 120 hpf (He et al., 2013; North et al., 2010; Verstraelen et al., 2016; Vliegthart et al., 2014b). Vliegthart and colleagues (2014) used adult zebrafish aged 5-24 months post-fertilisation and administered a higher concentration range of paracetamol: 20-40 mM. Although, the survival rate of the fish began to decline at the 30 mM concentration (Vliegthart et al., 2014a). Zebrafish are arguably the closest animal model to *Xenopus*. Subsequently, in order to determine the validity of paracetamol-induced liver injury in

Xenopus, the zebrafish paracetamol overdose model could be a useful model to compare results to.

4.2 Aim

Characterisation of *Xenopus laevis* as a model for paracetamol-induced liver injury and investigating the effects of additional compounds often affiliated with paracetamol toxicity models.

4.3 Hypothesis

Stage 38-45 *Xenopus laevis* embryos treated with paracetamol will exhibit characteristics of paracetamol-induced liver injury similar to other non-mammalian and mammalian animal models and humans.

4.4 Paracetamol Results

4.4.1 Paracetamol dose response in *Xenopus laevis*

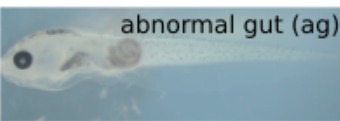
To test *Xenopus laevis* as a model for paracetamol-induced liver injury, I first investigated at what concentration paracetamol is toxic to the *Xenopus laevis* embryos. A concentration that is too high may not elicit paracetamol-specific toxicity, but the resultant phenotype could be due to general toxicity that occurs from overexposure to any chemical. The phenotypes observed in **chapter 3** for stage 38 to stage 45 embryos treated with a paracetamol concentration range 0-100 μ M did not indicate toxicity. Consequently, for this chapter, I began with a higher paracetamol concentration range of 0-5 mM. This range is consistent with zebrafish and *in vitro* models.

The *Xenopus laevis* embryos are transparent at these stages and so the liver is visible, however the aim of this experiment was to see if we could detect an obvious change in phenotype in the whole embryo (not just the liver) with increasing paracetamol treatment concentration. For the concentration range of 0-5 mM there was no significant change to overall embryo phenotype (**Figure 4-4**). This dose response was performed with 4 groups of embryos from 4 different *Xenopus laevis* mothers (n=4). The untreated embryos were similar to the known stage 45 wildtype phenotype for *Xenopus laevis*. The resultant phenotype observed was due to the paracetamol treatment alone. Embryos were separated in the screens to 1 embryo per well of a 96-well plate, therefore spontaneous or drug-induced death of an embryo did not affect the probability of another embryo's death. The incidence of oedema around the gastrointestinal region was higher with increasing concentration. The percentage survival decreased at the higher concentrations, for example, 4.5 mM and 5 mM to an average of 95 % and 90 % respectively (**Figure 4-5**). At all other concentrations the average survival percent remained at 100 %, with the

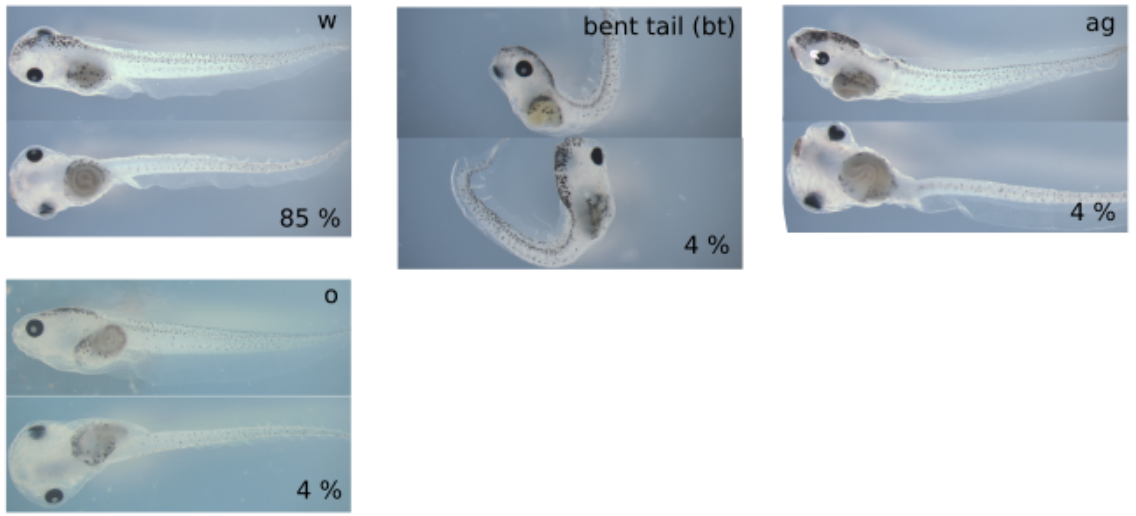
exception of 0.125 mM, where the 97.5 % average is due to the death of 1 embryo in all the dose response screens performed.

I decided to investigate a higher dose response range, that is 5.5-10 mM paracetamol (**Figure 4-6**). The occurrence of gastrointestinal oedema was higher in the 5.5-10 mM than the 0-5 mM paracetamol concentration range. In the 5.5-10 mM range, the intestines look abnormal in the higher concentrations compared to the untreated control embryos. From 6-10 mM, there were some embryos with elongated intestines along the sagittal plane; the intestines were less compact. This elongation often coincided with oedema in the same anatomical region. The survival rate decreased with increasing paracetamol concentration to 40 % at 8 mM and below 5 % from 9-10 mM, which reflected the survival of only 1 embryo in all the screens carried out (**Figure 4-7**).

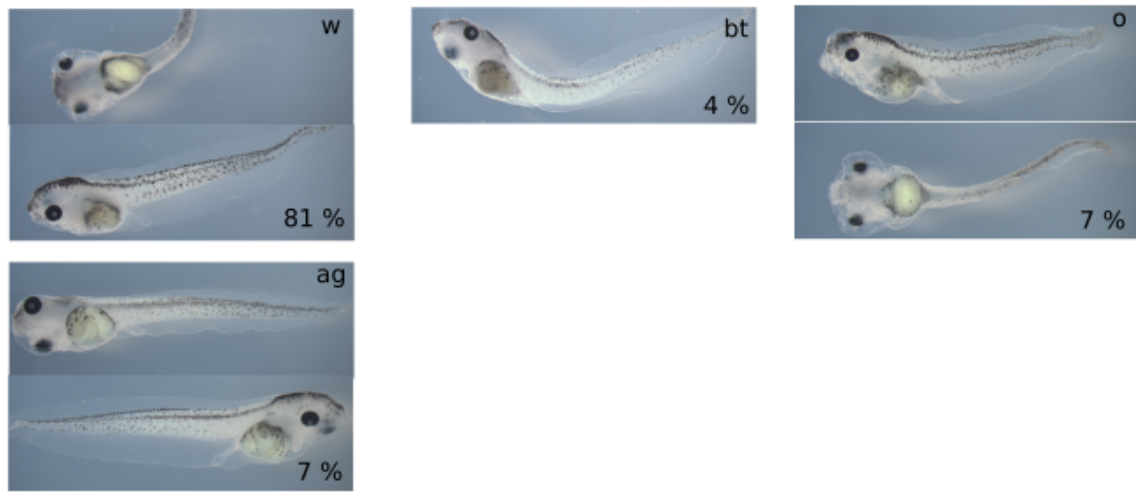
It is from these sets of dose response concentration ranges, that it was decided to continue with the 0-5 mM range for the investigation of paracetamol-induced DILI for the remainder of the experiments in this chapter. The reduced survival rate for the 5.5-10 mM range, suggests non-specific toxicity.

0 mM		
		
		
0.5 mM		
		
		
1 mM		
		
		
1.5 mM		
		
		
2 mM		
		
		
2.5 mM		
		
		

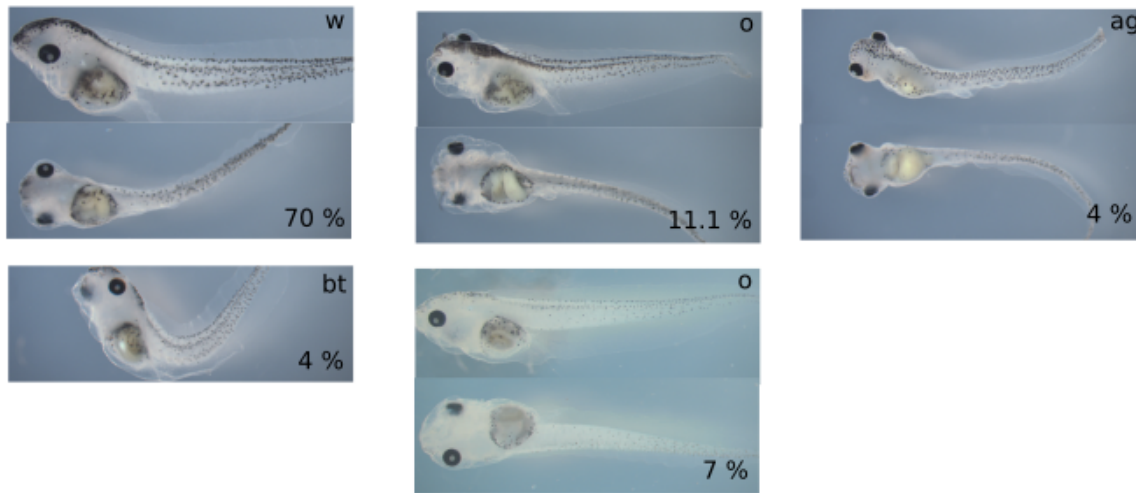
3 mM



3.5 mM



4 mM



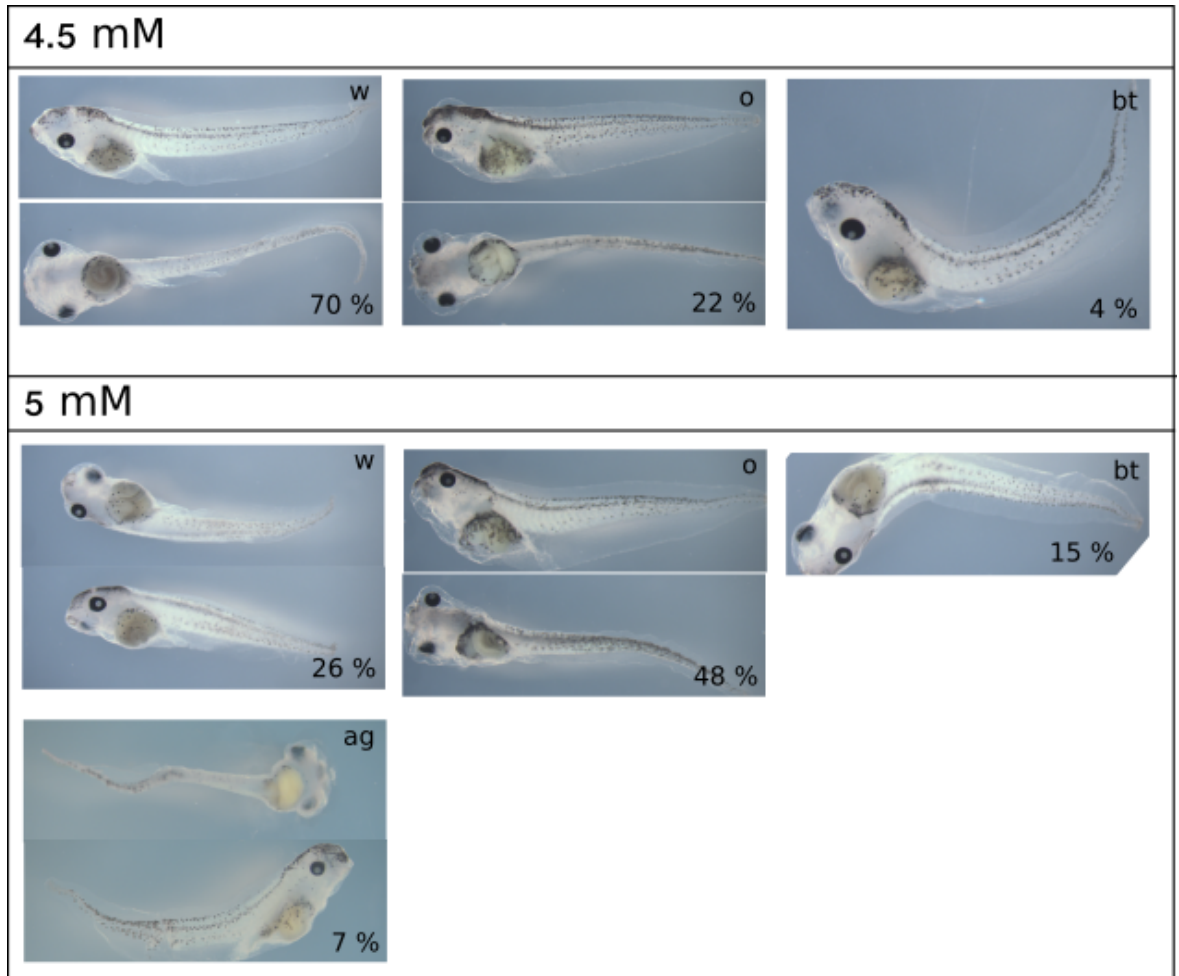


Figure 4-4: Paracetamol dose response 0-5 mM.

Xenopus laevis embryos were treated with a paracetamol concentration in the range 0-5 mM (n=4). The embryos were treated with paracetamol from stage 38 and harvested at stage 45. The surviving embryos at stage 45 were photographed and the different phenotypes found for each paracetamol concentration are shown and the percentage of embryos that had that phenotype. Phenotypes include wildtype (w), damaged tail (dt), bent tail (bt), oedema (o) and abnormal gut (ag). The percentage is calculated from the total number of embryos treated. Where possible, the embryos were photographed to show the lateral view and the ventral view.

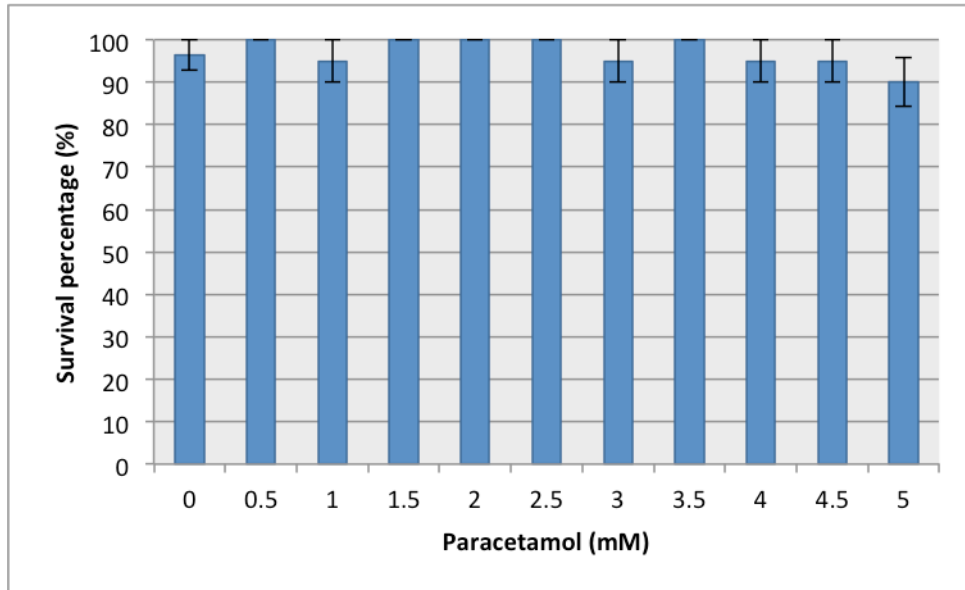
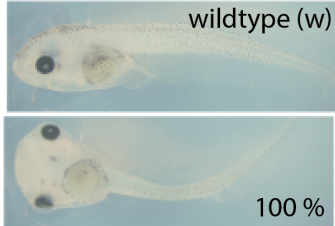
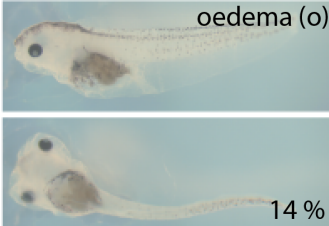
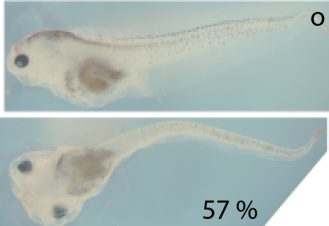
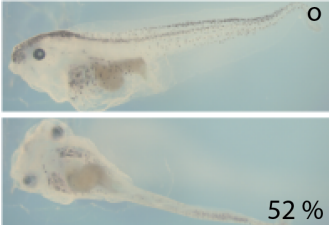
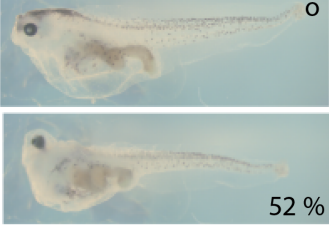


Figure 4-5: The percentage of *Xenopus* embryo survival with 0-5 mM paracetamol treatment.

The average (\pm SEM) amount of embryos that survived until the age of stage 45 to be harvested and photographed for **Figure 4-4** (n=4).

0 mM		
		
5.5 mM		
		
6 mM		
		
6.5 mM		
		
7 mM		
		
7.5 mM		
		

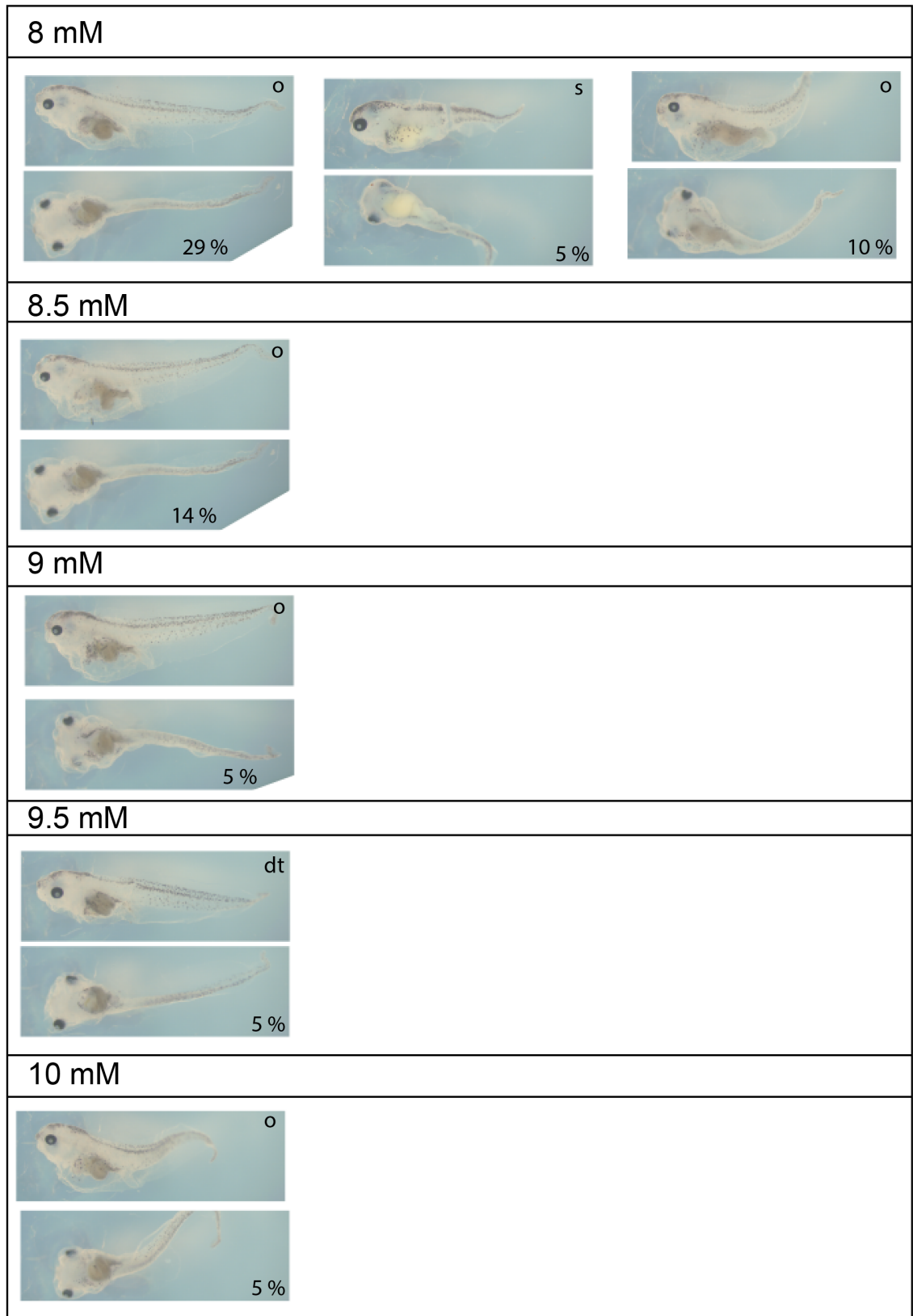


Figure 4-6: Paracetamol dose response 0, 5.5-10 mM.

Xenopus laevis embryos were treated with a paracetamol concentration in the range 5.5-10 mM (n=3) from stage 38 and harvested at stage 45. The surviving embryos at stage 45

were photographed. In this figure are the different phenotypes found for each paracetamol concentration and the percentage of embryos that had that phenotype. Phenotypes included wildtype (w), oedema (o), abnormal gut (ag), damaged tail (dt) and small (s). The percentage is calculated from the total number of embryos treated. Where possible, embryos were photographed to show the lateral view and the ventral view.

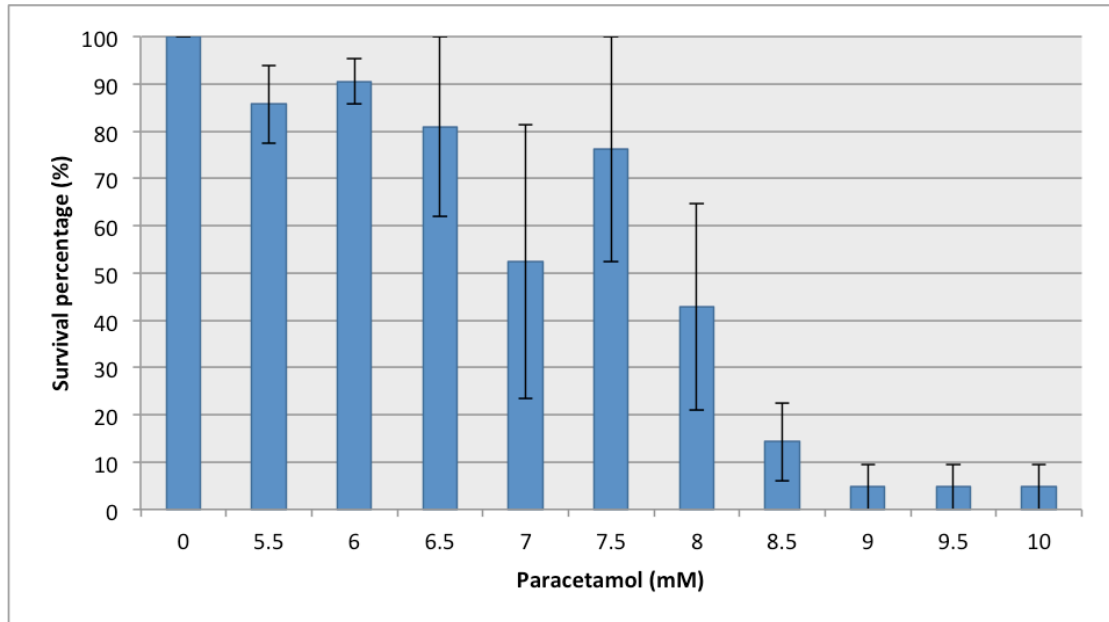


Figure 4-7: The percentage of *Xenopus* embryo survival with 5.5-10 mM paracetamol treatment.

The average (\pm SEM) amount of embryos that survived until the age of stage 45 to be harvested and photographed for **Figure 4-6** (n=3).

4.4.2 Free GSH content in Paracetamol Treated Embryos

In humans, the generation of the reactive metabolite, NAPQI, and the reduction of the neutralising agent, GSH, mediate paracetamol-induced liver injury. Consequently, the amount of free GSH can indicate the metabolism pathway of paracetamol and be an indirect measurement of paracetamol-induced liver injury. Existing *in vivo* or *in vitro* assays that imitate human paracetamol overdose and the associated acute liver failure, show a reduction of free GSH in the assay system (Goldring et al., 2004; Howell et al., 2014; Shenton et al., 2004; Vliegenthart et al., 2017).

Embryos at stage 38 were treated with a paracetamol concentration within the range 0-5 mM, harvested at stage 45, and processed to measure the amount of free GSH in them (n=10) (**Figure 4-8A**), normalised to the protein content using the Bradford assay. The amount of free GSH decreased from 47 nmol/mg to 22 nmol/mg with increasing concentration of paracetamol (0-5 mM). Embryos treated with a paracetamol concentration within the range 3-5 mM had statistically significantly less free GSH compared to untreated embryos ($P < 0.05$). *Xenopus laevis* embryos that are incubated at 23°C take 72h to develop from stage 38 to stage 45. In order to explore the time-dependency of the decline in free GSH, I treated stage 38 embryos with the same paracetamol concentration range (0-5 mM) and harvested them after 24h, at stage 41 (**Figure 4-8B**). There was no significant change in the relationship between paracetamol treatment and amount of free GSH when the embryos are treated for 24h.

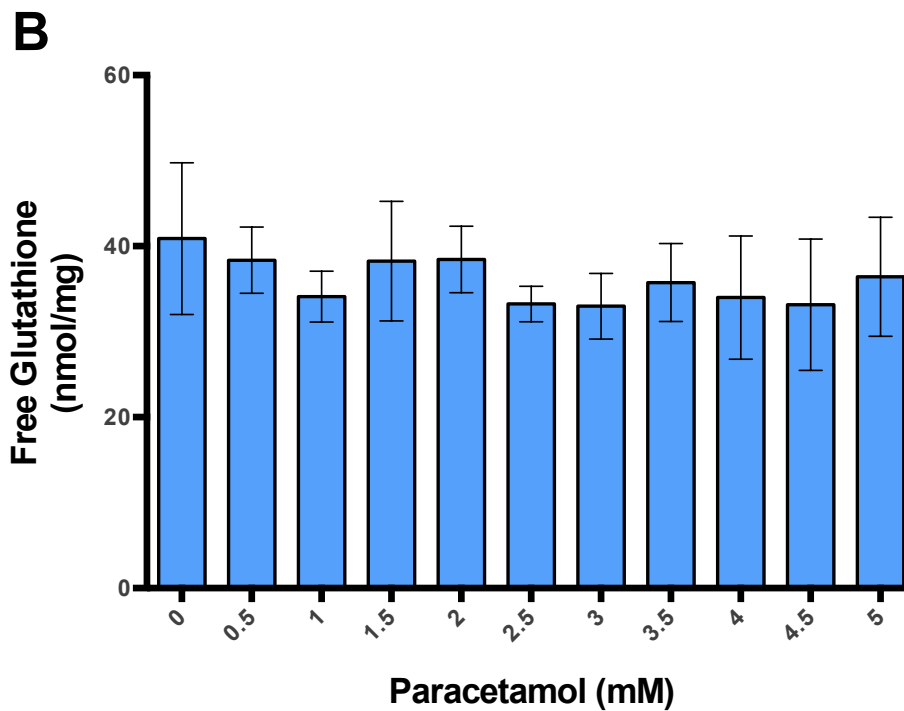
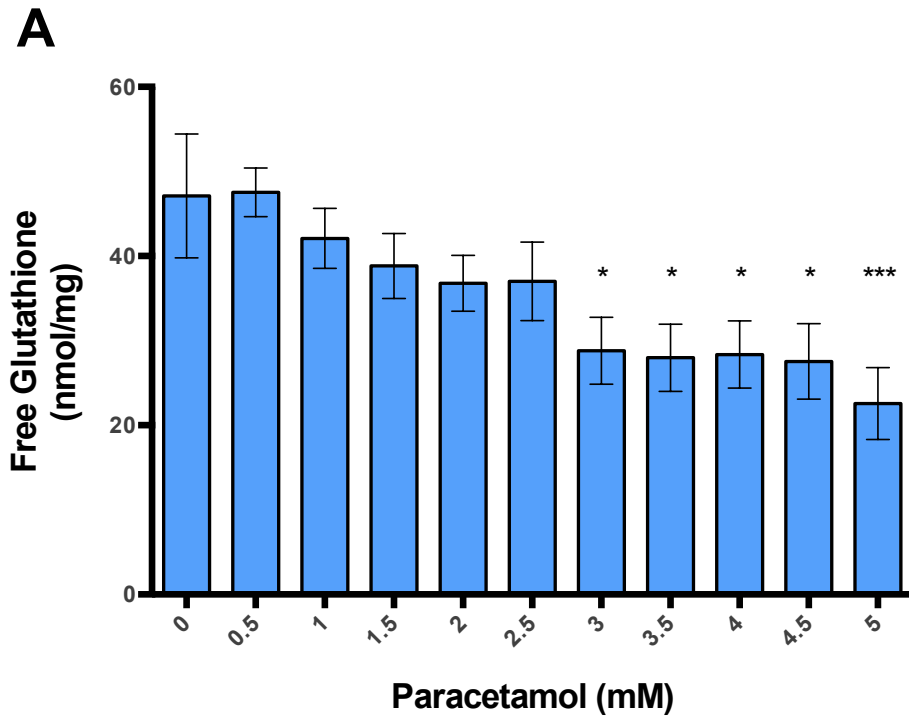


Figure 4-8: The amount of free GSH inside *Xenopus* embryos treated with paracetamol.

Xenopus laevis embryos were treated with 0-5 mM paracetamol from the age of stage 38, and harvested at stage 45 (A, n=10) or at stage 41 (B, n=3). The amount of free GSH (nmol/mL) was measured inside the embryos and normalised to the amount of protein (mg/mL). A one-way ANOVA compared each treatment group to the untreated group (0 mM). For the embryos treated until stage 45 (A), the amount of free GSH for 3, 3.5, 4 and

4.5 mM paracetamol treatment groups was statistically significant compared to the untreated group ($P < 0.05$). The 5 mM paracetamol treatment group was also statistically significantly different ($P < 0.01$). There was no significant difference between treated and untreated embryos that were harvested at stage 41 (B).

4.4.3 Liver expression pattern in *Xenopus laevis* and liver injury biomarker expression

4.4.3.1 Wholemout in situ hybridisation

The location of the liver is not always obvious in the *Xenopus laevis* embryo, it is < 0.5 mm at its widest diameter, and the colour of it is not notably different to the intestines. Thus, we used a probe to identify the liver using a wholemount *in situ* hybridisation (WISH) protocol. The location of the liver in a whole *Xenopus* embryo, at stages 38 and stage 45, has been described in the literature (Blitz et al., 2006; Zorn and Mason, 2001) and is illustrated in **Figure 4-9**. Alpha-1-microglobulin/bikunin precursor (AMBP) is a protein specifically expressed in the *Xenopus* liver (Zorn and Mason, 2001) and so I used it as a positive control for the WISH. Stage 38 and stage 45 embryos expressed AMBP in the presumed location of the liver (**Figure 4-10A**) ($n=10$).

Next, I decided to investigate the expression of miR-122 in the *Xenopus* embryos using the WISH assay. MiR-122 expression is specific to the liver in humans as well as rodent and zebrafish animal models (**Figure 4-10B**) ($n=10$). As previously mentioned in **chapter 1**, the presence of miR-122 in the circulation is abnormal, and it can indicate liver injury and therefore, miR-122 can be a good biomarker for DILI. The WISH for miR-122 stained the same area as AMBP in stage 38 and stage 45 embryos, so miR-122 expression in *Xenopus laevis* is specific to the liver tissue, comparable to rodent and zebrafish species.

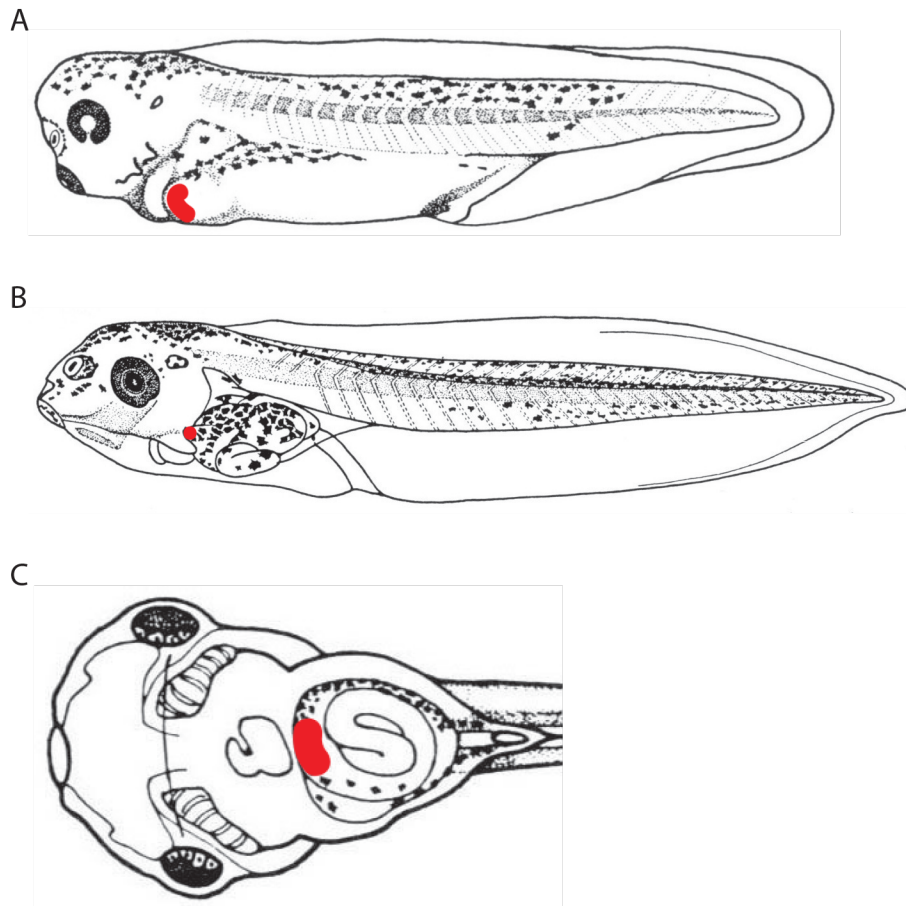


Figure 4-9: Illustration of the location of the liver in *Xenopus* embryos.

The *Xenopus* embryos at the age of stage 38 (A) and stage 45 (B and C) have liver tissue (red). This schematic displays the location of the liver as seen from a lateral view (A and B) and ventral view (C). Modified from Nieuwkoop & Faber (1994)

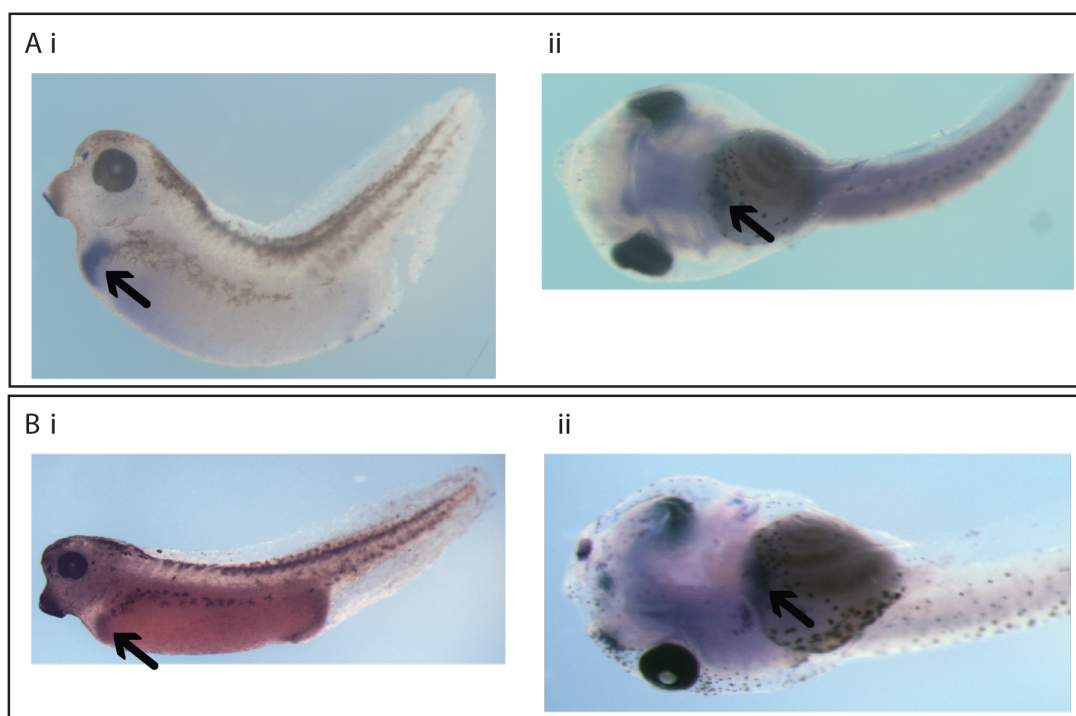


Figure 4-10: Wholemount *in situ* hybridisation (WISH) for liver markers.

WISH assay for AMBP (A) and miR-122 (B) at stage 38 (Ai and Bi) and stage 45 (Aii and Bii). The stage 38 embryos are shown in lateral view and the stage 45 embryos are shown ventrally. These embryos are representatives of the typical expression patterns seen (n=10).

4.4.3.2 Sections of WISH miR-122

When a liver is damaged, the expression of miR-122 in liver tissue becomes fragmented as the cells release it into the circulatory system. Consequently, I hypothesised that paracetamol-induced liver injury could be determined in the *Xenopus* embryos using fragmented miR-122 staining as an end-point. To test this hypothesis, I took untreated embryos that had been processed with the miR-122 probe using the WISH protocol, and sectioned them transversely; this was our negative control. I could clearly identify the liver in the transverse sections. Next, I treated the tissue sections with hematoxylin and eosin (H&E) that stain the nuclei and cytoplasm respectively. The H&E could help characterise the surrounding tissue in the sections. However, the WISH stain was not as easy to identify in these sections (**Figure 4-11Aii**). Finally, I treated embryos with paracetamol, then put them through the WISH protocol for miR-122 identification (**Figure 4-11B**), and sectioned them. It was difficult to observe paracetamol-induced liver damage in the results.

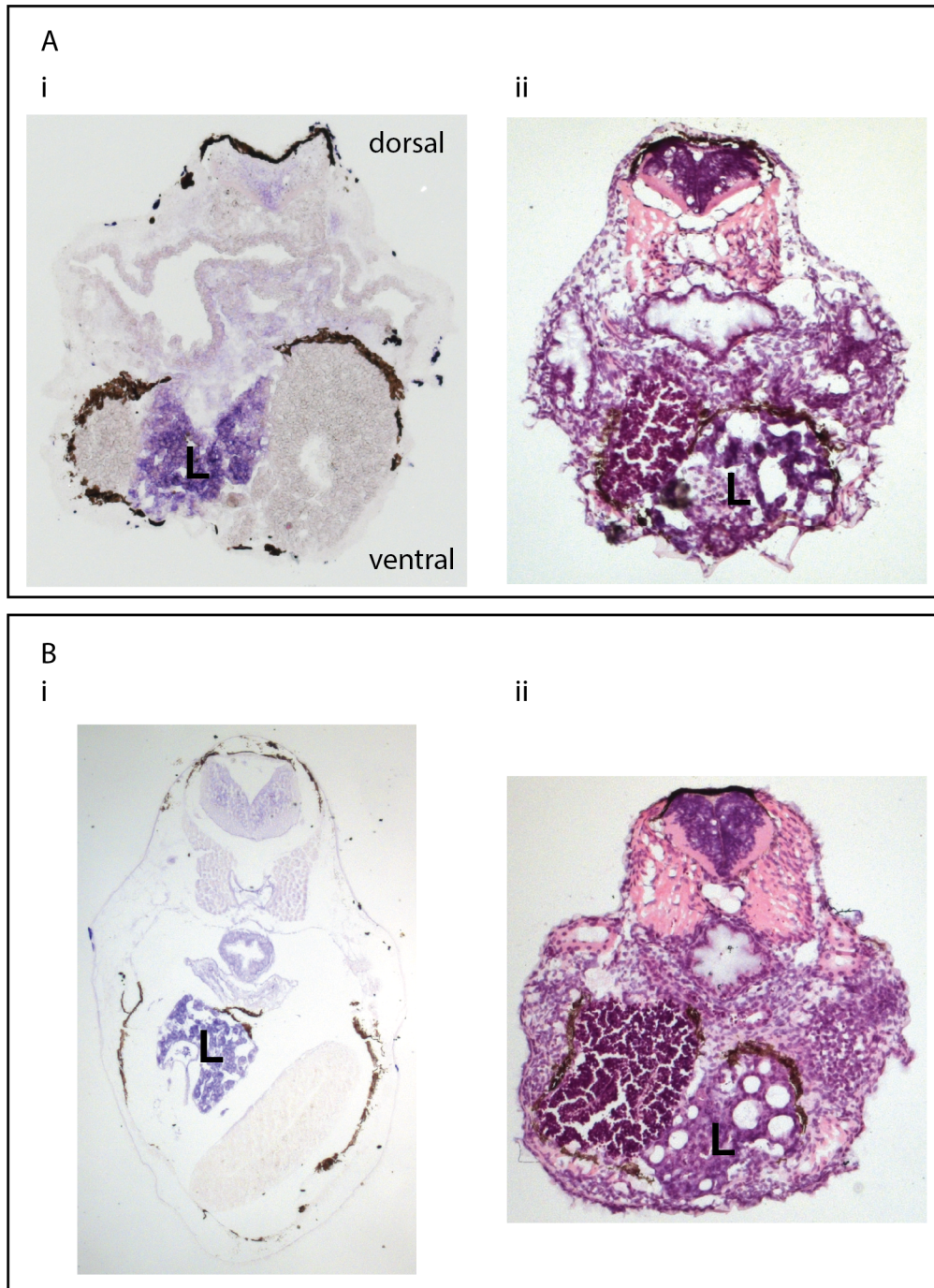


Figure 4-11: Sections of miR-122 WISH stage 45 embryos.

WISH using miR-122 probe stage 45 *Xenopus* embryos untreated (A) or treated (B) with 5 mM paracetamol from stage 38 until stage 45. 10 μ m sections were either left without additional histology staining (Ai and Bi) or stained with H&E (Aii and Bii). Representative sections are displayed. The location of the liver (L) is attained purple.

4.4.3.3 The expression of miR-122 in the different tissues of embryos treated with paracetamol

Stage 38 old embryos were treated with a paracetamol concentration within the 0-5 mM range, harvested at stage 45 and then processed to measure the expression of miR-122 using qRT-PCR. Embryos were dissected to obtain gut tissue that included the liver and tail tissue to represent the blood. The miR-122 expression levels were normalised to a miRNA (miR-103), which is not effected by paracetamol treatment. The miR-122 expression was also normalised to untreated (0 mM paracetamol) embryos (**Figure 4-12**). The expression of miR-122 increased in the tail tissue with increasing paracetamol concentration. In untreated wildtype embryos, the miR-122 expression in the tail was minimal. MiR-122 expression in the tail of embryos treated with 3 mM and 4 mM paracetamol was significantly different compared to the expression of miR-122 in the gut tissue from the same embryos treated with the same paracetamol treatment. In the gut tissue, the expression of miR-122 appears to be slightly reduced in treated embryos compared to untreated embryos, but the miR-122 expression does not change in relation to the paracetamol concentration, it remains level.

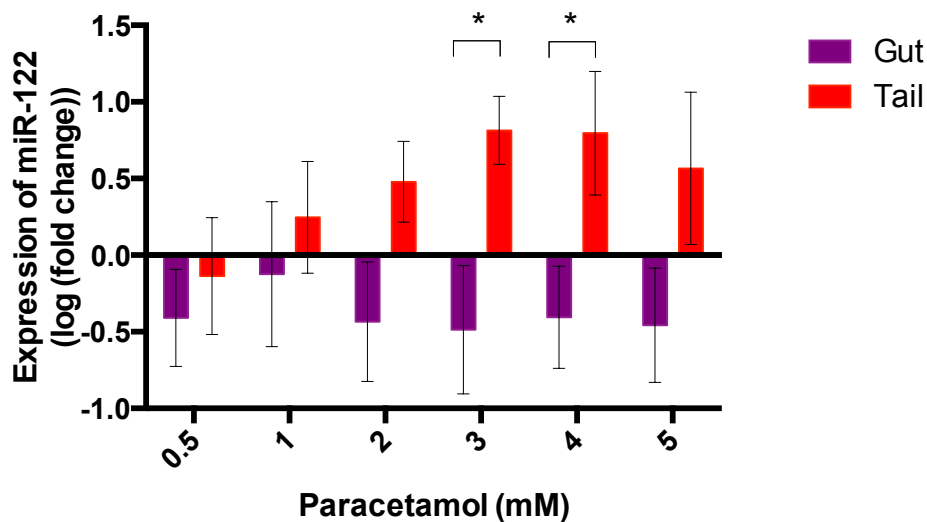


Figure 4-12: Expression of miR-122 in paracetamol-treated embryos.

Stage 38 embryos were treated with paracetamol (0-5 mM) and harvested at stage 45. The expression of miR-122 in gut (purple) and tail (red) was measured using qRT-PCR (log (fold change \pm SEM)) and normalised to untreated embryos (0 mM). The statistical significant difference of miR-122 expression between tissues from embryos with the same paracetamol concentration was measured using the Mann-Whitney test ($P < 0.05$) ($n = 5$).

4.4.4 Characterisation of the metabolic profile of paracetamol-treated *Xenopus laevis* embryos

As shown in **Figure 4-1**, paracetamol is metabolised into several small molecules in humans. I selected some of the major metabolites that are known to be produced in humans from paracetamol and investigated their production in our *Xenopus* paracetamol model. The metabolites I measured were: APAP-glucuronide, APAP-sulphate, APAP-GSH, APAP-cysteine, APAP-NAC and APAP-methoxy (**Figure 4-14**). I measured the metabolic profile present inside the embryos themselves and within the media the embryos were swimming in using mass spectrometry protocol already established for paracetamol metabolites in the laboratory. As per the previous experiments in this chapter, stage 38 embryos were treated with a concentration of paracetamol within the range 0-5 mM and harvested at stage 45. The concentration of the parent drug, paracetamol, was measured to check the dosing of the stage 38 embryos (theoretical APAP dose) was correct (**Figure 4-13**). The concentration of paracetamol actually in the media the embryos were incubated within, was correct for the 0-3 mM theoretical doses however the 3.5, 4, 4.5 and 5 mM theoretical doses were actually measured as 5.2, 2.1, 5.2 and 4.8 mM respectively. The APAP-sulphate metabolite is the dominant paracetamol metabolite produced in the *Xenopus* embryos and excreted into the incubation media. There were very small amounts of APAP-glucuronide and APAP-NAC detected in the media. The dominant metabolites present within the embryos were APAP-cysteine and APAP-GSH. Minimal amount (0-9.4 nmol/embryo) of the parent drug, paracetamol, was detected inside the embryo (**Figure 4-13A**).

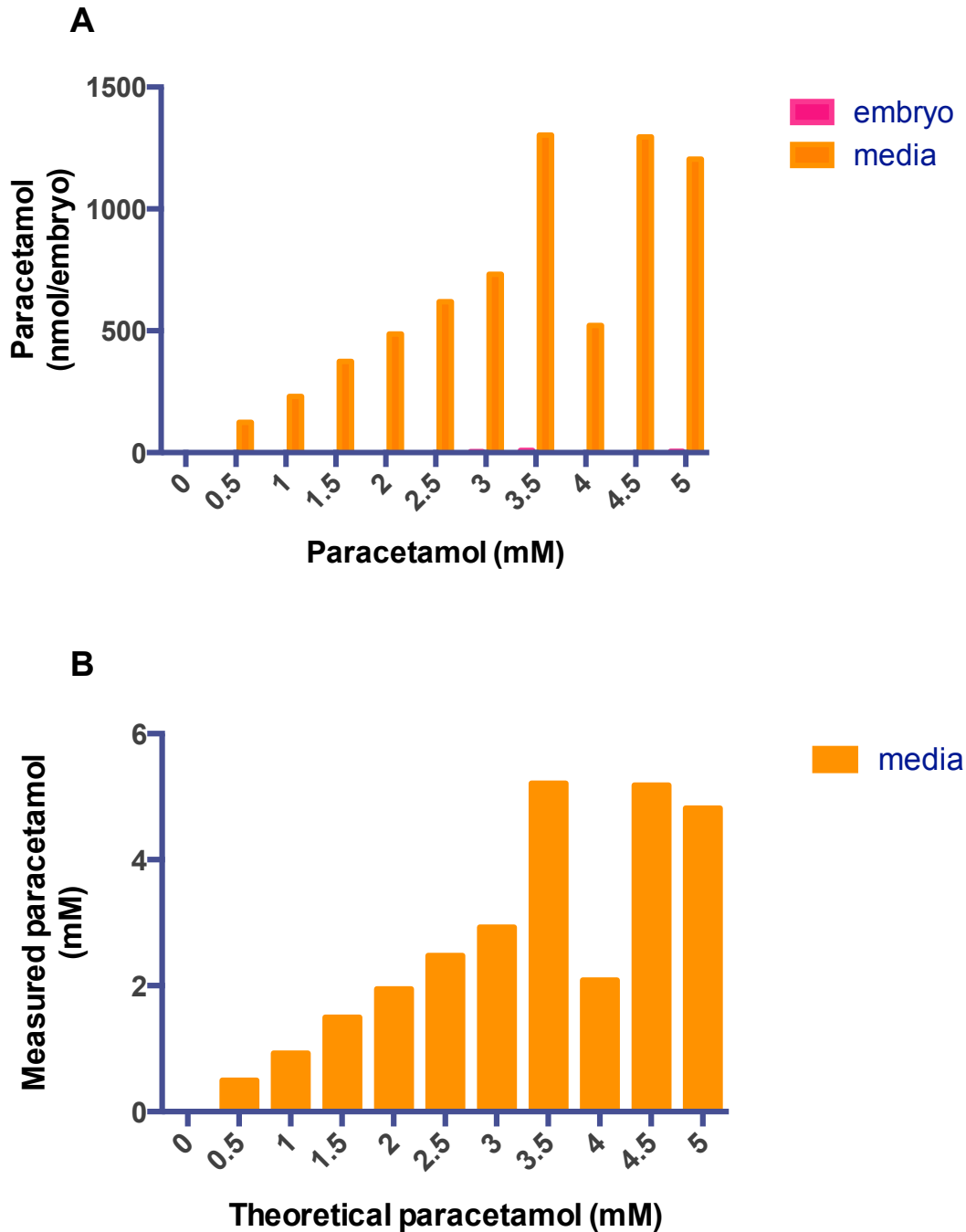
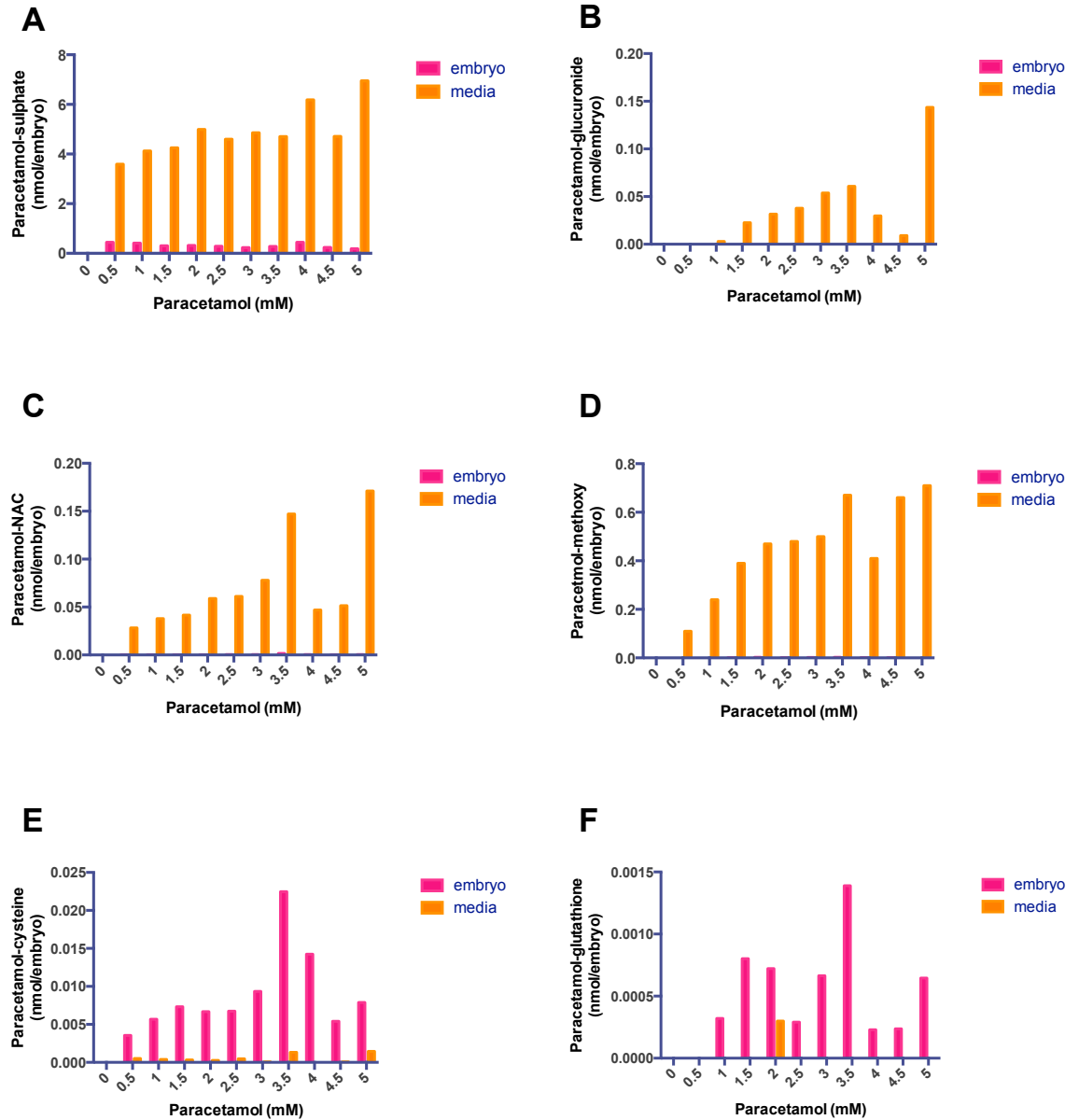


Figure 4-13: Mass spectrometry detection of paracetamol.

Embryos were treated with a paracetamol concentration (0-5 mM) in the embryo media. The embryos were pooled and mass spectrometry was carried out to measure the actual concentration of paracetamol in the media (orange) after 72h incubation (n=1). The amount of paracetamol was measured in nmol/embryo (A) and for ease, was then converted into mM (B). Minimal paracetamol was found inside the embryos (pink).



4.1.1

Figure 4-14: Mass spectrometry detection of paracetamol metabolites.

The amount of paracetamol metabolite present in the media (orange) and inside the embryo (pink) was measured after a 72h incubation with paracetamol (0-5 mM) (n=1). 6 major metabolites involved in human paracetamol metabolism were identified: sulphate (A), glucuronide (B), methoxy (C), NAC (D), cysteine (E) and glutathione (F) paracetamol conjugates.

4.4.5 Analysis of time-dependent and dose-dependent multidrug resistance-associated protein 2 (MRP2) expression

MRP2, also known as ABCC2, has 17 hydrophobic transmembrane regions, of which 3 span the membrane. In humans it is most highly expressed in the liver, however it is also found in the small intestine and kidney (Kool et al., 1997). APAP-glucuronide and APAP-sulphate are substrates for this transporter, MRP2 translocates them from inside the hepatocyte into the bile canaliculi (Klaassen and Aleksunes, 2014). I treated stage 38 *Xenopus* embryos with 5 mM APAP and harvested them at either stage 42, stage 44 or stage 45, that is 28 h, 48 h and 72 h respectively post-fertilisation (n=3, n=4 and n=4. respectively) (Figure 4-15). The mRNA expression for MRP2 was investigated in dissected gastrointestinal regions, and all results were normalised to untreated (0 mM APAP) embryos. The stage 42 harvested embryos had reduced MRP2 expression in comparison to untreated. The stage 44 and stage 45 embryos both had an average of increased MRP2 expression when compared to untreated embryos. The expression of MRP2 was greater in the stage 44 embryos than in the stage 45. There was not a statistically significant linear trend between MRP2 expression and increasing *Xenopus* embryo age.

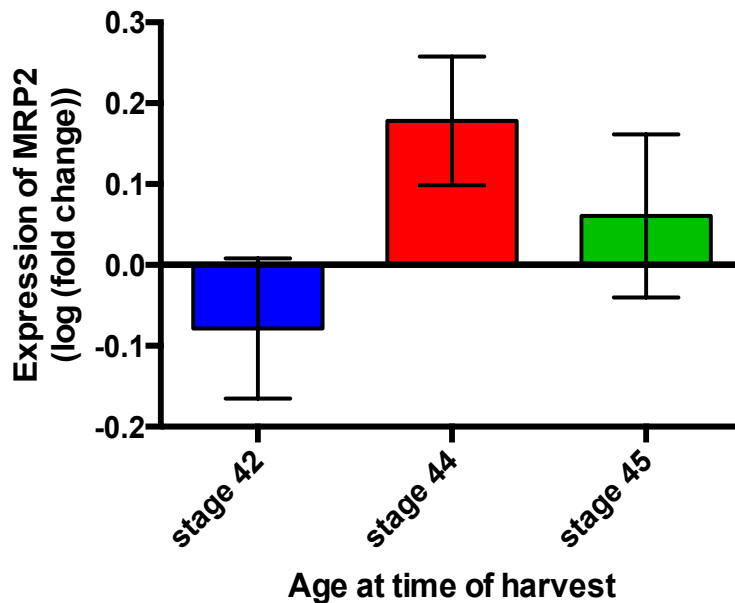


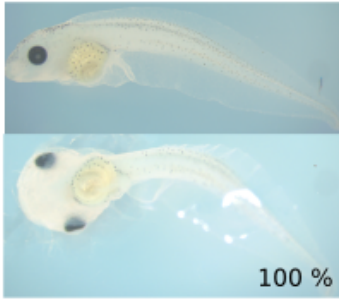
Figure 4-15: Expression of MRP2 in paracetamol-treated embryos.

Embryos were treated with 5 mM paracetamol at stage 38 and harvested at stage 42, 44 and 45, equivalent to 28 h, 48 h and 72 h incubation periods (n=3, n=4 and n=4. respectively). The gastrointestinal region was dissected and the expression of MRP2 measured in that tissue by qRT-PCR (log (fold change \pm SEM)) and normalised to untreated embryos (0 mM). No statistical significance was seen between samples.

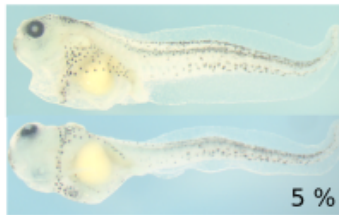
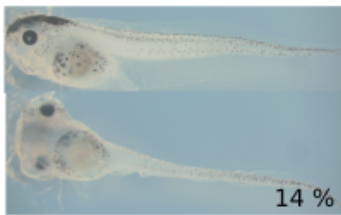
4.4.6 Treatment with acetyl-meta-aminophenol (AMAP)

AMAP is supposedly the non-toxic regioisomer version of APAP, but this appears to be species-dependent. I briefly investigated the *Xenopus* response to AMAP. Following the decline of survival percentage for the higher concentration range of APAP (5.5-10 mM), we decided to treat the embryos with that same concentration range and look at the resultant AMAP phenotype and survival percentage in comparison to APAP (**Figure 4-16**). The AMAP-treated embryos were increasingly more difficult to physically manipulate with increasing AMAP concentration to obtain the photographs. The embryos at the higher concentrations were more delicate, however they appeared similar to the stage 45 wildtype untreated embryos when I took photographs. The survival percentage decreased with increasing AMAP concentration (**Figure 4-17**). In comparison to the APAP survival for the same concentration range, less AMAP-treated embryos survived overall, and more embryos died at the AMAP lower concentrations. Finally, I compared the affect of GSH depletion, which was determined by measuring the amount of free GSH in embryos from the same mother, treated with either AMAP or APAP in the same concentration range (0-5 mM, n=3). These biological replicates for APAP produced the same depleting effect as shown with the previous result in this chapter; the amount of free GSH decreased with increasing APAP concentration. The embryos treated AMAP also produced a negative correlation: as the concentration of AMAP increased, the amount of free GSH detected decreased. The amount of GSH between embryos treated with the same concentration of either AMAP or APAP was not significantly different (**Figure 4-18**).

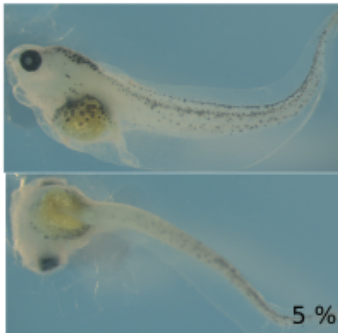
0 mM



5 mM

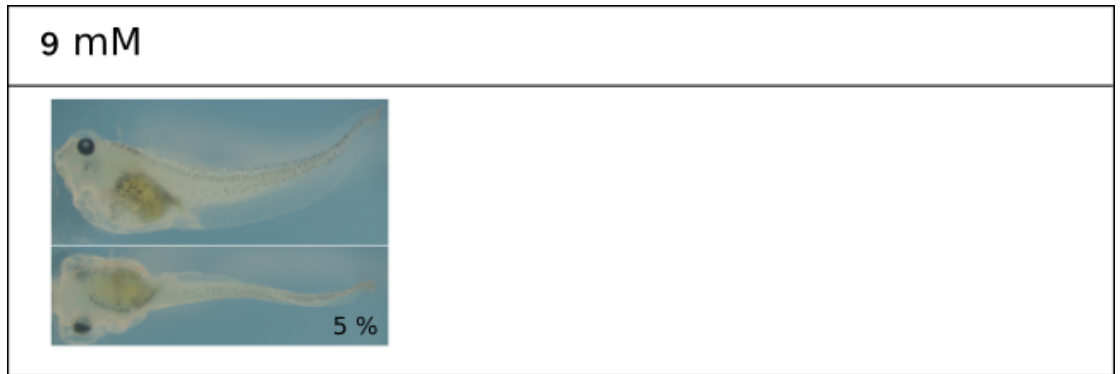


6 mM



7 mM





4.1.2

Figure 4-16: AMAP dose response 0, 5.5-10 mM.

Xenopus laevis embryos were treated with a AMAP concentration in the range 5.5-10 mM (n=3) from stage 38 and harvested at stage 45. The surviving embryos at stage 45 were photographed. There were no surviving embryos for 8 and 10 mM AMAP. In this figure are the different phenotypes found for each paracetamol concentration and the percentage of embryos that had that phenotype. The percentage is calculated from the total number of embryos treated. Where possible, the embryo was photographed to show the lateral view and the ventral view.

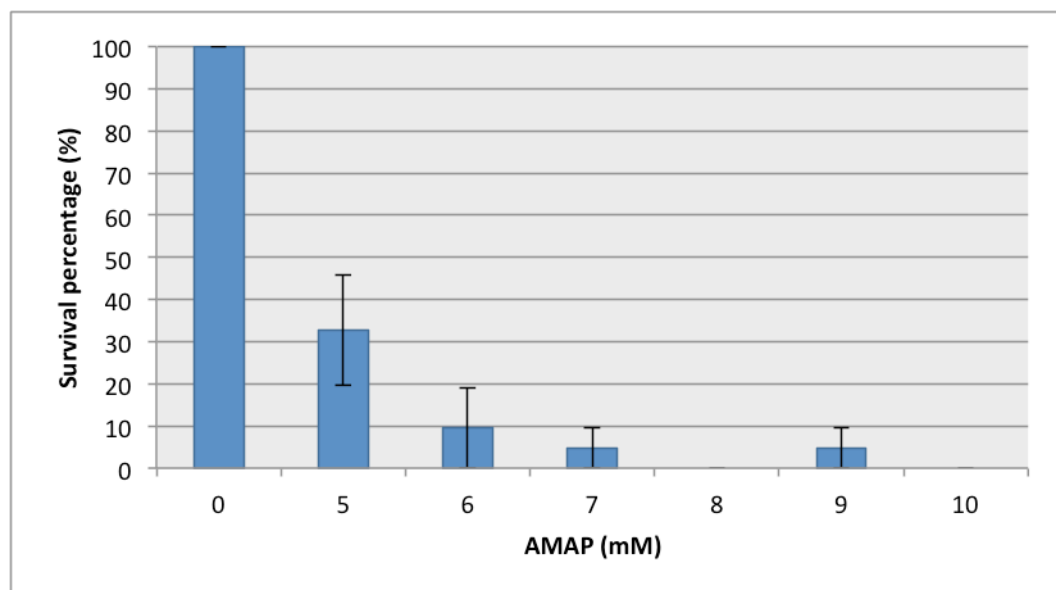


Figure 4-17: The percentage of *Xenopus* embryo survival with 5-10 mM AMAP treatment.

The average (\pm SEM) amount of embryos that survived until the age of stage 45 to be harvested and photographed for **Figure 4-16** (n=3).

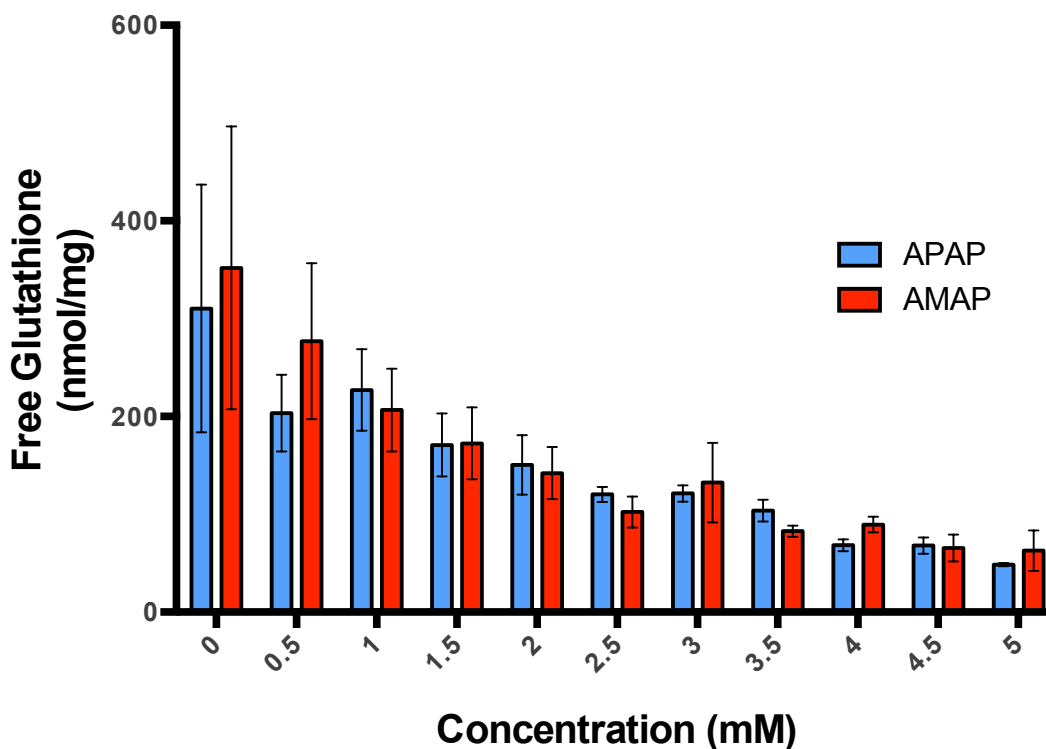


Figure 4-18: The amount of free GSH inside *Xenopus* embryos treated with paracetamol (APAP) or *N*-acetyl-meta-aminophenol (AMAP).

Xenopus laevis embryos were treated with 0-5 mM paracetamol (APAP) or 0-5 mM *N*-acetyl-meta-aminophenol (AMAP) from the age of stage 38, and harvested at stage 45 (n=3). The amount of free GSH (nmol/mL) was measured inside the embryos and normalised to the amount of protein (mg/mL). There was no significant difference between embryos treated with the same concentration of APAP and AMAP.

4.4.7 Characterisation of the metabolism of paracetamol in *Xenopus*

I attempted to determine the key steps of paracetamol metabolism in the *Xenopus* embryos that are crucial for the development of the paracetamol-associated DILI reaction seen in humans. To do this, I used 1-aminobenzotriazole (1-ABT), a known non-selective CYP450 inhibitor in humans and other mammalian models. The dose response with 1-ABT showed that significant oedema around the gastrointestinal region started developing at the 4 mM 1-ABT concentration and the incidence increased with increasing 1-ABT concentrations. The survival graph shows that death started occurring significantly at 6 mM 1-ABT. Subsequently, I decided to use the highest concentration of 1-ABT that did not cause death or a notably different phenotype, I decided to use 3 mM 1-ABT for the co-incubation with the APAP range of 0-5 mM.

At stage 38, *Xenopus* embryos were treated with 3 mM 1-ABT for 2h and then a concentration of APAP within the range 0-5 mM was added to the 1-ABT-containing incubation media and the embryo was harvested at stage 45 (**Figure 4-19**). The 3 mM 1-

ABT concentration was maintained throughout the entire incubation. The amount of free GSH was measured and compared between embryos treated with 1-ABT and APAP and embryos treated with APAP alone. As previously seen in this chapter, the amount of free GSH decreased in embryos treated with APAP alone with increasing APAP concentration. The same trend occurred for the embryos treated with 3 mM 1-ABT and APAP. However, the lower concentrations of the combined 1-ABT/APAP embryos had a lower free GSH compared to the APAP treated embryos of the same concentration. The embryos treated with 0-1 mM paracetamol and incubated with 3 mM 1-ABT, had less free GSH than the embryos treated with 0-1 mM paracetamol only.

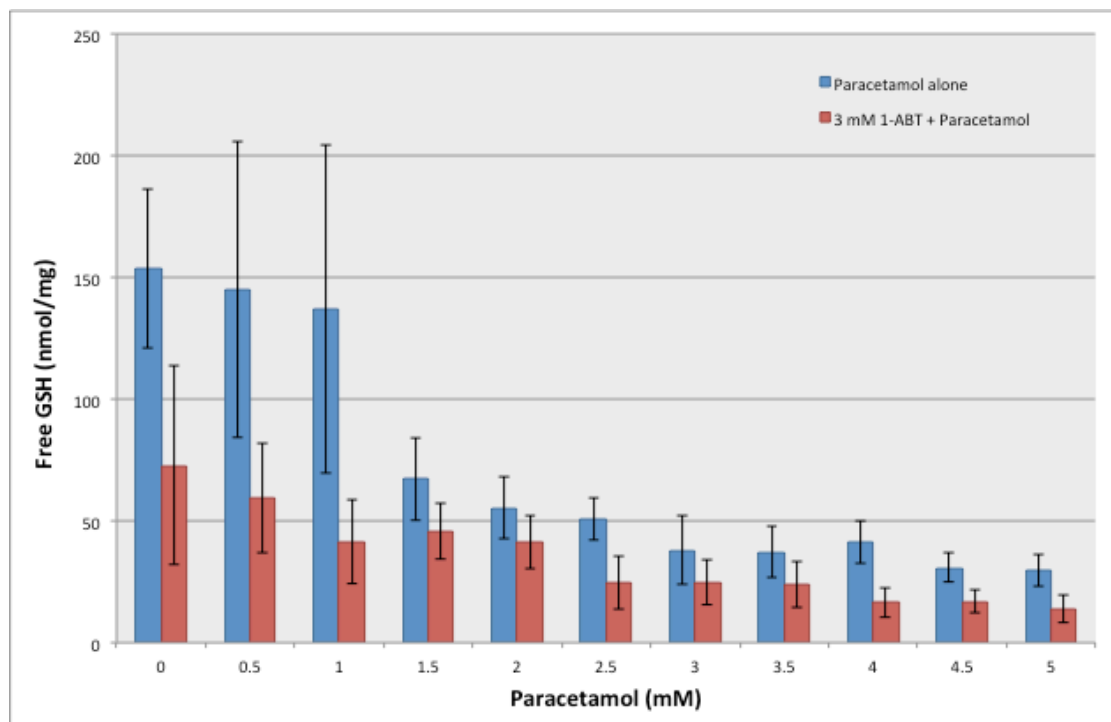


Figure 4-19: The amount of free GSH in embryos treated with 1-aminobenzotriazole (1-ABT) and paracetamol.

Xenopus laevis embryos were treated with 3 mM 1-ABT (red) and without 1-ABT (blue) with a concentration of paracetamol (0-5 mM) from the age of stage 38, and harvested at stage 45 (n=4). The amount of free GSH (nmol/mL) was measured inside the embryos and normalised to the amount of protein (mg/mL). The embryos treated with or without 1-ABT for the same concentration were not statistically significantly different.

4.4.8 *Xenopus* incubation with the human clinical treatment for paracetamol overdose

As mentioned in the earlier text of this chapter, NAC is used as the treatment for humans that have overdosed on paracetamol. I identified the highest dose of NAC that *Xenopus* embryos could tolerate by doing a dose response and noting the survival percentage. To begin with, I started with a concentration range of 0-10 mM NAC and the embryos were treated from stage 38 to stage 45. However all of the embryos treated with a concentration within 0-10 mM did not survive. So I lowered the dose range to 0-1 mM NAC. The survival percentage significantly decreased from 0.6-1 mM NAC. I decided to co-incubate *Xenopus* embryos with 0.5 mM NAC and a concentration within the range 0-5 mM APAP. Initially, I co-incubated NAC and APAP through 2 conditions: (1) incubation of the stage 38 embryos with 0.5 mM NAC for 2h and then the APAP concentration was added to the media and (2) concurrent 0.5 mM NAC and APAP (n=10) (**Figure 4-20A**). The embryos were harvested at stage 45 and compared to embryos treated with APAP alone. The free GSH concentration was measured and normalised to the untreated embryos for each condition which I denoted as a percentage of the 0 mM treatment group. Embryos treated with 0.5 mM NAC alone did not have a significantly different amount of free GSH to the untreated wildtype embryo (data not shown). Embryos that were pre-incubated with NAC before the APAP addition, had a decrease in free GSH with increasing APAP concentration, however the gradient was smaller in comparison to their counterparts that were treated with APAP only. The concurrent NAC and APAP co-incubation also had a negative correlation between free GSH and APAP concentration, but this gradient was, on average, smaller than the pre-incubation treatment.

Next, I decided to add the 0.5 mM NAC to APAP-treated embryos 24h, prior to their harvest at stage 45 (n=5) (**Figure 4-20B**). I saw that the free GSH measured in the embryos treated with NAC was, on average, higher than the counterpart embryos treated with the same APAP concentration but APAP alone. However the amount of free GSH measured in NAC-treated embryos did decrease with increasing APAP concentration.

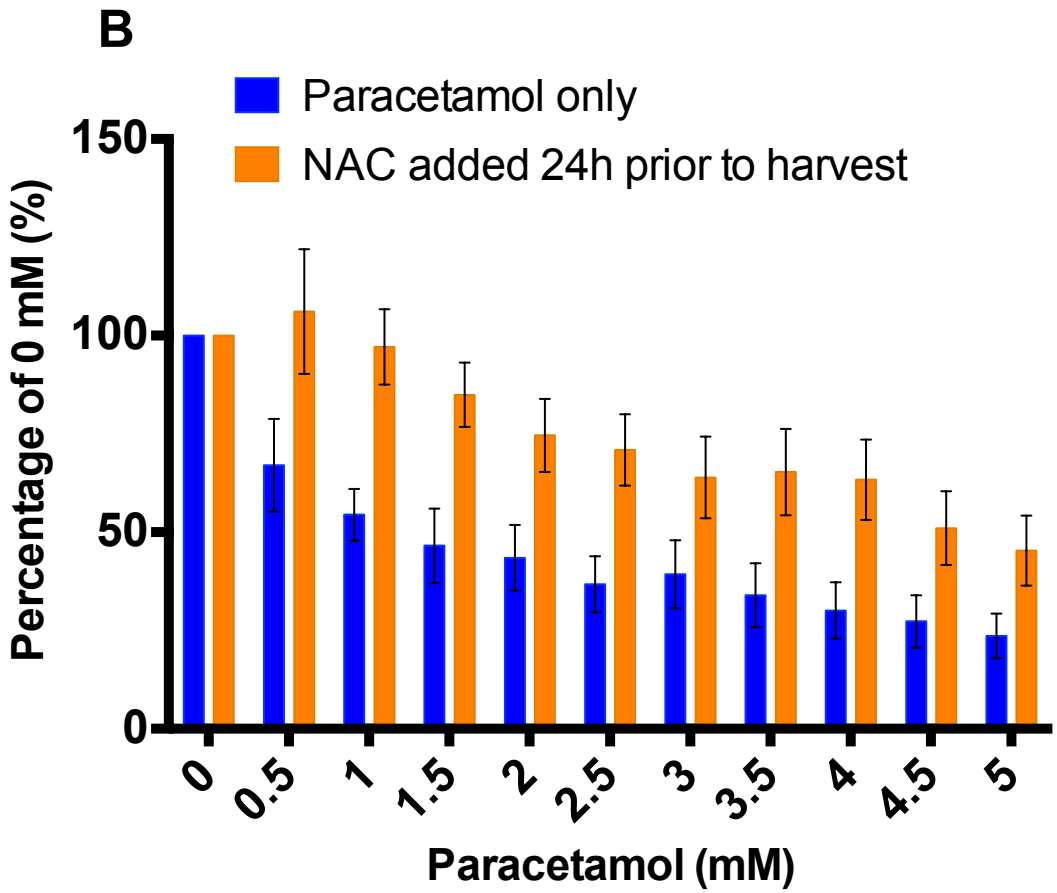
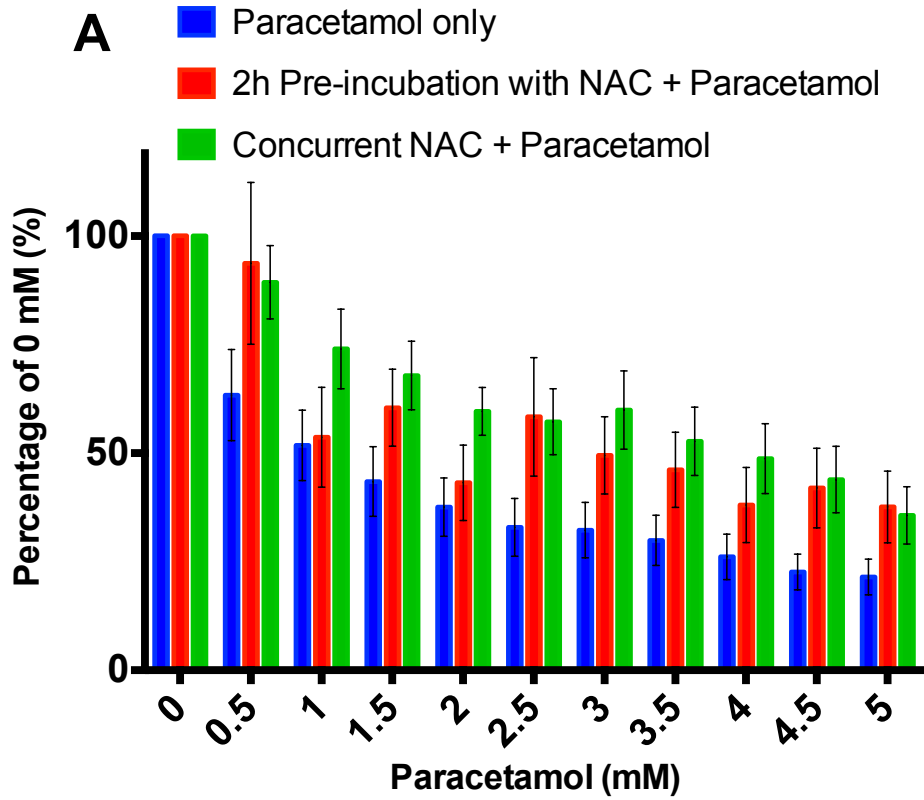


Figure 4-20: Free GSH in embryos treated with paracetamol and N-acetyl cysteine (NAC).

Embryos were treated with paracetamol (0-5 mM) for 72h with or without the addition of 0.5 mM NAC, they were harvested at stage 45. For the initial experiments (A) there were 3 conditions: treatment with paracetamol alone (blue), 2h incubation with NAC prior to the addition of paracetamol (red) and concurrent treatment with NAC and paracetamol (green) (n=10). The embryos were also treated with APAP and then with NAC for 24h prior to harvest (orange) or with paracetamol alone (blue) (B) (n=5). The amount of free GSH inside the embryos was measured and normalised to the amount of protein. This value was then normalised to the embryos treated with 0 mM paracetamol of the treatment group. The amount of free GSH measured was calculated as a percentage of the 0 mM paracetamol treatment group (\pm SEM).

4.5 Investigating an alternative drug known to be associated with drug-induced liver injury

4.5.1 Diclofenac-induced liver injury

Diclofenac is a non-steroidal anti-inflammatory drug (NSAID) that is taken for its analgesic, antipyretic and anti-inflammatory properties for diseases such as ankylosing spondylitis and rheumatoid arthritis (Boelsterli, 2003). However, it is the most commonly used NSAID that is still on the market but is also associated with drug-induced liver injury (DILI) (Thompson et al., 2012). The US Food and Drug Administration (FDA) have diclofenac under black box warning for its potential to cause mitochondrial damage, cardiovascular toxicity and hepatotoxicity (Dykens and Will, 2007). The majority of patients tolerate diclofenac but cases of hepatotoxicity and liver failure have been reported. Diclofenac is associated with idiosyncratic hepatotoxicity, and although the exact mechanisms of toxicity are unknown, the metabolites derived from diclofenac are thought to play a crucial role. 4'-OH-Dic and 5'-OH-Dic are diclofenac metabolites generated from phase I oxidation drug metabolism reactions from the activity of CYP2C9 and CYP3A4 respectively. Both of these oxidation products have the potential to be further oxidised to *p*-benzoquinone imines, which are very electrophilic and can covalently bind to non-protein and protein sulfhydryl groups (Syed et al., 2016). The phase II metabolite diclofenac 1-O-acyl glucuronide and its derivative diclofenac glutathione thioester have also been implicated in diclofenac-mediated liver injury. The acyl glucuronide metabolite is a product of the UGT2B7 (uridine 5'-diphospho-glucuronosyltransferase 2B7) isoenzyme and can covalently bind to hepatocellular proteins and impair their activity (Kretz-Rommel and Boelsterli, 1993). Diclofenac glutathione thioester is thought to be involved in

diclofenac-induced liver injury because it is highly reactive with thiol groups, even more so than the glucuronide metabolite (Grillo et al., 2003; Syed et al., 2016). Overall, studies suggest that diclofenac and its metabolites mediate hepatotoxicity via mitochondrial dysfunction (**Figure 4-21**) (Boelsterli, 2003; Gómez-Lechón et al., 2003; Masubuchi et al., 2002; Syed et al., 2016).

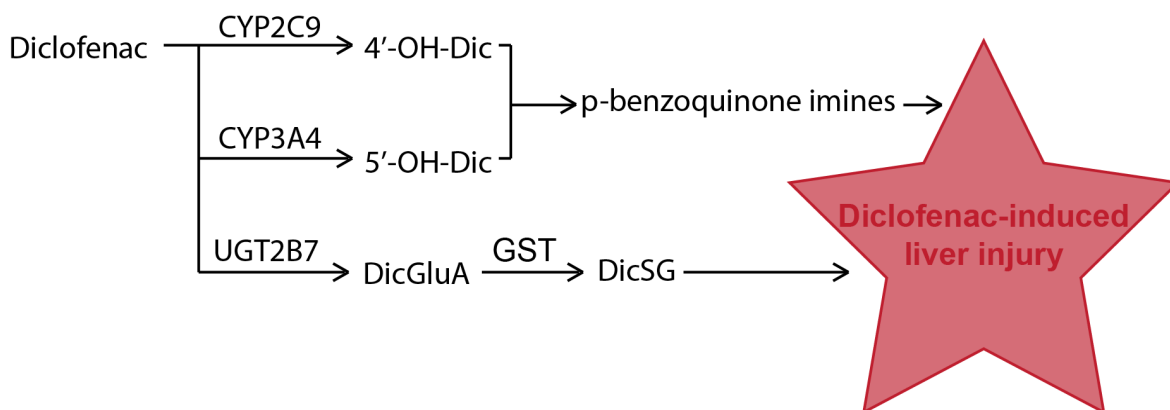


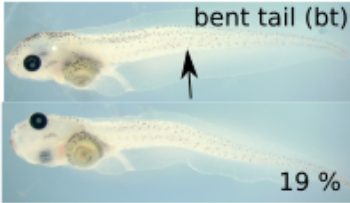
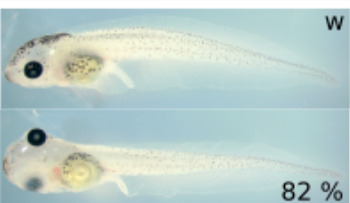
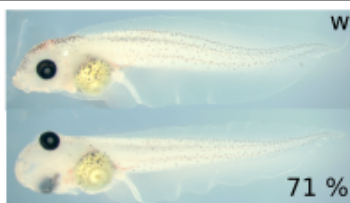
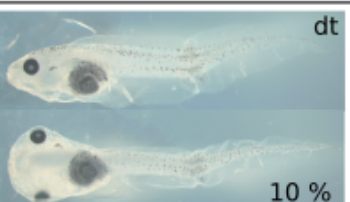
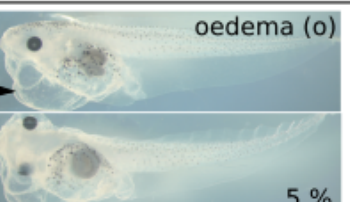
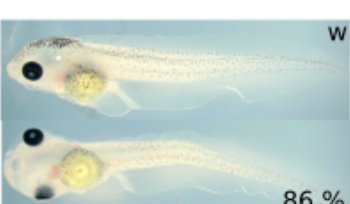
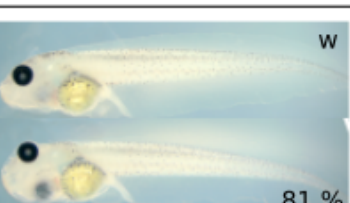
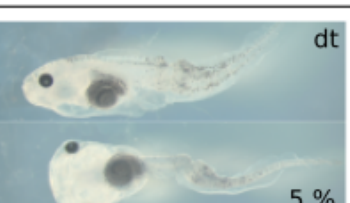
Figure 4-21: Diclofenac mechanism of toxicity

Diclofenac metabolites contribute to the generation of diclofenac-induced liver injury. Phase I metabolism produces hydroxyl metabolites via the CYP450 isoenzymes CYP2C9 and CYP3A4. The phase II metabolism enzyme uridine 5;-diphosphoglucuronosyltransferase 2B7 (UGT2B7) produces diclofenac 1-O-acyl glucuronide (DicGluA), which is conjugated to glutathione via glutathione S-transferase (GST) to produce diclofenac glutathione thioester (DicSG).

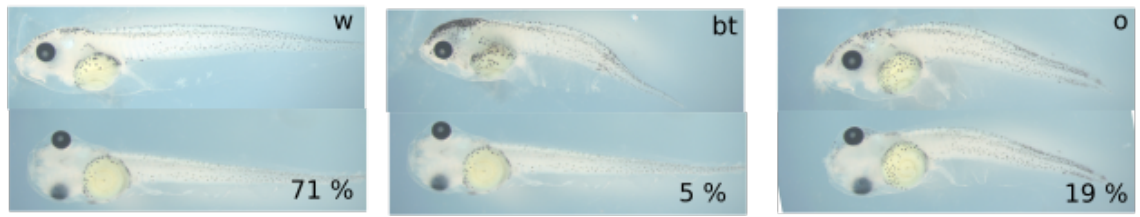
4.6 Diclofenac Results

4.6.1 Diclofenac dose response in *Xenopus laevis*

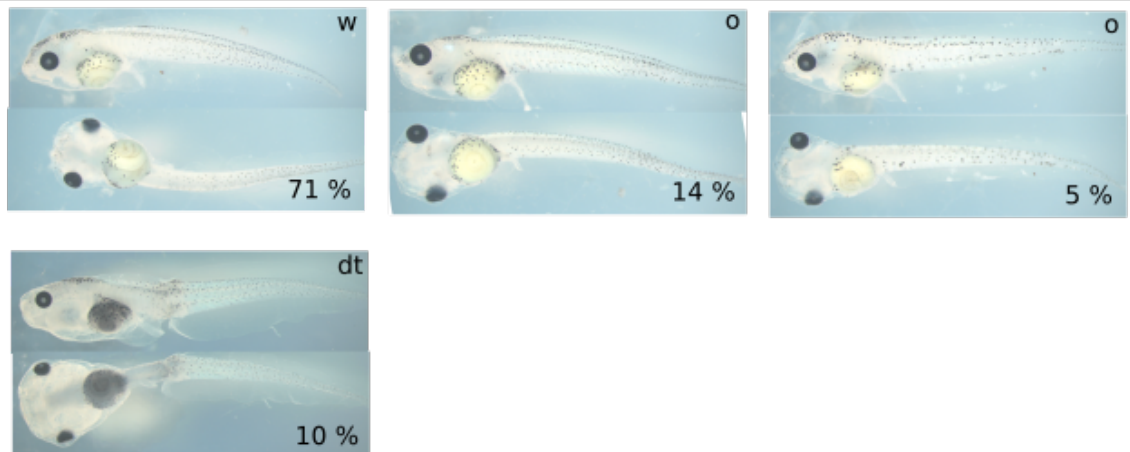
In the initial screens conducted with diclofenac in **chapter 3** using stage 38 to stage 45 embryos, the survival appeared to decrease after the 12.5 μM concentration. Consequently, I decided to start with a dose range of 0-10 μM (n=3) (**Figure 4-22**). For all of the concentrations in this range, the majority phenotype was the same as the untreated (0 μM diclofenac) embryos. One incidence of oedema in the gastrointestinal region occurred in the 1 μM diclofenac concentration group. A common phenotype that occurred in most of the concentrations was a damaged tail. The survival percentage did not significantly decrease for the 1-10 μM diclofenac concentration range (**Figure 4-23**), I decided to look at a higher range of 11-20 μM (n=1, data not shown). For this range, the survival significantly decreased to 0 % after 12 μM diclofenac, from 13-20 μM .

0 uM		
 <p>wildtype (w) 81 %</p>	 <p>bent tail (bt) 19 %</p>	
0.25 uM		
 <p>w 82 %</p>	 <p>damaged tail (dt) 14 %</p>	
0.5 uM		
 <p>w 71 %</p>	 <p>bt 29 %</p>	
1 uM		
 <p>w 76 %</p>	 <p>dt 10 %</p>	 <p>oedema (o) 5 %</p>
2 uM		
 <p>w 86 %</p>	 <p>bt 5 %</p>	
3 uM		
 <p>w 81 %</p>	 <p>dt 10 %</p>	 <p>dt 5 %</p>

4 uM



5 uM



6 uM



7 uM



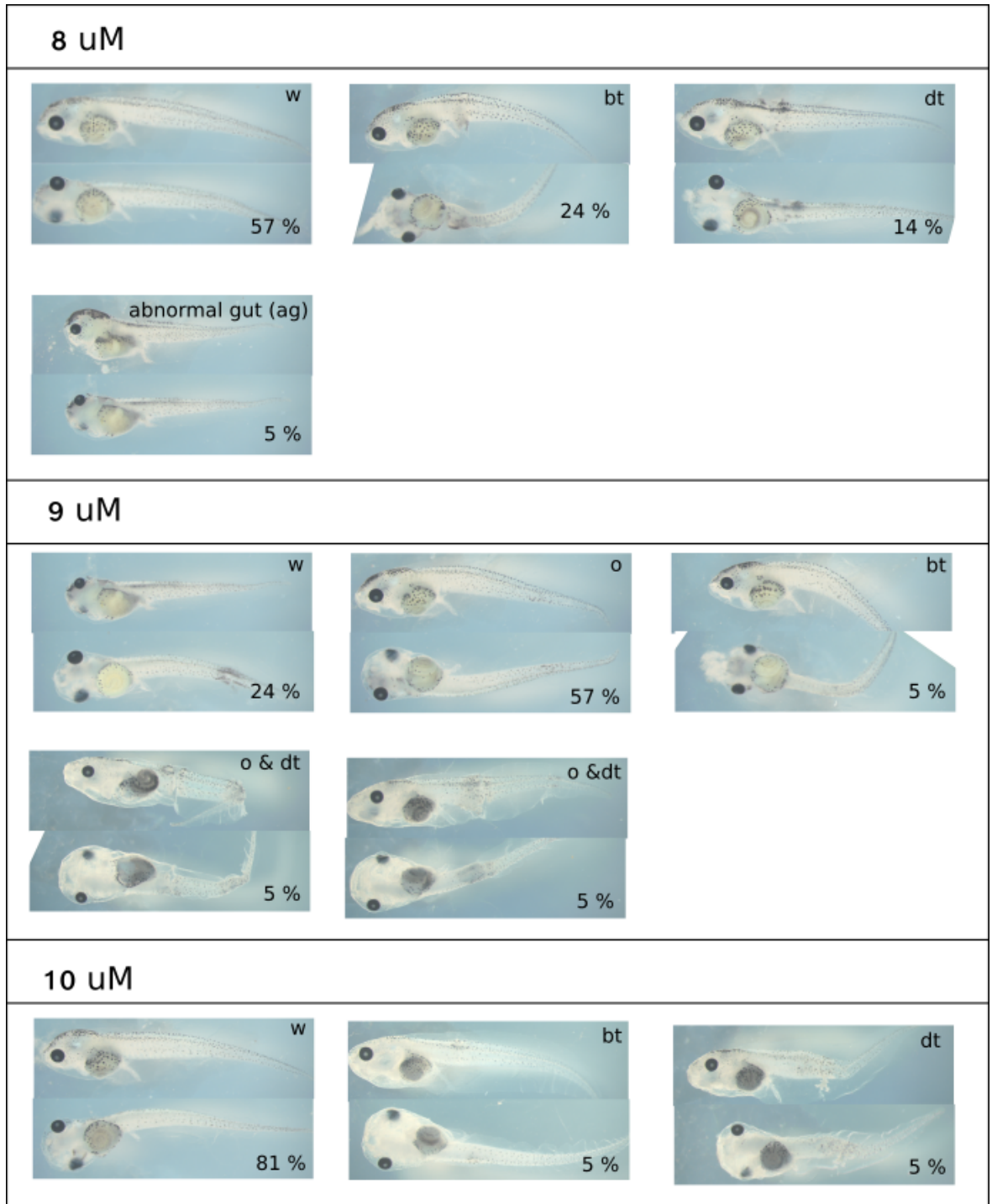


Figure 4-22: Diclofenac dose response 0-10 μM .

Xenopus laevis embryos were treated with a diclofenac concentration in the range 0-10 μM (n=3) from stage 38 and harvested at stage 45. Surviving embryos were photographed at stage 45. The different phenotypes are shown for each diclofenac concentration and the percentage of embryos that had that phenotype. The percentage is calculated from the total number of embryos treated. Phenotypes include wildtype (w), damaged tail (dt), bent tail (bt), oedema (o) and abnormal gut (ag). The percentage is

calculated from the total number of embryos treated. Where possible, the embryos were photographed to show the lateral view and the ventral view.

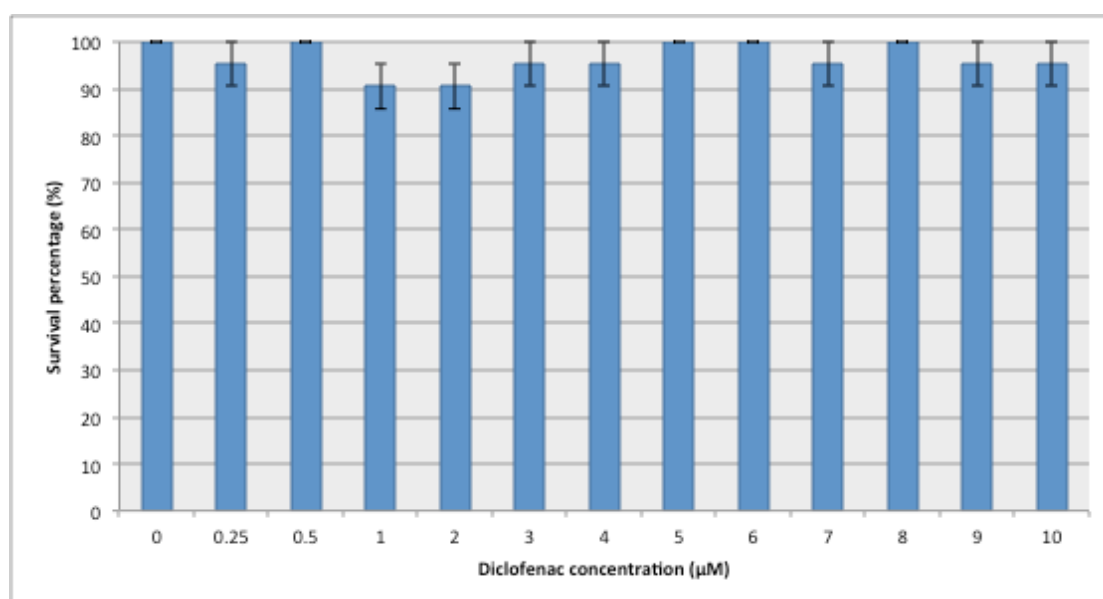


Figure 4-23: The percentage of *Xenopus* embryo survival with 1-10 µM diclofenac treatment.

The average (\pm SEM) amount of embryos that survived until the age of stage 45 to be harvested and photographed for **Figure 4-21** (n=3).

4.7 Discussion

As stated earlier the overall aim of the project is to assess the use of *Xenopus* as a model to predict drug-induced toxicity and this chapter predominantly focuses on one known hepatotoxic drug, paracetamol. Consequently, ultimately I have investigated the effect of paracetamol overdose on *Xenopus* embryos and can now compare the model to humans as well as mammalian and non-mammalian animal models. The results generated here can suggest the suitability of *Xenopus* as model to predict drug-induced hepatotoxicity.

4.7.1 Paracetamol Overdose Concentration Range and Phenotypes

In *in vitro* safety studies, the concentration of a drug candidate that exerts drug-specific toxicity mechanisms is defined as the highest concentration that induces approximately 20 % cell death. At least 80 % viability is required at this concentration. The ratio between this high concentration and the peak serum concentration of the drug candidate should be at least ten-fold, this ratio is called the safety margin (SM). A drug candidate with a value of $SM < 10$, is identified as a compound that has a high probability of causing a DILI reaction (Richert et al., 2016). In drug development, it is important to use the correct

concentration that is relative to the toxicity safety studies to be performed in higher-order animal models and humans.

The photographs in **Figure 4-4** depict the embryos that were alive at the harvest age, stage 45. The phenotypes of the embryos that died before stage 45 were not recorded. Therefore I was looking for a paracetamol concentration that was toxic, but did not kill the embryos, thus a concentration that would produce the pathophysiology of paracetamol-specific toxicity, not general toxicity that could occur if a system is given too many of any xenobiotic.

Despite the fact that they were sometimes difficult to manipulate, the embryos were photographed true to how they were found at their harvest age. The phenotype observed is a consequent of the paracetamol treatment. The gastrointestinal oedema phenotype in the *Xenopus* embryos was also observed in response to paracetamol in zebrafish larvae (Verstraelen et al., 2016). The paracetamol concentration range 0-5 mM is consistent with the dose used to investigate paracetamol-induced hepatotoxicity in zebrafish in the literature. Unlike the initial dose response screenings in **chapter 3**, the paracetamol used in this chapter was dissolved in the *Xenopus* media without the use of DMSO. This is important because DMSO is a known CYP450 inhibitor, and the pathophysiological mechanism of paracetamol-induced hepatotoxicity requires the generation of the reactive metabolite using CYP450 activity (Yoon et al., 2006). Overall the high mortality in the range 5.5-10 mM paracetamol coupled with some incidence of gastrointestinal oedema in the 0-5 mM range established the 0-5 mM concentration range as a sufficient dose to perform the following characterisation assays in this chapter, to observe *Xenopus* embryos and their response to a paracetamol overdose.

4.7.2 Characterising the *Xenopus* embryo response to paracetamol overdose

4.7.2.1 Free GSH

For a long time, it was thought that a significant reduction of free GSH upon drug candidate administration is indicative of oxidative stress and covalent binding and modification of proteins that leads to liver toxicity and activation of the innate immune system. A 90 % reduction of free GSH compared to the untreated normal value is considered significant (Geenen et al., 2013). However it has been argued that a reduction in free GSH is not necessary for covalent binding to proteins to occur (McGill and Jaeschke, 2013). In HepaRG cells treated with paracetamol, protein binding occurred before the GSH depletion (McGill et al., 2011). Furthermore, humans that have been administered therapeutic doses of paracetamol have protein adducts in their serum but their GSH level remains normal (Heard et al., 2011). Consequently the relationship between free GSH reduction and liver injury is not definitive. However, for paracetamol-

induced liver injury in humans, the reduced amount of free GSH is part of the pathophysiology mechanism as it allows the accumulation of the reactive metabolite NAPQI. Therefore it is an important assay to perform with the *Xenopus* embryos in order to determine if paracetamol is metabolised via the same pathway as mammals, and this would imply the embryos can be susceptible to a paracetamol-induced liver injury reaction.

The reduction of free GSH observed in the *Xenopus* embryos (**Figure 4-8A**) implies they have generated a small molecule from paracetamol, which depletes the free GSH store. The absence of the reduction in the embryos treated for only 24h shows the GSH depletion is time-dependent. Although statistically significant, the GSH depletion with the highest paracetamol concentration tested (5 mM) is a 52.1 % reduction compared to the untreated embryos, not the 90 % significant reduction as favoured by researchers that suggests a high risk DILI compound. It would be interesting to see if such a great reduction occurs with embryos treated with higher paracetamol concentrations.

4.7.2.2 The use of miR-122 as a biomarker for DILI in *Xenopus* embryos

The *Xenopus* miR-122 has the same nucleotide sequence as zebrafish, humans and rodents and the WISH results show that miR-122 is liver-specific in the *Xenopus*, much like these animal models as well (Vliegenthart et al., 2014a; Wienholds et al., 2005). Fragmented WISH miR-122 staining in the liver indicates hepatocyte injury. However, I could not detect a difference between the sections from paracetamol-treated embryos and untreated. The WISH protocol can make the embryo tissue more delicate and the size of the embryo can also contribute to the difficulty of obtaining good quality sections. To optimise the quality, I tried different embedding, sectioning and fixation techniques, such as embedding in OCT compound, sectioning using a cryostat, and fixing in a formaldehyde-containing solution for a longer period of time (data not shown). The best quality sections, shown here, were produced with wax embedding with a microtome and the fixation method stated in **chapter 2**. The incidence of holes in the tissue sections was similar in the untreated and treated embryos. In conclusion, we believe the holes seen in the sections were not paracetamol-specific, but possibly due to the technique.

Subsequently, I attempted to identify liver necrosis using the Terminal deoxynucleotidyl transferase dUTP nick end labelling (TUNEL) assay using a 12-UTP fluorescein label which has been shown to label necrotic cells as well as apoptosis (data not shown). The results were inconclusive and further work is needed to optimise this assay for use with *Xenopus* embryo sections.

The presence of miR-122 in the blood in humans is an indication of hepatotoxicity. The *Xenopus* embryos have a circulatory system at the age I was treating them, but the size of

the embryos is too small to be able to easily obtain a blood sample, and the volume of blood within the embryo is very little. Consequently, in order to measure the expression of miR-122 with paracetamol treatment, we decided to use the tail tissue to represent the blood. The tail contains a good vasculature and the liver tissue is not present in this body compartment. Under healthy circumstances there should not be a significant amount of miR-122 expression found in the tail. The size of the embryos means dissecting the liver alone would be difficult and time consuming. I therefore decided to dissect the whole gastrointestinal or gut region, including the liver, to represent the liver miR-122 expression. I normalised the miR-122 expression against miR-103 expression in the tissue of the embryos. Unlike U6, which is a small nuclear RNA (snRNA) that is traditionally used for miRNA quantification in qRT-PCR, miR-103 is not affected by paracetamol treatment (Wang et al., 2013). Vliegthart and colleagues (2015) identified a comprehensive list of endogenous miRNAs unaffected by paracetamol in humans, however unfortunately none of the best miRNAs mentioned are expressed in *Xenopus laevis* (Vliegthart et al., 2015).

The increase of miR-122 expression in the tail with increasing paracetamol concentration in **Figure 4-12** implies paracetamol-induced hepatotoxicity. The slight reduction of miR-122 expression in RNA isolated from gut tissue is indicative of liver damage, however there is no linear trend of miR-122 expression in the gut with regards to paracetamol concentration. This may be because miR-122 expression in the liver is so abundant, that a slight depletion cannot be detected.

4.7.2.3 Detection of Paracetamol Metabolites using HPLC-MS/MS

The mass spectrometry analysis was performed by Dr. Mark Bayliss at the MRC Centre for Drug Safety Science in the University of Liverpool using tissue samples generated in our laboratory. Unfortunately only one set of samples could be analysed (n=1) therefore I cannot perform statistical analysis on this data. The difference observed between theoretical and measured paracetamol concentrations must be taken into account when we interpret the detection of the paracetamol metabolites. Where the ratio of the analyte inside the embryo versus the analyte in the media is less than 0.02, the results for embryo represented the concentrations in residual media that was still attached to the outside of the embryo. For future experiments, I would suggest we washed the embryos with phosphate buffered saline (PBS) to remove this media and consequently ambiguous results. The detection of the presence of all the paracetamol metabolites we looked for is promising in so far as it suggests the embryos took up the parent drug from the media they were swimming in. The ratios of the paracetamol metabolites in the *Xenopus* embryos are more similar to the paracetamol metabolism observed in children than in

human adults (**Figure 4-14**). As previously described in this chapter, in human adults the ratio of the APAP-glucuronide to APAP-sulphate metabolites is approximately 2:1. Children produce more of the APAP-sulphate the ratio to APAP-glucuronide is more akin to 1:1. The reasons for the differences have not been established however it is thought that a more active SULT enzyme activity in children compared to adult, contributes to the different metabolic profiles (Barshop et al., 2011). In addition, although not that much data is available, the incidence of paracetamol-induced hepatotoxicity is lower in children than adults (W.M. Lee, 2003; Squires Jr. et al., 2006). But the oxidative pathway is more active in children than adults; children generate more of the reactive metabolite. The lower paracetamol-associated DILI incidence coupled with a higher production of NAPQI suggests children have more efficient detoxifying pathways (Penna and Buchanan, 1991). Furthermore, young mice are less susceptible to paracetamol-induced toxicity than their adult counterparts. This is thought to be attributed to a 4-fold higher GSH turnover and a more active GST system compared to adult mice (Adamson and Harman, 1989; Lauterburg et al., 1980). In summary, the results of the mass spectrometry analysis suggest the *Xenopus* embryos could be more similar to children and consequently they could be more adept at detoxifying xenobiotics. As stated, more experiments need to be carried out.

4.7.2.4 Investigating the expression of a transporter involved in paracetamol metabolite excretion: MRP2

For this experiment, all of the embryos were treated with 5 mM paracetamol at stage 38 and the gastrointestinal region was isolated and processed to investigate the change in MRP2 mRNA expression. Some of these embryos were harvested at stage 42, some at stage 44 and some at stage 45. The stage 45 harvested embryos were treated with paracetamol for the same amount of time as the dose response assays in this chapter. The expression of *Xenopus laevis* MRP2 was normalised to untreated embryos. The different harvest stages allowed us to analyse the expression of MRP2 over time following a single toxic dose of paracetamol. In male C57BL/6J mice, Mrp2 expression in the liver was significantly induced with a paracetamol dose ≥ 400 mg/kg (Aleksunes et al., 2006, 2005). This expression did not follow a time-dependent trend. The Mrp2 liver protein expression was upregulated in male Wister rats treated with 1 g/kg paracetamol (Ghanem et al., 2004). Studies involving the expression of MRP2 with paracetamol overdose in zebrafish are not available in the literature.

MRP2 expression increases in the stage 44 and stage 45 embryos compared to stage 42 and untreated embryos. However the absence of a positive linear correlation implies the expression is not time-dependent, indeed the expression of MRP2 appears to decrease

from stage 44 to stage 45. One explanation for this could be that the peak MRP2 expression is at stage 44 and by stage 45, the embryos have managed to control the accumulation of metabolites that require exportation from the hepatocyte via MRP2 activity. Perhaps the *Xenopus* have an alternative neutralising agent in their metabolic capacity to be able to do this. In order to clarify these results, further work should be done to explore the protein expression of MRP2. I would also suggest a greater range of harvest stages could help to establish the MRP2 expression pattern, and using a range of paracetamol doses would be interesting to ascertain the dose-dependent expression of MRP2. Characterising the expression of all the major efflux transporters involved in paracetamol excretion, for example MRP3, MRP4 and BCRP, could help determine the similarities or differences of paracetamol overdose in *Xenopus* and other animal models or humans.

4.7.2.5 Intervention with 1-ABT to elucidate the mechanisms of paracetamol-induced liver injury in *Xenopus* embryos

I hypothesised that 1-ABT will inhibit the CYP450 activity in the *Xenopus* embryos and consequently reduce the amount of reactive metabolite (NAPQI) produced. Therefore less GSH will be required to neutralise this reactive metabolite and a higher amount of free GSH will be detected in the GSH assay, compared to embryos not incubated with 1-ABT. I used 3 mM 1-ABT, which was the highest concentration of 1-ABT that the embryos could tolerate without any obvious phenotypic effects. All the embryos in the 1-ABT treatment group (**Figure 4-19** red bars) were incubated with 3 mM 1-ABT in addition to the paracetamol concentration noted on the X-axis. As per the previous GSH assay experiments in this chapter, the whole embryo was processed to measure the amount of free GSH. The amount of free GSH in 0 mM paracetamol control groups differed, although the difference is not statistically significant ($P=0.34$). However this difference suggests that the 1-ABT compound alone reduces the amount of free GSH available in the embryo. We do not understand the mechanism for this. The average free GSH for 0.5 mM and 1 mM paracetamol treatment also appears to be different for the 1-ABT group compared to paracetamol alone, but not statistically different ($P=0.34$ and $P=0.11$ respectively). I questioned if the 1-ABT compound has the same inhibitory affect in the non-mammalian *Xenopus* embryos as is established in mammalian models. To investigate this, I attempted to isolate *Xenopus* microsomes from adult liver homogenate that is available in our laboratory. In mammals, microsomes contain high concentrations of the CYP450 enzymes, I hypothesised the same traditional high centrifugation isolation method will obtain *Xenopus* microsomes that also contain CYP450s in abundance. The substrate *p*-nitrophenol is converted to 4-nitrocatechol in a hydroxylation reaction catalysed by

CYP450 enzymes (Monostory et al., 2004). This reaction can be used to measure CYP450 inhibition with 1-ABT. In the future I would like to optimise this experiment to determine the effectiveness of 1-ABT inhibition of *Xenopus* CYP450. This could help interpret the 1-ABT results I generated in this chapter.

4.7.2.6 Treatment with NAC, the clinical treatment for paracetamol overdose in humans

Overall 3 incubation conditions were carried out with 0.5 mM NAC and 0-5 mM paracetamol: (1) 2h NAC incubation prior to paracetamol addition (2) concurrent NAC and paracetamol treatment and (3) NAC incubation in paracetamol-treated embryos for 24h prior to harvest. Of the 3 conditions performed, the 24h incubation prior to harvest is the most clinically relevant to humans. However in all of the treatment conditions, the amount of free GSH measured is greater in the embryos of the NAC treatment group compared to the embryos without NAC, of the same paracetamol concentration group. This smaller decline of free GSH with NAC treatment suggests the embryos are metabolising paracetamol to generate a small molecule that depletes GSH, and this pathway can be reversed through the administration of NAC. This rescue mechanism implies but cannot confirm, that the reactive metabolite generated in the *Xenopus* embryos could be NAPQI, the same reactive metabolite produced in humans and animal models. The results are similar to the NAC response observed in zebrafish paracetamol overdose. In adult zebrafish treated with paracetamol, the amount of free GSH increased with NAC administration compared to zebrafish treated with paracetamol alone (North et al., 2010). Overall these NAC response results indicate that *Xenopus* embryos are a promising model as they exhibit reactivity to human treatments, which is similar to another promising non-mammalian model, the zebrafish.

4.7.3 AMAP: the non-toxic regioisomer of APAP

AMAP is the controversial, supposedly less toxic positional isomer to paracetamol. It has similar therapeutic indications to paracetamol, such as analgesic properties. Initially, I decided to use AMAP in comparison with paracetamol in **chapter 3** to determine if the *Xenopus* embryos can distinguish a non-toxic drug from a toxic drug. However literature suggests the AMAP lower risk of toxicity is species-dependent. Hadi and colleagues (2013) investigated the different AMAP toxicity susceptibility between rat, mouse and humans using precision-cut liver slices (PCLS). PCLS are an *ex vivo* tool that can be used in small studies to research drug-induced hepatotoxic reactions. In PCLS the liver structure and cell interactions are maintained and the gene expression profile is very similar to a functional, intact liver (Boess et al., 2003; Lerche-Langrand and Toutain, 2000; Olinga et al., 1997; Vickers and Fisher, 2004). In this study, the mouse PCLS incubated with paracetamol had a lower ATP content and lower histomorphological score than the

rat and human PCLS incubated with the same paracetamol concentration. This suggests mice are more susceptible to paracetamol than humans. Furthermore, AMAP showed a significantly lower toxicity profile than paracetamol in the mouse PCLS, whereas in rat and human PCLS, the AMAP toxicity phenotype appeared to be equal to or more toxic than the paracetamol. The mouse differential response to AMAP and paracetamol has been replicated in *in vitro* and *in vivo* experiments and is also true for the hamster model (Nelson, 1980; Rashed et al., 1990; Roberts et al., 1990; Tirmenstein and Nelson, 1989). The difference in toxicity in mouse is attributed to the lower production of reactive metabolite from AMAP compared to paracetamol, the GSH depletion is greater with paracetamol than AMAP, and the reactive metabolites produced do not bind to as many mitochondrial proteins as paracetamol (Howell et al., 2014; Rashed et al., 1990; Salminen et al., 1997; Tirmenstein and Nelson, 1989). But the absence of a difference for AMAP and paracetamol toxicity in rat and human models highlights the importance of using animal models that are relevant to humans and understanding the limitations of an animal model in order to improve drug toxicity prediction.

In our *Xenopus* embryos, the lack of significant difference between AMAP and paracetamol for the depletion of GSH indicates *Xenopus* could have a similar toxic reaction to AMAP as paracetamol. The embryos also have a similar concentration-dependent survival percentage for AMAP and paracetamol. Unfortunately, I could not find any literature researching AMAP versus paracetamol toxicity in zebrafish, which could be a useful comparison for our fellow non-mammalian animal model. I do not think this result diminishes the integrity of the *Xenopus* toxicity prediction model because toxicity associated with AMAP is not consistent across the existing animal models in drug development.

4.7.4 Investigating an additional hepatotoxin: diclofenac

In order to characterise the *Xenopus* embryos as a model of detecting hepatotoxicity, not just the paracetamol-specific phenotype, I decided to look at another drug known to cause hepatotoxicity, diclofenac. The concentration of diclofenac that did not cause a high percentage of mortality was approximately 1000-fold lower than the concentration of paracetamol the embryos received. I would like to compare the lipophilicity of diclofenac versus paracetamol, as this physicochemical property could be an important factor that contributes to the amount of drug that can pass from the *Xenopus* media into the embryo through the embryonic membrane. Unfortunately I did not have enough time to investigate the diclofenac phenotype further. It would be interesting to research the mechanism that caused the diclofenac-induced tail damage displayed in the phenotype photographs (Figure 4-22).

4.8 Conclusion

The scope for future work has been mentioned for individual experiments throughout the discussion. Overall our *Xenopus* embryo model appears to have the ability to react to paracetamol in a dose-dependent manner. The depletion of GSH with paracetamol treatment suggests the *Xenopus* embryo metabolic pathway is similar to that observed in humans and rodent paracetamol-induced liver injury models. Going forward it would be good to confirm the mechanism of toxicity using a CYP450 inhibitor that is valid for *Xenopus*. Furthermore, I would like to determine the CYP450 isoform that could be involved in the *Xenopus* metabolism of paracetamol. Although the dominant isoform in humans that generates the reactive metabolite NAPQI is the CYP2E1, in zebrafish the CYP3A65 isoform is predominantly responsible for NAPQI generation (Chng et al., 2012). In summary, these results represent the initial steps towards determining the advantages and limitations of our *Xenopus* embryo model as a predictive tool for drug-induced hepatotoxicity. It is promising that the embryos can react to paracetamol, a frequently used drug that is responsible for the largest proportion of drug-induced liver injury in humans.

5 Chapter 5: Assessing the use of *Xenopus* as a model for the prediction of Drug-induced Cardiotoxicity using doxorubicin and terfenadine as the model cardiotoxins

5.1 Introduction

5.1.1 Doxorubicin-induced cardiotoxicity

Doxorubicin is an anthracycline antibiotic that targets haematogenous and solid malignancies (Gu et al., 2015). The exact anti-cancer therapeutic mechanisms of doxorubicin are not completely understood but theories include: (1) inhibition of topoisomerase II which results in DNA damage so the cell cannot replicate, (2) interference with the separation of DNA strands and helicase activity, and (3) DNA alkylation (Hortobagyi, 1997). There are 2 topoisomerase enzymes: α and β . The topoisomerase II α enzyme is thought to be the main therapeutic target for doxorubicin as it is overexpressed in tumour cells (Zhang et al., 2012). Topoisomerase II β is expressed in quiescent cells (Capranico et al., 1992). Patients taking doxorubicin have a significantly high incidence of cardiovascular side effects including hypotension, tachycardia, arrhythmias and congestive heart failure (Singal and Iliskovic, 1998). In part, some of the doxorubicin-induced cardiotoxicity has been attributed to the inhibition of the topoisomerase II β in quiescent cardiomyocytes. Topoisomerase II β inhibition can cause a reduction of antioxidant enzyme gene transcription and a reduced activation of the p53 pathway for apoptosis (Zhang et al., 2012). Doxorubicin-induced cardiotoxicity can occur after a single dose, or after repeated administration for weeks or months. The acute cardiotoxic effects manifest within minutes to a week from the initial doxorubicin administration. They are normally reversible and include arrhythmias and inflammation of the heart muscle and the membrane surrounding the heart (myocarditis and pericarditis respectively) (Bristow et al., 1978). The temporary arrhythmias that occur in approximately 20-30 % of patients can be detected in the clinic by changes to the ECG. These electrophysiological abnormalities include T-wave flattening, a reduced QRS voltage and QT prolongation (Singal and Iliskovic, 1998). Chronic doxorubicin treatment is associated with congestive heart failure that correlates to a mortality rate of up to 50 % (Chatterjee et al., 2010). This mortality percentage increases with doxorubicin doses that are higher than 500 mg/m². A cardiotoxic phenotype associated with doxorubicin can also persist and progress after discontinuation of the drug. Chronic dilated cardiomyopathy, that is an enlarged and weakened left ventricle, can develop in patients 10 years after doxorubicin

treatment was stopped (Steinherz et al., 1991). It is unlikely that doxorubicin is still present in a patient body decades after treatment was stopped. The exact mechanisms of severely delayed doxorubicin-induced toxicity are unknown. The progressive impairment of the ability of the sarcoplasmic reticulum to regulate cellular calcium homeostasis could be a contributing factor (Chugun et al., 2000). A reduction of Ca^{2+} ATPase mRNA expression causes a reduction of cardiac contractility (Arai et al., 2000).

The intracellular characteristics of doxorubicin-induced cardiotoxicity include an increase of ROS production, a reduction of myocardial endogenous antioxidants, peroxynitrite formation, mitochondrial dysfunction and apoptosis (Vejpongsa and Yeh, 2014a). Doxorubicin-induced myocardial cell apoptosis can cause left ventricular thinning, an elevated afterload and subsequent increased stress on the heart (Wouters et al., 2005). It is thought that mitochondrial dysfunction is the major contributing factor towards the development of doxorubicin-induced cardiotoxicity. Doxorubicin is a favourable substrate for reduction, in particular, the NADH-dehydrogenase of mitochondrial complex I (Doroshov, 1983; Wallace, 2003). This reduction produces a highly reactive semiquinone radical that causes an increase of ROS generation which negatively impacts mitochondrial function: the mitochondrial transmembrane potential is disrupted, ATP production declines and the mitochondrial membrane permeability transition (MPT) pore forms allowing the release of pro-apoptotic proteins cytochrome *c* and AIF into the cytosol (Carvalho et al., 2013). These proteins activate caspase-mediated apoptosis. Doxorubicin also forms adducts with the circular DNA in mitochondria and consequently damages the mitochondrial DNA (Ashley and Poulton, 2009). The strong association with oxidative stress and mitochondrial dysfunction can explain why doxorubicin toxicity affects the heart in particular. The heart has a large density of mitochondria, this organelle accounts for approximately 35 % of the cellular volume of cells in the heart tissue. Mitochondria are a source and target for ROS and in heart cells, they have an elevated rate of oxygen consumption. Relative to the liver, the heart also has less antioxidant activity including a low expression of catalase (Doroshov et al., 1980; Quiles et al., 2002). Furthermore, doxorubicin-induced mitochondrial DNA alterations are only found in heart not skeletal muscle cells, in mice and in humans (Lebrecht et al., 2005, 2003).

Doxorubicin is a powerful iron chelator, the iron-doxorubicin complex can generate a large amount of ROS through iron cycling between Fe(II) and Fe(III) forms (Ichikawa et al., 2014). Doxorubicin contributes to the accumulation of iron inside mitochondria and the iron-doxorubicin complex can catalyse hydrogen peroxide to a reactive hydroxyl radical (Myers, 1998). The altered distribution of iron could be a result of doxorubicin interacting with iron regulatory proteins 1 and 2, which are involved in the regulation of proteins transferrin receptor 1 and ferritin. Transferrin receptor 1 is involved in iron uptake and

ferritin contributes to the regulation of cellular iron storage (Xu et al., 2005). Overall, iron plays a role in doxorubicin cardiotoxicity and exerts a considerable contribution to the generation of ROS.

Doxorubicin is a very effective anti-cancer drug, and it is an example of how in some circumstances, patients would prefer not to withdraw treatment that is causing inappropriate drug-induced toxicity. This can be because of the severity of their disease or the lack of alternative therapeutic treatment that is as effective. In this case, the risk/benefit of a drug for an individual patient must be weighed up and the drug implicated for toxicity is not always discontinued; if possible, a compound that can counter-act the toxic effects will be administered at the same time. Drugs with antioxidant properties can be used in conjunction with doxorubicin and have been proven to reduce doxorubicin-associated cardiac mitochondrial damage. One such drug is dexrazoxane. Dexrazoxane is the only drug that is approved by the FDA to prevent cardiotoxicity associated with doxorubicin (Swain and Vici, 2004). Dexrazoxane is hydrolysed inside cardiomyocytes to its metabolite ADR-925 (Popelova et al., 2008). This metabolite is a good iron chelator and this characteristic has been proposed as the dexrazoxane cardioprotective mechanism for reducing doxorubicin cardiotoxicity (Hasinoff and Herman, 2007). An additional mechanism is that dexrazoxane binds to topoisomerase II β , protecting it from doxorubicin and consequently reducing topoisomerase II β -mediated doxorubicin cardiotoxicity (Lyu et al., 2007). Other compounds that are associated with cardioprotective mechanisms, including neuregulin-1 β , a ErbB2 receptor agonist, and Cdk4/6 inhibitors (Cross et al., 2015).

5.1.2 Animal models for doxorubicin-induced cardiotoxicity

It is clear that the mechanism of doxorubicin-induced cardiotoxicity is multifactorial. Consequently, attempting to mimic the human pathophysiology in an animal model is difficult. Most of the animal models in the literature for doxorubicin-induced toxicity, or general anthracycline-induced cardiotoxicity, are altered to try to establish the mechanism of doxorubicin-induced cardiotoxicity and recapitulate the drug-induced phenotype manifested in humans. One example is the mouse model that has deleted the expression of topoisomerase II β in cardiomyocytes. This model appeared to be protected from anthracycline-induced cardiomyopathy (Vejpangsa and Yeh, 2014b). Furthermore, Li *et al* (2014) found that a nuclear factor erythroid-2 related factor 2 (Nrf2) knockout mouse (Nrf2^{-/-}) had a more exaggerated doxorubicin-induced cardiotoxicity phenotype, including cardiomyocyte necrosis and cardiac dysfunction, compared to the doxorubicin-treated wildtype mouse (Li et al., 2014). Nrf2 is a transcription factor that regulates the expression

of antioxidant proteins. Therefore, this model confirms the involvement of oxidative stress in the generation of cardiotoxicity induced by doxorubicin.

As mentioned in **chapter 4**, the closest animal model to the *Xenopus* that is frequently used in drug-induced toxicity research is the zebrafish. Ultimately, we would ideally want the *Xenopus* model to illicit a similar response as humans to drugs known to be cardiotoxic in humans. However it is useful to compare the *Xenopus* response to cardiotoxic drugs, for example doxorubicin, to zebrafish cardiotoxicity models, to help determine the validity of the model. Chang *et al* (2014) exposed 4 hpf zebrafish embryos to 0-100 mg/mL (approximately 0-170 μ M) doxorubicin and measured the effect the drug had on the heart rate, hatching rate, body length and survival. At 60 hpf, the zebrafish embryos treated with ≤ 10 mg/mL doxorubicin had a slightly increased heart rate however this declined significantly in embryos treated with ≥ 25 mg/mL doxorubicin (Chang *et al.*, 2014). This small study indicates non-mammalian animal models can present a cardiotoxic phenotype to doxorubicin. Furthermore Huang *et al* (2013) treated zebrafish embryos that were 6 hpf, until 96 hpf, with 0-100 μ M doxorubicin. The doxorubicin-treated zebrafish developed cardiac-specific phenotypes that included cardiac oedema and an elongated heart (Huang *et al.*, 2013).

Overall it is important to remember that the majority of *in vivo* doxorubicin studies reflect acute doxorubicin treatment. In general, not enough studies have been done to look at delayed doxorubicin-induced cardiotoxicity (Carvalho *et al.*, 2013). One example of the chronic doxorubicin cardiotoxicity model is a study which treated normotensive and spontaneously hypertensive rats with 0-1 mg/kg doxorubicin every week for 12 weeks (Herman *et al.*, 1985). The spontaneously hypertensive rats had higher arterial pressure, higher mortality rate and were overall more sensitive to doxorubicin cardiotoxic effects than the normotensive rats. However the normotensive rats did develop heart lesions such as cytoplasmic vacuoles and loss of myofibrils, but these were just less severe than the normotensive rats and developed at a later stage in the doxorubicin treatment course. A variety of animal and human studies have been conducted to investigate the mechanism of action of the cardioprotective agent dexrazoxane in combination with doxorubicin treatment. Rats treated with doxorubicin and dexrazoxane, had less adverse cardiac effects compared to doxorubicin-treated rats that did not receive dexrazoxane (Zhang *et al.*, 2015). Wiseman & Spencer (1998) summarise the key studies conducted in humans that demonstrates a reduction of cardiotoxicity in patients that have received dexrazoxane and doxorubicin combined, compared to doxorubicin alone (Wiseman and Spencer, 1998). As mentioned previously in this chapter, the FDA eventually supported these findings and implemented the use of dexrazoxane as a cardioprotective agent.

5.1.3 Terfenadine-induced cardiotoxicity

Terfenadine is a second-generation, non-sedating, H₁ antagonist antihistamine that was in the top 10 most prescribed drug in the US in 1991 (Simonsen, 1992). However in the 1980s there was an increase in reports that associated terfenadine with QT prolongation, ventricular arrhythmia and Torsade de Pointes, although the incidence overall was still quite rare (Monahan et al., 1990; Zimmermann et al., 1992). Originally, it was proposed that terfenadine primarily causes cardiotoxicity through the inhibition of the K_v1.5 channel. When the channel is open, the parent drug can enter the mouth and block it (Yang et al., 1995). The K_v1.5 channel contributes to the ultrarapid potassium ion efflux current (K_{ur}) (Crumb Jr. et al., 1995). However this channel is expressed more in the atrium than the ventricle, and it is ventricular arrhythmia that contributes to Torsade de Pointes more so than the atrium. The hERG channel is involved in the delayed rectifier current (I_{Kr}) in ventricular myocytes and it is more susceptible to terfenadine inhibition than the K_v1.5 channel. Roy and colleagues (1996) found that the hERG channel was 10-fold more sensitive to terfenadine block compared to K_v1.5. Furthermore the parent drug is responsible for the cardiotoxic effects whereas the major metabolite, terfenadine carboxylate, does not as great an affinity for the hERG and K_v1.5 channels (Woosley et al., 1993). Drug-drug interactions and environmental factors can inhibit the CYP450 isoenzyme CYP3A4, which reduces the amount of terfenadine carboxylate metabolite generated and cause an accumulation of the parent drug. Terfenadine patients that are also taking the antibiotic erythromycin or the antifungal agent ketoconazole, are more likely to develop terfenadine-induced cardiotoxicity because both of these drugs inhibit CYP3A4 activity (Crumb Jr. et al., 1995). Grapefruit is a well known CYP450 inhibitor that could also affect the toxicity of terfenadine. An accumulation to the extent of 0.2 µM terfenadine plasma concentration can result in cardiotoxicity (Zünkler et al., 2000). The therapeutic mechanism of terfenadine is attributed to the terfenadine carboxylate metabolite (Roy et al., 1996). This metabolite, known as fexofenadine, is used to treat allergic conditions and has markedly reduced incidence of cardiotoxicity compared to terfenadine. In addition, terfenadine inhibits L-type calcium current and induces spontaneous calcium release from the sarcoplasmic reticulum thus altering the intracellular calcium-handling in cardiomyocytes (Hove-Madsen et al., 2006). The increase of calcium ions in the cardiomyocytes induces apoptosis (Fearnley et al., 2011).

5.1.4 Animal models for terfenadine-induced cardiotoxicity

Terfenadine is frequently used as a model cardiotoxic drug in animal models, to compare other potentially cardiotoxic compounds to. One example is the Batey and colleagues (2002) laboratory group. They used an open-chest anaesthetised rabbit to compare the

cardiotoxicity mechanisms of the anti-malarial drug halofantrine, clofilium, a K⁺ channel blocker, and terfenadine (Batey and Coker, 2002). Clofilium and halofantrine caused TdP whereas terfenadine did not in this animal model. ECG analysis was used with this animal model to detect proarrhythmic activity. Another example is for the evaluation of a zebrafish embryo cardiotoxicity model, which analysed terfenadine alongside 6 other human cardiotoxic drugs including aspirin, clomipramine hydrochloride, cyclophosphamide, nimodipine, quinidine and verapamil hydrochloride (Zhu et al., 2014). In their project, terfenadine induced bradycardia and reduced the conduction from the atrium to the ventricle (atrioventricular block) in zebrafish embryos treated for 4h. In another project, transgenic zebrafish embryos that have GFP-labelled cardiomyocytes, showed reduced cardiac contractility, reduced heart rate and cardiomyocyte apoptosis when treated with 5-20 µM terfenadine for 24 h (Gu et al., 2017). The zebrafish treated with 20 µM terfenadine had an increased rate of arrhythmic beats. An arrhythmic beat was identified as an irregular atrium to ventricle contraction ratio. Survival of the zebrafish for Gu and colleagues (2017) decreased with embryos treated with more than 40 µM terfenadine for 24 h. It would be interesting to see if our *Xenopus* model generates similar results to the zebrafish models mentioned here as well as the human terfenadine toxicity phenotype. Zebrafish are the closest animal model to *Xenopus* and any drug response similarities could help validate the results of the following experiments.

5.2 Aim

Examine the use of *Xenopus laevis* embryos as a model for drug-induced cardiotoxicity.

5.3 Hypothesis

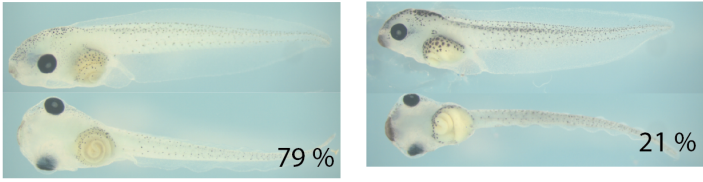
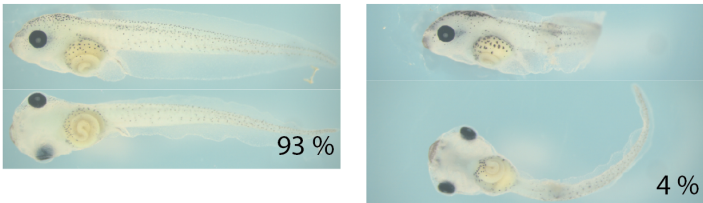
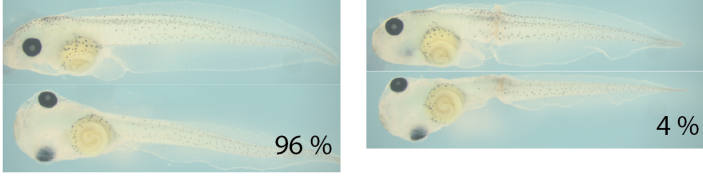
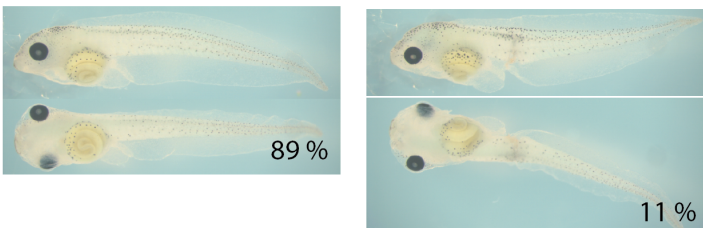
The *Xenopus laevis* embryos can be used to detect some markers of drug-induced cardiotoxicity that are in use in other animal models and humans.

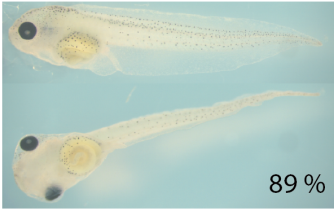
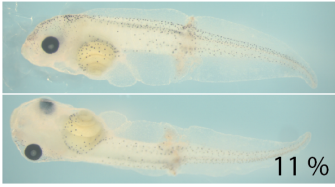
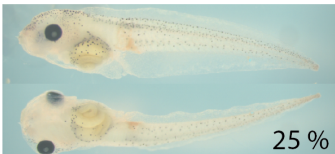
5.4 Results

5.4.1 Doxorubicin dose response in *Xenopus laevis* embryos

In order to test doxorubicin-induced cardiotoxicity in *Xenopus laevis* embryos, I carried out a dose response experiment to determine the concentration range at which the embryos have drug-specific toxicity. Further to the initial doxorubicin screens in **chapter 3**. I performed dose response screens in the concentration range 0-100 µM doxorubicin, in 10 µM increments (**Figure 5-1**). The embryos were incubated with doxorubicin from stage 38, harvested at stage 45 and photographed to investigate the presence of a visual phenotype (n=3). With increasing concentration, embryos have a red stain; this is particularly noticeable in 25 % of the embryos treated with 100 µM doxorubicin. I believe

this is because the doxorubicin solid compound is an orange-red powder and when dissolved in the *Xenopus* embryo media, it forms a orange-red solution. Therefore this is not a toxicity phenotype but it is a useful visual aid that confirms the *Xenopus* embryos are taking up the doxorubicin they are immersed within. By eye, the staining appears to be interior and the method of embryo processing to obtain the photograph of the embryos denotes the unlikelihood that the staining is just on the outside of the embryos. The most common phenotype observed with the doxorubicin-treated embryos is damage to the tail or a change in the tail shape. The incidence and variety of this tail phenotype increases with increasing doxorubicin concentration. From these photographs, I could not detect a significant heart-specific phenotype. The corresponding survival graph for these photographs shows that at 0-60 μM doxorubicin, the embryos survived, whereas from 70-100 μM there was a concentration-dependent decline in survival from 96 % to 75 % (**Figure 5-2**). I decided to perform further dose response screens to investigate the survival at higher concentrations, from 0-150 μM doxorubicin (n=4) (**Figure 5-3**). I observed a repeat of the concentration-dependent decline in survival, but this from an early concentration of 50 μM until 100 μM (96 -0 % survival respectively). It was decided to continue with the 0-100 μM doxorubicin concentration range for the investigation of doxorubicin-induced cardiotoxicity for the remainder of the doxorubicin experiments in this chapter. The reduced survival rate for the 100-150 μM range suggests non-specific toxicity.

0 uM			
10 uM			
20 uM			
30 uM			
40 uM			
50 uM			

60 uM		
		
70 uM		
		
80 uM		
		
		
90 uM		
		
		

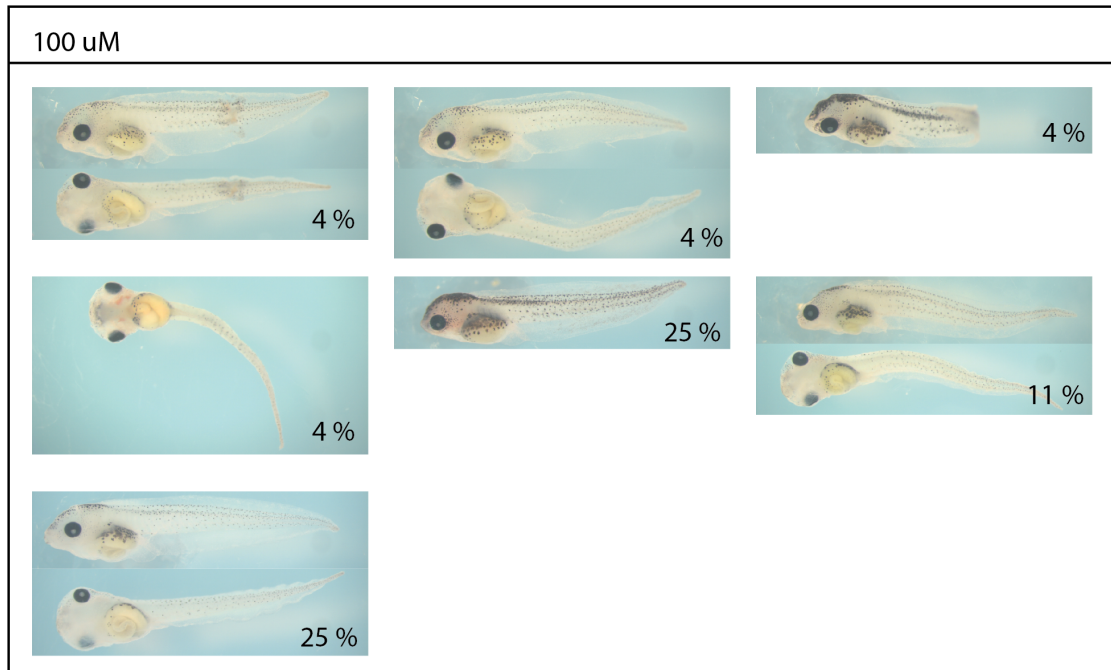


Figure 5-1: Doxorubicin dose response 0-100 μ M

Xenopus laevis embryos were treated with a doxorubicin concentration in the range 0-100 μ M (n=3). The embryos were treated with doxorubicin from stage 38 and harvested at stage 45. The surviving embryos at stage 45 were photographed. The different phenotypes found for each doxorubicin concentration and the percentage of embryos that had that phenotype are shown. The percentage is calculated from the total number of embryos treated. Where possible, the embryo was photographed to show the lateral view and the ventral view.

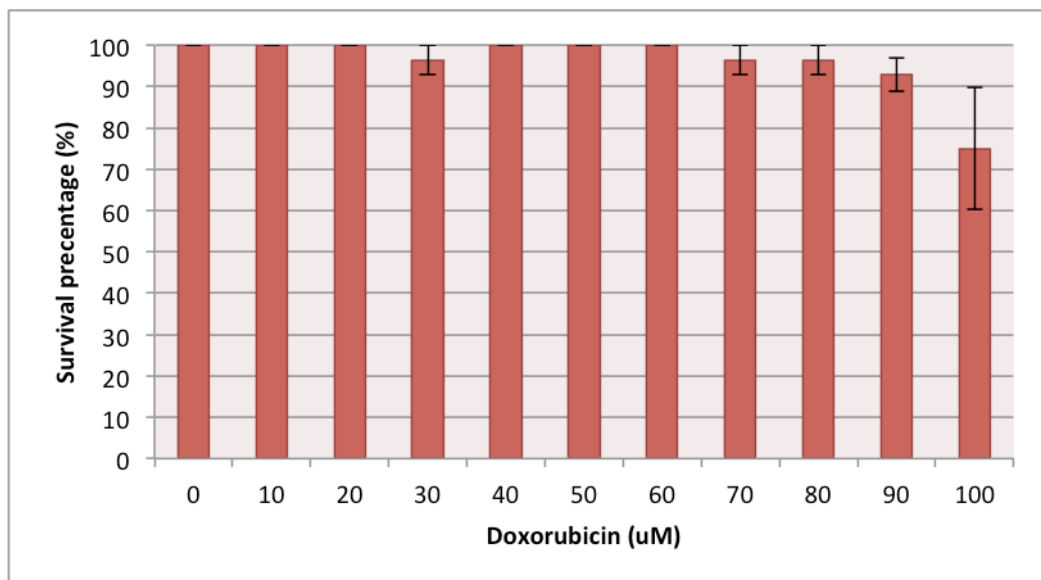


Figure 5-2: The percentage of *Xenopus* embryo survival with 0-100 μ M doxorubicin treatment.

The average (\pm SEM) amount of embryos that survived until the age of stage 45 to be harvested and photographed for **Figure 5-1** (n=3).

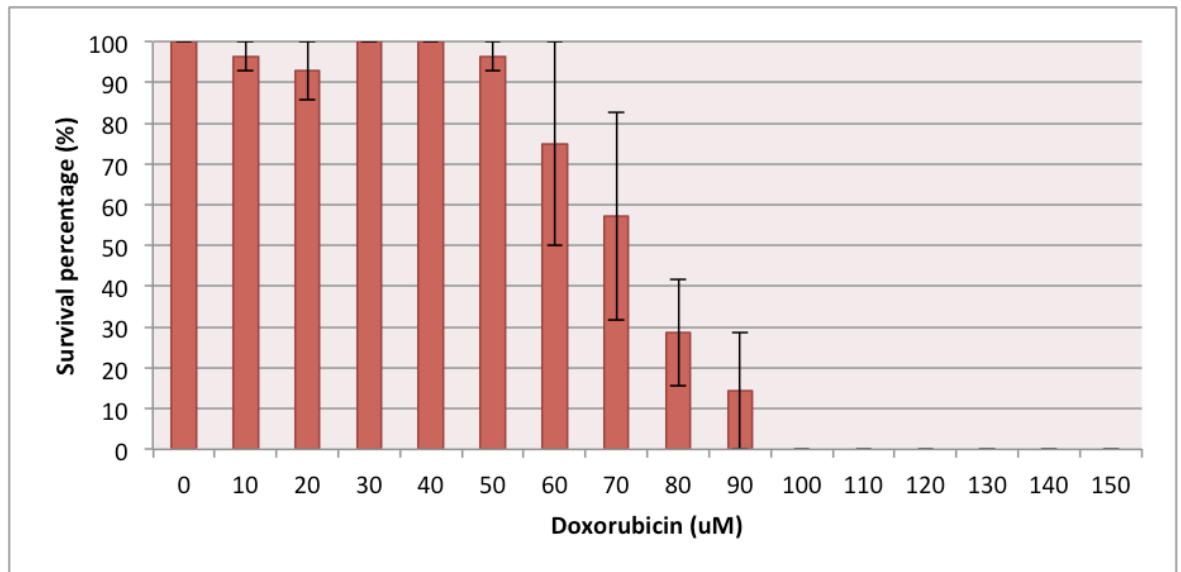
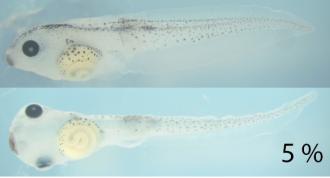
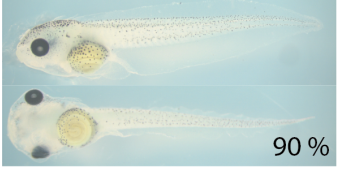


Figure 5-3: The percentage of *Xenopus* embryo survival with 0-150 μ M doxorubicin treatment.

The second set of doxorubicin dose response screens (n=4) to establish the average survival rate (\pm SEM) until the age of stage 45 for embryos treated from stage 38.

5.4.2 Dexrazoxane dose response in *Xenopus laevis* embryos

Dexrazoxane is a cardioprotective agent, administered to patients to minimise the cardiotoxic effects of their doxorubicin therapy. I hypothesised that the *Xenopus* embryos treated with the combination of dexrazoxane and doxorubicin will elicit a reduced amount of cardiotoxic effects compared to doxorubicin alone. I performed a dose response with the dexrazoxane alone, to determine if this compound alone produces any phenotypes (**Figure 5-4**). Stage 38 embryos were incubated with dexrazoxane (0-1 mM) and harvested at stage 45 (n=3). I did not detect any significant phenotype from the photographs. A minority of embryos displayed a damage tail phenotype, this did not appear to be concentration-dependent. The survival rate did not significantly reduce for the concentration range I tested (**Figure 5-5**).

0 mM			
0.1 mM			
0.2 mM			
0.3 mM			
0.4 mM			
0.5 mM			

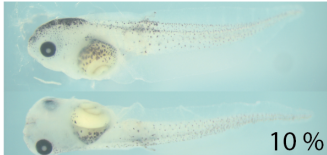
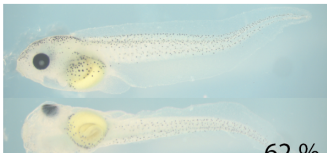
0.6 mM		
 72 %	 10 %	 19 %
0.7 mM		
 72 %	 29 %	
0.8 mM		
 19 %	 59 %	 14 %
 9 %		
0.9 mM		
 29 %	 5 %	 62 %
 33 %		



Figure 5-4: Dexrazoxane dose response 0-1 mM.

Xenopus laevis embryos were treated with a dexrazoxane concentration in the range 0-1 mM (n=3). The embryos were treated with dexrazoxane from stage 38 and harvested at stage 45. The surviving embryos were photographed at stage 45. The different phenotypes found for each dexrazoxane concentration shown and the percentage of embryos that had that phenotype. The percentage is calculated from the total number of embryos treated. Where possible, the embryos are photographed to show the lateral view and the ventral view.

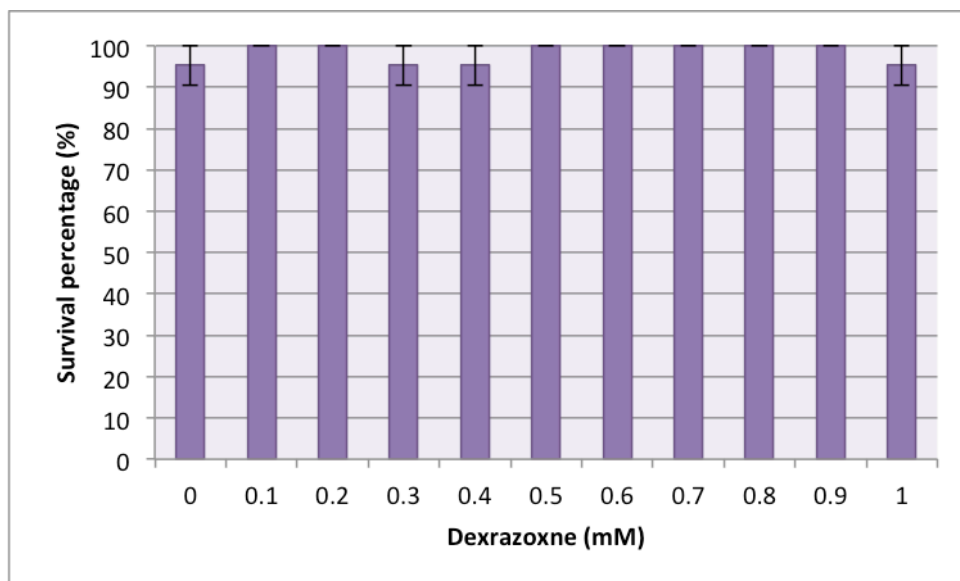
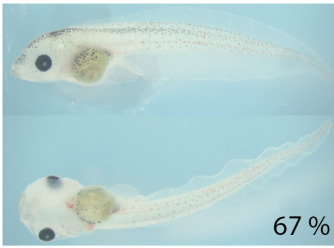
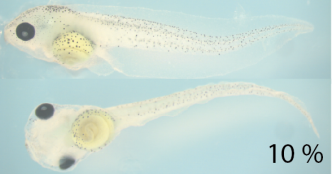
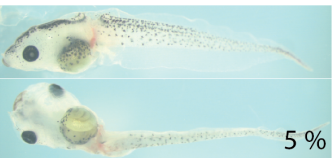
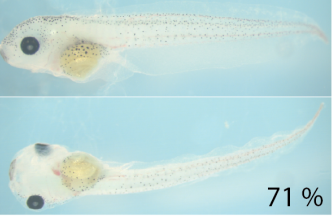
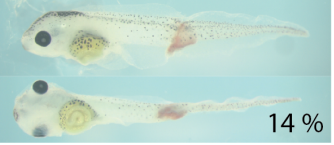


Figure 5-5: The percentage of *Xenopus* embryo survival with 0-1 mM dexrazoxane treatment.

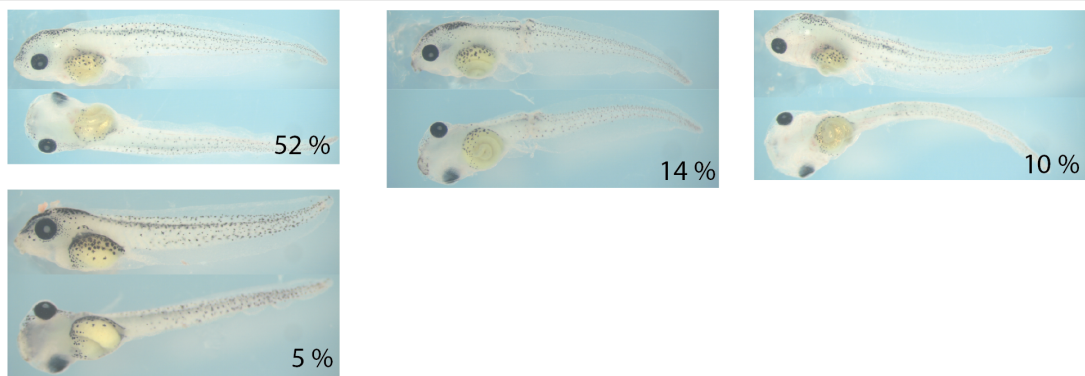
The average (\pm SEM) percentage of embryos treated with dexrazoxane (0-1 mM) that survived until stage 45 to be photographed in the dose response assay in **Figure 5-4** (n=3).

5.4.3 Treatment with combined doxorubicin and dexrazoxane incubation

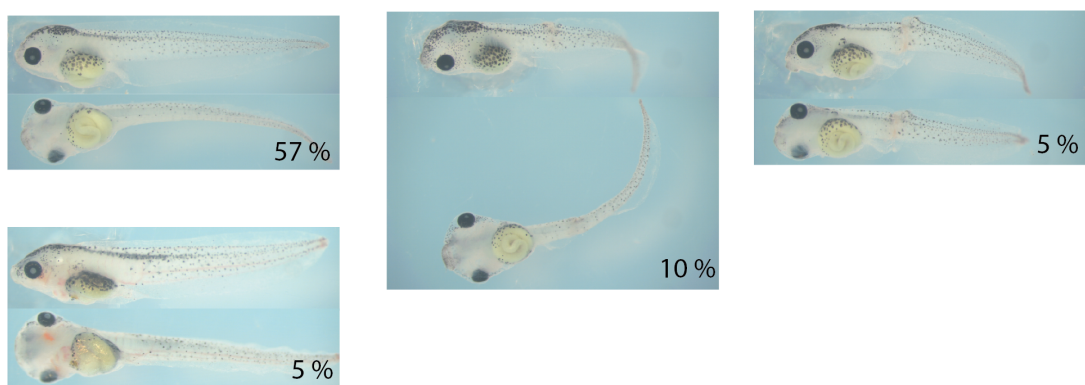
Stage 38 embryos were treated with doxorubicin (0-100 μ M and dexrazoxane (0-1 mM) at a concentration ratio of 1:10 (doxorubicin:dexrazoxane) (**Figure 5-6**). The embryos were harvested at stage 45, photographs were taken and we noted the survival rate. Damage to the tail was the most common alternative phenotype. The majority of the embryos appeared similar to wildtype, untreated embryos. The amount of embryos that survived declined with increasing concentration of the combined drugs from 100 to 33 % for the 0.04 mM doxorubicin and 0.4 mM dexrazoxane treatment to the 0.1 mM doxorubicin and 1 mM dexrazoxane treatment groups respectively (**Figure 5-7**).

0 uM doxorubicin + 0 mM dexrazoxane		
 67 %	 19 %	 10 %
10 uM doxorubicin + 0.1 mM dexrazoxane		
 95 %	 5 %	
20 uM doxorubicin + 0.2 mM dexrazoxane		
 86 %	 10 %	 5 %
30 uM doxorubicin + 0.3 mM dexrazoxane		
 71 %	 14 %	 5 %
 10 %		
40 uM doxorubicin + 0.4 mM dexrazoxane		
 95 %	 5 %	

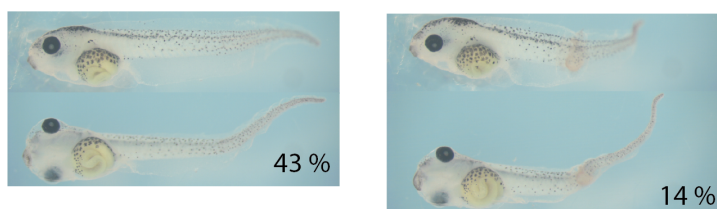
50 uM doxorubicin + 0.5 mM dexrazoxane



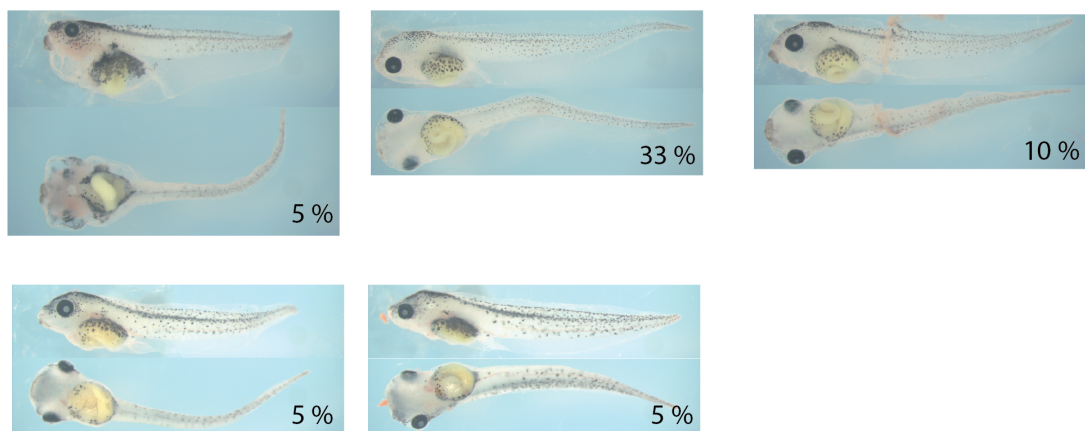
60 uM doxorubicin + 0.6 mM dexrazoxane



70 uM doxorubicin + 0.7 mM dexrazoxane



80 uM doxorubicin + 0.8 mM dexrazoxane



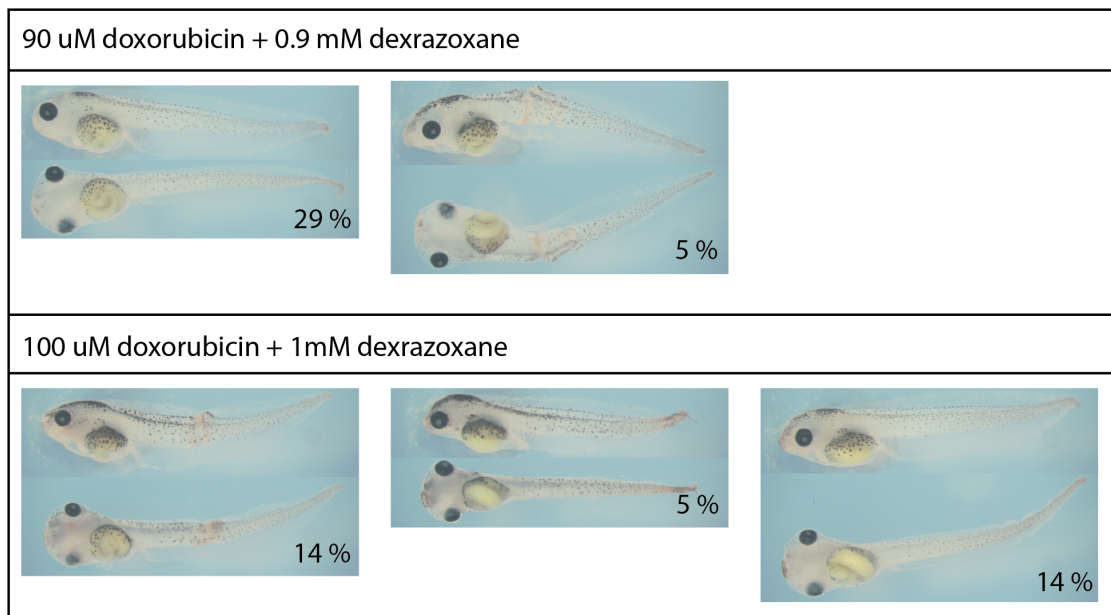


Figure 5-6: Doxorubicin (0-100 μ M) and Dexrazoxane (0-1 mM) treatment.

Xenopus embryos were treated with a combination of doxorubicin and dexrazoxane in the ratio 1:10 from stage 38 until stage 45. The embryos that survived at stage 45 were photographed. The percentage is calculated from the total number of embryos treated. Where possible, the embryos were photographed to show the lateral view and the ventral view (n=3).

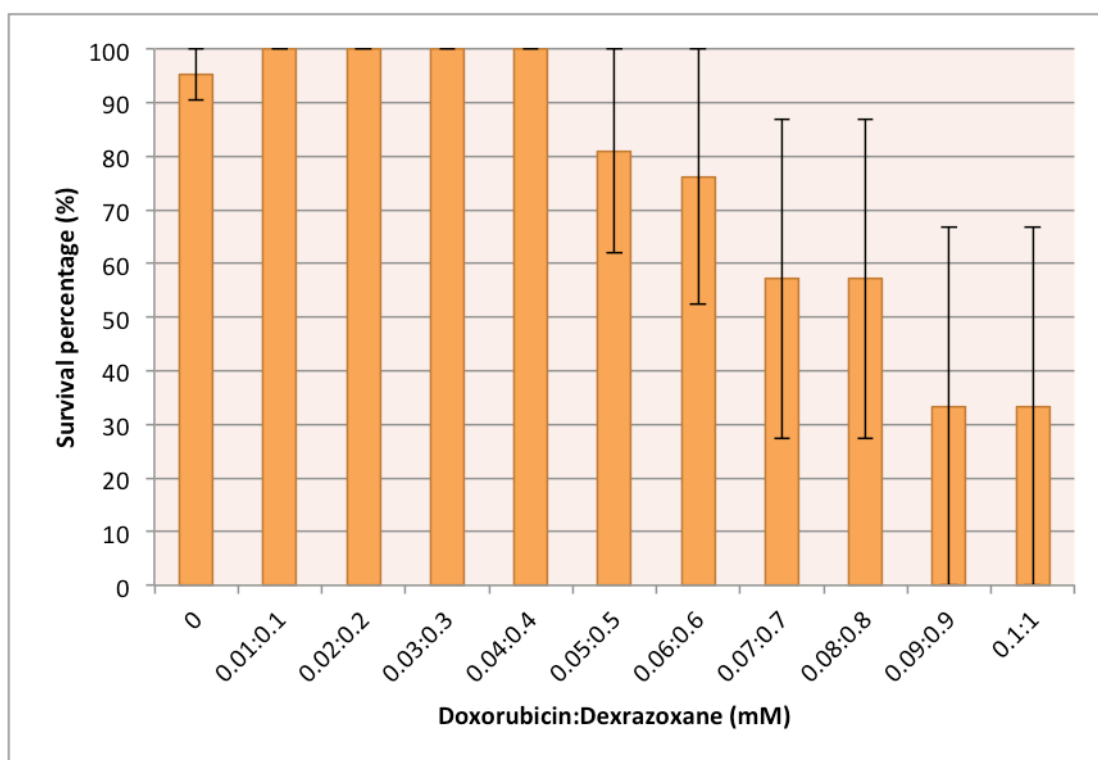


Figure 5-7: The percentage of *Xenopus* embryo survival with doxorubicin (0-100 μ M) and dexrazoxane (0-1 mM) treatment.

The average (\pm SEM) percentage of embryos treated with doxorubicin (0-100 μ M) and dexrazoxane (0-1 mM) in the ratio 1:10, that survived until stage 45 to be photographed in the dose response assay in **Figure 5-6** (n=3).

5.4.4 Identification of the anaesthetic concentration suitable for the experiments that will investigate *Xenopus* embryo heart rate

To investigate drug-induced cardiotoxicity, I decided to examine the heart rate of the *Xenopus* embryos at stage 45 after drug treatment. At stage 45 the embryos are very active in their incubation media, consequently, to be able to measure the heart rate I had to add a compound to make them stationary. I used tricaine, a soluble anaesthetic commonly used to anaesthetise *Xenopus* adults and tadpoles (see **chapter 2** for more detail). For the adult *Xenopus*, a concentration of 0.5 mg/mL tricaine is used for 1h to fully anaesthetise the frog. Consequently, I tested the *Xenopus* embryos with 0-0.5 mg/mL tricaine (n=3) (**Figure 5-8**). Stage 45 embryos were incubated with a concentration of tricaine for 1h and the heart rate was measured via the method described in **chapter 2**. For obvious reasons, the heart rate could not be measured for the 0 mg/mL tricaine group of embryos, however embryos from the same mother were incubated in untreated *Xenopus* media in parallel to the treated embryos for negative control. For all 3 biological replicates, the untreated embryos (0 mg/mL tricaine) appeared normal. The heart rate

increased from an average of 148 to 164 beats per minute (bpm) for 0.1-0.2 mg/mL tricaine respectively. The heart rate decreased for embryos treated with 0.3-0.5 mg/mL tricaine. At 0.1 mg/mL the embryos were not completely stationary (data not shown) and all the embryos treated with 0.5 mg/mL tricaine did not survive after the 1h incubation. I concluded that the best anaesthetic concentration for the following heart rate experiments was 0.2 mg/mL.

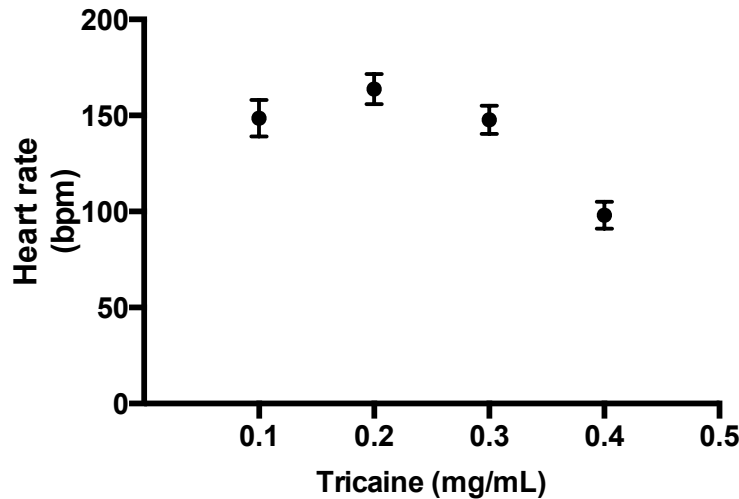


Figure 5-8: Investigation of anaesthetic concentration and heart rate.

The heart rate assay was used to measure the heart rate (\pm SEM) of stage 45 *Xenopus* embryos (n=3) that had been incubated with tricaine, an anaesthetic, for 1h before measurement. The embryos had not been treated with any other drugs.

5.4.5 Video analysis

An example of a heart rate assay video, video analysis and representative graphs for normal heart beat rhythm and arrhythmia is shown in the **Appendix Figures 8-1 and 8-2**.

5.4.6 Investigating the effect of doxorubicin treatment on *Xenopus* embryo heart rate

Embryos were treated with doxorubicin at stage 38 and their heart rate was measured at the age of stage 45 1 h after the addition of 0.2 mg/mL tricaine (n=3) (**Figure 5-9**). Of the embryos treated with 100 μ M doxorubicin, 0 % survived. The heart rate increased with increasing concentration of doxorubicin treatment from 0-80 μ M (110-141 bpm). However between 80-90 μ M doxorubicin, the heart rate decreased from an average of 141 to 107 bpm. The embryos treated with 30, 50-80 μ M doxorubicin had a statistically significantly difference heart rate compared to the untreated (0 μ M doxorubicin) embryos ($P < 0.05$). The heart rates plotted on this graph include regular and irregular heartbeats. The amount of embryos that survived to have their heart rates measured is plotted against the amount

of arrhythmias identified in the embryos that survived. The embryo survival decreased with increasing doxorubicin treatment: 50-100 μM saw a decline from 95-0 %. There does not seem to be a definitive pattern between incidence of arrhythmias and the concentration of doxorubicin (**Figure 5-10**). A regular rhythm was identified from the graphs generated, as having opposite peaks and troughs for the atrium and ventricle lines, which represents the heart chamber filling and emptying with blood respectively. An irregular rhythm can have 2 atrial peaks to 1 ventricular peak, the ventricular peak height can vary or the heart chambers can contract and relax simultaneously. A series of short and tall peaks can indicate sporadic filling of the heart chamber to its maximum capacity (**Appendix Figure 8-2**). For example, a tall peak occurs with a darker colour and therefore more blood in the chamber whereas a short peak is associated with less blood and often this is accompanied with a less dynamic contraction that is apparent in the video.

After this initial heart rate was measured, the same embryos were put into fresh media, that did not contain doxorubicin or tricaine, and incubated for 72 h (**Figure 5-11, red**). The heart rate was measured at 72 h and plotted against the primary heart rate measurement. The heart rates of the post-treatment embryos positively correlated with the doxorubicin concentration they received in their initial incubation. The gradient of the post-treatment heart rate looks similar to the gradient of the initial heart rate measurements. There is a shift of approximately +20 bpm for all the post-treatment measurements compared to the initial heart rate readings of the same doxorubicin concentration, including the untreated 0 μM doxorubicin treatment group. This will be discussed in more detail in the discussion later in this chapter.

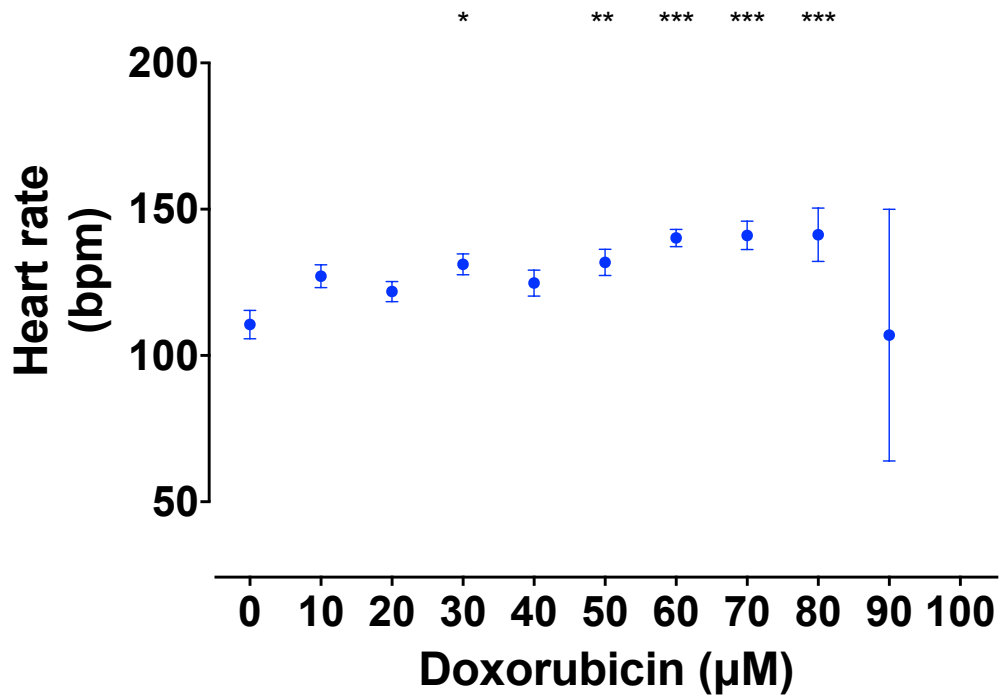


Figure 5-9: The effect of doxorubicin treatment on heart rate.

Xenopus embryos were treated with doxorubicin from stage 38 until stage 45 (n=3). The heart rate assay was used to measure the heart rate of the treated embryos after 1 h incubation with 0.2 mg/mL tricaine. The average heart rate (\pm SEM) of treated embryos was compared to untreated embryos (0 μ M doxorubicin) using a one-way ANOVA ($P < 0.05$).

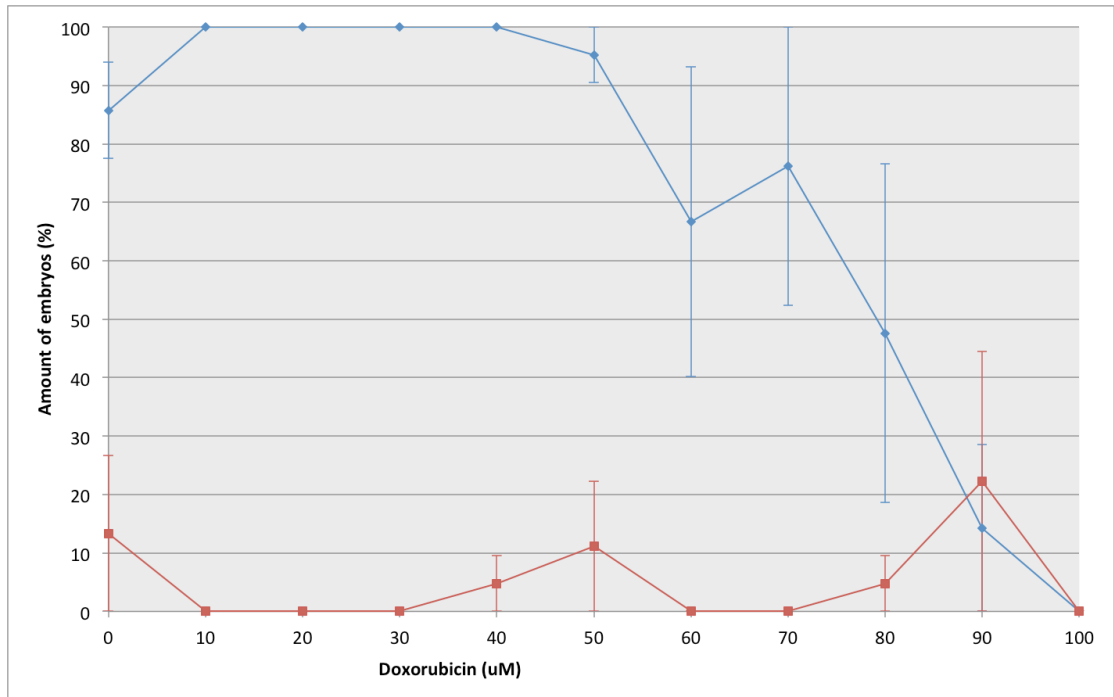


Figure 5-10: Heart rate assay embryo survival and incidence of arrhythmias with doxorubicin treatment.

The average survival rate (\pm SEM) (blue) of doxorubicin-treated *Xenopus* embryos that were used in the heart rate assay (Figure 5-9, $n=3$) and the amount of arrhythmias (red) as a percentage of the embryos that survived (\pm SEM).

- Doxorubicin treatment
- 3 days post-treatment

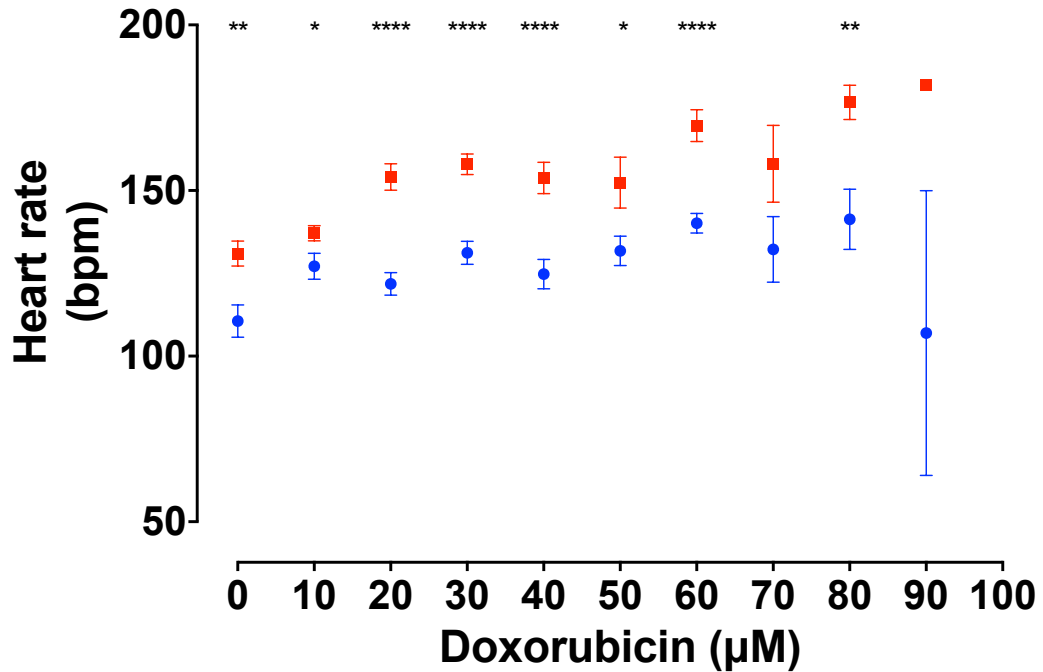


Figure 5-11: Characterisation of heart rate for doxorubicin-treated embryos after 3 days without treatment.

The *Xenopus* embryos that were treated with doxorubicin from stage 38 until stage 45 (n=3, blue) were left in fresh *Xenopus* media for 3 days. After 3 days the heart rate (\pm SEM) was measured after 1 h treatment with 0.2 mg/mL tricaine (red). The heart rates at stage 45 and 3 days post-treatment for a given doxorubicin concentration were compared using a paired T test ($P < 0.05$).

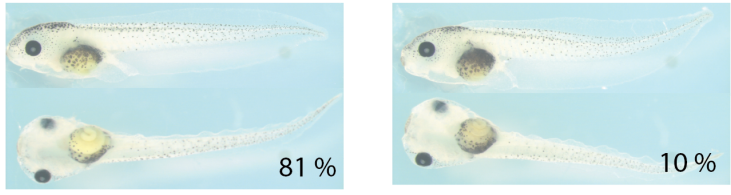
5.4.7 Terfenadine dose response in *Xenopus laevis* embryos

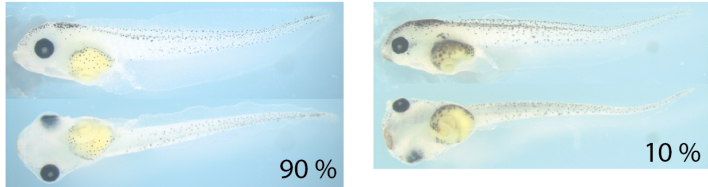
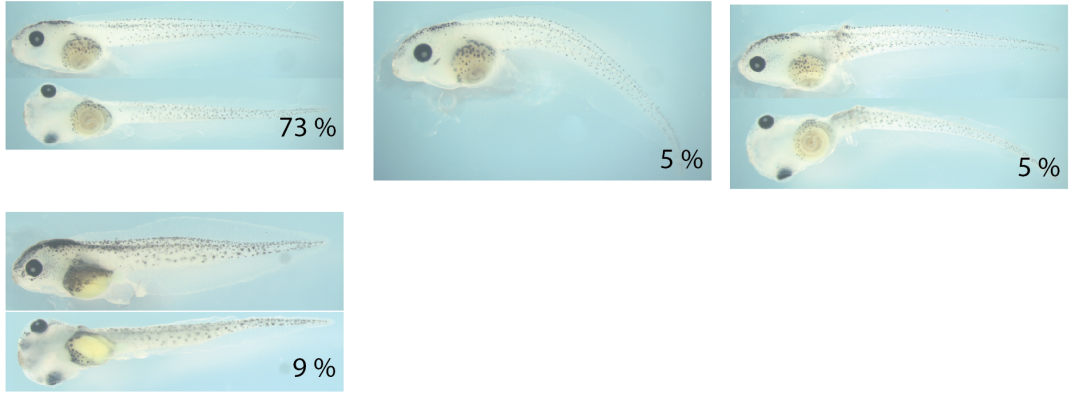
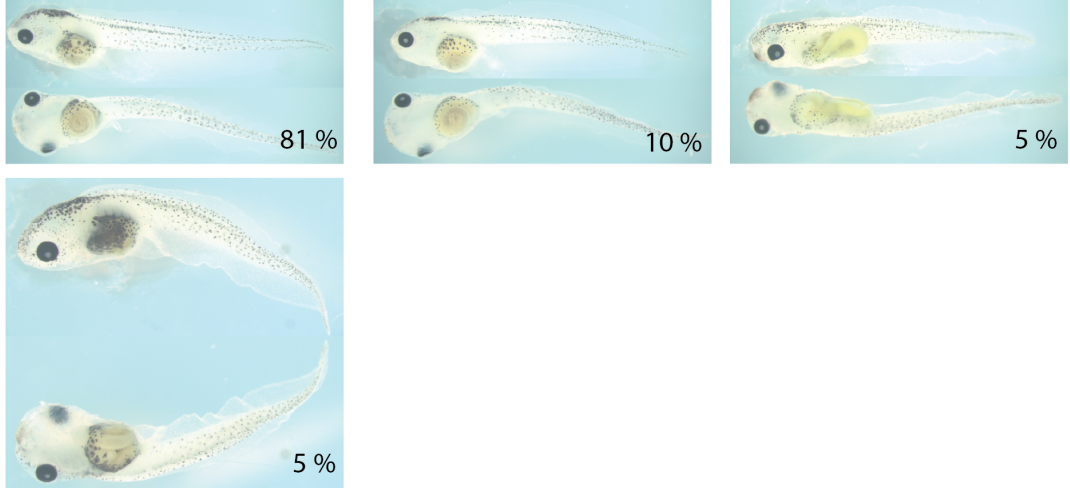
Xenopus embryos were treated with a concentration of terfenadine within the dose range 0-100 μM at stage 38 and harvested at stage 45 ($n=3$) (**Figure 5-12**). I took photographs and looked for a distinctive phenotype in the stage 45 embryos. A change in tail shape or tail damage was a frequent occurrence throughout the concentration range. At the high concentrations, from 20-80 μM , oedema around the heart and gastrointestinal region was a common phenotype. The embryos treated with 90 and 100 μM terfenadine did not survive to be photographed at the age of stage 45. The survival percentage began to decrease at 30 μM in a concentration-dependent manner. 90 % of the total embryos treated survived at 30 μM terfenadine, this decreased to 0 % at 100 μM terfenadine (**Figure 5-13**). I decided that the following experiments that explore terfenadine-induced cardiotoxicity would be performed in the range of 0-50 μM terfenadine.

5.4.8 Investigating the effect of terfenadine treatment on *Xenopus* embryo heart rate

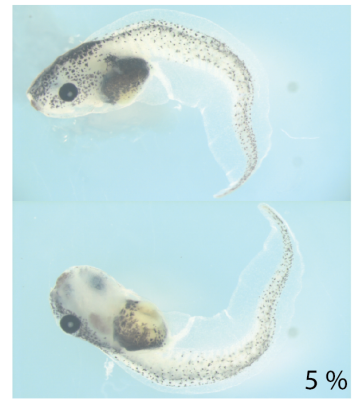
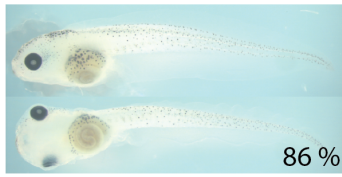
I treated stage 38 embryos with 0-50 μM terfenadine and measured their heart rates at stage 45 following 1h incubation with 0.2 mg/mL tricaine anaesthetic ($n=3$) (**Figure 5-14**). This is the same concentration of anaesthetic used for the embryos treated with doxorubicin earlier in this results chapter. Overall, the heart rates decreased in a concentration-dependent correlation from an average of 125 bpm to 82 bpm for untreated embryos (0 μM terfenadine) to embryos incubated with 30 μM terfenadine respectively. The average heart rates were statistically and significantly different compared to the untreated embryos (0 μM terfenadine) for the 10-30 μM terfenadine embryos ($P<0.05$). The embryos treated with 40 and 50 μM terfenadine did not survive to the age of stage 45 therefore we did not obtain heart rate measurements for these treatment groups.

For the terfenadine-treated embryos that were to be processed through the heart rate measurement method, the survival percentage decreased at 20 μM to 50 μM . On average, 76 % of embryos treated with 20 μM terfenadine survived until stage 45 and had their heart rates measured. This decreased to 0 % survival in embryos treated with 50 μM terfenadine. The frequency of arrhythmias occurring in embryos that survived does not appear to correlate with the concentration of terfenadine they were incubated with (**Figure 14**).

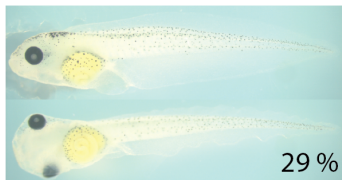
0uM

1 uM

2 uM

3 uM

4 uM


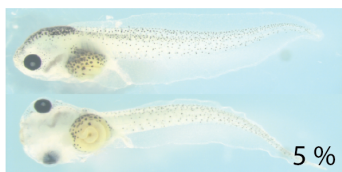
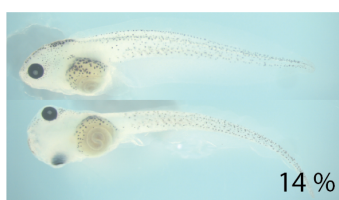
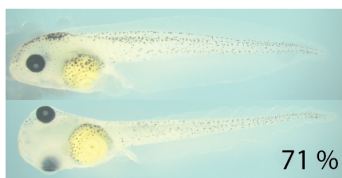
5 uM

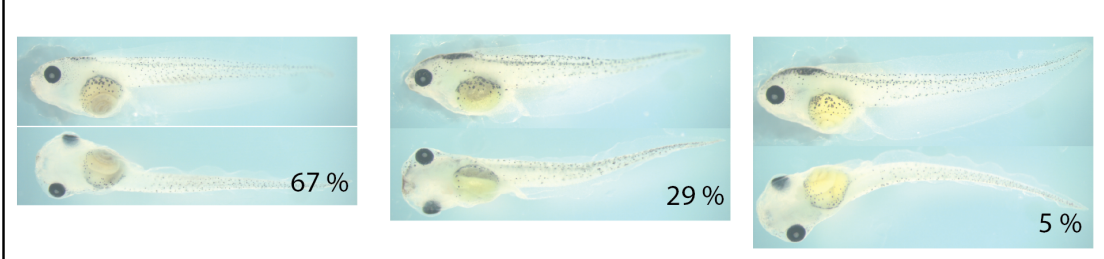
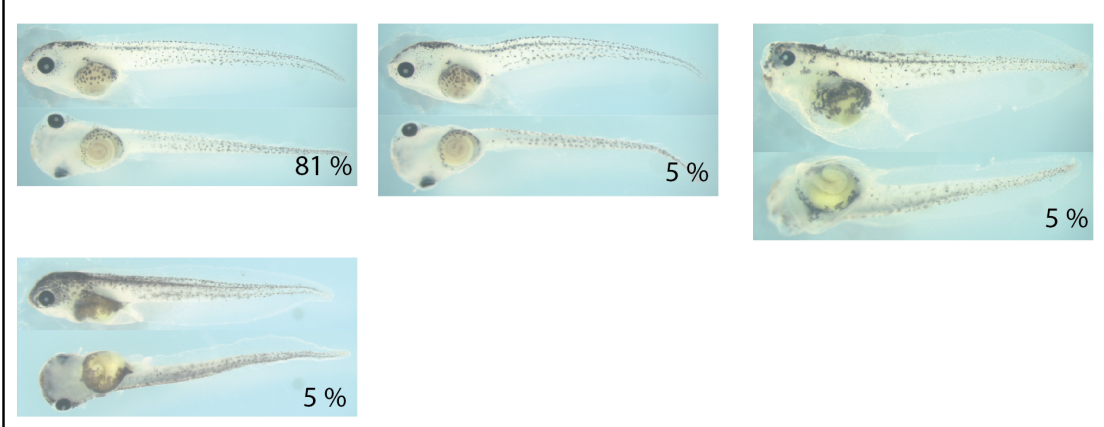


6 uM

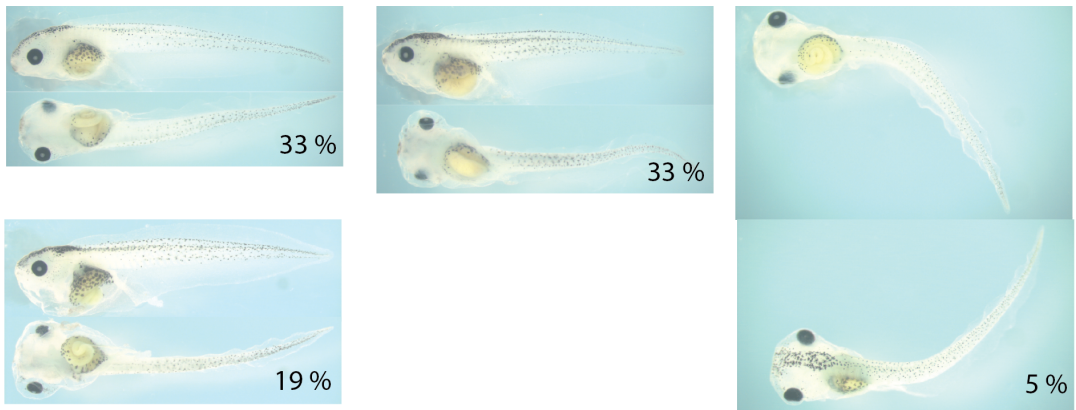


7 uM

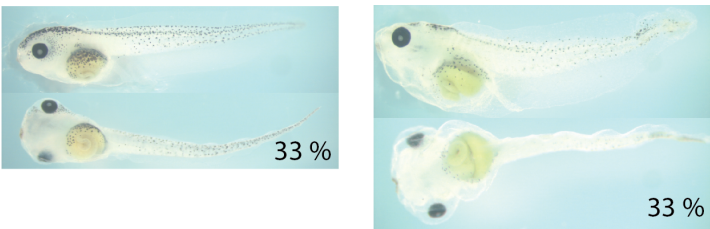


8 μ M			
9 μ M			
10 μ M			
20 μ M			

30 uM



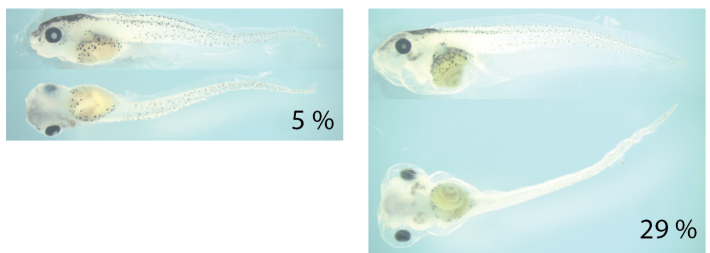
40 uM



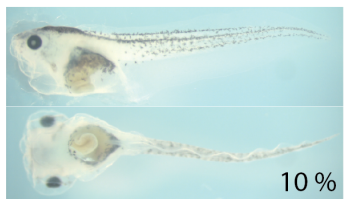
50 uM



60 uM



70 uM



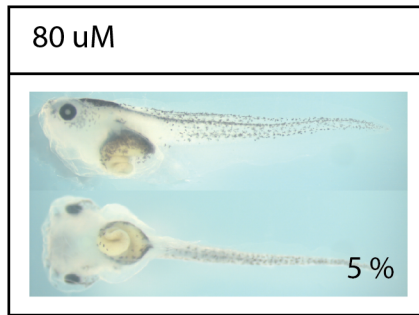


Figure 5-12: Terfenadine dose response 0-100 μ M.

Xenopus laevis embryos were treated with a terfenadine concentration in the range 0-100 μ M (n=3). The embryos were treated with terfenadine from stage 38 and harvested at stage 45. The surviving embryos at stage 45 were photographed. The different phenotypes found for each terfenadine concentration and the percentage of embryos that had that phenotype were photographed. The percentage is calculated from the total number of embryos treated. Where possible, the embryo was photographed to show the lateral view and the ventral view.

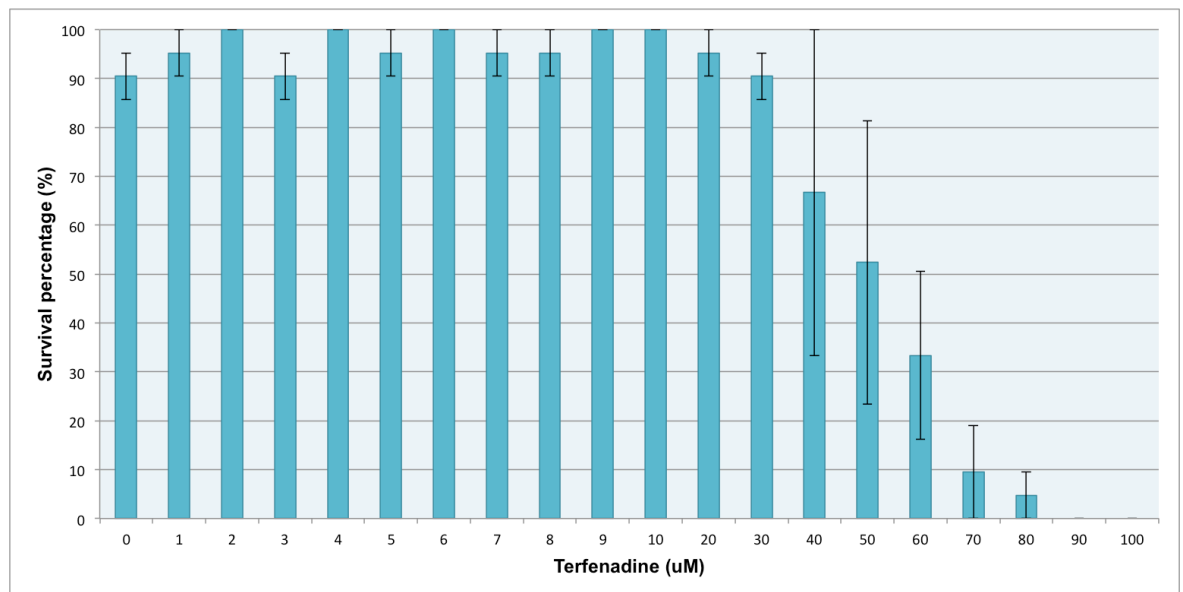


Figure 5-13: The percentage of *Xenopus* embryo survival with 0-100 μ M terfenadine treatment.

The average (\pm SEM) amount of embryos that survived until the age of stage 45 to be harvested and photographed for **Figure 5-12** (n=3).

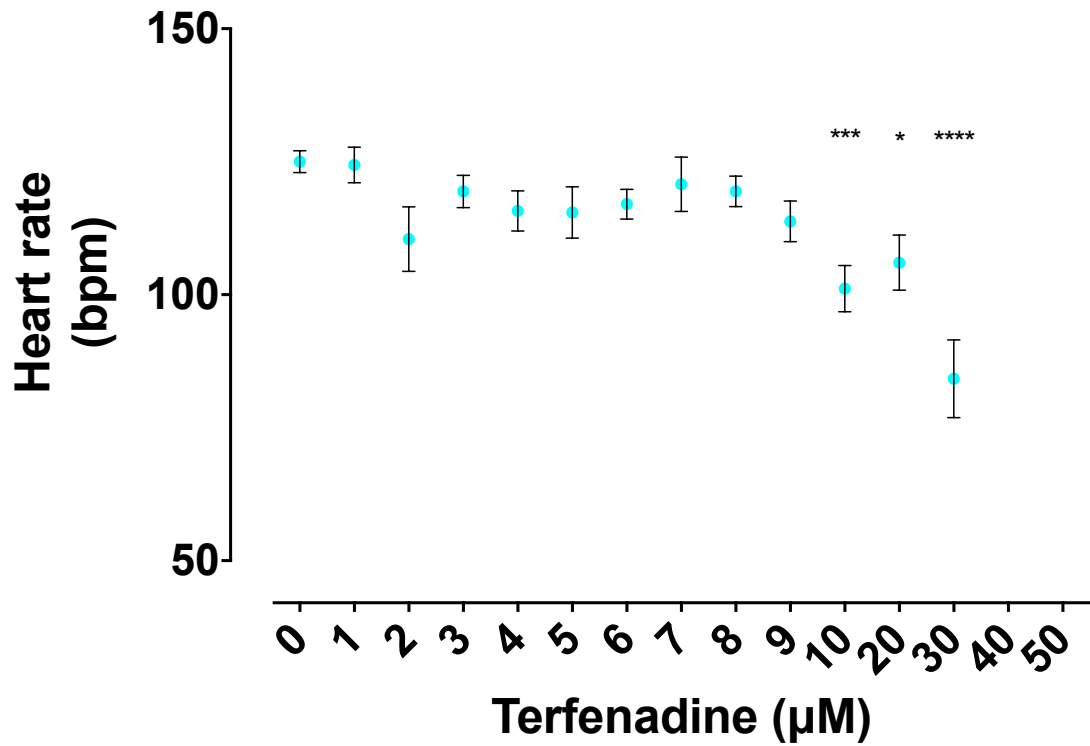


Figure 5-14: The effect of terfenadine treatment on heart rate.

Xenopus embryos were treated with terfenadine from stage 38 until stage 45 (n=3). The heart rate assay was used to measure the heart rate of the treated embryos after 1 h incubation with 0.2 mg/mL tricaine. The average heart rate (\pm SEM) of treated embryos was compared to untreated embryos (0 μ M terfenadine) using a one-way ANOVA ($P < 0.05$).

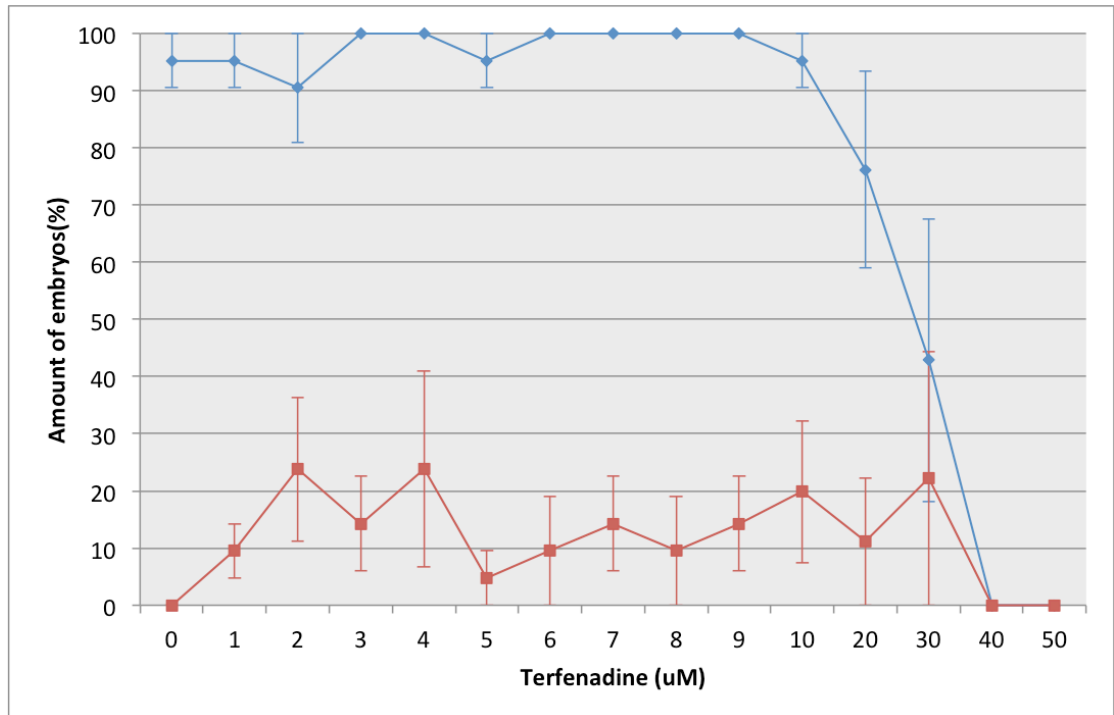


Figure 5-15: Heart rate assay embryo survival and incidence of arrhythmias with terfenadine treatment.

The average survival rate (\pm SEM) (blue) of terfenadine-treated *Xenopus* embryos that were used in the heart rate assay (**Figure 5-14**, n=3) and the amount of arrhythmias (red) as a percentage of the embryos that survived (\pm SEM).

5.4.9 Heart expression pattern in *Xenopus laevis*

5.4.9.1 Wholemount in situ hybridisation and transverse sections

The heart in the *Xenopus* embryo is easier to locate compared to the liver (**Figure 5-16**). The embryo retains its transparency for the duration of the stages I was observing for the drug-induced cardiotoxicity experiments. However I decided to use a probe that could stain the *Xenopus* embryo heart in order to investigate the expression pattern of miR-208. MiR-208 is a promising cardiotoxicity marker that is expressed in humans, zebrafish and rodents. I wanted to see if this expression pattern is conserved in the *Xenopus* embryos. First, I carried out a WISH assay on untreated stage 38 and stage 45 embryos using cardiac troponin 1c, a known *Xenopus* gene that is specific to the heart (n=5). These embryos were then sectioned and I could see the cardiac troponin 1c probe has stained the heart tissue (**Figure 5-17**).

Next, I conducted WISH assays using a probe for miR-208 (**Figure 5-18**). From the wholemount photographs I identified the probe stained the heart tissue in the stage 38 and stage 45 untreated embryos (n=10). Furthermore, the heart tissue is clearly stained in the sections taken from these same embryos in stage 38 and stage 45 embryos (**Figure 5-19**).

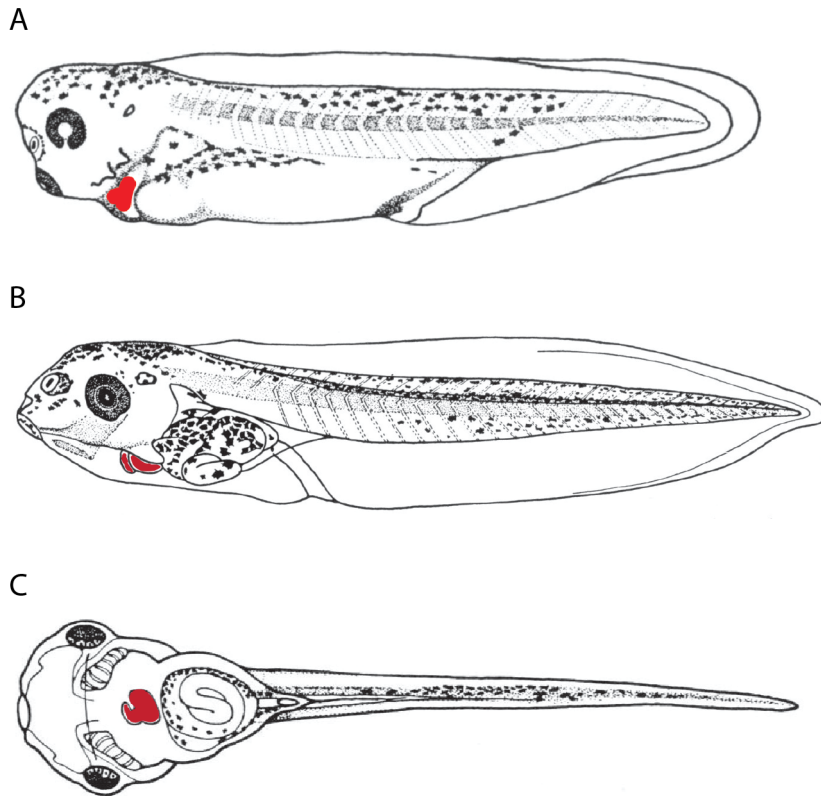


Figure 5-16: Illustration of heart location in *Xenopus laevis* embryo.

The *Xenopus* embryos at the age of stage 38 (A) and stage 45 (B and C) have heart tissue (red). This schematic displays the location of the heart as seen from a lateral view (A and B) and ventral view (C). Modified from Nieuwkoop & Faber (1994).

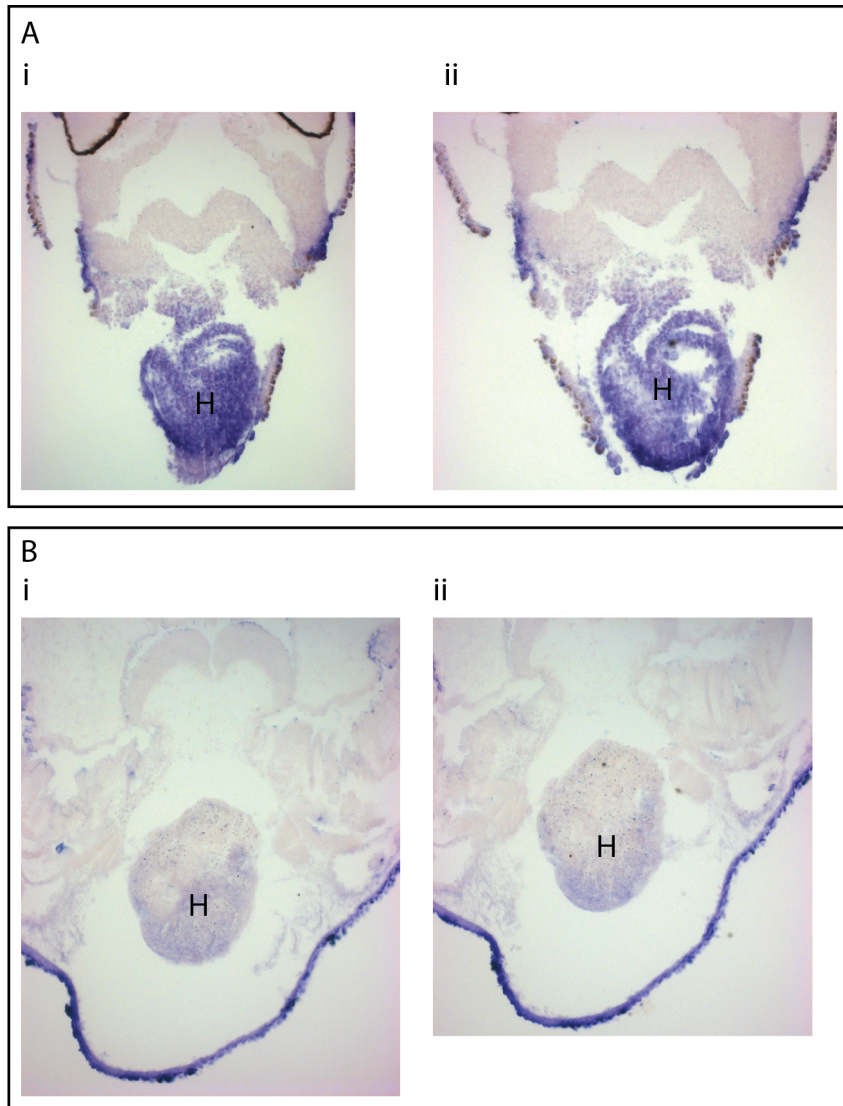


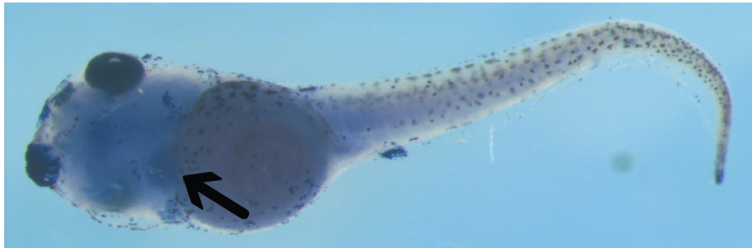
Figure 5-17: Cardiac troponin 1c sections.

Representative sections from stage 38 (A) and stage 45 (B) untreated embryos that had been processed through the WISH assay using a probe for cardiac troponin 1c (n=5). The heart (H) was stained purple in the WISH assay.

A



B



C

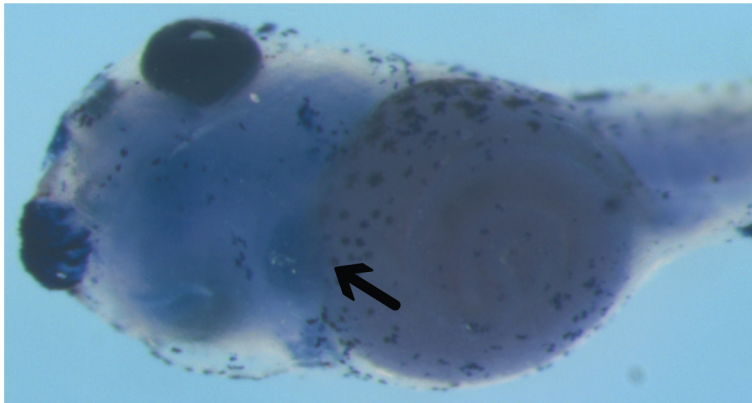


Figure 5-18: Wholemout *in situ* hybridisation (WISH) for miR-208.

A WISH assay with a probe for *Xenopus* miR-208 on stage 38 (A) and stage 45 (B and C). The stage 38 embryos were photographed to see the lateral view and the lateral (B) and ventral (C) view has been photographed for the stage 45. These embryos represent the stain (arrows) seen consistently for the embryos tested (n=10).

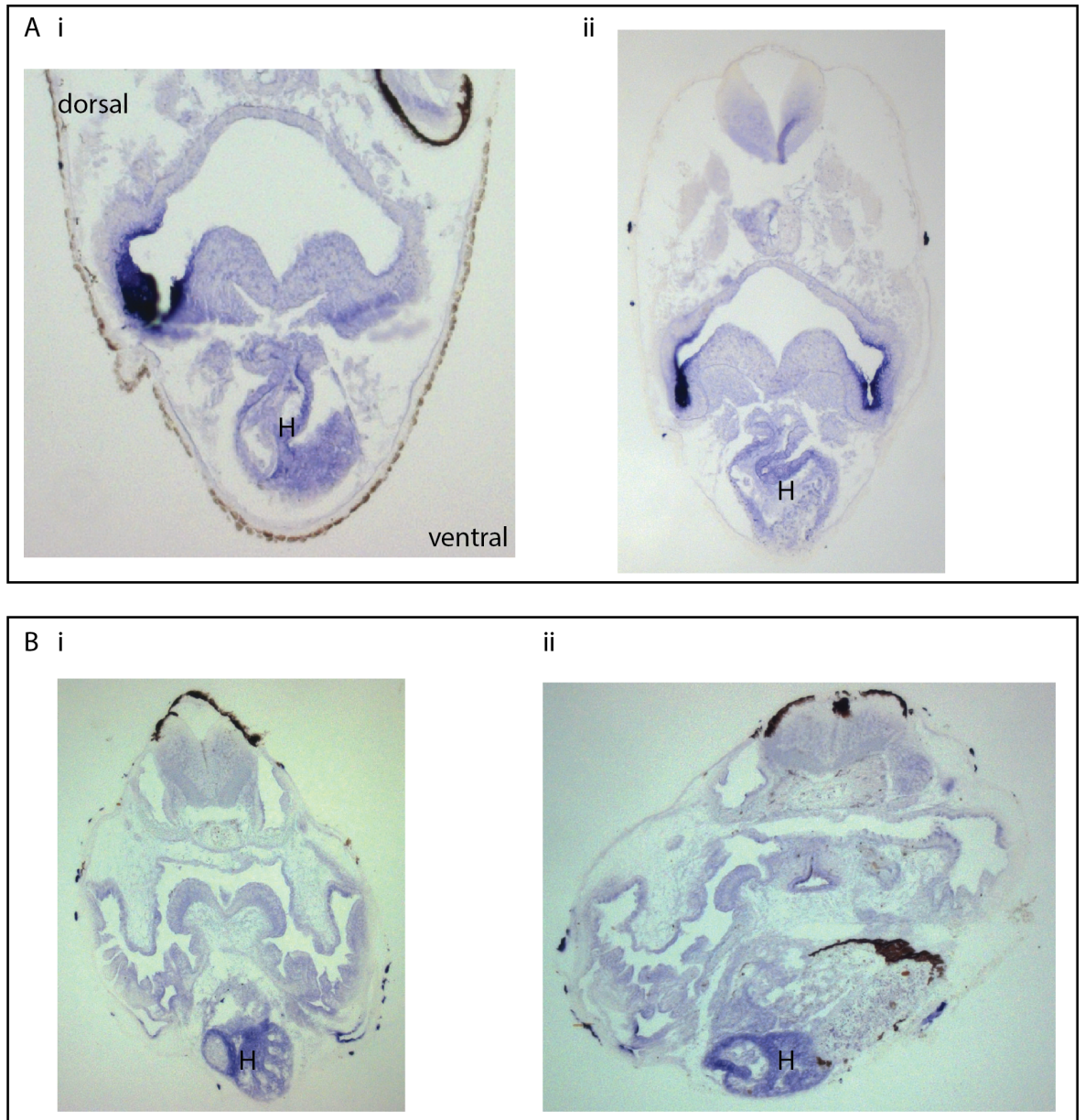


Figure 5-19: miR-208 sections for stage 38 *Xenopus* embryos.

Representative sections from stage 38 (A) and stage 45 (B) untreated embryos that had been processed through the WISH assay using a probe for *Xenopus* miR-208 (n=10). The heart (**H**) was stained purple in the WISH assay.

5.5 Discussion

In this chapter, we set out to explore the suitability of the *Xenopus* embryos for the prediction of drug-induced cardiotoxicity. To do this, I decided to use 2 drugs that are associated with cardiotoxicity in humans: doxorubicin and terfenadine. The mechanism of toxicity for doxorubicin is less certain and more multifactorial than terfenadine. Indeed, I deliberately chose to use these different drugs to see if our non-mammalian animal model is favourable to one or the other, or potentially neither. In order to conclude if the *Xenopus* embryos are a good model for the prediction of drug-induced cardiotoxicity in humans, a more comprehensive list of cardiotoxic and non-cardiotoxic drugs should be evaluated. However, this chapter can give an indication of the usefulness of the *Xenopus* embryo model for cardiotoxicity prediction.

5.5.1 Doxorubicin dose range and phenotype

The 0-100 μM doxorubicin concentration range I used to assess drug-induced cardiotoxicity in this chapter is similar to the dose used in zebrafish embryos. Huang and colleagues (2013) used doxorubicin to induce a heart failure model in zebrafish. Mild cardiac defects were detected in 20 % of the zebrafish given 50 μM doxorubicin and 60 % of the zebrafish given 90 μM doxorubicin developed heart failure. The zebrafish embryos Huang and colleagues used were of a similar age to the *Xenopus* embryos we used. All the zebrafish embryos given 100 μM doxorubicin, did not survive to the end of the 72h treatment period (Huang et al., 2013).

In the initial 3 screens of doxorubicin treatment I performed for this chapter, 75 % of the embryos survived with 100 μM doxorubicin for the 72 h period of treatment from stage 38 until stage 45. However, when I extended the dose range from a maximum of 100 μM doxorubicin to 150 μM in the second set of screens, the survival at 100 μM was 0 %. The reason for this difference is not clear. The first set of screens comprised of 3 biological replicates and the second set took an average of 4 biological replicates. The survival rate for the embryos in the experiments that followed these initial screenings in this chapter all showed 0 % survival with 100 μM treatment. It could be that the embryos treated for the first set of photographs were anomalies. I decided to use 0-100 μM doxorubicin because I believed this range incorporated the dose for which embryos that are likely to have a drug-specific cardiotoxic effect. A concentration of drug for which none of the embryos survive has an ambiguous causality. But a drug associated with toxicity is likely to reduce the survival rate because, for example, some embryos will not be able to tolerate the adverse effects and some embryos will. I believe the 0-100 μM doxorubicin concentration range takes into account these criteria and includes the dose that could cause doxorubicin-specific cardiotoxicity in the *Xenopus* embryos.

The embryos that survived the 72h treatment time were photographed. From the photographs we could not detect a phenotype that I could instinctively associate with heart pathophysiology in the *Xenopus* embryos. As mentioned in **chapter 4**, much like the liver, the heart is a very small organ in stage 38 – stage 45 *Xenopus laevis* embryos; it is difficult to detect microscopic changes to the heart structure. In future work it would be beneficial to use a marker for structural damage such as TUNEL, which can label necrotic cells with a fluorescent tag. Unintentionally, I was able to observe *Xenopus* embryo doxorubicin ingestion because the dissolved drug has a strong red pigment that is visible inside the transparent embryo body. For future work with the *Xenopus* embryos and drug toxicity, it could be useful to use drugs that have a natural pigment or label the drugs with a pigment that would not interfere with the drug toxicity mechanism. This could be an easy method to detect and maybe quantify drug uptake in the *Xenopus* embryos that doesn't require complex and expensive equipment, just a microscope colour camera.

5.5.2 Terfenadine dose range and phenotype

I used a dose range 0-50 μM to treat our stage 38 *Xenopus* embryos (72 hpf at 23°C) until stage 45 (72 h incubation). This is similar to the terfenadine concentration the 48 hpf zebrafish embryos were exposed to for 24 h in the Zhu *et al* (2014). And Gu *et al* (2017) also used similar terfenadine concentrations for 72 hpf zebrafish embryos, which were exposed to terfenadine for 24 h. The 24 h terfenadine exposure in both of these zebrafish models is considered acute exposure. In comparison, our *Xenopus* embryos were incubated in terfenadine for 72 h. However I observed similar phenotype endpoints such as some cardiac oedema. Overall, we chose to continue with the 0-50 μM terfenadine concentration range for the heart rate experiment because it incorporates treatment that produces phenotypes that are not dissimilar to untreated embryos, and a gradient of phenotypes across the middle concentrations, ending with a high mortality rate at the high concentrations. I concluded the 0-50 μM terfenadine concentration range should include terfenadine-specific effects. In future experiments I would like to identify any cardiomyocyte apoptosis in the wholemount embryos using a fluorescent label such as TUNEL or acridine orange staining.

5.5.3 The heart rate assay

An example of a heart rate assay video, video analysis and representative graphs for normal heart beat rhythm and arrhythmia is shown in the **Appendix Figures 8-1 and 8-2**. A change in heart rate can indicate a problem with the heart cellular components. It is also a very good method of identifying and quantifying heart function. A drug that alters the structure of an organ does not always correlate with a functional change. Sometimes the body has mechanisms that can compensate for the structural damage and keep the

function of the organ in fact. Often, drug-induced toxicity and adverse drug reactions are not detected in patients until they affect the organ function. Furthermore, as long as the drug does not affect the organ function, it can be argued that one can continue to administer the drug to the patient. Overall it is when the organ function is impaired, not necessarily the structural integrity, that the patient should consider withdrawal and seek alternatives. Consequently, I think heart rate is a good measure of cardiotoxicity.

A major advantage of *Xenopus* embryos is their transparency. This characteristic is useful because it means that we do not have to attach the embryos to an electrocardiograph to get the number of heart beats per minute. My heart rate protocol is adapted from Bartlett and colleagues (2004), I used the equipment available in our laboratory to update their protocol. Bartlett and colleagues compared cardiac recordings measured using fine glass microelectrodes to non-invasive digital video image analysis. They found that the non-invasive method was sufficient to obtain accurate cardiac cycle length readings (Bartlett et al., 2004). The full details of the heart rate protocol are described in **chapter 2**. Briefly, the stage 45 embryos were arranged ventral side up, I made sure the heart was in view down the microscope which translated to on the computer screen, and I obtained a 30 s black and white video of the heart beating using a camera that captured 50 frames per second (fps). I used my knowledge of the *Xenopus laevis* heart anatomy to identify an atrium and the ventricle to create the regions of interest (ROIs). The change in the shade of grey within the region corresponded to the blood flow; a darker shade indicates the heart chamber filling with blood, and a lighter shade is the heart chamber emptying. The heart rate (bpm) was calculated by counting the number of peaks in the graph created from the ROIs manually, I could not find a computational algorithm that could calculate this accurately. Consequently, this experiment is quite labour intensive and more work would be needed in order to make it an automated system that would be beneficial for drug safety studies in industry. It is important to note that through this method we can create a graph that illustrates the heart beat frequency, it does not show the changes in electrical activity, and consequently it is not an ECG. We cannot, for example, see the separate waves that are associated with the different stages of a heartbeat including the P and T waves and the QRS complex.

The heart rates recorded and plotted on the graphs included those that appeared to have an arrhythmic beat. A heart beat trace that depicted irregular peaks and troughs of greyscale intensity was identified as an arrhythmia. I verified this by going back to look at the video and deduce if the beat looks arrhythmic. It is possible that a heart with an arrhythmic beat will beat the same amount of times as a heart that has a regular rhythm and consequently produce a heart rate that is the same. However analysing the heart rate can still indicate cardiotoxicity. An increased heart rate can be caused from an increase of

stress on the heart that is a result of cardiomyocyte apoptosis and the loss of myofibrils. Drug-induced cardiomyocyte apoptosis can therefore be detected through changes in the heart rate. In research, commonly the left ventricular ejection fraction (LVEF) is used to identify heart stress or heart dysfunction. LVEF or ejection fraction is the volume of blood ejected from the heart with each heart beat. A shortened left ventricular ejection fraction can be an indication of a heart that is struggling to pump and move blood effectively because it has less of its functional subunits i.e. cardiomyocytes, due to cardiomyocyte apoptosis. I hypothesise, that with more time, our heart protocol can be adapted to measure the change in LVEF.

One problem with my heart rate assay was that I needed to be able to immobilise the embryos to get an accurate heart rate video, to do this I used anaesthetic. Consequently I was not able to measure the heart rate in completely untreated stage 45 embryos. The effect of the drug on the heart rate measurements can be determined by comparing the change relative to the embryos that have not received drug treatment but have still been anaesthetised; therefore I may not have measured the “true” heart rate of the stage 45 embryos. Ideally in the future, I would like to be able to conduct this assay without the anaesthetic to reduce the intervention with the embryos that could affect the drug-induced cardiotoxicity results. Suggestions for this include minimising the space in which the embryo can swim and Bartlett and colleagues (2004) used superglue. However these methods could also cause the embryos stress and affect the heart rate results. More work needs to be done to improve this part of the method. When I was investigating which concentration of anaesthetic to use for my heart rate assay, I was looking for the concentration at which the embryo is stationary for the videos but it was not so high so as to slow down the heart rate. In our laboratory, it is known that 0.5 mg/mL tricaine slows and sometimes stops the heart beating altogether in adult male *Xenopus laevis*. So I started with 0.5 mg/mL as the highest concentration to test on the embryos. I concluded 0.2 mg/mL was the tricaine concentration best to use for the heart experiments. When I created the ROIs to determine the change of grey intensity, the ROI area is fixed, it does not move with the embryo. Therefore the 0.1 mg/mL tricaine concentration was not sufficient because although the *Xenopus* embryos stopped swimming at this concentration, they still twitched, and the heart chambers would move in and out of the ROIs set on the screen. When the embryos were incubated in 0.2 mg/mL tricaine for 1 h I did not want to give them the chance to recover from the doxorubicin treatment before we filmed them. Therefore I decided to incubate them in a combination of 0.2 mg/mL tricaine and fresh doxorubicin of the same concentration they had been incubated in since stage 38.

5.5.3.1 Investigating the effect of drug treatment on the *Xenopus* embryo heart rate:

Doxorubicin

The concentration-dependent increase of heart rate for embryos treated with doxorubicin indicates that the drug has had an effect. The same result was achieved with zebrafish embryos treated with doxorubicin (Chang et al., 2014). Although the change in heart rate with doxorubicin treatment implies there is a cardiotoxic effect, the incidence of arrhythmias can provide a better indication of drug-induced cardiotoxicity. The occurrence of arrhythmia was concentration-dependent for doxorubicin-treated *Xenopus* embryos, but as the concentration of doxorubicin increased the survival of the embryos decreased. It could be possible that the embryos that didn't survive to stage 45 have had an arrhythmic heart beat and therefore the arrhythmia incidence could be higher. A useful experiment to carry out in the future would include the monitoring and characterisation of the heartbeat at more than 1 time point to include the embryos that don't survive to the age of stage 45. The increase in heart rate for all of the doxorubicin concentrations and untreated embryos (0 μ M doxorubicin) at 3 days post-treatment was also observed by Chang and colleagues in zebrafish embryos. This heart rate increase is likely to be as a result of the ageing of the embryos over the 3 days. It is a time-dependent increase irrespective of the doxorubicin concentration. The heart has developed further and become stronger from stage 38 to stage 45 in the *Xenopus* embryos. In future experiments this should be taken into account when analysing the results.

5.5.3.2 Investigating the effect of drug treatment on the *Xenopus* embryo heart rate:

Terfenadine

Terfenadine is a known hERG blocker that is associated with QT-prolongation, arrhythmias and TdP in humans. My results suggest that our *Xenopus* model correlates with the human terfenadine-induced cardiotoxicity response. The incidence of arrhythmia is not dose-dependent in my results, but this could be explained by the decline in survival at higher concentrations, therefore I could be missing arrhythmic heart rates in embryos that did not survive until stage 45. The concentration-dependent reduction in heart rate with our *Xenopus* model was also observed in zebrafish embryos exposed to acute terfenadine cardiotoxic concentrations (Gu et al., 2017). I used DMSO as a solvent for terfenadine, the final incubation concentration contained 0.5 % DMSO. DMSO is a known human CYP450 inhibitor (Chauret et al., 1998). As I have mentioned previously in this chapter, the presence of a CYP450 inhibitor can reduce the amount of terfenadine that is metabolised to terfenadine carboxylate, a known non-cardiotoxic molecule, and lead to terfenadine accumulation. The accumulation of the parent drug terfenadine increases the risk of drug-induced cardiotoxicity. The terfenadine was not soluble in the *Xenopus* media

alone, but in future experiments I would like to use a different solvent to DMSO to remove possible pro-cardiotoxic effects.

5.5.4 Doxorubicin and dexrazoxane combined treatment

In humans taking doxorubicin, dexrazoxane is a cardioprotective agent often prescribed to help minimise the doxorubicin cardiotoxic effects. Our aim was to explore this using the heart rate assay. In the literature, the ratio of doxorubicin to dexrazoxane used in drug safety models varies. Zhang and colleagues (2015) used a doxorubicin to dexrazoxane ratio of 1:50 to investigate the combined effects of doxorubicin, dexrazoxane and trastuzumab on the cardiotoxicity in rats. They found that the rats that had dexrazoxane in their treatment had a bigger LVEF than the rats that did not (Zhang et al., 2015). Lyu and colleagues (2007) used a ratio range of 1:20 to 1:2000 doxorubicin to dexrazoxane to treat H9C2 cardiomyocytes. A retrospective study looked at cardiotoxicity in children and teenagers treated with doxorubicin alone or in combination with dexrazoxane in a ratio of 1:10 (Paiva et al., 2005). In another retrospective study, children received doxorubicin alone, or in combination with dexrazoxane in a ratio of 1:10 (Lipshultz et al., 2012). In conclusion, I decided to use a ratio of doxorubicin to dexrazoxane 1:10 to treat the *Xenopus* embryos. The doxorubicin concentration range was 0-100 μM (10 μM integrals), therefore the dexrazoxane concentration range was 0-1 mM (100 μM integrals). Before I performed the dose response with the combination of doxorubicin and dexrazoxane treatment, I examined the phenotype and survival rate of the embryos with the 0-1 mM dexrazoxane treatment alone. Unlike the majority of the dose response assays performed in this project, I did not want a change in survival rate with dexrazoxane treatment. There was no change in survival for embryos treated with 0-1 mM dexrazoxane; therefore I concluded that changes in the combined doxorubicin and dexrazoxane treatment are likely to be due to the doxorubicin compound. I hypothesised the survival rate for the combined doxorubicin and dexrazoxane treatment would be higher than the survival rate for embryos treated with doxorubicin alone. However in the combined treatment the survival rate was similar to the doxorubicin alone treatment. In future experiments I would like to explore the reason for this result. As mentioned above, dexrazoxane binds to topoisomerase II β in humans, this is one of the cardioprotective mechanisms proposed that reduces doxorubicin cardiotoxicity. The *Xenopus laevis* topoisomerase II β protein has 84 % homology to the human protein. Therefore it could be that the dexrazoxane cannot carry out the cardioprotective mechanism in the *Xenopus* embryos.

5.5.5 MiR-208 expression in *Xenopus* embryos

The *Xenopus laevis* miR-208 mature sequence has 95 % homology to the mature human miR-208a-3p sequence; 1 out of the 22 nucleotides differs. My results clearly show that

the *Xenopus* miR-208 is specifically expressed in the heart (**Figure 5-18**), this is similar to humans and other animal models such as rats. I did perform qRT-PCR to identify the expression of miR-208 in the *Xenopus* heart compared to the tail (tissue that does not express miR-208) in doxorubicin-treated embryos (data not shown). However unfortunately I did not have enough time to optimise the primers. In future work I would like to investigate the change of miR-208 expression in *Xenopus* plasma for embryos treated with known cardiotoxic drugs. This experiment would be similar to the miR-122 qRT-PCR paracetamol experiment performed in **chapter 4** and it would explore if the role of miR-208 as a drug-induced cardiotoxicity biomarker is conserved in *Xenopus* embryos.

5.6 Conclusion

In this chapter I have used 2 drugs that in rare cases, are known to cause cardiotoxicity in humans through different mechanisms. Unlike **chapter 4**, which focused on structural and metabolic changes to the target organ for toxicity, I was able to assess the effect of the drugs associated with toxicity on organ function in this chapter. There is room for improvement in heart rate assay, limitations and future experimental ideas have been mentioned in the text above. In addition, I would like to test more known cardiotoxic compounds and drugs that are not associated with heart-specific ADRs to validate the heart rate assay protocol. In **chapter 3** I identified the expression of the *Xenopus* equivalent hERG gene in stage 38 and stage 45 embryos. However, in the future I would like to determine the activity of the *Xenopus* hERG channel when the embryos are treated with cardiotoxic drugs and if the drugs associated with significant hERG inhibition in humans, perform the same mechanism of action with the *Xenopus* hERG channel. With regards to the wholemount phenotype, I would like to add a more comprehensive specification of endpoints to look for that is decided on prior to the experiment, for example, haemorrhage and thrombosis. The transparency of the *Xenopus* implies it should be simple to spot the pooling of blood outside the heart and blood clots, however I think that this could be undetectable in the photographs I have taken due to the fixation process we perform prior to photographing. Indeed the red blood colour is not visible in the *Xenopus* embryos hearts in my photographs.

Overall the arrhythmias and statistically significant changes in heart rate in *Xenopus* embryos treated with doxorubicin and terfenadine suggests that the *Xenopus* could be useful for identifying drug-induced cardiotoxicity that is applicable to humans.

6 Chapter 6: General discussion

6.1 Project aims

During this project our project aims were to:

- Characterise the functional capacity of *Xenopus laevis* embryos functional capacity in relation to drug metabolism and drug toxicity
- Optimise and adapt assays used in other drug toxicity models to the *Xenopus* system
- Investigate organ-specific toxicity in *Xenopus* embryos with drugs that are associated with hepatotoxic, cardiotoxic and nephrotoxic reactions in humans

6.2 Introduction

Current drug safety assessment animal models do not reliably predict drug-induced toxicity events in man. In a large retrospective study of 150 compounds, 221 human toxicity events were generated, 63 % were detected in non-rodent models (mostly dogs) and there was a 43 % concordance with rodent models (mainly rats) (Olson et al., 2000). Improving the current models or finding better alternatives can help to reduce drug attrition in the later phases of drug development and therefore decrease the amount of time and money wasted in pharmaceutical companies for drugs that are not going to be approved. A more efficient and successful assessment of drug toxicity potential in animal models could improve drug development productivity, thus having a positive impact on hospitals and patients. If the drug candidates associated with toxicity were identified and terminated early in development, more effort can be put towards the safer drugs and a pharmaceutical company could potentially deliver more drugs to the market each year. This could benefit a larger number of patients and consequently hospitals.

The use of traditional animal models, which in the past were sometimes used by default for safety predictions, is on the decline. There is increasing pressure to produce drug safety data that is as relevant to humans as possible. Researchers need to think about what the best animal model is for their experiments and not just use the one they have always used. In drug development, the best animal model for each safety assessment is chosen carefully. In particular, in the UK the NC3Rs, which was launched in 2004, encourages the development of research methods that can replace, reduce and refine the use of animals in scientific research (NC3Rs, 2017). The replacement principle refers to using a technology or alternative tool that is just as good or better than the animal model to be able to replace the animal entirely. Good experimental design and analysis can reduce the number of animals used, whilst still generating accurate and reproducible data that has good statistical power. Finally, animal welfare can affect the validity of the results

produced and so by refining the experiment to minimise animal suffering, it is not only considered more ethical, but the results can be interpreted more accurately (Prescott and Lidster, 2017). This project was funded by the NC3Rs. We hypothesised that a non-mammalian *Xenopus laevis* embryo model for drug-induced toxicity prediction could contribute to the reduction principle. A successful *Xenopus laevis* model could aid lead drug candidate prioritisation and reduce the number of toxic compounds getting through to the mammalian animal models as well as reduce the number of mammalian animal models to be used.

The *Xenopus laevis* embryo model has several characteristics that are in line with an ideal animal model for the prediction of drug toxicity. It can also help bridge the gap between the *in vitro* and the first mammalian *in vivo* studies conducted in drug development.

A large number of *Xenopus* embryos can be produced from an adult female *Xenopus*, approximately 1000 a day. The embryos develop quickly *ex utero* after *in vitro* fertilisation (IVF) and the cost for keeping adult females is relatively low compared to mammalian models. Furthermore, the embryos are small and up to 5 can comfortably fit into 1 well of a 96-well plate. This makes them amenable for medium to high throughput compound screening and advantageous for early preclinical studies, as they require only a small amount of the test compound. *Xenopus laevis* embryos are transparent, a useful characteristic for imaging techniques and phenotype analysis. Unlike other mammalian models, the *Xenopus* model does not necessarily require time-consuming dissection to visualise the effect of the test compound and we can obtain real-time information. However it is likely the *Xenopus laevis* embryo model does have some limitations that are possibly similar to other non-mammalian models such as zebrafish. For this project we decided to characterise the *Xenopus laevis* embryos capability to act as a model for the prediction of drug toxicity, exploring the model's advantages and disadvantages using drugs associated with toxicity in humans. The results are summarised in **Figure 6-1**.

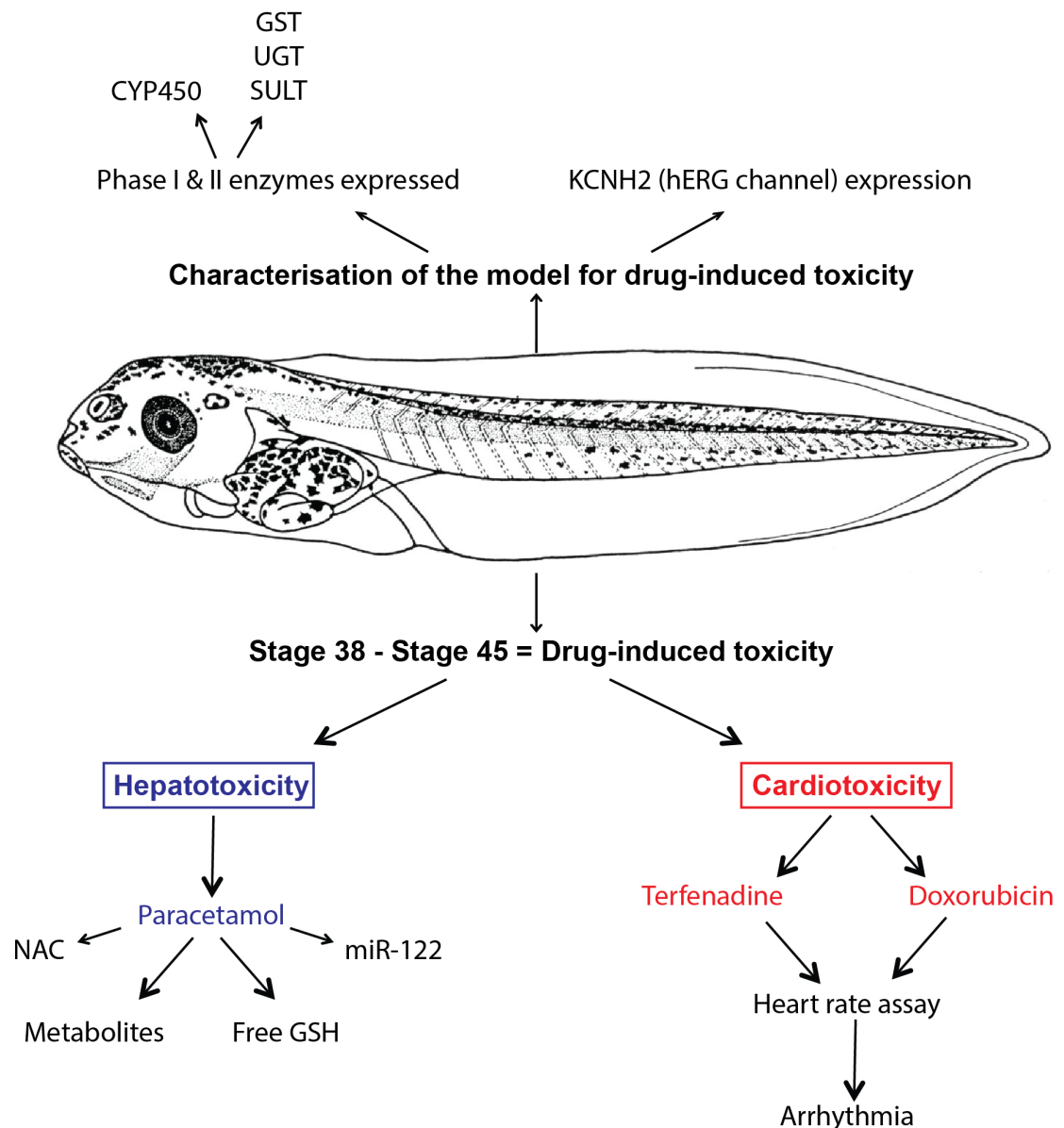


Figure 6-1: Summary of project results.

A schematic to summarise the main results generated in this project including the expression of the *Xenopus laevis* gene equivalent to the hERG (human Ether-à-go-go-Related Gene) also known as KCNH2. Stage 38 embryos incubated with a drug for 72 h, until the age of stage 45, measures drug-induced toxicity as opposed to teratogenicity, as organogenesis is near completion. CYP450, cytochrome P450; GSH, glutathione; GST, glutathione S-transferase; miR-122, microRNA-122; NAC, N-acetylcysteine; SULT, sulphotransferase; UGT, Uridine-5'-triphosphate-glucuronosyl transferase.

6.3 Characterisation of the *Xenopus laevis* embryo as a model for drug-induced toxicity

In **chapter 3** we conducted preliminary dose response assays with 2 different *Xenopus* embryo age groups: stage 15 to stage 38 and stage 38 to stage 45. Overall, we proved our **chapter 3** hypothesis is correct, that is that the stage 38 to stage 45 embryos were suitable for drug-induced toxicity screening. In the dose response assays for the embryos incubated with the test drug at stage 38 and harvested at stage 45, the number of different abnormal phenotypes was less compared to the stage 15 - stage 38 screens. This indicates the stage 38 - stage 45 embryos have more functional organ systems compared to younger embryos. There is only 1 dominant abnormal phenotype generated from the stage 38 - stage 45 embryo screen, that is gastrointestinal oedema, which suggests the reaction drug-specific. It would be ideal if we could correlate specific organ toxicity to a visual phenotype. For example, oedema around the cardiac tissue would indicate cardiotoxicity. Unfortunately, there was not a clear correlation between this abnormal phenotype and the embryo treatment of drugs associated with cardiotoxicity such as doxorubicin.

These screens also demonstrate that the drug is at least getting into the embryo and causing an effect. The *Xenopus laevis* embryos do not have an open mouth until stage 40, however the gills are open and the skin is permeable to small molecules such as phenylthiourea (PTU) therefore, drugs present in the media the *Xenopus* embryos swim in, should still be able to enter the embryo system (Brandli, 2004; Chen et al., 2017). It is not known if the physicochemical properties of each individual drug will affect the efficiency of drug diffusion through the *Xenopus* embryo skin. For example, a more lipophilic drug could diffuse at a different rate to a hydrophilic drug. One of the disadvantages of using non-mammalian models for drug or chemical screens, is that it is difficult to determine what percentage of the dose they are exposed to translates to an internal concentration (van Vliet, 2011). We explored this with *Xenopus* embryos treated with paracetamol and using mass spectrometry in **chapter 4**. These mass spectrometry results revealed the presence of paracetamol metabolites APAP-cysteine and APAP-glutathione inside the embryos, although the presence of the parent drug paracetamol was minimal. We hypothesise this is because paracetamol is quickly metabolised inside the embryos, or it could be that the parent drug is rapidly excreted. The internal concentration of the test drug inside the embryos should be relevant to the human C_{max} (peak serum drug concentration after a dose) value in order for the model to be applicable for the prediction of drug-induced toxicity in humans. Consequently, we need to be able to measure the amount of drug inside the embryos. We believe mass spectrometry is the

best method to measure internal drug concentration inside *Xenopus* embryos. Vliegenthart and colleagues (2014) developed a method to extract blood from zebrafish through the retro orbital sinus. This could be useful to determine the C_{max} of drug candidates in *Xenopus*. But this laboratory group used adult zebrafish aged 5 months to 2 years old post fertilisation; we imagine it would difficult to apply the same technique to *Xenopus* embryos. This zebrafish laboratory group found that the zebrafish plasma concentration of paracetamol 4 h after an overdose was 962 mg/mL. They stated this was similar to the 10-340 mg/mL plasma concentration measured in humans that have taken a paracetamol overdose (Dargan et al., 2001; Prescott et al., 1979; Vliegenthart et al., 2014a). The fact that a non-mammalian model can possess similar pharmacokinetics to humans means the *Xenopus* model could be useful too.

At the ages of stage 38 and stage 45, the embryos expressed phase I and phase II drug metabolism enzymes: (a) CYP450 isoenzymes 2D6, 3A4 and 2E1 (b) GST (glutathione-S-transferase) P1, T1 and M1 (c) SULT (sulphotransferase) 1A1 and 2A1 and (d) UGT (UDP-glucuronosyltransferase) 1A1 and 1A6. The human drug metabolism enzymes of the same names metabolise a high percentage of drugs taken. We decided to look for the expression of these enzymes especially, because the CYP2E1 and all the phase II enzymes are known to be important for paracetamol metabolism, which is the main hepatotoxic drug we explored in **chapter 4**. The mRNA expression of these enzymes does not necessarily correlate with a functional CYP450 enzyme. In addition, the *Xenopus* CYP2E1 enzyme may not be the major enzyme involved in the generation of the paracetamol reactive metabolite NAPQI, as is the case in humans. Consequently it would be useful to measure the activity of the drug metabolism enzymes in *Xenopus* at stages 38 and stages 45 to characterise their drug metabolism capacity. Possible methods for this are outlined in the future experiments sections below.

6.4 *Xenopus laevis* embryos and the prediction of DILI: paracetamol

Drug-induced liver injury (DILI) is the leading cause of drug attrition in the later phases of drug development. Each drug associated with DILI in man presents as a specific liver injury phenotype. In addition, a drug candidate that causes idiosyncratic DILI is rare and often not detected in the clinical phases of drug development because the size of the study cohorts are too small. Consequently, it is impossible for one animal model to be able to detect all DILI reactions. We proposed the *Xenopus laevis* embryos could be an additional animal model to detect drug candidates that are associated with DILI in the very early phases of drug development. They could bridge the gap between *in vitro* studies and the first *in vivo* studies. To investigate if the *Xenopus* embryos have the ability to detect DILI, we used the dose-dependent hepatotoxin paracetamol in **chapter 4**. Paracetamol

overdose is a major contributor to the incidence of acute liver failure in the US and the UK. We hypothesised that stage 38-45 *Xenopus laevis* embryos treated with paracetamol will exhibit characteristics of paracetamol-induced liver injury similar to other non-mammalian and mammalian animal models and humans. We established this hypothesis is correct according to our results that measured: (1) miR-122 expression, (2) free GSH concentration, (3) paracetamol metabolite generation and (4) NAC intervention. *Xenopus* embryos treated with paracetamol had an increased miR-122 expression in isolated tissue that does not normally express miR-122. In humans, other mammalian animal models, and non-mammalian models, miR-122 expression is abundant in the liver. Liver injury causes an increase of miR-122 expression in the blood. The *Xenopus* embryo tail was used as a substitute for mammalian blood in our experiment, as it is very difficult to obtain enough blood from a stage 45 to measure the serum miR-122 concentration. We also adapted an *in vitro* assay that measures free GSH concentration for paracetamol-treated *Xenopus* embryos. This adaptation produced results that show that as the concentration of paracetamol the embryos were incubated with increased, the concentration of free GSH inside the embryos decreased. In humans that take a therapeutic dose of paracetamol, the paracetamol reactive metabolite NAPQI is neutralised with GSH. A paracetamol overdose leads to a higher production of NAPQI and consequently less endogenous free GSH is available to reduce the toxic effects of NAPQI that provokes liver function impairment. The GSH result for *Xenopus* embryos implies they metabolise paracetamol via a similar pathway to humans. Moreover, the *Xenopus* embryos generate paracetamol metabolites that are also detected with human paracetamol metabolism. This is demonstrated in our HPLC-MS/MS results in **chapter 4**. Finally, when *Xenopus* embryos are treated with paracetamol for 72 h and NAC for the last 24 h of the incubation, the reduction of free GSH is not as considerable as without NAC treatment. NAC is the therapeutic treatment for humans that have taken a paracetamol overdose. These last 3 experiments (free GSH reduction, HPLC-MS/MS and NAC treatment) indicate the *Xenopus* embryos have the ability to process paracetamol and therefore potentially other drugs as well, using the same metabolic pathways and mechanisms as humans. This is important for the detection of DILI, because often an adverse hepatotoxic reaction occurs due to a drug metabolite, not the parent drug. So a good animal model for the prediction of DILI should be able to generate the same or similar metabolites that will be produced in humans.

6.5 *Xenopus laevis* embryos and the prediction of cardiotoxicity: doxorubicin and terfenadine

The second organ-specific toxicity we investigated with the *Xenopus* embryos was drug-induced cardiotoxicity. The introduction of a compulsory evaluation of the potential for a drug candidate to cause delayed ventricular repolarisation has reduced the incidence of drug attrition due to cardiotoxicity associated with TdP. In the past, the majority of assays that assessed drug-induced cardiotoxicity analysed the drug candidate's interaction and ability to block the potassium ion hERG channel and consequently the I_{Kr} current. But in 2014, the CiPA initiative recognised that there are other ion channels that the drug candidate could interfere with and contribute to the generation of a cardiotoxicity reaction. As a result, the CiPA method was introduced which is comprised of 3 elements: (1) *in vitro* evaluation of drug effect on multiple individual currents, (2) *in silico* computational reconstruction to assess proarrhythmic liability and (3) confirm any effects found using *in vitro* electrophysiological techniques. The models to predict drug-induced cardiotoxicity are clearly still developing and we think there is room for the *Xenopus* embryo model at the early phases of drug development. Non-mammalian animal models can still be relevant to humans even though the heart structure does not have 4 chambers. For example, the zebrafish has a 2-chambered heart it has an average heart rate of 120-180 bpm and the QT intervals are 400-500 ms (Hassel et al., 2008; Leong et al., 2010). Whereas mice have a much higher heart rate at 300-600 bpm and their QT intervals are shorter at 50 ms (Dhillon et al., 2013). Humans have an average heart of 60-100 bpm and a QT interval of 350-440 ms (Li et al., 2016). Thus, the non-mammalian zebrafish could be just as relevant as the mammalian models for the prediction of drugs that affect human heart rhythm.

In **chapter 5** we investigated if the *Xenopus* embryo could be a good model for the prediction of cardiotoxicity. To do this, we used doxorubicin and terfenadine, which are 2 drugs known to be associated with cardiotoxicity in humans. The mechanism of toxicity is slightly different between doxorubicin and terfenadine, so by using these test drugs we were able to analyse if the *Xenopus* embryos can aid the identification of different types of drug-induced cardiotoxicity. The generation of doxorubicin-induced cardiotoxicity is attributed to the production of free radical oxygen species that damage cardiac tissue. Terfenadine is known to block the hERG channel and therefore negatively impact on the delayed rectifier current and subsequently cause arrhythmia. One of the advantages of the *Xenopus* embryos, is their transparency, the heart can be observed beating in real time. We exploited this with our heart rate assay. The heart rate of treated embryos increased with increasing doxorubicin concentration and decreased with increasing

terfenadine concentration. The incidence of arrhythmias increased with increasing doxorubicin concentration. But for terfenadine-treated embryos, arrhythmias occurred at every concentration and were not dose-dependent. All of these results demonstrate that cardiotoxic drugs affect the *Xenopus* embryo hearts and the trends also correlate with other animal models. Overall, we reached the aim of **chapter 5** and demonstrated that the *Xenopus* embryos can be useful for the prediction of cardiotoxicity.

6.6 Limitations and future experiments

We have addressed the majority of the aims for this project in **chapters 3 – 5** and the advantages of the *Xenopus* embryos for the prediction of drug-induced toxicity are summarised in the sections above. However, we understand this non-mammalian model is not likely to correlate completely with humans and we discovered some limitations in this project. We think some of these limitations can be improved with future experiments (**Figure 6-2**). First of all, we did not have the time to explore a large number of drugs associated with organ-specific toxicity in the *Xenopus* embryos. To help further characterisation of the *Xenopus* embryo model, we would like to use a list of test drugs that have different mechanisms of toxicity for hepatotoxicity and cardiotoxicity. We also think it would be beneficial to add drugs to the list that are not associated with toxicity and conduct a blind experiment to determine if the *Xenopus* embryos can help differentiate between the toxic and non-toxic compounds. This is an important feature of an ideal animal model to be used in drug development.

In **chapter 3** we measured drug metabolism enzyme expression but not activity. It is important to characterise the *Xenopus* embryo drug metabolism capability because sometimes it is the drug metabolite, not the parent drug, which is vital for a drug-induced toxicity reaction to occur. In future experiments we would like to measure drug metabolism enzyme activity in the stage 38 to stage 45 *Xenopus* embryos to examine if they are functional at this age. Once we have established their functionality, we could also use enzyme inhibitors to decipher the mechanisms and pathways for drug-induced toxicity reactions in the *Xenopus*. We attempted to isolate microsomes from an adult *Xenopus* in **chapter 4** to investigate CYP450 activity in the presence of 1-ABT, a known CYP450 inhibitor in mammalian models. To quantify CYP450 activity, we used the substrate p-nitrophenol and tried to measure the rate of the production of the product 4-nitrocatechol (Monostory et al., 2004). However the protocol required more time to be optimised for the *Xenopus*. We would like to measure SULT activity in the *Xenopus* embryos to determine their ability to process drugs using the sulphation metabolic pathway. Typically, the activity of the SULT enzymes is determined by measuring the transfer of a PAP³⁵S sulpho group to a substrate, and then quantifying the ³⁵S-labelled products (Paul et al., 2012). PAPS is

the coenzyme or conjugating agent involved in sulphotransferase reactions. We would also like to measure the activity of the UGT enzymes in the *Xenopus* embryos, as glucuronidation is a major drug metabolism pathway in humans for many drugs. There are compounds specific to UGT isoforms such as azidothymidine for UGT2B7 and propofol for UGT1A9. UGT activity can be quantified using fluorescence, HPLC and mass spectrometry techniques that detect the products of these substrates (Donato et al., 2010).

One of the major aims we did not achieve for this project was the evaluation of *Xenopus* embryos for the prediction of nephrotoxicity. Drug-induced nephrotoxicity accounts for 18-27 % of acute kidney injury cases in the US (Taber and Pasko, 2008). It is responsible for 2 % of drug attrition in preclinical studies and 19 % in the clinical phase of drug development (Jang et al., 2013). In the literature and to our knowledge, *Xenopus* embryos have not been characterised for the prediction of drug-induced nephrotoxicity. Christensen *et al* (2008) have detected the expression of megalin and cubilin in stage 35 *Xenopus tropicalis* embryos. The expression was specific to the proximal tubule of the pronephric kidney (Christensen et al., 2008). Megalin and cubilin are endocytic receptors that are co-expressed in the apical membrane of the proximal tubule. In humans, they are predominantly involved in the reabsorption of albumin. However these receptors also play a pathophysiological role in the uptake of aminoglycosides, such as gentamicin. The accumulation of aminoglycosides in the proximal tubule is associated with the mechanism of drug-induced nephrotoxicity. In summary, Christensen *et al* indicate the *Xenopus* embryo has some of the mechanistic tools that suggest it could be a good animal model to help predict drug-induced nephrotoxicity, and it would be interesting to investigate this in the future. In **chapter 3** we looked at 2 drugs associated with nephrotoxicity: cisplatin and gentamicin. In the stage 38 – stage 45 screens, a common abnormal phenotype observed in embryos treated with 0.78-100 μ M gentamicin was gastrointestinal oedema. This indicates that the *Xenopus* embryo could be a promising model to help identify drug-induced nephrotoxicity. However all of the embryos treated with cisplatin generated a wildtype phenotype, no abnormal phenotypes were identified. We hypothesise this is because the dose range 0.78-100 μ M was not high enough to cause cisplatin-induced toxicity in the *Xenopus* embryos.

It is difficult to determine what is the correct concentration range to use that can potentially cause drug-induced toxicity in a new animal model. For *in vitro* safety studies, the drug concentration that causes 20 % cell death is the highest concentration that should be used to test for drug-specific toxicity. A higher percentage of cell death could be caused by general toxicity mechanisms that occur if the cells were treated with too much of any compound. In addition, the highest concentration treatment that maintains 80 % cell

viability can be used to decide if the test drug is likely to generate a toxicity reaction in humans. The ratio between this high concentration and the C_{max} of the drug candidate in patients should be at least ten-fold, this ratio is called the safety margin (SM). A drug candidate with a value of $SM < 10$, is identified as a compound that has a high probability of causing a toxicity reaction (Richert et al., 2016). We applied the same principle to our *Xenopus* embryo toxicity studies and used a concentration range that we believe investigates drug-specific toxicity, not general toxicity.

It would be useful to measure the *Xenopus* embryo C_{max} of the drugs we researched in this project for 2 reasons: (1) we can establish how much of the drug the embryo has taken up (the “internal dose” mentioned previously in this chapter) and (2) we can see if this is similar to C_{max} in humans and therefore deduce the relevance of the *Xenopus* embryo as a model for the prediction of drug toxicity. HPLC-MS/MS can be used to measure the *Xenopus* C_{max} . The concentration of paracetamol metabolites inside and outside the *Xenopus* embryos treated with paracetamol was measured after a 72 h incubation using HPLC-MS/MS in **chapter 4**. However we could not perform a statistical analysis on this experiment because it was only conducted once ($n=1$). We would like to repeat this experiment in the future and modify it to include more time points so we can analyse the concentration of the parent drug and its metabolites throughout the stage 38 – stage 45 paracetamol screen. As explained in the discussion of **chapter 4**, the 1 set of results we did obtain from HPLC-MS/MS analysis of paracetamol-treated *Xenopus* embryos indicate the embryos could be more representative of a child than an adult human. The APAP-glucuronide to APAP-sulphate metabolite ratio in adult humans is approximately 2:1 whereas in children it is closer to a 1:1 ratio. The APAP-glucuronide and APAP-sulphate metabolites detected in *Xenopus* treated with a concentration of paracetamol within the range 0-5 mM were closer to the ratio for children. If this result is reproducible, we will conduct further experiments to determine if the *Xenopus* behaves more like a child in terms of drug metabolism and pharmacokinetics than an adult. This could impact upon what the *Xenopus* should be used for in drug development. For the most part, in drug development the drugs are assessed for adult administration.

Finally, in future experiment we would like to determine the impact of the test drug on organ function in the *Xenopus* embryos. Our experiments in **chapter 4** focused on characterising drug-induced liver injury, however we did not investigate if the liver function was impaired. This is important because in humans, the body sometimes has the ability to compensate for drug-induced toxicity reactions. The human liver is particularly capable of adapting to chemical insults and it is able to regenerate after liver resection (Eakins et al., 2015; Riehle et al., 2011). Adverse drug reactions could go undetected in the clinic until the body is no longer able to tolerate them and organ function is impaired. Furthermore, if

the toxicity reaction is reversible after administration stops and organ function is adequate, then it can be argued that the drug benefits outweigh the risks. We would to adapt the liver function tests used in other animal models and humans to measure liver function in *Xenopus* embryos treated with drugs associated with liver injury in humans. Typically, liver function impairment can be characterised by measuring the concentration of liver biomarkers in the plasma as previously mentioned in **chapter 1** such as ALT, AST, ALP and total bilirubin. However 1 method to truly measure liver function is using Indocyanine green (ICG) dye, which is exclusively cleared from the body via the liver. The elimination rate of ICG has been used to measure hepatic blood flow, hepatosplanchnic haemodynamics, and liver function (Brillant et al., 2017; Imamura et al., 2005; Levesque et al., 2016; Sakka, 2007). In the future, we would like to investigate the use of ICG dye to evaluate *Xenopus* embryo liver function.

Our heart rate assay assessed *Xenopus* embryo heart function in the presence of drugs associated with cardiotoxicity in humans. In particular, we think that the incidence of arrhythmias measured with our heart rate assay method, is a good reflection of drug-induced cardiac injury. However in future experiments with the *Xenopus* embryos we would like to add more time points to assess the incidence of arrhythmia over the 72 h incubation period and detect embryos that had arrhythmic heart beats but died before they could be detected at 72 h. In addition, it would be interesting to see if we could adapt the heart rate assay to detect changes in left ventricular ejection fraction (LVEF), which is a common measure of heart function in other animal models for the prediction of drug-induced cardiotoxicity. Our heart assay protocol includes a computational element that eliminates some personal bias but it is still requires further development to become a more automated experiment. Currently, we counted the peaks and troughs of the graph generated from the change in greyscale due to the movement of blood through the *Xenopus* embryo heart, in order to get the number of beats per minute.

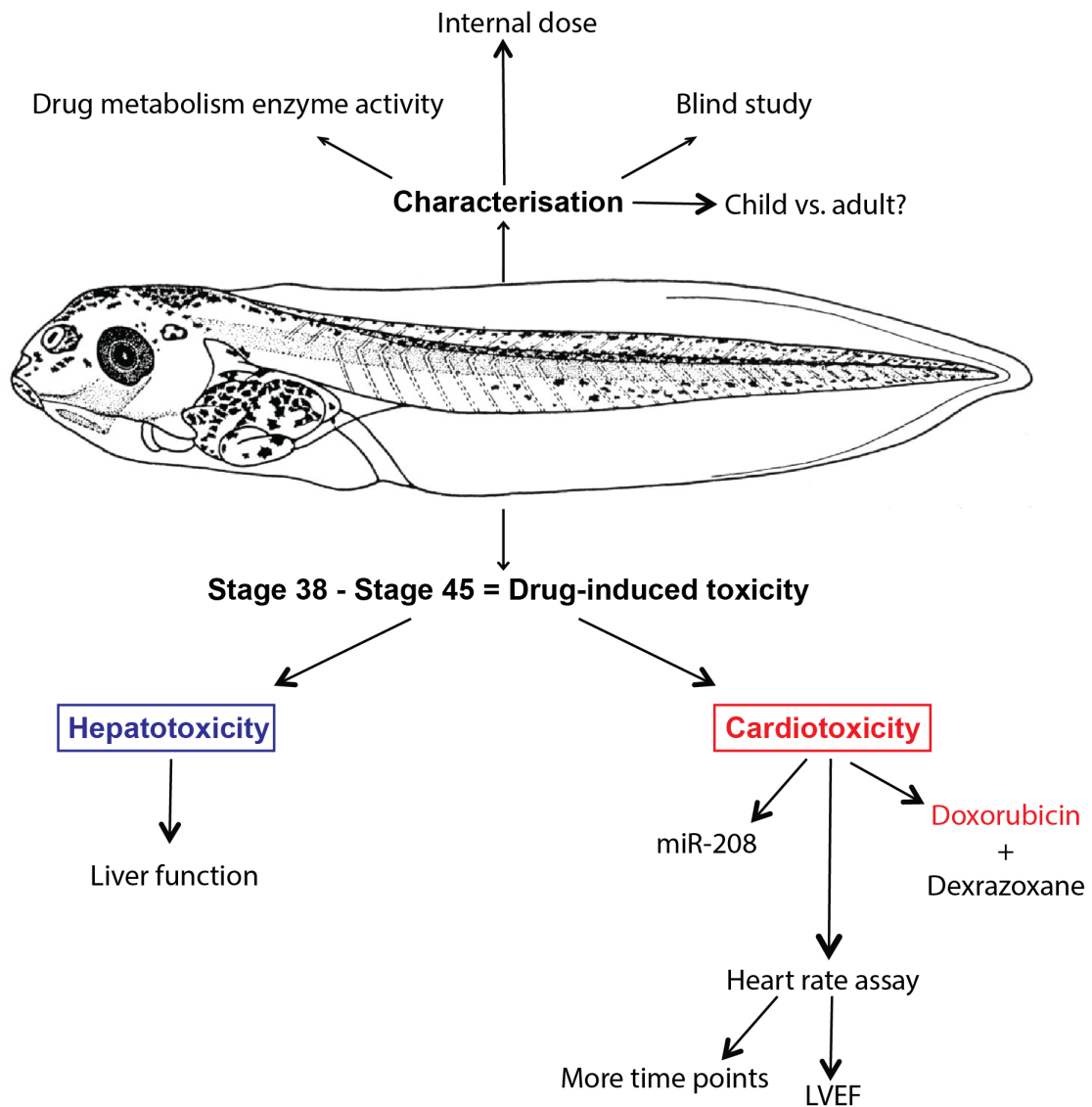


Figure 6-2: Future experiments to be conducted

A schematic that displays examples of future experiments that would be required to further characterise the *Xenopus laevis* embryo as a model for the prediction of drug-induced toxicity. The internal dose the embryo receives from the dose they are exposed to should be characterised to determine *Xenopus* embryo pharmacokinetics and relevance to human peak plasma concentration. The paracetamol metabolite ratio was similar to that observed in children; future experiments should explore if this model is closer to human adults or representative of children. Finally, a more comprehensive list of compounds associated and not associated with toxicity reactions in humans should be performed in a blind study to see if this model can differentiate these groups.

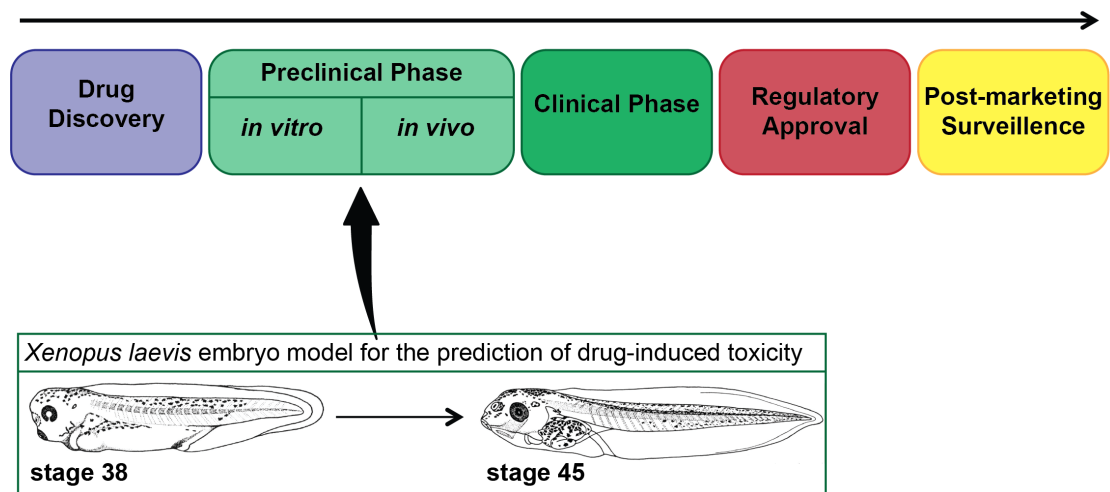


Figure 6-3: Drug development with *Xenopus laevis*

The proposed use of *Xenopus laevis* embryos in drug development would be in the early preclinical phase for the prediction of drug-induced toxicity. *Xenopus* embryos could bridge the gap between *in vitro* and *in vivo* safety studies.

6.7 Conclusion and the ‘bigger picture’

In this project, we aimed to investigate the use of *Xenopus* embryos for the prediction of drug-induced toxicity in humans. We propose a non-mammalian animal model such as the *Xenopus* could be useful to bridge the gap between *in vitro* and *in vivo* drug safety studies in the early preclinical phase of drug development (**Figure 6-3**). Currently, our results indicate that the *Xenopus* embryos could be useful and relevant model. A lot of the methods for the detection of drug-induced toxicity are conserved. In particular, the organ-specific expression of miR-122 and miR-208 for the liver and heart respectively suggests a simple qRT-PCR experiment with treated *Xenopus* embryos can indicate drug-induced toxicity. This experiment combined with the fact that at least 5 embryos can fit into 1 well of a 96 well plate, demonstrates *Xenopus* embryos could be useful for medium throughput screening. In addition, this is translatable to other animal models and humans that also express these organ-specific biomarker miRNAs. However we think that further characterisation is required to determine the limitations of the model and therefore understand the value of the data it generates. This animal model could adhere to the reduction principle defined by the NC3Rs. In research, much effort has been made to characterise the zebrafish as a model for drug-induced toxicity. However the *Xenopus*, an alternative non-mammalian model, has a closer anatomic proximity to humans than the zebrafish. The *Xenopus* has lungs, a 3-chambered heart (as opposed to the 2-chambered zebrafish heart) and amphibians have a common evolutionary history with mammals that is an estimated 100 million years longer than between zebrafish and mammals (Kälin et

al., 2009). Unfortunately commercial research tools for the *Xenopus* such as antibodies are currently not readily available. Consequently it can be difficult to adapt common drug toxicity experiments. However we believe that with time, further characterisation and by developing the experimental methods to be become more automated, the *Xenopus* embryo could be a useful tool for the prediction of drug toxicity in drug development.

7 Chapter 7: References

- Adams, J.E., Schechtman, K.B., Landt, Y., Ladenson, J.H., Jaffet, A.S., 1994. Comparable Detection of Acute Myocardial Infarction by Creatine Kinase MB Isoenzyme and Cardiac Troponin I. *Clin. Chem.* 40, 1291–1295.
- Adamson, G.M., Harman, A.W., 1989. A role for the glutathione peroxidase/reductase enzyme system in the protection from paracetamol toxicity in isolated mouse hepatocytes. *Biochem. Pharmacol.* 38, 3323–3330.
- Adjel, A.A., Gaedigk, A., Simon, S.D., Weinshilboum, R.M., Leeder, J.S., 2008. Interindividual variability in acetaminophen sulfation by human fetal liver: implications for pharmacogenetic investigations of drug-induced birth defects. *Birth Defects Res. A. Clin. Mol. Teratol.* 82, 155–165.
- Ahmadi, F., Dolatkhani, F., Lessan-Pezeshki, M., Mahdavi-Mazdeh, M., Abbasi, M.R., Mohebi-Nejad, A., 2014. Cardiac troponins in patients with chronic kidney disease and kidney transplant recipients without acute cardiac symptoms. *Iran. J. Kidney Dis.* 8, 31–36.
- Aithal, G.P., Watkins, P.B., Andrade, R.J. Larrey, D., Molokhia, M., Takikawa, H., Hunt, C.M., Wilke, R.A., Avigan, M., Kaplowitz, N., Bjornsson, E., Daly, A.K., 2011. Case definition and phenotype standardization in drug-induced liver injury. *Clin. Pharmacol. Ther.* 89, 806–815.
- Albano, E., Tomasi, A., 1987. Spin trapping of free radical intermediates produced during the metabolism of isoniazid and iproniazid in isolated hepatocytes. *Biochem. Pharmacol.* 36, 2913–2920.
- Aleksunes, L.M., Scheffer, G.L., Jakowski, A.B., Pruijboom-Brees, I.M., Manautou, J.E., 2006. Coordinated expression of multidrug resistance-associated proteins (Mrps) in mouse liver during toxicant-induced injury. *Toxicol. Sci.* 89, 370–379.
- Aleksunes, L.M., Slitt, A.M., Cherrington, N.J., Thibodeau, M.S., Klaassen, C.D., Manautou, J.E., 2005. Differential Expression of Mouse Hepatic Transporter Genes in Response to Acetaminophen and Carbon Tetrachloride. *Toxicol. Sci.* 83, 44–52.
- Ames, B.N., Joyce, M., Yamasaki, E., 1975. Methods for Detecting Carcinogens and Mutagens With. *Mutat. Res.* 31, 347–363.
- Anonymous, 1972. International drug monitoring: the role of national centres. Report of a WHO meeting. *World Health Organ. Tech. Rep. Ser.* 498, 1–25.
- Antoine, D.J., Dear, J.W., Lewis, P.S., Platt, V., Coyle, J., Masson, M., Thanacoody, R.H., Gray, A.J., Webb, D.J., Moggs, J.G., Bateman, D.N., Goldring, C.E., Park, B.K., 2013. Mechanistic biomarkers provide early and sensitive detection of acetaminophen-induced acute liver injury at first presentation to hospital. *Hepatology*

58, 777–787.

- Antoine, D.J., Jenkins, R.E., Dear, J.W., Williams, D.P., McGill, M.R., Sharpe, M.R., Craig, D.G., Simpson, K.J., Jaeschke, H., Park, B.K., 2012. Molecular forms of HMGB1 and keratin-18 as mechanistic biomarkers for mode of cell death and prognosis during clinical acetaminophen hepatotoxicity. *J. Hepatol.* 56, 1070–1079.
- Antoine, D.J., Mercer, A.E., Williams, D.P., Park, B.K., 2009. Mechanism-based bioanalysis and biomarkers for hepatic chemical stress. *Xenobiotica* 39, 565–577.
- Arai, M., Yoguchi, A., Takizawa, T., Yokoyama, T., Kanda, T., Kurabayashi, M., Nagai, R., 2000. Mechanism of Doxorubicin-Induced Inhibition of Sarcoplasmic Reticulum Ca²⁺-ATPase Gene Transcription 86, 8–14.
- Arany, I., Safirstein, R.L., 2003. Cisplatin nephrotoxicity. *Semin. Nephrol.* 23, 460–464.
- Arbour, N.C., Lorenz, E., Schutte, B.C., Zabner, J., Kline, J.N., Jones, M., Frees, K., Watt, J.L., Schwartz, D.A., 2000. TLR4 mutations are associated with endotoxin hyporesponsiveness in humans. *Nat. Genet.* 25, 187–191.
- Ashley, N., Poulton, J., 2009. Mitochondrial DNA is a direct target of anti-cancer anthracycline drugs. *Biochem. Biophys. Res. Commun.* 378, 450–455.
- Bacon, B.R., O'grady, J.G., Di bisceglie, A.M., Lake, J.R., 2006. *Comprehensive clinical hepatology*. Elsevier Health Sciences.
- Bailey, D.G., Malcolm, J., Arnold, O., Spence, J.D., 1998. Grapefruit juice-drug interactions. *Br. J. Clin. Pharmacol.* 46, 101–110.
- Baillie, T.A., Cayen, M.N., Fouda, H., Gerson, R.J., Green, J.D., Grossman, S.J., Klunk, L.J., LeBlanc, B., Perkins, D.G., Shipley, L.A., 2002. Contemporary issues in toxicology: Drug metabolites in safety testing. *Toxicol. Appl. Pharmacol.* 182, 188–196.
- Barnes, S.N., Aleksunes, L.M., Augustine, L., Scheffer, G.L., Goedken, M.J., Jakowski, A.B., Pruiomboom-Brees, I.M., Cherrington, N.J., Manautou, J.E., 2007. Induction of Hepatobiliary Efflux Transporters in Acetaminophen- Induced Acute Liver Failure Cases. *Drug Metab. Dispos.* 35, 1963–1969.
- Barshop, N.J., Capparelli, E. V, Sirlin, C.B., Jeffrey, B., Lavine, J.E., 2011. Acetaminophen Pharmacokinetics in Children with Nonalcoholic Fatty Liver Disease 52, 198–202.
- Bartel, D.P., 2004. MicroRNAs: Genomics, Biogenesis, Mechanism, and Function. *Cell* 116, 281–297.
- Bartlett, H.L., Scholz, T.D., Lamb, F.S., Weeks, D.L., 2004. Characterization of embryonic cardiac pacemaker and atrioventricular conduction physiology in *Xenopus laevis* using noninvasive imaging. *Am. J. Physiol. Circ. Physiol.* 286, H2035–H2041.
- Bateman, D.N., Carroll, R., Pettie, J., Yamamoto, T., Elamin, M.E.M.O., Peart, L., Dow,

- M., Coyle, J., Cranfield, K.R., Hook, C., Sandilands, E.A., Veiraiah, A., Webb, D., Gray, A., Dargan, P.I., Wood, D.M., Thomas, S.H.L., Dear, J.W., Eddleston, M., 2014. Effect of the UK's revised paracetamol poisoning management guidelines on admissions, adverse reactions and costs of treatment. *Br. J. Clin. Pharmacol.* 78, 610–618.
- Batey, A.J., Coker, S.J., 2002. Proarrhythmic potential of halofantrine, terfenadine and clofilium in a modified in vivo model of torsade de pointes. *Br. J. Pharmacol.* 135, 1003–12.
- Begg, E.J., Barclay, M.L., 1995. Aminoglycosides--50 years on. *Br. J. Clin. Pharmacol.* 39, 597–603.
- Bell, C.C., Hendriks, D.F.G., Moro, S.M.L., Ellis, E., Walsh, J., Renblom, A., Fredriksson Puigvert, L., Dankers, A.C.A., Jacobs, F., Snoeys, J., Sison-Young, R.L., Jenkins, R.E., Nordling, Å., Mkrtchian, S., Park, B.K., Kitteringham, N.R., Goldring, C.E.P., Lauschke, V.M., Ingelman-Sundberg, M., 2016. Characterization of primary human hepatocyte spheroids as a model system for drug-induced liver injury, liver function and disease. *Sci. Rep.* 6, 25187.
- Benichou, C., 1990. Criteria of drug-induced liver disorders. Report of an international consensus meeting. *J. Hepatol.* 11, 272–276.
- Bertolini, A., Ferrari, A., Ottani, A., Guerzoni, S., Tacchi, R., Leone, S., 2006. Paracetamol: New vistas of an old drug. *CNS Drug Rev.* 12, 250–275.
- Bertz, R.J., Granneman, G.R., 1997. Use of in vitro and in vivo data to estimate the likelihood of metabolic pharmacokinetic interactions. *Clin. Pharmacokinet.* 32, 210–258.
- Bessems, J.G.M., Vermeulen, N.P.E., 2001. Paracetamol (Acetaminophen)-Induced Toxicity: Molecular and Biochemical Mechanisms, Analogues and Protective Approaches. *Crit. Rev. Toxicol.* 31, 55–138.
- Biomarkers Definitions Working Group, 2001. Biomarkers and surrogate endpoints: Preferred definitions and conceptual framework. *Clin. Pharmacol. Ther.* 69, 89–95.
- Blitz, I.L., Andelfinger, G., Horb, M.E., 2006. Germ layers to organs: Using *Xenopus* to study “later” development. *Semin. Cell Dev. Biol.* 17, 133–145.
- Boelsterli, U.A., 2003. Diclofenac-induced liver injury: A paradigm of idiosyncratic drug toxicity. *Toxicol. Appl. Pharmacol.* 192, 307–322.
- Boelsterli, U.A., Redinbo, M.R., Saitta, K.S., 2013. Multiple NSAID-induced hits injure the small intestine: Underlying mechanisms and novel strategies. *Toxicol. Sci.* 131, 654–667.
- Boess, F., Kamber, M., Romer, S., Gasser, R., Muller, D., Albertini, S., Suter, L., 2003. Gene expression in two hepatic cell lines, cultured primary hepatocytes, and liver

- slices compared to the in vivo liver gene expression in rats: Possible implications for toxicogenomics use of in vitro systems. *Toxicol. Sci.* 73, 386–402.
- Bourdi, M., Amouzadeh, H.R., Rushmore, T.H., Martin, J.L., Pohl, L.R., 2001. Halothane-Induced Liver Injury in Outbred Guinea Pigs: Role of Trifluoroacetylated Protein Adducts in Animal Susceptibility. *Chem. Res. Toxicol.* 14, 362–370.
- Bowes, J., Brown, A.J., Hamon, J., Jarolimek, W., Sridhar, A., Waldron, G., Whitebread, S., 2012. Reducing safety-related drug attrition: The use of in vitro pharmacological profiling. *Nat. Rev. Drug Discov.* 11, 909–922.
- Brander, C., Mauri-hellweg, D., Bettens, F., Rolli, H., Coldman, M., Pichler, W.J., 1995. Heterogeneous T Cell Responses to P-Lactam-Modified Self- Structures Are Observed in Penicillin-Allergic Individuals '.
- Brandli, A.W., 2004. Prospects for the *Xenopus* embryo model in therapeutics technologies. *Chimia (Aarau).* 58, 694–702.
- Brase, J.C., Wuttig, D., Kuner, R., Sülthmann, H., 2010. Serum microRNAs as non-invasive biomarkers for cancer. *Mol. Cancer* 9, 306.
- Bril, A., Gout, B., Bonhomme, M., Landais, L., Faivre, J., Linee, P., Poyser, R.H., Ruffolo, R.R., 1996. Combined Potassium and Calcium Channel Blocking Activities as a Basis for Antiarrhythmic Efficacy with Low Proarrhythmic Risk : Experimental Profile of BRL-32872. *J. Pharmacol. Exp. Ther.* 276, 637–646.
- Brillant, N., Elmasry, M., Burton, N.C., Rodriguez, J.M., Sharkey, J.W., Fenwick, S., Poptani, H., Kitteringham, N.R., Goldring, C.E., Kipar, A., Park, B.K., Antoine, D.J., 2017. Dynamic and accurate assessment of acetaminophen-induced hepatotoxicity by integrated photoacoustic imaging and mechanistic biomarkers in vivo. *Toxicol. Appl. Pharmacol.* 332, 64–74.
- Brink, A., Pähler, A., Funk, C., Schuler, F., Schadt, S., 2017. Minimizing the risk of chemically reactive metabolite formation of new drug candidates: implications for preclinical drug design. *Drug Discov. Today* 22, 751–756.
- Bristow, M.R., Billingham, M.E., Mason, J.W., Daniels, J.R., 1978. Clinical spectrum of anthracycline antibiotic cardiotoxicity. *Cancer Treat. Rep.* 62, 873–879.
- Busch, A.E., Suessbrich, H., Waldegger, S., Sailer, E., Greger, R., Lang, H., Lang, F., Gibson, K.J., Maylie, J.G., 1996. Inhibition of IKs in guinea pig cardiac myocytes and guinea pig IsK channels by the chromanol 293B. *Pflugers Arch. Eur. J. Physiol.* 432, 1094–1096.
- Bushel, P.R., Heinloth, A.N., Li, J., Huang, L., Chou, J.W., Boorman, G.A., Malarkey, D.E., Houle, C.D., Ward, S.M., Wilson, R.E., Fannin, R.D., Russo, M.W., Watkins, P.B., Tennant, R.W., Paules, R.S., 2007. Blood gene expression signatures predict exposure levels. *Proc. Natl. Acad. Sci.* 104, 18211–18216.

- Capranico, G., Tinelli, S., Austin, C.A., Fisher, M.L., Zunino, F., 1992. Different patterns of gene expression of topoisomerase II isoforms in differentiated tissues during murine development. *Gene Struct. Expr.* 1132, 43–48.
- Cardinale, D., Sandri, M.T., Colombo, A., Colombo, N., Boeri, M., Lamantia, G., Civelli, M., Peccatori, F., Martinelli, G., Fiorentini, C., Cipolla, C.M., 2004. Prognostic value of troponin I in cardiac risk stratification of cancer patients undergoing high-dose chemotherapy. *Circulation* 109, 2749–2754.
- Carr, R.E., Henkind, P., Rothfield, N., Siegel, I.M., 1968. OCULAR TOXICITY OF ANTIMALARIAL DRUGS - LONG-TERM FOLLOW-UP. *Am. J. Ophthalmol.* 66, 738+.
- Carvalho, F.S., Burgeiro, A., Garcia, R., Moreno, A.J., Carvalho, R.A., Oliveira, P.J., 2013. Doxorubicin-Induced Cardiotoxicity: From Bioenergetic Failure and Cell Death to Cardiomyopathy. *Med. Res. Rev.* 34, 106–135.
- Cavero, I., Holzgrefe, H., 2014. Comprehensive in vitro Proarrhythmia Assay, a novel in vitro/in silico paradigm to detect ventricular proarrhythmic liability: a visionary 21st century initiative. *Expert Opin. Drug Saf.* 13, 745–758.
- Chalmers, A.D., Slack, J.M., 2000. The *Xenopus* tadpole gut: fate maps and morphogenetic movements. *Development* 127, 381–392.
- Chang, C., Wu, S.L., Zhao, X.D., Zhao, C.T., Li, Y.H., 2014. Developmental toxicity of doxorubicin hydrochloride in embryo-larval stages of zebrafish. *Biomed. Mater. Eng.* 24, 909–916.
- Chang, T.T., Hughes-Fulford, M., 2008. Monolayer and spheroid culture of human liver hepatocellular carcinoma cell line cells demonstrate distinct global gene expression patterns and functional phenotypes. *Tissue Eng. Part A* 15, 559–567.
- Chatterjee, K., Zhang, J., Honbo, N., Karliner, J.S., 2010. Doxorubicin cardiomyopathy. *Cardiology* 115, 155–162.
- Chaudhary, K.W., O'Neal, J.M., Mo, Z.L., Fermini, B., Gallavan, R.H., Bahinski, A., 2006. Evaluation of the Rubidium Efflux Assay for Preclinical Identification of hERG Blockade. *Assay Drug Dev. Technol.* 4, 73–82.
- Chauret, N., Gauthier, A., Nicoll-Griffith, D.A., 1998. Effect of common organic solvents on in vitro cytochrome P450-mediated metabolic activities in human liver microsomes. *Drug Metab. Dispos.* 26, 1–4.
- Chen, C., Hennig, G.E., Manautou, J.E., 2003. Hepatobiliary excretion of acetaminophen glutathione conjugate and its derivatives in transport-deficient (TR-) hyperbilirubinemic rats. *Drug Metab. Dispos.* 31, 798–804.
- Chen, J., Jacox, L.A., Saldanha, F., Sive, H., 2017. Mouth development. *Wiley Interdiscip. Rev. Dev. Biol.* 6, 1–16.

- Chen, M., Borlak, J., Tong, W., 2013. High lipophilicity and high daily dose of oral medications are associated with significant risk for drug-induced liver injury. *Hepatology* 58, 388–396.
- Cheng, C.S., Alderman, D., Kwash, J., Dessaint, J., Patel, R., Lescoe, M.K., Kinrade, M.B., Yu, W., 2002. A High-Throughput HERG Potassium Channel Function Assay: An Old Assay with a New Look. *Drug Dev. Ind. Pharm.* 28, 177–191.
- Chiu, P.J.S., Marcoe, K.F., Bounds, S.E., Lin, C.-H., Feng, J.-J., Lin, A., Cheng, F.-C., Crumb, W.J., Mitchell, R., 2004. Validation of a [³H]astemizole binding assay in HEK293 cells expressing HERG K⁺ channels. *J. Pharmacol. Sci.* 95, 311–319.
- Chng, H.T., Ho, H.K., Yap, C.W., Lam, S.H., Chan, E.C.Y., 2012. An investigation of the bioactivation potential and metabolism profile of zebrafish versus human. *J. Biomol. Screen.* 17, 974–986.
- Chorghade, M.S., 2006. *Drug discovery and development*. Hoboken, N.J.: Wiley-Interscience, c2006-2007.
- Christensen, E.I., Raciti, D., Reggiani, L., Verroust, P.J., Brändli, A.W., 2008. Gene expression analysis defines the proximal tubule as the compartment for endocytic receptor-mediated uptake in the *Xenopus* pronephric kidney. *Pflugers Arch. Eur. J. Physiol.* 456, 1163–1176.
- Chugun, A., Temma, K., Oyamada, T., Suzuki, N., Kamiya, Y., Hara, Y., Sasaki, T., Kondo, H., Akera, T., 2000. Doxorubicin-induced late cardiotoxicity: delayed impairment of Ca²⁺-handling mechanisms in the sarcoplasmic reticulum in the rat. *Can. J. Physiol. Pharmacol.* 78, 329–338.
- Clark, R.A., Chong, B., Mirchandani, N., Brinster, N.K., Yamanaka, K. -i., Dowgiert, R.K., Kupper, T.S., 2006. The Vast Majority of CLA⁺ T Cells Are Resident in Normal Skin. *J. Immunol.* 176, 4431–4439.
- Clements, M., 2016. Multielectrode Array (MEA) Assay for Profiling Electrophysiological Drug Effects in Human Stem Cell-Derived Cardiomyocytes. *Curr. Protoc. Toxicol.* 4, 1–22.
- Colatsky, T., Fermini, B., Gintant, G., Pierson, J.B., Sager, P., Sekino, Y., Strauss, D.G., Stockbridge, N., 2016. The Comprehensive in Vitro Proarrhythmia Assay (CiPA) initiative — Update on progress. *J. Pharmacol. Toxicol. Methods* 81, 15–20.
- Cooper, D.S., Kaplan, M.M., Ridgway, E.C., Maloof, F., Daniels, G.H., 1979. Alkaline phosphatase isoenzyme patterns in hyperthyroidism. *Ann. Intern. Med.* 90, 164–168.
- Corsini, A., Ganey, P., Ju, C., Kaplowitz, N., Pessayre, D., Roth, R., Watkins, P., Albassam, M., Liu, B., Stancic, S., Suter, L., Bortolini, M., 2012. Current Challenges and Controversies in Drug-Induced Liver Injury. *Drug Saf.* 35, 1099–1117.
- Court, M.H., Duan, S.X., von Moltke, L.L., Greenblatt, D.J., Patten, C.J., Miners, J.O.,

- Mackenzie, P.I., 2001. Interindividual variability in acetaminophen glucuronidation by human liver microsomes: identification of relevant acetaminophen UDP-glucuronosyltransferase isoforms. *J. Pharmacol. Exp. Ther.* 299, 998–1006.
- Cross, M.J., Berridge, B.R., Clements, P.J.M., Cove-Smith, L., Force, T.L., Hoffmann, P., Holbrook, M., Lyon, A.R., Mellor, H.R., Norris, A.A., Pirmohamed, M., Tugwood, J.D., Sidaway, J.E., Park, B.K., 2015. Physiological, pharmacological and toxicological considerations of drug-induced structural cardiac injury. *Br. J. Pharmacol.* 172, 957–974.
- Crumb Jr., W.J., Wible, B., Arnold, D.J., Payne, J.P., Brown, A.M., 1995. Blockade of multiple human cardiac potassium currents by the antihistamine terfenadine: possible mechanism for terfenadine-associated cardiotoxicity. *Mol Pharmacol* 47, 181–190.
- Cummings, J., Ranson, M., Lacasse, E., Ganganagari, J.R., St-Jean, M., Jayson, G., Durkin, J., Dive, C., 2006. Method validation and preliminary qualification of pharmacodynamic biomarkers employed to evaluate the clinical efficacy of an antisense compound (AEG35156) targeted to the X-linked inhibitor of apoptosis protein XIAP. *Br. J. Cancer* 95, 42–48.
- Dagil, R., O’Shea, C., Nykjaer, A., Bonvin, A.M.J.J., Kragelund, B.B., 2013. Gentamicin binds to the megalin receptor as a competitive inhibitor using the common ligand binding motif of complement type repeats insight from the nmr structure of the wth complement type repeat domain alone and in complex with gentamicin. *J. Biol. Chem.* 288, 4424–4435.
- Dargan, P.I., Ladhani, S., Jones, A.L., 2001. Measuring plasma paracetamol concentrations in all patients with drug overdose or altered consciousness: does it change outcome? *Emerg. Med. J.* 18, 178–82.
- Dart, R.C., Erdman, A.R., Olson, K., Christianson, G., Manoguerra, A.S., Chyka, P.A., Caravati, E.M., Wax, P.M., Keyes, D.C., Woolf, A.D., Scharman, E.J., Booze, L.L., Troutman, W.G., 2006. Acetaminophen poisoning: an evidence-based consensus guideline for out-of-hospital management. *Clin. Toxicol.* 44, 1–18.
- Davis, D.C., Potter, W.Z., Jollow, D.J., Mitchell, J.R., 1974. Species differences in hepatic glutathione depletion, covalent binding and hepatic necrosis after acetaminophen. *Life Sci.* 14, 2099–2109.
- De Luca, E., Zaccaria, G.M., Hadhoud, M., Rizzo, G., Ponzini, R., Morbiducci, U., Santoro, M.M., 2014. ZebraBeat : A flexible platform for the analysis of the cardiac rate in zebrafish embryos. *Sci. Rep.* 4, 1–13.
- De Ponti, F., Poluzzi, E., Montanaro, N., 2001. Organising evidence on QT prolongation and occurrence of Torsades de Pointes with non-antiarrhythmic drugs: A call for consensus. *Eur. J. Clin. Pharmacol.* 57, 185–209.

- De Rosa, S., Curcio, A., Indolfi, C., 2014. Emerging Role of MicroRNAs in Cardiovascular Diseases. *Circ. J.* 78, 567–575.
- Dessertenne, F., 1966. [Ventricular tachycardia with 2 variable opposing foci]. *Arch. des Maladies du Coeur des Vaiss.* 59, 263–272.
- Dhillon, S.S., Dórá, É., Magyary, I., Egginton, S., Sík, A., Müller, F., 2013. Optimisation of Embryonic and Larval ECG Measurement in Zebrafish for Quantifying the Effect of QT Prolonging Drugs. *PLoS One* 8.
- Di Veroli, G.Y., Davies, M.R., Zhang, H., Abi-Gerges, N., Boyett, M.R., 2014. HERG inhibitors with similar potency but different binding kinetics do not pose the same proarrhythmic risk: Implications for drug safety assessment. *J. Cardiovasc. Electrophysiol.* 25, 197–207.
- Donato, M.T., Montero, S., Castell, J. V., Gómez-Lechón, M.J., Lahoz, A., 2010. Validated assay for studying activity profiles of human liver UGTs after drug exposure: Inhibition and induction studies. *Anal. Bioanal. Chem.* 396, 2251–2263.
- Dong, H., Haining, R.L., Thummel, K.E., Rettie, A.E., Nelson, S.D., 2000. Involvement of Human Cytochrome P450 2D6 in the Bioactivation of Acetaminophen 28, 1397–1400.
- Doroshov, J.H., 1983. Anthracycline Antibiotic-stimulated Superoxide, Hydrogen Peroxide, and Hydroxyl Radical Production by NADH Dehydrogenase. *Cancer Res.* 43, 4543–4551.
- Doroshov, J.H., Locker, G.Y., Myers, C.E., 1980. Enzymatic Defenses of the Mouse Heart Against Reactive Oxygen Metabolites. *J. Clin. Invest.* 65, 128–135.
- Dorr, R.T., Shipp, N.G., Lee, K.M., 1991. Comparison of cytotoxicity in heart cells and tumor cells exposed to DNA intercalating agents in vitro. *Anticancer. Drugs* 2, 27–33.
- Dragovic, S., Vermeulen, N.P.E., Gerets, H.H., Hewitt, P.G., Ingelman-Sundberg, M., Park, B.K., Juhila, S., Snoeys, J., Weaver, R.J., 2016. Evidence-based selection of training compounds for use in the mechanism-based integrated prediction of drug-induced liver injury in man. *Arch. Toxicol.* 90, 2979–3003.
- Drake, R.L., Vogl, W., Mitchell, A.W.M., 2012. Liver. In: *Gray's Basic Anatomy*. Philadelphia, PA : Elsevier Churchill Livingstone, c2012., pp. 164–168.
- Dykens, J.A., Will, Y., 2007. The significance of mitochondrial toxicity testing in drug development. *Drug Discov. Today* 12, 777–785.
- Eakins, R., Walsh, J., Randle, L., Jenkins, R.E., Schuppe-Koistinen, I., Rowe, C., Starkey Lewis, P., Vasieva, O., Prats, N., Brillant, N., Auli, M., Bayliss, M., Webb, S., Rees, J.A., Kitteringham, N.R., Goldring, C.E., Park, B.K., 2015. Adaptation to acetaminophen exposure elicits major changes in expression and distribution of the hepatic proteome. *Sci. Rep.* 5, 1–13.

- Edwards, I.R., Aronson, J.K., 2000. Adverse drug reactions: definitions, diagnosis, and management. *Lancet* (London, England) 356, 1255–9.
- Eichelbaum, M., Evert, B., 1996. Influence of pharmacogenetics on drug disposition and response. *Clin. Exp. Pharmacol. Physiol.* 23, 983–985.
- Fearnley, C.J., Roderick, H.L., Bootman, M.D., 2011. Calcium signaling in cardiac myocytes.
- Feng, W.Y., 2004. Mass Spectrometry in Drug Discovery: A Current Review. *Curr. Drug Discov. Technol.* 1, 295–312.
- Fourmy, D., Recht, M., Blanchard, S.C., Puglisi, J.D., 1996. Structure of the A Site of *Escherichia coli* 16S Ribosomal RNA Complexed with an Aminoglycoside Antibiotic. *Science* (80-.). 274.
- Fowler, W.M.J., Chowdhury, S.R., Pearson, C.M., Gardner, G., Bratton, R., 1962. Changes in serum enzyme levels after exercise in trained and untrained subjects. *J. Appl. Physiol.* 17, 943–946.
- Friedrich, J., Seidel, C., Ebner, R., Kunz-Schughart, L.A., 2009. Spheroid-based drug screen: considerations and practical approach. *Nat. Protoc.* 4, 309–324.
- Funk, C., Pantze, M., Jehle, L., Ponelle, C., Scheuermann, G., Lazendic, M., Gasser, R., 2001. Troglitazone-induced intrahepatic cholestasis by an interference with the hepatobiliary export of bile acids in male and female rats. Correlation with the gender difference in troglitazone sulfate formation and the inhibition of the canalicular bile salt. *Toxicology* 167, 83–98.
- Funk, C., Roth, A., 2017. Current limitations and future opportunities for prediction of DILI from in vitro. *Arch. Toxicol.* 91, 131–142.
- Galloway, S.M., Aardema, M.J., Ishidate, M., Ivett, J.L., Kirkland, D.J., Morita, T., Mosesso, P., Sofuni, T., 1994. Report from working group on in vitro tests for chromosomal aberrations. *Mutat. Res.* 312, 241–261.
- Geenen, S., Du Preez, F.B., Snoep, J.L., Foster, A.J., Sarda, S., Kenna, J.G., Wilson, I.D., Westerhoff, H. V., 2013. Glutathione metabolism modeling: A mechanism for liver drug-robustness and a new biomarker strategy. *Biochim. Biophys. Acta - Gen. Subj.* 1830, 4943–4959.
- Ghanem, C.I., Gómez, P.C., Arana, M.C., Perassolo, M., Ruiz, M.L., Villanueva, S.S.M., Ochoa, E.J., Catania, V.A., Bengochea, L.A., Mottino, A.D., 2004. Effect of acetaminophen on expression and activity of rat liver multidrug resistance-associated protein 2 and P-glycoprotein. *Biochem. Pharmacol.* 68, 791–798.
- Ghanem, C.I., Ruiz, M.L., Villanueva, S.S.M., Luquita, M., Llesuy, S., Catania, V.A., Bengochea, L.A., Mottino, A.D., 2009. Effect of repeated administration with subtoxic doses of acetaminophen to rats on enterohepatic recirculation of a subsequent toxic

- dose. *Biochem. Pharmacol.* 77, 1621–1628.
- Giboney, P.T., 2005. Mildly elevated liver transaminase levels in the asymptomatic patient. *Am. Fam. Physician* 71, 1105–1110.
- Gintant, G.A., Limberis, J.T., McDermott, J.S., Wegner, C.D., Cox, B.F., 2001. The canine Purkinje fiber: An in vitro model system for acquired long QT syndrome and drug-induced arrhythmogenesis. *J. Cardiovasc. Pharmacol.* 37, 607–618.
- Gintant, G., Sager, P.T., Stockbridge, N., 2016. Evolution of strategies to improve preclinical cardiac safety testing. *Nat. Rev. Drug Discov.* 15, 457–471.
- Glineur, S.F., De Ron, P., Hanon, E., Valentin, J.P., Dremier, S., da Costa, A.N., 2016. Paving the route to plasma miR-208a-3p as an acute cardiac injury biomarker: Preclinical rat data supports its use in drug safety assessment. *Toxicol. Sci.* 149, 89–97.
- Godoy, P., Hewitt, N.J., Albrecht, U., Andersen, M.E., Ansari, N., Bhattacharya, S., Bode, J.G., Bolleyn, J., Borner, C., Böttger, J., Braeuning, A., Budinsky, R.A., Burkhardt, B., Cameron, N.R., Camussi, G., Cho, C.S., Choi, Y.J., Craig Rowlands, J., Dahmen, U., Damm, G., Dirsch, O., Donato, M.T., Dong, J., Dooley, S., Drasdo, D., Eakins, R., Ferreira, K.S., Fonsato, V., Fraczek, J., Gebhardt, R., Gibson, A., Glanemann, M., Goldring, C.E.P., Gómez-Lechón, M.J., Groothuis, G.M.M., Gustavsson, L., Guyot, C., Halifax, D., Hammad, S., Hayward, A., Häussinger, D., Hellerbrand, C., Hewitt, P., Hoehme, S., Holzhütter, H.G., Houston, J.B., Hrach, J., Ito, K., Jaeschke, H., Keitel, V., Kelm, J.M., Kevin Park, B., Kordes, C., Kullak-Ublick, G.A., Lecluyse, E.L., Lu, P., Luebke-Wheeler, J., Lutz, A., Maltman, D.J., Matz-Soja, M., McMullen, P., Merfort, I., Messner, S., Meyer, C., Mwinyi, J., Naisbitt, D.J., Nussler, A.K., Olinga, P., Pampaloni, F., Pi, J., Pluta, L., Przyborski, S.A., Ramachandran, A., Rogiers, V., Rowe, C., Schelcher, C., Schmich, K., Schwarz, M., Singh, B., Stelzer, E.H.K., Stieger, B., Stöber, R., Sugiyama, Y., Tetta, C., Thasler, W.E., Vanhaecke, T., Vinken, M., Weiss, T.S., Widera, A., Woods, C.G., Xu, J.J., Yarborough, K.M., Hengstler, J.G., 2013. Recent advances in 2D and 3D in vitro systems using primary hepatocytes, alternative hepatocyte sources and non-parenchymal liver cells and their use in investigating mechanisms of hepatotoxicity, cell signaling and ADME, *Archives of Toxicology*.
- Goldring, C.E.P., Kitteringham, N.R., Elsby, R., Randle, L.E., Clement, Y.N., Williams, D.P., McMahon, M., Hayes, J.D., Itoh, K., Yamamoto, M., Park, B.K., 2004. Activation of Hepatic Nrf2 in Vivo by Acetaminophen in CD-1 Mice. *Hepatology* 39, 1267–1276.
- Goldstein, R.S., Mayor, G.H., 1983. Minireview. The nephrotoxicity of cisplatin. *Life Sci.* 32, 685–690.

- Gomes, E.R., Demoly, P., 2005. Epidemiology of hypersensitivity drug reactions. *Curr. Opin. Allergy Clin. Immunol.* 5, 309–316.
- Gomez-Lechon, M.J., Castell, J. V., Donato, M.T., 2010. The Use of Hepatocytes to Investigate Drug Toxicity, *Hepatocytes*. Humana Press.
- Gomez-Lechon, M.J., Donato, M.T., Castell, J. V., Jover, R., 2003. Human Hepatocytes as a Tool for Studying Toxicity and Drug Metabolism. *Curr. Drug Metab.* 4, 292–312.
- Gómez-Lechón, M.J., Ponsoda, X., O'Connor, E., Donato, T., Jover, R., Castell, J. V., 2003. Diclofenac induces apoptosis in hepatocytes. *Toxicol. Vitro.* 17, 675–680.
- Grillo, M.P., Knutson, C.G., Sanders, P.E., Waldon, D.J., Hua, F., Ware, J.A., 2003. Studies on the chemical reactivity of diclofenac acyl glucuronide with glutathione: Identification of diclofenac-S-acyl-glutathione in rat bile. *Drug Metab. Dispos.* 31, 1327–1336.
- Gu, G., Na, Y., Chung, H., Seok, S.H., Lee, H.Y., 2017. Zebrafish larvae model of dilated cardiomyopathy induced by terfenadine. *Korean Circ. J.* 47, 960–969.
- Gu, J., Hu, W., Zhang, D.D., 2015. Resveratrol, a polyphenol phytoalexin, protects against doxorubicin-induced cardiotoxicity. *J. Cell. Mol. Med.* 19, 2324–2328.
- Gu, X., Manautou, J.E., 2010. Regulation of hepatic ABC transporters by xenobiotics and in disease states. *Drug Metab. Rev.* 42, 482–538.
- Guengerich, F.P., 2005. Generation of reactive intermediates. *J. Biochem. Mol. Toxicol.* 19, 173–174.
- Gyselynck, A.M., Forrey, A., Cutler, R., 1971. Pharmacokinetics of gentamicin: distribution and plasma and renal clearance. *J. Infect. Dis.* 124, S70–S76.
- Hadi, M., Dragovic, S., Van Swelm, R., Herpers, B., Van De Water, B., Russel, F.G.M., Commandeur, J.N.M., Groothuis, G.M.M., 2013. AMAP, the alleged non-toxic isomer of acetaminophen, is toxic in rat and human liver. *Arch. Toxicol.* 87, 155–165.
- Hamdam, J., Sethu, S., Smith, T., Alfirevic, A., Alhaidari, M., Atkinson, J., Ayala, M., Box, H., Cross, M., Delaunois, A., Dermody, A., Govindappa, K., Guillon, J.M., Jenkins, R., Kenna, G., Lemmer, B., Meecham, K., Olayanju, A., Pestel, S., Rothfuss, A., Sidaway, J., Sison-Young, R., Smith, E., Stebbings, R., Tingle, Y., Valentin, J.P., Williams, A., Williams, D.P., Park, K., Goldring, C., 2013. Safety pharmacology - Current and emerging concepts. *Toxicol. Appl. Pharmacol.* 273, 229–241.
- Harrill, A.H., Roach, J., Fier, I., Eaddy, J.S., Kurtz, C.L., Antoine, D.J., Spencer, D.M., Kishimoto, T.K., Pisetsky, D.S., Park, B.K., Watkins, P.B., 2012. The effects of heparins on the liver: Application of mechanistic serum biomarkers in a randomized study in healthy volunteers. *Clin. Pharmacol. Ther.* 92, 214–220.
- Hartmann, J.T., Lipp, H.-P., 2003. Toxicity of platinum compounds. *Expert Opin. Pharmacother.* 4, 889–901.

- Hasinoff, B.B., Herman, E.H., 2007. Dexrazoxane: How it works in cardiac and tumor cells. Is it a prodrug or is it a drug? *Cardiovasc. Toxicol.* 7, 140–144.
- Hassel, D., Scholz, E.P., Trano, N., Friedrich, O., Just, S., Meder, B., Weiss, D.L., Zitron, E., Marquart, S., Vogel, B., Karle, C.A., Seemann, G., Fishman, M.C., Katus, H.A., Rottbauer, W., 2008. Deficient zebrafish ether-à-go-go-related gene channel gating causes short-QT syndrome in zebrafish reggae mutants. *Circulation* 117, 866–875.
- Hawton, K., Bergen, H., Simkin, S., Dodd, S., Pocock, P., Bernal, W., Gunnell, D., Kapur, N., 2013. Long term effect of reduced pack sizes of paracetamol on poisoning deaths and liver transplant activity in England and Wales: Interrupted time series analyses. *BMJ* 346, 1–9.
- He, J.H., Guo, S.Y., Zhu, F., Zhu, J.J., Chen, Y.X., Huang, C.J., Gao, J.M., Dong, Q.X., Xuan, Y.X., Li, C.Q., 2013. A zebrafish phenotypic assay for assessing drug-induced hepatotoxicity. *J. Pharmacol. Toxicol. Methods* 67, 25–32.
- Heard, K.J., Green, J.L., James, L.P., Judge, B.S., Zolot, L., Rhyee, S., Dart, R.C., 2011. Acetaminophen-cysteine adducts during therapeutic dosing and following overdose. *BMC Gastroenterol.* 11.
- Hempel, A., Kühn, M., 2016. A Matter of the Heart: The African Clawed Frog *Xenopus* as a Model for Studying Vertebrate Cardiogenesis and Congenital Heart Defects. *J. Cardiovasc. Dev. Dis.* 3, 21.
- Herman, E.H., El-Hage, A.N., Ferrans, V.J., Ardan, B., 1985. Comparison of the severity of the chronic cardiotoxicity produced by doxorubicin in normotensive and hypertensive rats. *Toxicol. Appl. Pharmacol.* 78, 202–214.
- Heywood, R., 1990. Clinical Toxicity – Could it have been predicted? Post-marketing experience. In: *Animal Toxicity Studies: Their Relevance for Man*. pp. 57–67.
- Hinz, B., Cheremina, O., Brune, K., 2007. Acetaminophen (paracetamol) is a selective cyclooxygenase-2 inhibitor in man. *FASEB J.* 22, 383–390.
- Hollenberg, P.F., Kent, U.M., Bumpus, N.N., 2008. Mechanism-based inactivation of human cytochromes P450s: Experimental characterization, reactive intermediates, and clinical implications. *Chem. Res. Toxicol.* 21, 189–205.
- Holmgren, G., Synnergren, J., Bogestål, Y., Améen, C., Åkesson, K., Holmgren, S., Lindahl, A., Sartipy, P., 2015. Identification of novel biomarkers for doxorubicin-induced toxicity in human cardiomyocytes derived from pluripotent stem cells. *Toxicology* 328, 102–111.
- Hortobagyi, G.N., 1997. Anthracyclines in the treatment of cancer. An overview. *Drugs* 54, 1–7.
- Hove-Madsen, L., Llach, A., Molina, C.E., Prat-Vidal, C., Farré, J., Roura, S., Cinca, J., 2006. The proarrhythmic antihistaminic drug terfenadine increases spontaneous

- calcium release in human atrial myocytes. *Eur. J. Pharmacol.* 553, 215–221.
- Howell, B.A., Siler, S.Q., Watkins, P.B., 2014. Use of a systems model of drug-induced liver injury (DILIsym®) to elucidate the mechanistic differences between acetaminophen and its less-toxic isomer, AMAP, in mice. *Toxicol. Lett.* 226, 163–172.
- Hsiao, Y.W., Petersson, C., Svensson, M.A., Norinder, U., 2012. A pragmatic approach using first-principle methods to address site of metabolism with implications for reactive metabolite formation. *J. Chem. Inf. Model.* 52, 686–695.
- Hu, Y., Benedict, M. a, Ding, L., Nu, G., 1999. Role of cytochrome c and dATP / ATP hydrolysis in Apaf-1-mediated caspase-9 activation and apoptosis. *EMBO J.* 18, 3586–3595.
- Huang, C.-C., Monte, A., Cook, J.M., Kabir, M.S., Peterson, K.P., 2013. Zebrafish Heart Failure Models for the Evaluation of Chemical Probes and Drugs. *Assay Drug Dev. Technol.* 11, 561–572.
- Hunt, C.M., Westerkam, W.R., Stave, G.M., 1992. Effect of age and gender on the activity of human hepatic CYP3A. *Biochem. Pharmacol.* 44, 275–83.
- Hunziker, T., Künzi, U.P., Braunschweig, S., Zehnder, D., Hoigné, R., 1997. Comprehensive hospital drug monitoring (CHDM): Adverse skin reactions, a 20-year survey. *Allergy Eur. J. Allergy Clin. Immunol.* 52, 388–393.
- Hutchin, T., Cortopassi, G., 1994. Proposed molecular and cellular mechanism for aminoglycoside ototoxicity. *Antimicrob. Agents Chemother.* 38, 2517–2520.
- ICH (International Conference, 2009. ICH M3(R2) - Guidance on non-clinical safety studies for the conduct of human clinical trials and marketing authorization for pharmaceuticals [WWW Document]. Int. Conf. Harmon. URL http://www.ich.org/fileadmin/Public_Web_Site/ICH_Products/Guidelines/Multidisciplinary/M3_R2/Step4/M3_R2__Guideline.pdf
- ICH (International Conference on Harmonization), 2005. ICH Topic S 7 B The nonclinical Evaluation of the Potential for delayed Ventricular Repolarization (QT Interval Prolongation) by Human Pharmaceuticals [WWW Document]. Int. Conf. Harmon. URL http://www.ema.europa.eu/docs/en_GB/document_library/Scientific_guideline/2009/09/WC500002841.pdf
- ICH (International Conference on Harmonization), 2014. ICH Topic S7A: Safety pharmacology studies for human pharmaceuticals. [WWW Document]. Int. Conf. Harmon. URL http://www.ema.europa.eu/docs/en_GB/document_library/Scientific_guideline/2009/09/WC500002831.pdf

- Ichikawa, Y., Ghanefar, M., Bayeva, M., Wu, R., Khechaduri, A., Naga Prasad, S. V., Mutharasan, R.K., Jairaj Naik, T., Ardehali, H., 2014. Cardiotoxicity of doxorubicin is mediated through mitochondrial iron accumulation. *J. Clin. Invest.* 124, 617–630.
- Illing, P.T., Vivian, J.P., Dudek, N.L., Kostenko, L., Chen, Z., Bharadwaj, M., Miles, J.J., Kjer-Nielsen, L., Gras, S., Williamson, N.A., Burrows, S.R., Purcell, A.W., Rossjohn, J., McCluskey, J., 2012. Immune self-reactivity triggered by drug-modified HLA-peptide repertoire. *Nature* 486, 554–558.
- Imamura, H., Sano, K., Sugawara, Y., Kokudo, N., Makuuchi, M., 2005. Assessment of hepatic reserve for indication of hepatic resection: Decision tree incorporating indocyanine green test. *J. Hepatobiliary. Pancreat. Surg.* 12, 16–22.
- Isogai, S., Horiguchi, M., Weinstein, B.M., 2001. The vascular anatomy of the developing zebrafish: An atlas of embryonic and early larval development. *Dev. Biol.* 230, 278–301.
- Jaeschke, H., Gores, G.J., Cederbaum, A.I., Hinson, J.A., Pessayre, D., Lemasters, J.J., 2002. Mechanisms of hepatotoxicity. *Toxicol. Sci.* 65, 166–176.
- Jaeschke, H., McGill, M.R., Ramachandran, A., 2012. Oxidant stress, mitochondria, and cell death mechanisms in drug-induced liver injury: lessons learned from acetaminophen hepatotoxicity. *Drug Metab. Rev.* 44, 88–106.
- Jang, K.-J., Mehr, A.P., Hamilton, G.A., McPartlin, L.A., Chung, S., Suh, K.-Y., Ingber, D.E., 2013. Human kidney proximal tubule-on-a-chip for drug transport and nephrotoxicity assessment. *Integr. Biol.* 5, 1119.
- Ji, X., Takahashi, R., Hiura, Y., Hirokawa, G., Fukushima, Y., Iwai, N., 2009. Plasma miR-208 as a biomarker of myocardial injury. *Clin. Chem.* 55, 1944–1949.
- Jonsson, J.R., Edwards-smith, C.J., Catania, S.C., Morotomi, Y., Hogan, P.G., Clouston, A.D., Bansa, A.S., Lynch, S. V., Strongly, R.W., Powell, E.E., 2000. Expression of cytokines and factors modulating apoptosis by human sinusoidal leucocytes. *J. Hepatol.* 32, 392–398.
- Jost, N., Papp, J.G., Varró, A., 2007. Slow Delayed Rectifier Potassium Current (I_{Ks}) and the Repolarization Reserve. *Ann. Noninvasive Electrocardiol.* 12, 64–78.
- Kälin, R.E., Bänziger-Tobler, N.E., Detmar, M., Brändli, A.W., 2009. An in vivo chemical library screen in *Xenopus* tadpoles reveals novel pathways involved in angiogenesis and lymphangiogenesis. *Blood* 114, 1110–1122.
- Kelm, J.M., Timmins, N.E., Brown, C.J., Fussenegger, M., Nielsen, L.K., 2003. Method for generation of homogeneous multicellular tumor spheroids applicable to a wide variety of cell types. *Biotechnol. Bioeng.* 83, 173–180.
- Kienhuis, A.S., Van de Poll, M.C.G., Wortelboer, H., Van Herwijnen, M., Gottschalk, R., Dejong, C.H.C., Boorsma, A., Paules, R.S., Kleinjans, J.C.S., Stierum, R.H., Van

- Delft, J.H.M., 2009. Parallelogram approach using rat-human In vitro and rat in vivo toxicogenomics predicts acetaminophen-induced hepatotoxicity in humans. *Toxicol. Sci.* 107, 544–552.
- King, E.J., 1953. Plasma Alkaline Phosphatase in Disease. *Br. Med. Bull.* 9, 160–164.
- Kirpnick, Z., Homiski, M., Rubitski, E., Repnevskaya, M., Howlett, N., Aubrecht, J., Schiestl, R.H., 2005. Yeast DEL assay detects clastogens. *Mutat. Res. - Genet. Toxicol. Environ. Mutagen.* 582, 116–134.
- Klaassen, C.D., Aleksunes, L.M., 2014. Xenobiotic , Bile Acid , and Cholesterol Transporters : *Pharmacol. Rev.* 62, 1–96.
- Knapp, A.C., Todesco, L., Beier, K., Terracciano, L., Sagesser, H., Reichen, J., Krahenbuhl, S., 2008. Toxicity of valproic acid in mice with decreased plasma and tissue carnitine stores. *J Pharmacol Exp Ther* 324, 568–575.
- Köck, K., Ferslew, B.C., Netterberg, I., Yang, K., Urban, T.J., Swaan, P.W., Stewart, P.W., Brouwer, K.L.R., 2014. Risk factors for development of cholestatic drug-induced liver injury: Inhibition of hepatic basolateral bile acid transporters multidrug resistance-associated proteins 3 and 4. *Drug Metab. Dispos.* 42, 665–674.
- Kodama, I., Kamiya, K., Toyama, J., 1997. Cellular electropharmacology of amiodarone. *Cardiovasc. Res.* 35, 13–29.
- Kon, K., Kim, J.-S., Jaeschke, H., Lemasters, J.J., 2004. Mitochondrial permeability transition in acetaminophen-induced necrosis and apoptosis of cultured mouse hepatocytes. *Hepatology* 40, 1170–1179.
- Kool, M., Haa, M. De, Scheffer, G.L., Scheper, R.J., Eijk, M.J.T. Van, Juijn, J. a, 1997. Analysis of expression of cMOAT (MRP2), MRP3, MRP4, and MRP5, homologues of the multidrug resistance-associated protein gene (MRP1), in human cancer cell lines. 3537–3547.
- Kostrubsky, V.E., Strom, S.C., Hanson, J., Urda, E., Rose, K., Burliegh, J., Zocharski, P., Cai, H., Sinclair, J.F., Sahi, J., 2003. Evaluation of hepatotoxic potential of drugs by inhibition of bile-acid transport in cultured primary human hepatocytes and intact rats. *Toxicol. Sci.* 76, 220–228.
- Kramer, J.A., Sagartz, J.E., Morris, D.L., 2007. The application of discovery toxicology and pathology towards the design of safer pharmaceutical lead candidates. *Nat. Rev. Drug Discov.* 6, 636–649.
- Kramer, J., Obejero-Paz, C.A., Myatt, G., Kuryshev, Y.A., Bruening-Wright, A., Verducci, J.S., Brown, A.M., 2013. MICE models: Superior to the HERG model in predicting torsade de pointes. *Sci. Rep.* 3, 1–7.
- Kretz-Rommel, A., Boelsterli, U.A., 1993. Diclofenac covalent protein binding is dependent on acyl glucuronide formation and is inversely related to P450-mediated acute cell

- injury in cultured rat hepatocytes. *Toxicol. Appl. Pharmacol.*
- Kubes, P., Mehal, W.Z., 2012. Sterile inflammation in the liver. *J. Gastroenterol. Hepatol.* 143, 1158–1172.
- Langheinrich, U., Vacun, G., Wagner, T., 2003. Zebrafish embryos express an orthologue of HERG and are sensitive toward a range of QT-prolonging drugs inducing severe arrhythmia. *Toxicol. Appl. Pharmacol.* 193, 370–382.
- Larrey, D., 2002. Epidemiology and individual susceptibility to adverse drug reactions affecting the liver. *Semin. Liver Dis.* 22, 145–155.
- Larson, A.M., Polson, J., Fontana, R.J., Davern, T.J., Lalani, E., Hynan, L.S., Reisch, J.S., Schiødt, F. V., Ostapowicz, G., Shakil, A.O., Lee, W.M., 2005. Acetaminophen-induced acute liver failure: Results of a United States multicenter, prospective study. *Hepatology* 42, 1364–1372.
- Lauterburg, B.H., Vaishnav, Y., Stillwell, W.G., Mitchell, J.R., 1980. The effects of age and glutathione depletion on hepatic glutathione turnover in vivo determined by acetaminophen probe analysis. *J. Pharmacol. Exp. Ther.* 213, 54 LP-58.
- Lavergne, S.N., Park, B.K., Naisbitt, D.J., 2008. The roles of drug metabolism in the pathogenesis of T-cell-mediated drug hypersensitivity. *Curr. Opin. Allergy Clin. Immunol.* 8, 299–307.
- Lebrecht, D., Kokkori, A., Ketelsen, U.P., Setzer, B., Walker, U.A., 2005. Tissue-specific mtDNA lesions and radical-associated mitochondrial dysfunction in human hearts exposed to doxorubicin. *J. Pathol.* 207, 436–444.
- Lebrecht, D., Setzer, B., Ketelsen, U.P., Haberstroh, J., Walker, U.A., 2003. Time-Dependent and Tissue-Specific Accumulation of mtDNA and Respiratory Chain Defects in Chronic Doxorubicin Cardiomyopathy. *Circulation* 108, 2423–2429.
- LeCluyse, E.L., 2001. Human hepatocyte culture systems for the in vitro evaluation of cytochrome P450 expression and regulation. *Eur. J. Pharm. Sci.* 13, 343–368.
- Lee, W.M., 2003. Drug-Induced Hepatotoxicity 474–485.
- Lee, W.M., 2003. Acute liver failure in the United States. *Semin. Liver Dis.* 23, 217–226.
- Leong, I.U.S., Skinner, J.R., Shelling, A.N., Love, D.R., 2010. Zebrafish as a model for long QT syndrome: The evidence and the means of manipulating zebrafish gene expression. *Acta Physiol.* 199, 257–276.
- Lerche-Langrand, C., Toutain, H.J., 2000. Precision-cut liver slices : characteristics and use for in vitro. *Toxicology* 153, 221–253.
- Levesque, E., Martin, E., Dudau, D., Lim, C., Dhonneur, G., Azoulay, D., 2016. Current use and perspective of indocyanine green clearance in liver diseases. *Anaesth. Crit. Care Pain Med.* 35, 49–57.
- Li, A.P., Kaminski, D.L., Rasmussen, A., 1995. Substrates of human hepatic cytochrome

P450 3A4. *Toxicology* 104, 1–8.

- Li, B., Li, S., Wang, W., Niu, T., Wang, H., Li, B., Shao, L., Lai, Y., Li, H., Janicki, J.S., Wang, X.L., Tang, D., Cui, T., 2014. Nrf2 Deficiency Exaggerates Doxorubicin-Induced Cardiotoxicity and Cardiac Dysfunction Nrf2 Deficiency Exaggerates Doxorubicin-Induced Cardiotoxicity and Cardiac Dysfunction 2014.
- Li, X., Zhang, R., Zhao, B., Lossin, C., Cao, Z., 2016. Cardiotoxicity screening: a review of rapid-throughput in vitro approaches. *Arch. Toxicol.* 90, 1803–1816.
- Liew, C.Y., Pan, C., Tan, A., Ang, K.X.M., Yap, C.W., 2012. QSAR classification of metabolic activation of chemicals into covalently reactive species. *Mol. Divers.* 16, 389–400.
- Lindsay, J., Wang, L., Li, Y., Zhou, S., 2008. Structure, Function and Polymorphism of Human Cytosolic Sulfotransferases. *Curr. Drug Metab.* 9, 99–105.
- Lione, A., Scialli, A.R., 1995. The developmental toxicity of indomethacin and sulindac. *Reprod. Toxicol.* 9, 7–20.
- Lipshultz, S.E., Miller, T.L., Scully, R.E., Lipsitz, S.R., Rifai, N., Silverman, L.B., Colan, S.D., Neuberg, D.S., Dahlberg, S.E., Henkel, J.M., Asselin, B.L., Athale, U.H., Clavell, L.A., Laverdière, C., Michon, B., Schorin, M.A., Sallan, S.E., 2012. Changes in cardiac biomarkers during doxorubicin treatment of pediatric patients with high-risk acute lymphoblastic leukemia: Associations with long-term echocardiographic outcomes. *J. Clin. Oncol.* 30, 1042–1049.
- Liu, T., Brown, B.S., Wu, Y., Antzelevitch, C., Kowey, P.R., Yan, G.X., 2006. Blinded validation of the isolated arterially perfused rabbit ventricular wedge in preclinical assessment of drug-induced proarrhythmias. *Hear. Rhythm* 3, 948–956.
- Livak, K.J., Schmittgen, T.D., 2001. Analysis of relative gene expression data using real-time quantitative PCR and the 2- $\Delta\Delta$ CT method. *Methods* 25, 402–408.
- Lübberstedt, M., Müller-Vieira, U., Mayer, M., Biemel, K.M., Knöspel, F., Knobloch, D., Nüssler, A.K., Gerlach, J.C., Zeilinger, K., 2011. HepaRG human hepatic cell line utility as a surrogate for primary human hepatocytes in drug metabolism assessment in vitro. *J. Pharmacol. Toxicol. Methods* 63, 59–68.
- Lucas, R., Warner, T.D., Vojnovic, I., Mitchell, J.A., Pharmacology, C., Hospital, R.B., Street, D., Kingdom, U., William, T., Hospital, B., 2005. Cellular mechanisms of acetaminophen: role of cyclo-oxygenase 15, 1–15.
- Lucena, M.I., Molokhia, M., Shen, Y., Urban, T.J., Aithal, G.P., Andrade, R.J., Day, C.P., Ruizcabello, F., Donaldson, P.T., Stephens, C., Pirmohamed, M., Romerogomez, M., Navarro, J.M., Fontana, R.J., Miller, M., Groome, M., Bondonguiton, E., Conforti, A., Stricker, B.H.C., Carvajal, A., Ibanez, L., Yue, Q., Eichelbaum, M., Floratos, A., Pe'Er, I., Daly, M.J., Goldstein, D.B., Dillon, J.F., Nelson, M.R., Watkins, P.B., Daly,

- A.K., 2011. Susceptibility to amoxicillin-clavulanate-induced liver injury is influenced by multiple HLA class I and II alleles. *Gastroenterology* 141, 338–347.
- Luft, F.C., Bloch, R., Sloan, R.S., Yum, M.N., Costello, R., Maxwell, D.R., 1978. Comparative nephrotoxicity of aminoglycoside antibiotics in rats. *J. Infect. Dis.* 138, 541–545.
- Lyu, Y.L., Kerrigan, J.E., Lin, C.P., Azarova, A.M., Tsai, Y.C., Ban, Y., Liu, L.F., 2007. Topoisomerase II β -mediated DNA double-strand breaks: Implications in doxorubicin cardiotoxicity and prevention by dexrazoxane. *Cancer Res.* 67, 8839–8846.
- MacDonald, J.S., Robertson, R.T., 2009. Toxicity testing in the 21st century: A view from the pharmaceutical industry. *Toxicol. Sci.* 110, 40–46.
- Mackenzie, P.I., Bock, K.W., Burchell, B., Guillemette, C., Ikushiro, S., Iyanagi, T., Miners, J.O., Owens, I.S., Nebert, D.W., 2005. Nomenclature update for the mammalian UDP glycosyltransferase (UGT) gene superfamily. *Pharmacogenet. Genomics* 15, 677–685.
- Madias, N.E., Harrington, J.T., 1978. Platinum nephrotoxicity. *Am. J. Med.* 65, 307–314.
- Maron, D.M., Ames, B.N., 1983. Revised methods for the Salmonella mutagenicity test. *Mutat. Res. Mutagen. Relat. Subj.* 113, 173–215.
- Marroquin, L.D., Hynes, J., Dykens, J.A., Jamieson, J.D., Will, Y., 2007. Circumventing the crabtree effect: Replacing media glucose with galactose increases susceptibility of hepG2 cells to mitochondrial toxicants. *Toxicol. Sci.* 97, 539–547.
- Masubuchi, Y., Nakayama, S., Horie, T., 2002. Role of mitochondrial permeability transition in diclofenac-induced hepatocyte injury in rats. *Hepatology* 35, 544–551.
- Mayr, L.M., Fuerst, P., 2008. The future of high-throughput screening. *J. Biomol. Screen.* 13, 443–448.
- McGill, M.R., Jaeschke, H., 2013. Metabolism and disposition of acetaminophen: Recent advances in relation to hepatotoxicity and diagnosis. *Pharm. Res.* 30, 2174–2187.
- McGill, M.R., Williams, C.D., Xie, Y., Ramachandran, A., Jaeschke, H., 2012. Acetaminophen-induced liver injury in rats and mice: Comparison of protein adducts, mitochondrial dysfunction, and oxidative stress in the mechanism of toxicity. *Toxicol. Appl. Pharmacol.* 264, 387–394.
- McGill, M.R., Yan, H.-M., Ramachandran, A., Murray, G.J., Rollins, D.E., Jaeschke, H., 2011. HepaRG cells: A human model to study mechanisms of acetaminophen hepatotoxicity. *Hepatology* 53, 974–982.
- McGrath, P., Li, C.Q., 2008. Zebrafish: a predictive model for assessing drug-induced toxicity. *Drug Discov. Today* 13, 394–401.
- Messner, S., Agarkova, I., Moritz, W., Kelm, J.M., 2013. Multi-cell type human liver microtissues for hepatotoxicity testing. *Arch. Toxicol.* 87, 209–213.

- Mewe, M., Mauerhöfer, M., Wulfsen, I., Szlachta, K., Zhou, X.B., Schwarz, J.R., Bauer, C.K., 2010. Modulation of cardiac ERG1 K⁺ channels by cGMP signaling. *J. Mol. Cell. Cardiol.* 49, 48–57.
- Miller, R.P., Tadagavadi, R.K., Ramesh, G., Reeves, W.B., 2010. Mechanisms of cisplatin nephrotoxicity. *Toxins (Basel)*. 2, 2490–2518.
- Miller, T.J., Knapton, A., Adeyemo, O., Noory, L., Weaver, J., Hanig, J.P., 2008. Cytochrome c: a non-invasive biomarker of drug-induced liver injury. *J. Appl. Toxicol.* 28, 815–828.
- Mingeot-Leclercq, M.P., Tulkens, P.M., 1999. Aminoglycosides: Nephrotoxicity. *Antimicrob. agents Chemother.* 43, 1003–1012.
- Mizuta, K., Saito, A., Watanabe, T., Nagura, M., Arakawa, M., Shimizu, F., Hoshino, T., 1999. Ultrastructural localization of megalin in the rat cochlear duct. *Hear. Res.* 129, 83–91.
- Moghe, P. V., Cogger, R.N., Toner, M., Yarmush, M.L., 1997. Cell-cell interactions are essential for maintenance of hepatocyte function in collagen gel but not on matrigel. *Biotechnol. Bioeng.* 56, 706–711.
- Monahan, B.P., Ferguson, C.L., Killeavy, E.S., Lloyd, B.K., Troy, J., Cantilena Jr, L.R., 1990. Torsades de Pointes Occurring in Association With Terfenadine Use. *J. Am. Med. Assoc.* 264, 2788–2790.
- Monostory, K., Hazai, E., Vereczkey, L., 2004. Inhibition of cytochrome P450 enzymes participating in p-nitrophenol hydroxylation by drugs known as CYP2E1 inhibitors. *Chem. Biol. Interact.* 147, 331–340.
- Monshi, M.M., Faulkner, L., Gibson, A., Jenkins, R.E., Farrell, J., Earnshaw, C.J., Alfirevic, A., Cederbrant, K., Daly, A.K., French, N., Pirmohamed, M., Park, B.K., Naisbitt, D.J., 2013. Human leukocyte antigen (HLA)-B*57:01-restricted activation of drug-specific T cells provides the immunological basis for flucloxacillin-induced liver injury. *Hepatology* 57, 727–739.
- Murphy, S.M., Palmer, M., Poole, M.F., Padegimas, L., Hunady, K., Danzig, J., Gill, S., Gill, R., Ting, A., Sherf, B., Brunden, K., Stricker-Krongrad, A., 2006. Evaluation of functional and binding assays in cells expressing either recombinant or endogenous hERG channel. *J. Pharmacol. Toxicol. Methods* 54, 42–55.
- Myers, C., 1998. The role of iron in doxorubicin-induced cardiomyopathy. *Semin. Oncol.* 25, 10–14.
- Nassar, A.F., Hollenberg, P.F., Scatina, J., 2009. *Drug Metabolism Handbook: Concepts and Applications*, 1st ed. John Wiley & Sons.
- Nattrass, R., Faulkner, L., Vocanson, M., Antoine, D.J., Kipar, A., Kenna, G., Nicolas, J.F., Park, B.K., Naisbitt, D.J., 2015. Activation of flucloxacillin-specific CD8⁺ T-cells with

- the potential to promote hepatocyte cytotoxicity in a mouse model. *Toxicol. Sci.* 146, 146–156.
- NC3Rs, 2017. Responsibility in the use of animals in bioscience research: expectations of the major research councils and charitable funding bodies. [WWW Document]. URL [https://www.nc3rs.org.uk/sites/default/files/documents/Guidelines/Responsibility in the use of animals in bioscience research- expectations of the major research councils and charitable funding bodies April 2017.pdf](https://www.nc3rs.org.uk/sites/default/files/documents/Guidelines/Responsibility%20in%20the%20use%20of%20animals%20in%20bioscience%20research-%20expectations%20of%20the%20major%20research%20councils%20and%20charitable%20funding%20bodies%20April%202017.pdf)
- Nebert, D.W., Wikvall, K., Miller, W.L., 2013. Human cytochromes P450 in health and disease. *Philos. Trans. R. Soc. Lond. B. Biol. Sci.* 368, 20120431.
- Nelson, F.B., 1980. The pharmacology and toxicology of meta-substituted acetanilide I: acute toxicity of 3-hydroxyacetanilide in mice. *Res. Commun. Chem. Pathol. Pharmacol.* 28, 447–456.
- Nieuwkoop, P.D., Faber, J., 1994. Normal table of *Xenopus laevis* (Daudin): a systematical and chronological survey of the development from the fertilized egg till the end of metamorphosis. Garland, New York.
- Nishimura, Y., Kondo, C., Morikawa, Y., Tonomura, Y., Torii, M., Yamate, J., Uehara, T., 2015. Plasma miR-208 as a useful biomarker for drug-induced cardiotoxicity in rats. *J. Appl. Toxicol.* 35, 173–180.
- Norcross, M.A., Luo, S., Lu, L., Boyne, M.T., Gomarteli, M., Rennels, A.D., Woodcock, J., Margulies, D.H., McMurtrey, C., Vernon, S., Hildebrand, W.H., Buchli, R., 2012. Abacavir induces loading of novel self-peptides into HLA-B*57: 01: an autoimmune model for HLA-associated drug hypersensitivity 26, F21–F29.
- North, T.E., Babu, I.R., Vedder, L.M., Lord, A.M., Wishnok, J.S., Tannenbaum, S.R., Zon, L.I., Goessling, W., 2010. PGE2-regulated wnt signaling and N-acetylcysteine are synergistically hepatoprotective in zebrafish acetaminophen injury. *Proc. Natl. Acad. Sci.* 107, 17315–17320.
- Novik, E., Maguire, T.J., Chao, P., Cheng, K.C., Yarmush, M.L., 2010. A microfluidic hepatic coculture platform for cell-based drug metabolism studies. *Biochem. Pharmacol.* 79, 1036–1044.
- Obiol-Pardo, C., Gomis-Tena, J., Sanz, F., Saiz, J., Pastor, M., 2011. A multiscale simulation system for the prediction of drug-induced cardiotoxicity. *J. Chem. Inf. Model.* 51, 483–492.
- Olinga, P., Meijer, D.K., Slooff, M.J., Groothuis, G.M., 1997. Liver slices in in vitro pharmacotoxicology with special reference to the use of human liver tissue. *Toxicol. Vitro.* 12, 77–100.
- Olson, H., Betton, G., Robinson, D., Thomas, K., Monro, A., Kolaja, G., Lilly, P., Sanders, J., Sipes, G., Bracken, W., Dorato, M., Van Deun, K., Smith, P., Berger, B., Heller,

- A., 2000. Concordance of the toxicity of pharmaceuticals in humans and in animals. *Regul. Toxicol. Pharmacol.* 32, 56–67.
- Osaki, M., Kosaka, N., Okada, F., Ochiya, T., 2014. Circulating microRNAs in drug safety assessment for hepatic and cardiovascular toxicity: The latest biomarker frontier? *Mol. Diagnosis Ther.* 18, 121–126.
- Ostapowicz, G., RJ, F., FV, S., AI, E., 2002. Results of a prospective study of acute liver failure at 17 tertiary care centers in the united states. *Ann. Intern. Med.* 137, 947–954.
- Ostrov, D.A., Grant, B.J., Pompeu, Y.A., Sidney, J., Harndahl, M., Southwood, S., Oseroff, C., Lu, S., Jakoncic, J., de Oliveira, C.A.F., Yang, L., Mei, H., Shi, L., Shabanowitz, J., English, A.M., Wriston, A., Lucas, A., Phillips, E., Mallal, S., Grey, H.M., Sette, A., Hunt, D.F., Buus, S., Peters, B., 2012. Drug hypersensitivity caused by alteration of the MHC-presented self-peptide repertoire. *Proc. Natl. Acad. Sci.* 109, 9959–9964.
- Paiva, M.G., Petrilli, A.S., Moisés, V.A., Macedo, C.R.D., Tanaka, C., Campos, O., 2005. Cardioprotective effect of dexrazoxane during treatment with doxorubicin: A study using low-dose dobutamine stress echocardiography. *Pediatr. Blood Cancer* 45, 902–908.
- Pammolli, F., Magazzini, L., Riccaboni, M., 2011. The productivity crisis in pharmaceutical R&D. *Nat. Rev. Drug Discov.* 10, 428–438.
- Park, B.K., Boobis, A., Clarke, S., Goldring, C.E.P., Jones, D., Kenna, J.G., Lambert, C., Lavery, H.G., Naisbitt, D.J., Nelson, S., Nicoll-Griffith, D.A., Obach, R.S., Routledge, P., Smith, D.A., Tweedie, D.J., Vermeulen, N., Williams, D.P., Wilson, I.D., Baillie, T.A., 2011. Managing the challenge of chemically reactive metabolites in drug development. *Nat. Rev. Drug Discov.* 10, 292–306.
- Park, B.K., Kitteringham, N.R., Maggs, J.L., Pirmohamed, M., Williams, D.P., 2005a. The Role of Metabolic Activation in Drug-Induced Hepatotoxicity. *Annu. Rev. Pharmacol. Toxicol.* 45, 177–202.
- Park, B.K., Williams, D.P., Naisbitt, D.J., Kitteringham, N.R., Pirmohamed, M., 2005b. Investigation of toxic metabolites during drug development. *Toxicol. Appl. Pharmacol.* 207, 425–434.
- Patten, C.J., Thomas, P.E., Guy, R., Lee, M., Gonzalez, F.J., Guengerich, F.P., Yang, C.S., 1993. Cytochrome P450 enzymes involved in acetaminophen activation by rat and human liver microsomes and their kinetics. *Chem. Res. Toxicol.* 6, 511–518.
- Paul, P., Suwan, J., Liu, J., Dordick, J.S., Linhardt, R.J., 2012. Recent advances in sulfotransferase enzyme activity assays. *Anal. Bioanal. Chem.* 403, 1491–1500.
- Penna, A., Buchanan, N., 1991. Paracetamol poisoning in children and hepatotoxicity. *Br. J. Clin. Pharmacol.* 143-149), 1991. 143–149.

- Pichler, W.J., Naisbitt, D.J., Park, B.K., 2011. Immune pathomechanism of drug hypersensitivity reactions. *J. Allergy Clin. Immunol.* 127, S74–S81.
- Pirmohamed, M., James, S., Meakin, S., Green, C., 2004. Adverse drug reactions as cause of admission to hospital. *BMJ Br. Med. J.* 329, 460.
- Pirmohamed, M., Naisbitt, D.J., Gordon, F., Park, B.K., 2002. The danger hypothesis—potential role in idiosyncratic drug reactions. *Toxicology* 181–182, 55–63.
- Popelova, O., Sterba, M., Simunek, T., Mazurova, Y., Guncova, I., Hroch, M., Adamcova, M., Gersl, V., 2008. Deferiprone Does Not Protect against Chronic Anthracycline Cardiotoxicity in Vivo. *J. Pharmacol. Exp. Ther.* 326, 259–269.
- Pouna, P., Bonoron-Adèle, S., Gouverneur, G., Tariosse, L., Besse, P., Robert, J., 1996. Development of the model of rat isolated perfused heart for the evaluation of anthracycline cardiotoxicity and its circumvention. *Br. J. Pharmacol.* 117, 1593–1599.
- Prakash, C., Sharma, R., Gleave, M., Nedderman, A., 2008. In Vitro Screening Techniques for Reactive Metabolites for Minimizing Bioactivation Potential in Drug Discovery. *Curr. Drug Metab.* 9, 952–964.
- Prescott, L.F., 1980. Kinetics and Metabolism of Paracetamol and Phenacetin. *Br. J. clin. Pharmac.* 10, 291–298.
- Prescott, L.F., 1983. Paracetamol overdose. Pharmacological considerations and clinical management. *Drugs* 25, 290–314.
- Prescott, L.F., Illingworth, R.N., Critchley, J.A., Stewart, M.J., Adam, R.D., Proudfoot, A.T., 1979. Intravenous N-acetylcystine: the treatment of choice for paracetamol poisoning. *Br. Med. J.* 2, 1097–100.
- Prescott, M.J., Lidster, K., 2017. Improving quality of science through better animal welfare: The NC3Rs strategy. *Lab Anim. (NY)*. 46, 152–156.
- Prestwich, G.D., Liu, Y., Yu, B., Shu, X.Z., Scott, A., 2007. 3-D culture in synthetic extracellular matrices: New tissue models for drug toxicology and cancer drug discovery. *Adv. Enzyme Regul.* 47, 196–207.
- Qin, S., Zhou, Y., Gray, L., Kusebauch, U., McEvoy, L., Antoine, D.J., Hampson, L., Park, K.B., Campbell, D., Caballero, J., Glusman, G., Yan, X., Kim, T.K., Yuan, Y., Wang, K., Rowen, L., Moritz, R.L., Omenn, G.S., Pirmohamed, M., Hood, L., 2016. Identification of Organ-Enriched Protein Biomarkers of Acute Liver Injury by Targeted Quantitative Proteomics of Blood in Acetaminophen- and Carbon-Tetrachloride-Treated Mouse Models and Acetaminophen Overdose Patients. *J. Proteome Res.* 15, 3724–3740.
- Quiles, J.L., Huertas, J.R., Battino, M., Mataix, J., Ramírez-Tortosa, M.C., 2002. Antioxidant nutrients and adriamycin toxicity. *Toxicology* 180, 79–95.
- Rang, H.P., Ritter, J., Flower, R.J., Henderson, G., Rang, H.P., 2016. Rang and Dale's

- pharmacology. [Edinburgh?]: Elsevier, Churchill Livingstone, [2016].
- Rashed, M.S., Myers, T.G., Nelson, S.D., 1990. Hepatic protein arylation, glutathione depletion, and metabolite profiles of acetaminophen and a non-hepatotoxic regioisomer, 3'-hydroxyacetanilide, in the mouse. *Drug Metab. Dispos.* 18, 765–770.
- Redfern, W., Wakefield, I., Prior, H., Pollard, C., Hammond, T., Valentin, J., 2002. Safety Pharmacology a progressive approach.pdf. *Fundam. Clin. Pharmacol.* 16, 161–173.
- Redfern, W.S., Carlsson, L., Davis, A.S., Lynch, W.G., MacKenzie, I., Palethorpe, S., Siegl, P.K.S., Strang, I., Sullivan, A.T., Wallis, R., Camm, A.J., Hammond, T.G., 2003. Relationships between preclinical cardiac electrophysiology, clinical QT interval prolongation and torsade de pointes for a broad range of drugs: Evidence for a provisional safety margin in drug development. *Cardiovasc. Res.* 58, 32–45.
- Richert, L., Baze, A., Parmentier, C., Gerets, H.H.J., Sison-Young, R., Dorau, M., Lovatt, C., Czich, A., Goldring, C., Park, B.K., Juhila, S., Foster, A.J., Williams, D.P., 2016. Cytotoxicity evaluation using cryopreserved primary human hepatocytes in various culture formats. *Toxicol. Lett.* 258, 207–215.
- Riehle, K.J., Dan, Y.Y., Campbell, J.S., Fausto, N., 2011. New concepts in liver regeneration. *J. Gastroenterol. Hepatol.* 26, 203–212.
- Roberts, S.A., Price, V.F., Jollow, D.J., 1990. Acetaminophen structure-toxicity studies: in vivo covalent binding of a nonhepatotoxic analog, 3-hydroxyacetanilide. *Toxicol. Appl. Pharmacol.* 105, 195–208.
- Robles-Díaz, M., Medina-Caliz, I., Stephens, C., Andrade, R.J., Lucena, M.I., 2016. Biomarkers in DILI: One more step forward. *Front. Pharmacol.* 7, 1–7.
- Roth, R.A., Ganey, P.E., 2011. Animal models of idiosyncratic drug-induced liver injury - Current status. *Crit. Rev. Toxicol.* 41, 723–739.
- Rowe, C., Gerrard, D.T., Jenkins, R., Berry, A., Durkin, K., Sundstrom, L., Goldring, C.E., Park, B.K., Kitteringham, N.R., Hanley, K.P., Hanley, N.A., 2013. Proteome-wide analyses of human hepatocytes during differentiation and dedifferentiation. *Hepatology* 58, 799–809.
- Rowland, A., Miners, J.O., Mackenzie, P.I., 2013. The UDP-glucuronosyltransferases: their role in drug metabolism and detoxification. *Int. J. Biochem. cell Biol.* 45, 1121–1132.
- Roy, M.L., Dumaine, R., Brown, A.M., 1996. HERG, a primary human ventricular target of the nonsedating antihistamine terfenadine. *Circulation* 94, 817–823.
- Sager, P.T., Gintant, G., Turner, J.R., Pettit, S., Stockbridge, N., 2014. Rechanneling the cardiac proarrhythmia safety paradigm: A meeting report from the Cardiac Safety Research Consortium. *Am. Heart J.* 167, 292–300.
- Sakka, S.G., 2007. Assessing liver function. *Curr. Opin. Crit. Care* 13, 207–214.

- Salata, J.J., Jurkiewicz, N.K., Sanguinetti, M.C., Siegl, P.K., Claremon, D.A., Remy, D.C., Elliott, J.M., Libby, B.E., 1996. The novel class III antiarrhythmic agent, L-735,821 is a potent and selective blocker of IKs in guinea pig ventricular myocytes. *Circulation* 94, 3095.
- Salata, J.J., Jurkiewicz, N.K., Wallace, A.A., Stupienski, R.F., Guinosso, P.J., Lynch, J.J., 1995. Cardiac electrophysiological actions of the histamine H1-receptor antagonists astemizole and terfenadine compared with chlorpheniramine and pyrilamine. *Circ. Res.* 76, 110–119.
- Salliot, C., Van Der Heijde, D., 2009. Long-term safety of methotrexate monotherapy in patients with rheumatoid arthritis: A systematic literature research. *Ann. Rheum. Dis.* 68, 1100–1104.
- Salminen, W.F., Voellmy, R., Roberts, S.M., 1997. Differential heat shock protein induction by acetaminophen and a nonhepatotoxic regioisomer, 3'-hydroxyacetanilide, in mouse liver. *J. Pharmacol. Exp. Ther.* 282, 1533–40.
- Sanguinetti, M.C., Jiang, C., Curran, M.E., Keating, M.T., 1995. A mechanistic link between an inherited and an acquired cardiac arrhythmia: HERG encodes the IKr potassium channel. *Cell* 81, 299–307.
- Scaffidi, P., Misteli, T., Bianchi, M.E., 2002. Release of chromatin protein HMGB1 by necrotic cells triggers inflammation. *Nature* 418, 191–195.
- Scannell, J.W., Blanckley, A., Boldon, H., Warrington, B., 2012. Diagnosing the decline in pharmaceutical R&D efficiency. *Nat. Rev. Drug Discov.* 11, 191–200.
- Schutte, B., Henfling, M., Kölgen, W., Bouman, M., Meex, S., Leers, M.P.G., Nap, M., Björklund, V., Björklund, P., Björklund, B., Lane, E.B., Omary, M.B., Jörnvall, H., Ramaekers, F.C.S., 2004. Keratin 8/18 breakdown and reorganization during apoptosis. *Exp. Cell Res.* 297, 11–26.
- Selnick, H.G., Liverton, N.J., Baldwin, J.J., Butcher, J.W., Claremon, D.A., Elliott, J.M., Freidinger, R.M., King, S.A., Libby, B.E., McIntyre, C.J., Pribush, D.A., Remy, D.C., Smith, G.R., Tebben, A.J., Jurkiewicz, N.K., Lynch, J.J., Salata, J.J., Sanguinetti, M.C., Siegl, P.K.S., Slaughter, D.E., Vyas, K., 1997. Class III antiarrhythmic activity in vivo by selective blockade of the slowly activating cardiac delayed rectifier potassium current I(Ks) by (R)- 2-(2,4-trifluoromethyl)-N-[2-oxo-5-phenyl-1-(2,2,2-trifluoroethyl)-2,3-dihydro-1h-benzo[e][1,4]diazepin-3-yl. *J. Med. Chem.* 40, 3865–3868.
- Shenton, J.M., Chen, J., Uetrecht, J., 2004. Animal Models of Idiosyncratic Drug Reactions. *Chem. Biol. Interact.* 6150, 53–70.
- Silverblatt, F.J., Kuehn, C., 1979. Autoradiography of gentamicin uptake by the rat proximal tubule cell. *Kidney Int.* 15, 335–345.

- Simonsen, L.L., 1992. What are pharmacists dispensing most often? *Pharm. Times* April, 47–65.
- Singal, P.K., Iliskovic, N., 1998. Doxorubicin-induced cardiomyopathy. *N. Engl. J. Med.* 339, 900–905.
- Smilkstein, M.J., Knapp, G.L., Kulig, K.W., Rumack, B.H., 1988. Efficacy of Oral N-Acetylcysteine in the Treatment of Acetaminophen Overdose. *N. Engl. J. Med.* 319, 1557–1562.
- Spriet-Pourra, C., Auriche, M., 1994. *Drug Withdrawal from Sale*, 2nd ed. New York.
- Squires Jr., R.H., Shneider, B.L., Bucuvalas, J., Alonso, E., Sokol, R.J., Narkewicz, M.R., Dhawan, A., Rosenthal, P., Rodriguez-Baez, N., Murray, K.F., Horslen, S., Martin, M.G., Lopez, M.J., Soriano, H., McGuire, B.M., Jonas, M.M., Yazigi, N., Shepherd, R.W., Schwarz, K., Lobritto, S., Thomas, D.W., Lavine, J.E., Karpen, S., Ng, V., Kelly, D., Simonds, N., Hynan, L.S., 2006. Acute liver failure in children: the first 348 patients in the pediatric acute liver failure study group. *J. Pediatr.* 148, 652–658.
- Stachulski, A.V., Baillie, T.A., Park, B.K., Obach, R.S., Dalvie, D.K., Williams, D.P., Srivastava, A., Regan, S.L., Antoine, D.J., Goldring, C.E.P., Chia, A.J.L., Kitteringham, N.R., Randle, L.E., Callan, H., Castrejon, J.L., Farrell, J., Naisbitt, D.J., Lennard, M.S., 2013. The Generation, Detection, and Effects of Reactive Drug Metabolites. *Med. Res. Rev.* 33, 985–1080.
- Stark, W.M., Hoehn, M.M., Knox, N.G., 1967. Nebramycin, a new broad-spectrum antibiotic complex. I. Detection and biosynthesis. *Antimicrobial agents Chemother.* 7.
- Starkey Lewis, P.J., Dear, J., Platt, V., Simpson, K.J., Craig, D.G.N., Antoine, D.J., French, N.S., Dhaun, N., Webb, D.J., Costello, E.M., Neoptolemos, J.P., Moggs, J., Goldring, C.E., Park, B.K., 2011. Circulating microRNAs as potential markers of human drug-induced liver injury. *Hepatology* 54, 1767–1776.
- Steinherz, L., Steinherz, P., Tan, C., Heller, G., Murphy, L., 1991. Cardiac toxicity 4 to 20 years after completing anthracycline therapy. *JAMA* 266, 1672–1677.
- Stepan, A.F., Walker, D.P., Bauman, J., Price, D.A., Baillie, T.A., Kalgutkar, A.S., Aleo, M.D., 2011. Structural Alert/Reactive Metabolite Concept as Applied in Medicinal Chemistry to Mitigate the Risk of Idiosyncratic Drug Toxicity: A Perspective Based on the Critical Examination of Trends in the Top 200 Drugs Marketed in the United States. *Chem. Res. Toxicol.* 24, 1345–1410.
- Stevens, J.L., 2006. Future of toxicology - Mechanisms of toxicity and drug safety: Where do we go from here? *Chem. Res. Toxicol.* 19, 1393–1401.
- Sullivan, A., 1995. Good laboratory practices and other regulatory issues: A European view. *Drug Dev. Res.* 35, 145–149.

- Swain, S.M., Vici, P., 2004. The current and future role of dexrazoxane as a cardioprotectant in anthracycline treatment: Expert panel review. *J. Cancer Res. Clin. Oncol.* 130, 1–7.
- Swift, B., Pfeifer, N.D., Brouwer, K.L., 2010. Sandwich-Cultured Hepatocytes: An In Vitro Model to Evaluate Hepatobiliary Transporter-Based Drug Interactions and Hepatotoxicity. *Drug Metab. Rev.* 42, 446–471.
- Syed, M., Skonberg, C., Hansen, S.H., 2016. Mitochondrial toxicity of diclofenac and its metabolites via inhibition of oxidative phosphorylation (ATP synthesis) in rat liver mitochondria: Possible role in drug induced liver injury (DILI). *Toxicol. Vitro.* 31, 93–102.
- Taber, S.S., Pasko, D.A., 2008. The epidemiology of drug-induced disorders: the kidney. *Expert Opin. Drug Saf.* 7, 679–690.
- Takakusa, H., Masumoto, H., Yukinaga, H., Makino, C., Nakayama, S., Okazaki, O., Sudo, K., 2008. Covalent binding and tissue distribution/retention assessment of drugs associated with idiosyncratic drug toxicity. *Drug Metab. Dispos.* 36, 1770–1779.
- Tang, W., Kang, J., Wu, X., Rampe, D., Wang, L., Shen, H., Li, Z., Dunnington, D., Garyantes, T., 2001. Development and Evaluation of High Throughput Functional Assay Methods for hERG Potassium Channel. *J. Biomol. Screen.*
- Tennant, B.C., Baldwin, B.H., Graham, L. a, Ascenzi, M. a, Hornbuckle, W.E., Rowland, P.H., Tochkov, I. a, Yeager, a E., Erb, H.N., Colacino, J.M., Lopez, C., Engelhardt, J. a, Bowsher, R.R., Richardson, F.C., Lewis, W., Cote, P.J., Korba, B.E., Gerin, J.L., 1998. Antiviral activity and toxicity of fialuridine in the woodchuck model of hepatitis B virus infection. *Hepatology* 28, 179–91.
- Thompson, R.A., Isin, E.M., Li, Y., Weidolf, L., Page, K., Wilson, I., Swallow, S., Middleton, B., Stahl, S., Foster, A.J., Dolgos, H., Weaver, R., Kenna, J.G., 2012. In vitro approach to assess the potential for risk of idiosyncratic adverse reactions caused by candidate drugs. *Chem. Res. Toxicol.* 25, 1616–1632.
- Thompson, R.A., Isin, E.M., Ogese, M.O., Mettetal, J.T., Williams, D.P., 2016. Reactive Metabolites: Current and Emerging Risk and Hazard Assessments. *Chem. Res. Toxicol.* 29, 505–533.
- Thulin, P., Nordahl, G., Gry, M., Yimer, G., Aklillu, E., Makonnen, E., Aderaye, G., Lindquist, L., Mattsson, C.M., Ekblom, B., Antoine, D.J., Park, B.K., Linder, S., Harrill, A.H., Watkins, P.B., Glinghammar, B., Schuppe-Koistinen, I., 2014. Keratin-18 and microRNA-122 complement alanine aminotransferase as novel safety biomarkers for drug-induced liver injury in two human cohorts. *Liver Int.* 34, 367–378.
- Tirmenstein, M.A., Nelson, S.D., 1989. Subcellular binding and effects on calcium

- homeostasis produced by acetaminophen and a nonhepatotoxic regioisomer, 3'-hydroxyacetanilide, in mouse liver. *J. Biol. Chem.* 264, 9814–9819.
- Tomlinson, M.L., Hendry, A.E., Wheeler, G.N., 2012. *Xenopus Protocols* 917, 155–166.
- Tortora, G.J., Derrickson, B., 2014. The Digestive System. In: *Principles of Anatomy & Physiology*. Wiley, pp. 886–939.
- Townsend, D.M., Deng, M., Zhang, L., Lopus, M.G., Hanigan, M.H., 2003. Metabolism of cisplatin to a nephrotoxin in proximal tubule cells. *J. Am. Soc. Nephrol.* 14, 1–10.
- Ulrich, R.G., Bacon, J.A., Cramer, C.T., Petrella, D.K., Sun, E.L., Meglasson, M.D., Holmuhamedov, E., 1998. Disruption of mitochondrial activities in rabbit and human hepatocytes by a quinoxalinone anxiolytic and its carboxylic acid metabolite. *Toxicology* 131, 33–47.
- Utkarsh, D., Loretz, C., Li, A.P., 2016. In vitro evaluation of hepatotoxic drugs in human hepatocytes from multiple donors: Identification of P450 activity as a potential risk factor for drug-induced liver injuries. *Chem. Biol. Interact.* 255, 12–22.
- Valentin, J.P., Hoffmann, P., De Clerck, F., Hammond, T.G., Hondeghe, L., 2004. Review of the predictive value of the Langendorff heart model (Screenit system) in assessing the proarrhythmic potential of drugs. *J. Pharmacol. Toxicol. Methods* 49, 171–181.
- van Vliet, E., 2011. Current standing and future prospects for the technologies proposed to transform toxicity testing in the 21st century. *ALTEX Altern. zu Tierexperimenten* 28, 17–44.
- Vandewalle, A., Farman, N., Morin, J.P., Fillastre, J.P., Hatt, P.Y., Bonvalet, J.P., 1981. Gentamicin incorporation along the nephron: Autoradiographic study on isolated tubules. *Kidney Int.* 19, 529–539.
- Vejpongsa, P., Yeh, E.T.H., 2014a. Prevention of anthracycline-induced cardiotoxicity: Challenges and opportunities. *J. Am. Coll. Cardiol.* 64, 938–945.
- Vejpongsa, P., Yeh, E.T.H., 2014b. Topoisomerase 2 β : A promising molecular target for primary prevention of anthracycline-induced cardiotoxicity. *Clin. Pharmacol. Ther.* 95, 45–52.
- Verstraelen, S., Peers, B., Maho, W., Hollanders, K., Remy, S., Berckmans, P., Covaci, A., Witters, H., 2016. Phenotypic and biomarker evaluation of zebrafish larvae as an alternative model to predict mammalian hepatotoxicity. *J. Appl. Toxicol.* 36, 1194–1206.
- Vickers, A.E.M., Fisher, R.L., 2004. Organ slices for the evaluation of human drug toxicity. *Chem. Biol. Interact.* 150, 87–96.
- Vliegthart, A.D.B., Kimmitt, R.A., Seymour, J.H., Homer, N.Z., Clarke, J.I., Eddleston, M., Gray, A., Wood, D.M., Dargan, P.I., Cooper, J.G., Antoine, D.J., Webb, D.J.,

- Lewis, S.C., Bateman, D.N., Dear, J.W., 2017. Circulating acetaminophen metabolites are toxicokinetic biomarkers of acute liver injury. *Clin. Pharmacol. Ther.* 101, 531–540.
- Vliegenthart, A.D.B., Shaffer, J.M., Clarke, J.I., Peeters, L.E.J., Caporali, A., Bateman, D.N., Wood, D.M., Dargan, P.I., Craig, D.G., Moore, J.K., Thompson, A.I., Henderson, N.C., Webb, D.J., Sharkey, J., Antoine, D.J., Park, B.K., Bailey, M.A., Lader, E., Simpson, K.J., Dear, J.W., 2015. Comprehensive microRNA profiling in acetaminophen toxicity identifies novel circulating biomarkers for human liver and kidney injury. *Sci. Rep.* 5, 15501.
- Vliegenthart, A.D.B., Starkey Lewis, P., Tucker, C.S., Del Pozo, J., Rider, S., Antoine, D.J., Dubost, V., Westphal, M., Moulin, P., Bailey, M.A., Moggs, J.G., Goldring, C.E., Park, B.K., Dear, J.W., 2014a. Retro-Orbital Blood Acquisition Facilitates Circulating microRNA Measurement in Zebrafish with Paracetamol Hepatotoxicity. *Zebrafish* 11, 219–26.
- Vliegenthart, A.D.B., Tucker, C.S., Del Pozo, J., Dear, J.W., 2014b. Zebrafish as model organisms for studying drug-induced liver injury. *Br. J. Clin. Pharmacol.* 78, 1217–1227.
- Wallace, K.B., 2003. Doxorubicin-induced cardiac mitochondrionopathy. *Pharmacol. Toxicol.* 93, 105–115.
- Wang, D., Lippard, S.J., 2005. Cellular processing of platinum anticancer drugs. *Nat. Rev. Drug Discov.* 4, 307–320.
- Wang, G.-K., Zhu, J.-Q., Zhang, J.-T., Li, Q., Li, Y., He, J., Qin, Y.-W., Jing, Q., 2010. Circulating microRNA: a novel potential biomarker for early diagnosis of acute myocardial infarction in humans. *Eur. Heart J.* 31, 659–666.
- Wang, J. feng, Yu, M. li, Yu, G., Bian, J. jun, Deng, X. ming, Wan, X. jian, Zhu, K. ming, 2010. Serum miR-146a and miR-223 as potential new biomarkers for sepsis. *Biochem. Biophys. Res. Commun.* 394, 184–188.
- Wang, K., Zhang, S., Marzolf, B., Troisch, P., Brightman, A., Hu, Z., Hood, L.E., Galas, D.J., 2009. Circulating microRNAs, potential biomarkers for drug-induced liver injury. *Proc. Natl. Acad. Sci. U. S. A.* 106, 4402–7.
- Wang, Y., Tang, N., Hui, T., Wang, S., Zeng, X., Li, H., Ma, J., 2013. Identification of endogenous reference genes for RT-qPCR analysis of plasma microRNAs levels in rats with acetaminophen-induced hepatotoxicity. *J. Appl. Toxicol.* 33, 1330–1336.
- Waring, W.S., 2012. Criteria for acetylcysteine treatment and clinical outcomes after paracetamol poisoning. *Expert Rev. Clin. Pharmacol.* 5, 311–318.
- Watanabe, T., Tanigawa, T., Nadatani, Y., Otani, K., Machida, H., Okazaki, H., Yamagami, H., Watanbe, K., Tominaga, K., Fujiwara, Y., Arakawa, T., 2011.

- Mitochondrial disorders in NSAIDs-induced small bowel injury. *J. Clin. Biochem. Nutr* 48, 117–121.
- Weber, J.A., Baxter, D.H., Zhang, S., Huang, D.Y., Huang, K.H., Lee, M.J., Galas, D.J., Wang, K., 2010. The microRNA spectrum in 12 body fluids. *Clin. Chem.* 56, 1733–1741.
- Weinstein, M.J., Luedemann, G.M., Oden, E.M., Wagman, G.H., Rosselet, J.P., Marquez, J.A., Coniglio, C.T., Charney, W., Herzog, H.L., Black, J., 1963. GENTAMICIN, A NEW ANTIBIOTIC COMPLEX FROM MICROMONOSPORA. *J. Med. Chem.* July, 463–464.
- Wheeler, G.N., Brändli, A.W., 2009. Simple vertebrate models for chemical genetics and drug discovery screens: Lessons from zebrafish and *Xenopus*. *Dev. Dyn.* 238, 1287–1308.
- Wheeler, G.N., Liu, K.J., 2012. *Xenopus*: An ideal system for chemical genetics. *Genesis* 50, 207–218.
- Wienholds, E., Kloosterman, W.P., Miska, E., Alvarez-saavedra, E., Berezikov, E., Bruijn, E. De, Horvitz, H.R., Kauppinen, S., Plasterk, R.H., 2005. MicroRNA Expression in Zebrafish Embryonic Development. *Science* (80-.). 309, 310–311.
- Wienkers, L.C., Heath, T.G., 2005. Predicting in vivo drug interactions from in vitro drug discovery data. *Nat. Rev. Drug Discov.* 4, 825–833.
- Wilson, D.E., Kaymakalan, H., 1981. Prostaglandins: gastrointestinal effects and peptic ulcer disease. *Med. Clin. north Am.* 65, 773–787.
- Wiseman, L.R., Spencer, C.M., 1998. Dexrazoxane A Review of its Use as a Cardioprotective Agent in Patients Receiving Anthracycline-Based Chemotherapy. *Drugs* 56, 385–403.
- Wong, A., Gaudins, A., Kerr, F., Greene, S.L., 2014. Paracetamol toxicity: What would be the implications of a change in Australian treatment guidelines? *EMA - Emerg. Med. Australas.* 26, 183–187.
- Wosley, R.L., Chen, Y., Freiman, J.P., Gillis, R.A., 1993. Mechanism of the Cardiotoxic Actions of Terfenadine. *J. Am. Med. Assoc.* 269, 1532–1536.
- Wouters, K.A., Kremer, L.C.M., Miller, T.L., Herman, E.H., Lipshultz, S.E., 2005. Protecting against anthracycline-induced myocardial damage: A review of the most promising strategies. *Br. J. Haematol.* 131, 561–578.
- Wu, Y., Geng, X. chao, Wang, J. feng, Miao, Y. fa, Lu, Y. li, Li, B., 2016. The HepaRG cell line, a superior in vitro model to L-02, HepG2 and hiHeps cell lines for assessing drug-induced liver injury. *Cell Biol. Toxicol.* 32, 37–59.
- Xu, X., Persson, H.L., Richardson, D.R., 2005. Molecular Pharmacology of the Interaction of Anthracyclines with Iron. *Mol. Pharmacol.* 68, 261–271.

- Yang, T., Prakash, C., Roden, D.M., Snyders, D.J., 1995. Mechanism of block of a human cardiac potassium channel by terfenadine racemate and enantiomers. *Br. J. Pharmacol.* 115, 267–274.
- Yoon, M.Y., Kim, S.J., Lee, B.-H., Chung, J.-H., Kim, Y.C., 2006. Effects of dimethylsulfoxide on metabolism and toxicity of acetaminophen in mice. *Biol. Pharm. Bull.* 29, 1618–24.
- Yu, Z., IJzerman, A.P., Heitman, L.H., 2015. Kv11.1 (hERG)-induced cardiotoxicity: A molecular insight from a binding kinetics study of prototypical Kv11.1 (hERG) inhibitors. *Br. J. Pharmacol.* 172, 940–955.
- Zhang, B., Ramesh, G., Uematsu, S., Akira, S., Reeves, W.B., 2008. TLR4 Signaling Mediates Inflammation and Tissue Injury in Nephrotoxicity. *J. Am. Soc. Nephrol.* 19, 923–932.
- Zhang, J., Doshi, U., Suzuki, A., Chang, C.W., Borlak, J., Li, A.P., Tong, W., 2016. Evaluation of multiple mechanism-based toxicity endpoints in primary cultured human hepatocytes for the identification of drugs with clinical hepatotoxicity: Results from 152 marketed drugs with known liver injury profiles. *Chem. Biol. Interact.* 255, 3–11.
- Zhang, S., Liu, X., Bawa-Khalfe, T., Lu, L.-S., Lyu, Y.L., Liu, L.F., Yeh, E.T.H., 2012. Identification of the molecular basis of doxorubicin-induced cardiotoxicity. *Nat. Med.* 18, 1639–1642.
- Zhang, S., Meng, T., Liu, J., Zhang, X., Zhang, J., 2015. Cardiac protective effects of dexrazoxane on animal cardiotoxicity model induced by anthracycline combined with trastuzumab is associated with upregulation of calpain-2. *Medicine (Baltimore).* 94, e445.
- Zhang, S., Zhou, Z., Gong, Q., Makielski, J.C., January, C.T., 1999. Mechanism of block and identification of the verapamil binding domain to HERG potassium channels. *Circ. Res.* 84, 989–998.
- Zhao, R., Duncan, S.A., 2005. Embryonic development of the liver. *Hepatology* 41, 956–967.
- Zhu, J.J., Xu, Y.Q., He, J.H., Yu, H.P., Huang, C.J., Gao, J.M., Dong, Q.X., Xuan, Y.X., Li, C.Q., 2014. Human cardiotoxic drugs delivered by soaking and microinjection induce cardiovascular toxicity in zebrafish. *J. Appl. Toxicol.* 34, 139–148.
- Zimmerman, H.J., 1978. Drug-Induced Liver Disease. In: *Hepatotoxicity, The Adverse Effects of Drugs and Other Chemicals on the Liver.* Appleton-Century-Crofts, New York, pp. 351–353.
- Zimmerman, H.J., 1999. Drug-Induced Liver Disease. In: *Heptotoxicity, The Adverse Effects of Drugs and Other Chemicals on the Liver.* Lippincott Williams & Wilkins,

Philadelphia, pp. 428–433.

- Zimmermann, M., Duruz, H., Guinand, O., Broccard, O., Levy, P., Lacatis, D., Bloch, A., 1992. Torsades de Pointes after treatment with terfenadine and ketoconazole. *Eur. Heart J.* 13, 1002–1003.
- Zon, L.I., Peterson, R.T., 2005. In vivo drug discovery in the zebrafish. *Nat. Rev. Drug Discov.* 4, 35–44.
- Zorn, A.M., Mason, J., 2001. Gene expression in the embryonic *Xenopus* liver. *Mech. Dev.* 103, 153–157.
- Zütkler, B.J., Kühne, S., Rustenbeck, I., Ott, T., 2000. Mechanism of terfenadine block of ATP-sensitive K(+) channels. *Br. J. Pharmacol.* 130, 1571–4.

8 Chapter 8: Appendix

Genes were retrieved from GenBank (www.ncbi.nlm.nih.gov) and primers were designed using Primer3 (<http://primer3.ut.ee/>).

The miRCURY™ LNA PCR Primer mixes used were:

Table 8-1: miRNA qRT-PCR primer sets

<i>Xenopus laevis</i> experimental target gene	Product name (Exiqon)	Target sequence 5'-3'
miR-122	ssc-miR-122	UGGAGUGUGACAAUGGUGUUU GU
miR-103	hsa-miR-103a-3p	AGCAGCAUUGUACAGGGCUAU GA

Custom designed miRCURY™ locked nucleic acid (LNA) probes

Table 8-2 miRNA LNA probes

<i>Xenopus laevis</i> experimental target gene	Target sequence 5'-3'
miR-122	UGGAGUGUGACAAUGGUGUUUGU
miR-208	AUAAGACGAGCAUAAAGCUUGU

Table 8-3: mRNA qRT-PCR primers

Gene	Forward primer	Reverse primer
mrp2	CTGCACAACATCCTACGGG T	TCCAGCTGCGGAATGACA TT
odc	CATGGCATTCTCCCTGAAG T	TGGTCCCAAGGCTAAAGTT G

Table 8-4: mRNA RT-PCR primers

Gene	Forward primer	Reverse primer
CYP2E1	CCGCTCATTGGAAATCTGCA	CGGTGGTTGAGCAGTATG TG

CYP2D6	TCACACTGGGCATCATCTGT	TTTCCCATGCCAAAATCC C
CYP3A4	ACCTACTCCATTGCCGTTCA	TGAGGTGCTGGTGATGAC AT
GSTP1 set 1	GTATTCGGTCAGCTGCCTCA	CGTTTATTGCGGGCATCTG A
GSTP1 set 2	GGCAGATCAGGGCATTTC	AAGGGTAGGCTGAAAGGG AC
GSTT1 set 1	TGGCCGATCTCACACTCTAC	TGCCACAGAGATCTCATCC C
GSTT1 set 2	GTGTGCCCGTGTTGATGAAT	GGGTAGAGGTTCACTTGC CA
GSTM1 set 1	CGATGGATTTTCGCATGGGT	AGGACATCAGGTAGGGGA GA
GSTM1 set 2	CGTGGATGGTGATGTGAAG C	CCATGCGGTTGTTAATCG GT
SULT1A1 set 1	CCATTGCGTCAGACAGGAA G	TAAGACACCGCCACATCCT T
SULT1A1 set 2	GGCATCCCCTCGTATCATCA	CATCACAGAGCTTGGAAC CG
SULT2A1 set 1	TGCTTTCTCGCTGTAGGTGA	AAGAACCCTTGGGCTGGA AA
SULT2A1 set 2	CCCCAGGCTCATACTCACAA	CTGACGTGCTCAAACCAA GA
UGT1A6 set 1	TCCTCTTGTTGGTGTTGGGT	GGGATGGAAAGGTGTTCA GC
UGT1A6 set 2	TCCCAGACCTGTAATGCCAA	ACTGAGAGTCAACCCTGC TC
UGT1A1 set 1	AGAATGCTCTGGTGTTGGTCA	CATGTGATCCAGCGTGAG TG
UGT1A1 set 2	CACTCACGCTGGATCACATG	GCGAAAGACAAAAGTGCA GC
KCNH2	TGGTGGCAGCTATACCCTTT	GTGTTGGGAGAGACATTG CC
AMBP	CGACTATTTCAACGCACGGT	CGCCATACTGAAACGTCTC

		G
MRP2	CCTTCCCCTGTGCTTTGAAC	CGCCTGGTGTGATGAATG AG
Cardiac troponin 1c	AAAGAGCCCGGACAAGATG T	TCACTTCGGCTTCCATGTC A

8.1 Heart rate assay

An example of a video used for the heart rate assay can be found at the following link:

https://drive.google.com/drive/folders/1uoxGkKr1NsYniqqHgzigQa4Bdf_HGEKg?usp=sharing

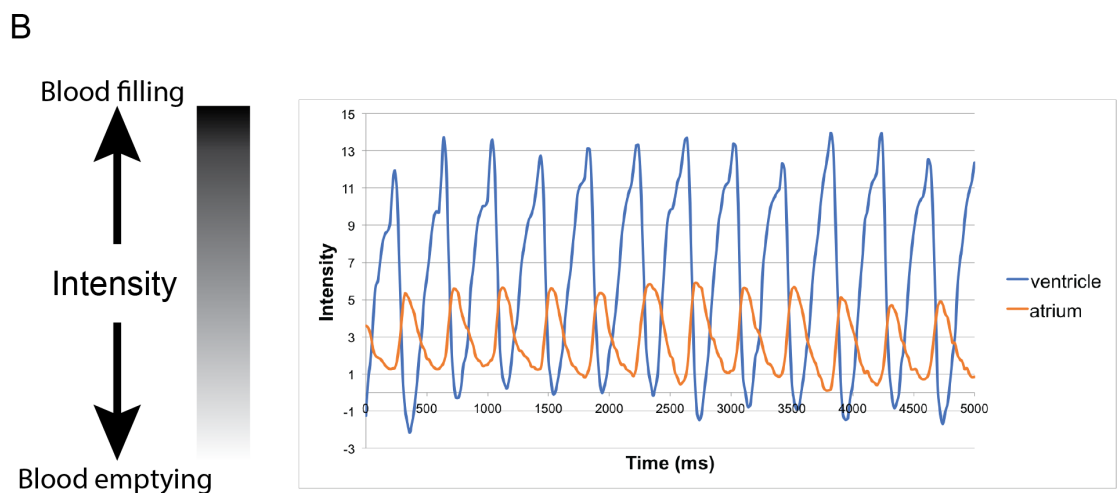
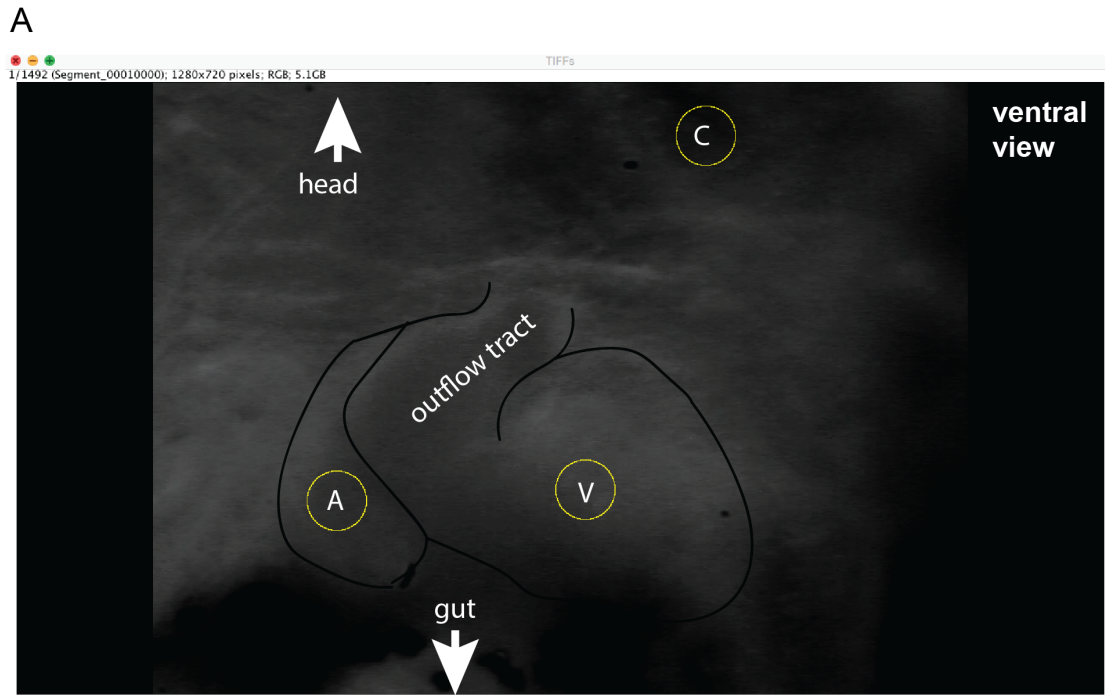


Figure 8-1: Heart rate analysis and an example of a physiological heart beat

Schematic to show the analysis process of the videos taken for the heart rate assay. Shown here, is a screenshot of the video once it has been imported into the video analysis software, ImageJ (**Panel A**). A more detailed description of the method is in **chapter 2**. The heart is outlined with a black line and the three regions of interest (ROIs) are shown here in yellow circles that are 70 pixels in diameter. ROIs were placed in the *Xenopus* atrium (A), ventricle (V) and in an area outside of the heart for control (C). The average intensity for each ROI over time was plotted. Shown here is an example of a graph generated for a normal, physiological heart beat (**Panel B**). The intensity peaks and troughs are opposite for the ventricle (blue) and atrium (orange).

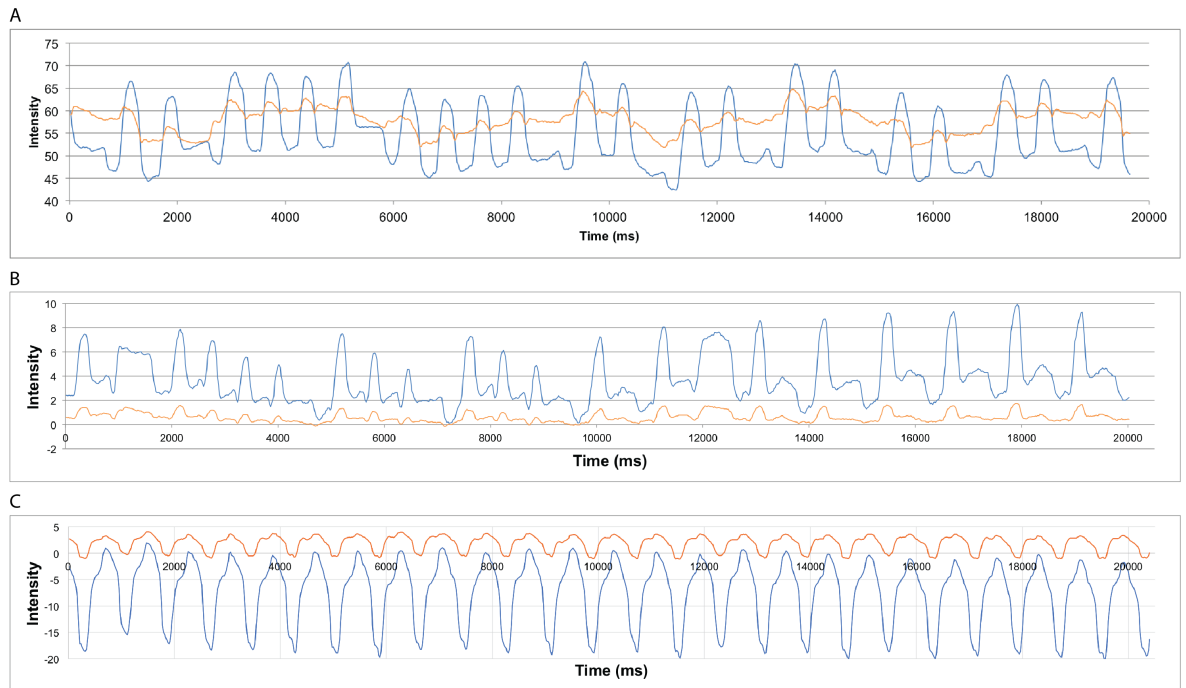


Figure 8-2: Graphs that indicate arrhythmic heart beats

3 representative arrhythmic heart beat graphs generated from videos analysed using the heart rate assay. The average intensity within the ROI for the ventricle (blue line) and the atrium (orange line) were plotted against time. An abnormal heart beat pattern can be presented as irregular ventricular peaks or shallow atrium peaks (A and B). Alternatively, simultaneous atrial and ventricular peaks also indicates an arrhythmic beat (C).